1995

Effect of various mixing devices and patterns on flocculation kinetics in water treatment

Md. Wahid Sajjad
Iowa State University

INFORMATION TO USERS

This manuscript has been reproduced from the microfilm master. UMI films the text directly from the original or copy submitted. Thus, some thesis and dissertation copies are in typewriter face, while others may be from any type of computer printer.

The quality of this reproduction is dependent upon the quality of the copy submitted. Broken or indistinct print, colored or poor quality illustrations and photographs, print bleedthrough, substandard margins, and improper alignment can adversely affect reproduction.

In the unlikely event that the author did not send UMI a complete manuscript and there are missing pages, these will be noted. Also, if unauthorized copyright material had to be removed, a note will indicate the deletion.

Oversize materials (e.g., maps, drawings, charts) are reproduced by sectioning the original, beginning at the upper left-hand corner and continuing from left to right in equal sections with small overlaps. Each original is also photographed in one exposure and is included in reduced form at the back of the book.

Photographs included in the original manuscript have been reproduced xerographically in this copy. Higher quality 6" x 9" black and white photographic prints are available for any photographs or illustrations appearing in this copy for an additional charge. Contact UMI directly to order.

UMI

A Bell & Howell Information Company
300 North Zeeb Road, Ann Arbor, MI 48106-1346 USA
313/761-4700 800/521-0600

Effect of various mixing devices and patterns on flocculation kinetics in water treatment

by

Md. Wahid Sajjad

A Dissertation Submitted to the

Graduate Faculty in Partial Fulfillment of the

Requirements for the Degree of

DOCTOR OF PHILOSOPHY

Department: Civil and Construction Engineering
Major: Civil Engineering (Environmental Engineering)

Approved:

Signature was redacted for privacy.

In Charge of Major Work

Signature was redacted for privacy.

For the Major Department

Signature was redacted for privacy.

For the Graduate College

Iowa State University
Ames, Iowa

1995

TABLE OF CONTENTS

LIST OF TABLES

LIST OF FIGURES

1. INTRODUCTION

The role of the environmental engineers is to remove pollutants from three spheres of the world, water, air and soil. One of their primary duties is to provide society with safe (from a public health standpoint) and aesthetically pleasing water. They mainly depend on two sources of water supply for potable and other uses. These are surface water sources and ground water sources. Surface water sources are usually contaminated by particulates (clay and silt particles) and other chemical and biological contaminants (humic acids, fulvic acids, color causing compounds, bacteria, viruses, fungi, algae etc.). Most of the chemical or biological contaminants mentioned above are often associated with the particulates (Lawler et al., 1980). That is why removal of particulates is the first and prime concern of environmental engineers in the production of a safe water supply.

Particles with a size near 1 μm are problematic because they can not be removed easily by simple physical methods, such as, sedimentation and filtration. Yao et al. (1971) illustrated that removal efficiency of particles in a granular media filter is minimum for particles with size near 1 μm. The particles much smaller than 1μm will be transported to the filter media for removal by Brownian motion and particles much larger than 1 μm will be transported to the filter media or to the bottom of the tank by gravity and/or inertial forces. Particles near the size range of 1 μm can not be removed by either means with reasonable cost benefit ratio. These particles and smaller particles are kinetically stable and are often called colloids and/or primary particles.

The coagulation-flocculation process comes into the picture for taking care of those kinetically stable particles. The whole process of coagulation-flocculation is divided into two parts: rapid mixing and flocculation. The principal aim of the rapid mixing step is to disperse the coagulants uniformly and quickly so as to cause destabilization of primary particles. Four distinct mechanisms can cause particle destabilization such as, compression of double layer, adsorption to produce charge neutralization, enmeshment in a precipitate or sweep flocculation, and adsorption to permit interparticle bridging. Charge neutralization and sweep flocculation are the two predominant mechanisms associated with the destabilization of particulates by metal coagulants.

Flocculation is the formation of aggregates, i.e., floc, by transport of the particles to cause collision and growth. Collisions among particles can be caused by three well defined mechanisms, such as, brownian or perikinetic flocculation due to the thermal energy of the fluid, velocity gradient or orthokinetic flocculation due to bulk fluid motion and differential settling due to a larger particle overtaking and colliding with a slower settling particle. The velocity gradient or the orthokinetic flocculation is the prime interest of the environmental engineers for both research and practical applications.

The process of orthokinetic flocculation, because of its physical nature, should be studied predominantly from a hydrodynamic/ fluid mechanics standpoint. Rapid mixing on the other hand is a physico-chemical phenomenon and needs to be studied from a joint chemical and hydrodynamics standpoint. Often times, the influence of mixing is

overshadowed by chemical overdosing in practical water treatment plants. Cleasby et al. (1989) surveyed 21 surface water treatment plants. Among those 21, eighteen used alum as coagulant. Most of those alum treatment plants used a dose above 10 mg/l as dry alum (as $Al_2(SO_4)_3.14H_2O$, molecular weight about 600 gm/mole) for a pH range of 7.2 to 8.6. Some used as high as 50 mg/l as dry alum. In addition to that, they used organic polymers as flocculation and/or filter aid chemicals. So any inefficiency of mixing during the coagulation-flocculation process was compensated by those heavy arsenal of chemicals for overall process performance.

Most of the researchers in the coagulation arena have engaged themselves in unraveling the mystery of chemistry in coagulation. They tried to show the behavior of coagulant ions during coagulation with or without the presence of other ions. Very little research has been performed involving the hydrodynamic aspects of mixing in the coagulation-flocculation process. Some researchers in environmental engineering have shown in isolated studies that both rapid and slow mixing stages are important to the coagulation-flocculation process in water treatment. But most of them have failed to comprehend a global picture of mixing associated with the coagulation and flocculation process due to a general lack of understanding of the phenomenon of turbulent flow of fluid and its influence on chemical reactions and particle transport.

Recently, advances in the theory of fluid mixing, turbulent flows in various reactors and mixing with fast chemical reactions in turbulent flows have provided some material that can be used to construct a conceptual model which combines the chemical and hydrodynamic aspects of the coagulation-flocculation process. Attempts will be

made in this study to achieve better understanding of chemical and physical phenomena which underlie the processes of mixing, colloid destabilization and flocculation. Efforts will be made to illustrate experimentally the various aspects of mixing involved in a coagulation flocculation process.

2. OBJECTIVES

Mixing in the coagulation-flocculation process can be varied in two different ways; first, by changing the mixing equipment and second, by changing the mixing pattern. Thus the prime objective of this study was to investigate and determine the effect of different mixing devices and patterns on the kinetics of flocculating kaolin clay suspension at both warm and cold water temperatures using metal coagulants under a number of physico-chemical conditions. In addition, attempts have been made to understand various aspects of the coagulation-flocculation process, such as, colloid, colloid stability, destabilization, aggregation, flocculation modeling, etc. Thus the specific objectives of this study can be stated as follows:

1. Understand the general behavior of the colloids.
2. Understand the general behavior of the metal coagulants in water and their interaction with colloids.
3. Define and understand the process of mixing and its influence on fast chemical reactions.
4. Study the phenomena of turbulent flow and determine its effect on mixing, fast chemical reactions and particle transport.
5. Study the effects of various rapid mixing variables (e.g., intensity, pattern, coagulant injection type, concentration of dosing solution etc.)
6. Study the effects of various slow mixing variables (e.g., intensity, constant intensity or tapered intensity).

7. Based on flow patterns, construct various types of mixing devices (impellers) and compare their effects during both rapid mixing and flocculation on the kinetics of the process.

Objectives 1 through 4 were accomplished by a thorough review of the literature pertaining to those areas and objectives 5 through 7 were accomplished by detailed experimental investigations in the laboratory. The flocculation experiments were performed in a bench scale batch reactor inside a walk-in constant temperature room. Impeller performance was judged on constant power input which was calculated based on measured torque. All the variables chosen for experimental studies were based on extensive literature review and their effects have been explained theoretically based on the information available in the literature. Some mathematical modeling of flocculation has been reviewed in order to understand the two directions of flocculation (growth of particles and their breakup).

This study made no attempt to address:

- The effect of various mixing variables on flocculation kinetics in a continuous flow flocculator.
- The issue of mathematical model development for the overall process of coagulation and flocculation.

3. LITERATURE REVIEW

3.1 General

Coagulation-flocculation is the first step of the three-step process for solid-liquid separation used in water and wastewater treatment. The performance of the sedimentation and filtration is very much dependent on the performance of this first step. Particles which are to be flocculated may initially be very small and fall in the colloidal range, i.e. 0.003 to 5 mm, which are distributed in a liquid suspension homogeneously and isotropically. These small particles are stable in colloidal sense, that is, given a long time, they would not aggregate into larger particles. Electrostatic repulsion induced by a negative charge on the particles causes this particle stability in a natural system.

The purpose of coagulation and flocculation is to destabilize these stable particles and then cause the individual primary particles to stick together and form aggregates (floc). This destabilization of primary particles is usually achieved by adding a small amount of positively charged material, called the coagulant, to the suspension. Depending on the amount added, this coagulant either reduces or eliminates nearly all of the electrostatic repulsion between the particles by adsorbing onto the surface of the particles. Intense mixing is required while coagulant is added, to prevent nonuniform distribution of coagulant in the suspension. This intense mixing is termed as rapid mixing which is fully turbulent in nature.

Flocculation can then be achieved in a turbulent flow field created by paddle mixer in the reactor to bring these destabilized particles closer and the van der Waals attractive force acts to stick the particles together and to form flocs. This stage of mixing is called slow mixing or velocity gradient flocculation.

From the above discussions, it is clear that mixing, turbulence, chemical reaction and flocculation kinetics are the four major topics that need to be reviewed. The literature concerning each of these four areas will be discussed in this chapter. Before discussing the above mentioned four venues of this literature review, the colloid and colloidal stability that are often found in a natural water will be discussed first.

3.2 Colloids

3.2.1. Introduction

The International Union of Pure and Applied Chemistry (IUPAC) defines a colloid as any material for which one or more of its three dimensions lie within the range of 1-1000 nm (Hirtzel and Rajagopalan, 1985). **Figure 3.1** shows the size spectrum of particles found in water. Relatively large contact area between the dispersed particles and the dispersion medium as well as the significant energy associated with creating and maintaining that interface are the two most fundamental distinguishing features of all colloidal systems. The Tyndal effect, i.e. ability to scatter light, is another distinguishing characteristic displayed by colloids (Edzwald, 1981 and Hunter, 1987). True solutions scatter very little light. The scattering pattern of colloidal dispersions

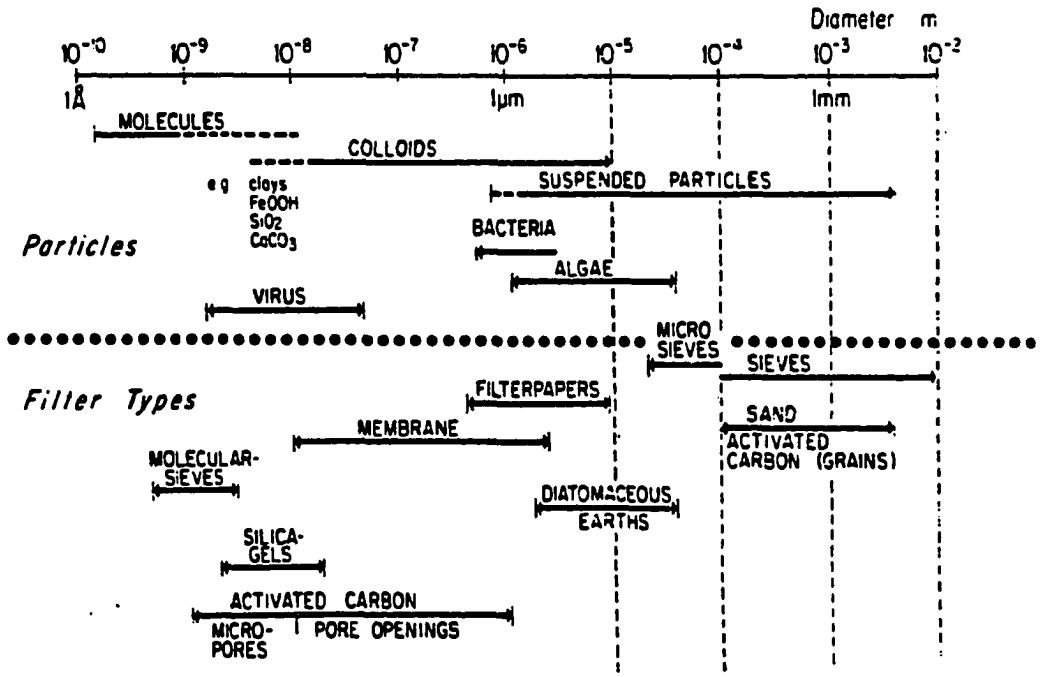

Figure 3.1. Size spectrum of waterborne particles and filter pores (Stumm and Morgan,1981)

depends very strongly on the particle size and the wavelength of the light (Hunter, 1987).

According to Kavanaugh and Leckie (1980), the size spectrum of particulates in water extends from colloidal humic substances, 1 nm in size to large aggregates such as fecal pellets or marine snow with sizes up to 10^{-2} m (10 mm), covering about 6-7 orders of magnitude. The distribution of shapes, densities, surface chemical properties and chemical composition may vary widely with size, making the complete characterization of a given water sample fairly difficult (Montgomery, 1985; and Kavanaugh and Leckie, 1980).

Environmental Engineers use a fairly simple measure of the presence of colloids in water. They measure turbidity, which is an easily determined and practically useful parameter by which a gross measure of the colloidal content of a water can be made. Very small particles with maximum dimension less than about 0.1 μm scatter very little visible light. Therefore, a water containing asbestos fibers, viruses, or humic substances have lower turbidity with a larger particle number concentration when compared with larger particles such as clay or plankton. Clay and plankton have particle diameters close to wavelength of visible light, scatter light more effectively and thereby, yield higher turbidities (Edzwald, 1981).

Based on these facts, turbidity is used as a surrogate measure of colloidal particle concentration and turbidity removal indicates the removal of such particulate contaminants of near micron size from water. But it has to be remembered that very low turbidity does not necessarily mean low total particle concentrations. It simply means

that the water does not have many particulates of a near micron size. It may still have large count of sub-micron particles. In recent years attempts have been made to measure the total number and to characterize the size distribution of particles in water suspension. One such attempt was made by Hanson and Cleasby (1990). They counted the number of particles of clay suspensions and classified the size ranges with a fair amount of accuracy down to about 0.7 mm using an Automatic Image Analyzer (AIA).

3.2.2. Colloidal interactions

When two particles approach each other, several types of interparticle forces come into play which may have a major effect on the flocculation process. These interparticle forces include van der Waals attractive forces, electrostatic repulsive forces, hydrodynamic repulsive forces, solvation repulsive forces, and steric repulsive forces. The flocculation process is influenced by colloid interactions in two different but related ways. First, colloid interactions have a direct effect on the collision efficiency, the probability of a pair of colliding particles to form aggregate. If there is strong repulsion between the particles, then the chance of aggregate formation will be very low and the flocculation will occur very slowly, if at all. One of the principal objectives of the coagulation (i.e. destabilization) process is to either reduce or eliminate this interparticle repulsion. The other aspect of colloid interactions is their effect on the strength of aggregates, which is much less understood but of great practical importance (Gregory, 1989).

Colloidal interactions are highly complex and depend on many physical and

chemical, and in some cases, biological factors. The properties that are of primary significance in determining the nature of these interactions and their outcome are as follows (Hirtzel and Rajagopalan, 1985):

1. The size and shape of the particle.

2. The chemical and electrical properties, such as, charge and charge distribution of the particle surface.

3. The interactions of the particle with other particles and with the solvent and finally

4. Particle size distribution in the solvent.

Based on their interactions with the solvent, colloidal dispersions can be classified as being lyophilic(solvent loving) or hydrophilic when solvent is water and lyophobic (solvent hating) or hydrophobic when solvent is water. **Table 3.1** (Hunter, 1987) shows some of the properties of both kinds of colloids.

The role of surface area in colloid chemistry is very important, particularly in determining the differences in behavior of both lyophilic and lyophobic colloids. One contributing factor to these differences is the extent to which the dispersion medium is able to interact with the atoms of the suspended particles. When solvent comes in contact with all or most of the atoms of the dispersed phase, then the solvation energy will be important and the colloid should be lyophilic in some suitable solvent. But when solvent is prevented, by the structure of the suspended particle, from coming in contact with any but a small fraction of the atoms of those particles then the colloid will almost certainly be lyophobic in its behavior, even if the surface atoms interact strongly with the solvent.

Table 3.1. Lyophilic and Lyophobic Colloids (Hunter, 1987)

Lyophilic	Lyophobic
o High concentrations of disperse phase frequently stable.	o Only low concentrations of disperse phase stable[a].
o Unaffected by small amounts of electrolytes. 'Salted out by large amounts.	o Very easily precipitated by electrolytes.
o Stable to prolonged dialysis[b].	o Unstable on prolonged dialysis[c] (due to removal of the small amount of electrolyte necessary for stabilization).
o Residue after desiccation will take up dispersion medium spontaneously.	o Irreversibly coagulated on desiccation.
o Coagulation gives a gel or jelly.	o Coagulation gives definite granules[d].
o Usually give a weak Tyndall beam.	o Very marked light scattering and Tyndall beam.
o Surface tension generally lower than dispersion medium.	o Surface tension not affected.
o Viscosity frequently much higher than that of medium.	o Viscosity only slightly increased[e].

[a]This is no longer true, especially if one allows the possibility of an adsorbed stabilizing layer of lyophilic material

[b]Dialysis refers to a membrane filtration technique for separating colloidal particles from small molecules or ions.

[c]Note that this is not true of lyophobic sols with dissociable ionic surface groups attached.

[d]Except for concentrated systems.

[e]This is true only for dilute, *stable* sols with more or less spherical particles.

The different interactions of these two types of colloids with the solvent determine the nature of stability of these colloids. Lyophilic colloids are soluble in solvent. Because of their solubility, these colloids are thermodynamically stable and they can be induced to aggregate or precipitate only by changing the solvency conditions, i.e., by changing the temperature or by adding large quantities of inorganic salts ("salting out"). These types of colloids consist of water-soluble macromolecules such as starches, proteins, and many others. Although these are in true solution, their size gives them some properties of dispersed particles or colloids (Gregory, 1989). In water, hydrophilic particulates are primarily of organic origin and include a wide variety of bio-colloids (humic and fulvic acids, viruses etc.) and suspended living or dead microorganisms (bacteria, algae, etc.) (Edzwald, 1981).

On the other hand lyophobic colloids consist of less soluble materials which exist in a finely divided state. These colloids are not stable in a thermodynamic sense, but may be kinetically stable because of interparticle repulsion. In most cases the repulsion is electrical in nature, since the great majority of aqueous colloids are negatively charged (Gregory, 1989). Hydrophobic particulates are primarily of an inorganic origin and include some clay particles and non-hydrated metal oxides (Montgomery, 1985).

3.2.3. Dynamics of a colloidal system

In order to understand the behavior of a colloidal system, it is necessary to observe the fundamental forces that govern the actions of lyophobic colloidal particles.

In the water industry, the term hydrophobic is frequently applied to clays, and implies that clay materials do not dissolve and remain thermodynamically unstable. But the forces that make the clay kinetically stable are as follows:

1. Electrostatic repulsion (double-layer forces): Most particles in aqueous systems are charged for various reasons, e.g., surface ionization, specific ion adsorption etc. (Gregory, 1989). Kaolin clay has a net negative surface charge of 0.15 to 0.20 C/m^2, where C is coulombs and m is meter (Hanson, 1989). Because of this net surface charge, a layer of counter ions is developed surrounding the particle. This distribution of ions around the charged particle is not uniform and creates an electrical double layer. The combination of the surface charge on the particles and the sum of the counter-ion region around the particle develop an electrically neutral system. That is why, a colloidal suspension does not have a net electrical charge. The inner layer of the double-layer is called stern layer, which is comparatively rigid, attached to particle surface and contains mainly the charge opposite to particle charge. The density of opposite charge is very high in this layer, and the thickness of this layer is much less compared to that of the outer layer. The outer plane of stern layer is called the slipping plane or the plane of shear. The outer layer is called the diffuse layer and contains mostly the same charge as the particle and some opposite charge. The density of charge is much less in this layer and the thickness is much higher than the stern layer thickness. This layer results from electrostatic attraction of counterions to the particle, electrostatic repulsion of ions of the same charge as the particle (similions), and thermal or molecular diffusion that acts against the concentration gradients produced by electrostatic effects to evenly distribute

the ions. **Figure 3.2** shows schematically a negatively charged colloidal particle with a cloud of ions (double-layer) around the particle (Amirtharajah and O'Melia, 1990).

When a voltage is applied across a suspension, the potential that causes the motion of the particles is called the zeta potential or electrokinetic potential which is developed at the plane of shear, between a particle and a fluid, when there is a relative motion between them. **Figure 3.2** also shows the location of zeta potential plane. Zeta potential and other parameters such as streaming current measurements are indirect measures of particle charge. Zeta potential has the maximum value at the plane of shear and decreases with distance from the surface. This decrease is effected by the characteristics of the double layer and by the type and concentration of ions in the bulk solution. Zeta potential is often expressed in millivolt (mv) and Bennett and Hulbert (1986) have suggested that a zeta potential on the order of 20-30 mv is the "critical zeta potential", which needs to be exceeded in absolute value if the particle suspension is to be stable. **Figure 3.3** (Zeta Meter, Inc., see page 16 please) shows the relative stability of particle systems at different zeta potential.

When two charged particles approach each other, their diffuse layers overlap and begin to interact. In the case of identical particles, the electrostatic interaction between the particles results in a repulsive force between them. A repulsive potential energy Ψ_R is produced that increases as the distance separating the particles decreases. These repulsive interactions are shown in **Figure 3.4 c and d** (Amirtharajah and O'Melia, 1990). This energy acts as a barrier for particle contact.

2. Attractive forces: London-van der Waals attractive forces are very important and

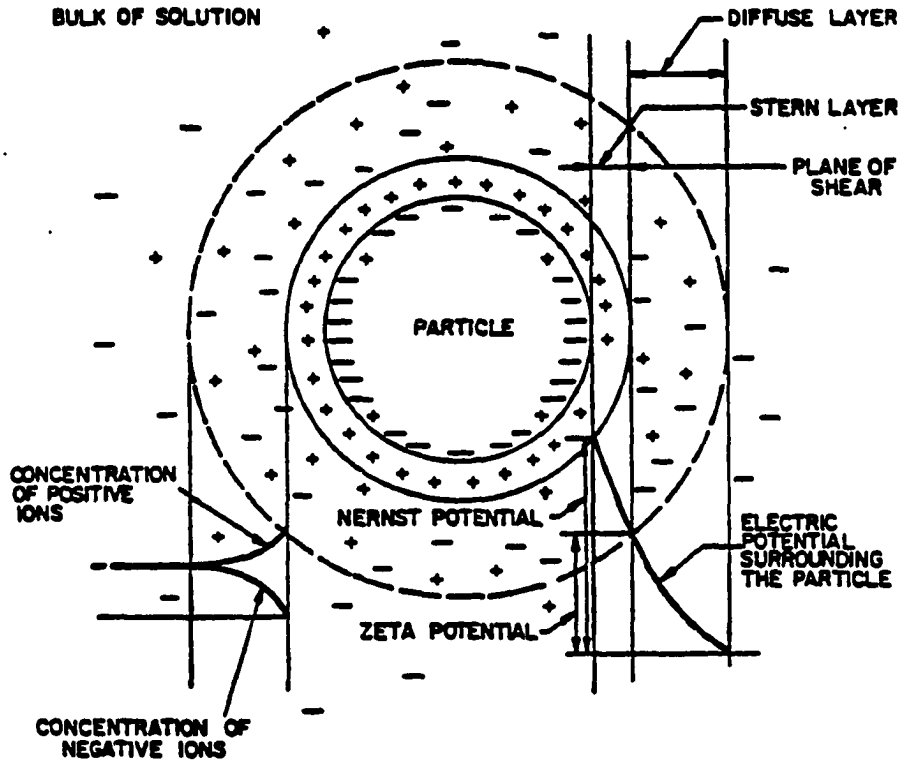

Figure 3.2. Schematic representation of a colloidal particle (Amirtharajah and O'Melia, 1990)

What ZP values reflect stability? How about flocculation?

−120	−70	−50	−30		−20	−10	−5	0 +3
excellent	good	moderate		transition	poor	fair	excellent	
DISPERSION					AGGLOMERATION			

Figure 3.3. The effect of zeta potential (ZP) on particle stability; ZP values are in millivolts (Zeta Meter, Inc.)

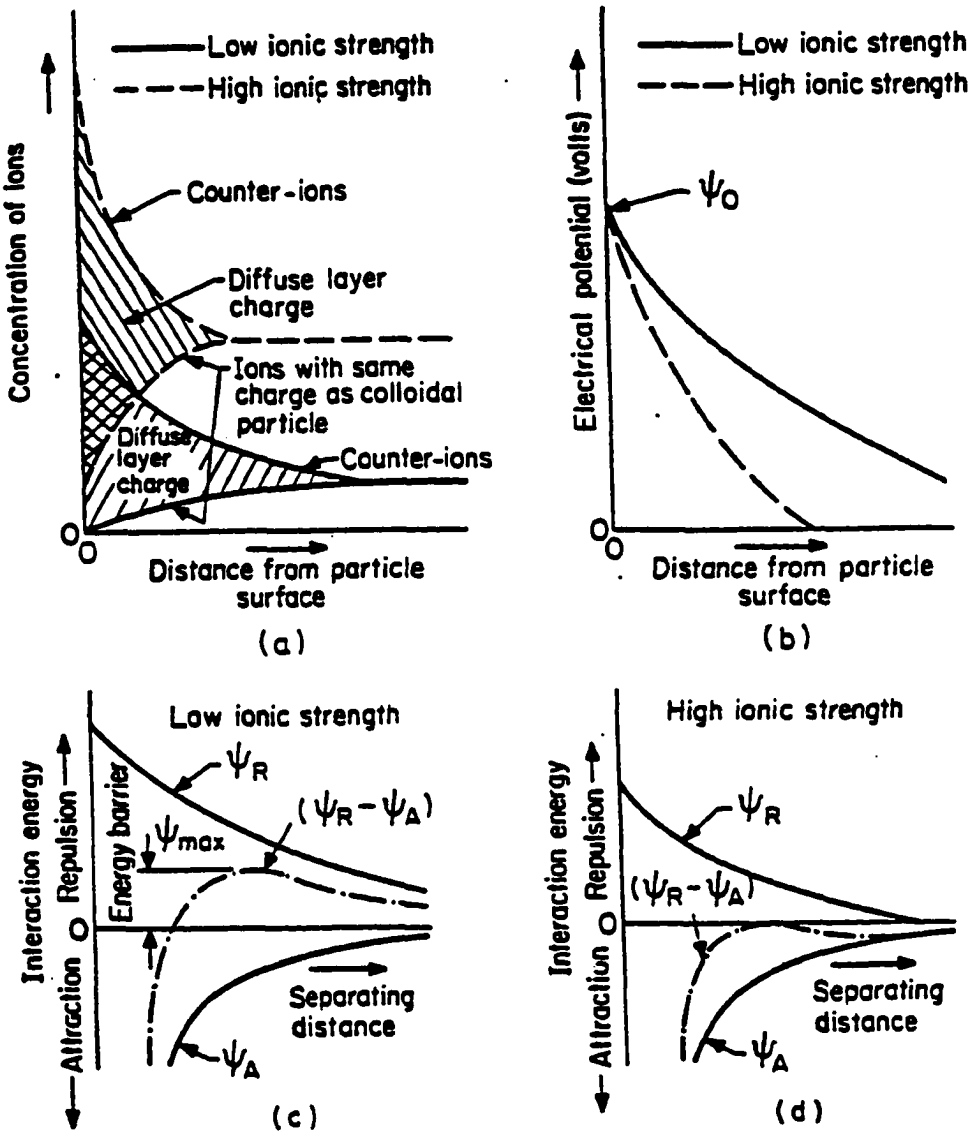

Figure 3.4. Schematic representations of (a) the diffuse double layer; (b) the diffuse layer potential; and (c and d) two cases of particle-particle interaction energies in electrostatically stabilized colloidal systems (Amirtharajah and O'Melia, 1990)

probably the only kind of attractive force existent in a coagulation-flocculation process. They arise from dipole interactions, either permanent or induced, in the atoms comprising the colloidal particles and water. Although the strength of these forces is small compared to the forces developed by a chemical bond, as seen in **Table 3.2**, these forces are strong enough to cause irreversible flocculation under some conditions.

Table 3.2. Relative bond strength of different types of bond.

Bond Type	Strength (KJ/mole)	
	(Israelachvili, 1985)	(Camp, 1968)
Co-valent	500	210-420
Hydrogen	10-40	12-42
Van der Waals	1	4-8

Based on quantum mechanical perturbation theory, London in 1930, derived an expression for the interaction energy between two identical atoms as follows (Israelachvili, 1985):

$$W(r) = [(-3/4)\alpha^2 h\nu)]/[(4\pi\varepsilon_o)^2 r^6] = -C_k/r^6 \qquad 3.1$$

α = Electronic polarizability of second atom ($C^2m^2J^{-1}$)

h = Plank's constant; 6.626×10^{-34} J.s

ν = Orbiting frequency of electron, which for the Bohr atom is 3.3×10^{15} sec^{-1}. In the simplest Bohr atom, electron orbits a proton, and there is no permanent dipole moment. However an instantaneous dipole of moment whose field will polarize a nearby neutral

atom giving rise to an attractive interaction will exist at any instant (Israelachvili, 1985).

ε_o = Permittivity of free space ($C^2J^{-1}m^{-1}$)

r = Separation distance of the atoms (m)

W(r) = London dispersion interaction free energy (J).

C = Coulombs

C_k = A constant

The main intention of the introduction of this expression is to show that the interaction energy of two identical, single atoms, the attractive energy varies inversely with the sixth power of the intermolecular distance. This analysis of London has two limiting ends: (i) very large separation distance between attracting molecules or atoms and (ii) very small separation distance between attracting molecules or atoms. The expression is not accurate in the above two cases. Two different quantitative theories for London-van der Waals interaction between two macroscopic bodies were proposed by Hamaker and later by Lifshitz.

The interaction potential between two bodies is the summed or integrated interactive energies of all of the atoms in one body with all of the atoms in a second body. This summed interaction is material and geometry specific. For a flat geometry the equation for van der Waals attraction is given by (Hanson, 1989):

$$\Phi = \{-A/(12\pi)\}\{(1/d^2)+1/(d+2\delta)^2-2/(d+2\delta)^2\} \qquad 3.2$$

Φ = van der Waals attraction for infinite flat plate ($J\ m^{-2}$)

A = Hamaker's constant (J)

d = plate separation distance (m)

δ = plate thickness (m)

The parameter "A" is material specific and has been named after H. C. Hamaker, who did much of the original work in this area. The expression for the constant A for two identical materials interacting across a third can be given as follows (Israelachvili, 1985):

$$A=(3/4)KT[(\varepsilon_1-\varepsilon_3)/(\varepsilon_1+\varepsilon_3)]^2+[(3h\nu_e)/16\sqrt{2}]*[(n_1^2-n_3^2)^2/(n_1^2+n_3^2)^{3/2}]$$

ν_e = adsorption frequency (s^{-1})

n_i = refractive index of material i

ε_i = dielectric permittivity of material i

K = Boltzman's constant (J/°K)

T = absolute temperature (°K)

h = Planck's constant, defined earlier.

Frequently the constant "A" is written as A_{123} meaning that Hamaker's constant for materials 1 and 2 acting across material 3. In case of colloid stability and flocculation, materials 1 and 2 are colloids and material 3 is the liquid medium. Hamaker's constant is much affected by the presence of dissolved salts and is considerably reduced at high ionic strengths, essentially by a "damping effect" (Gregory, 1989), but it is not sensitive to large temperature change. Practically for all aqueous dispersions, Hamaker's constant lies in the range (0.3 to 10) X 10^{-20} J. Dense mineral particles have values toward the upper end of the range, whereas low density, especially biological, materials have quite low values, and for materials with Hamaker's constants greater than about 10^{-20}J, the van der Waals interaction can be assumed to be

independent of ionic strength.

The van der Waals potential energy is usually represented by Ψ_A and is schematically shown in **Figure 3.4c and d**. This energy acts against the repulsive energy to reduce the repulsive energy barrier and yields the net interaction energy between two colloids which is also shown in the above mentioned figures.

3. Steric forces: These forces are usually generated in polymer added colloidal suspensions. When a suspension is overdosed by polymer, long-chain molecules of polymer adsorbed onto the particle surface repel each other, resulting in large interparticle forces. **Figure 3.5** (Amirtharajah and O'Melia, 1990) shows the two processes that can produce a repulsion when two polymer-coated surfaces interact at close distances. First, the adsorbed layers can be compressed by collision, reducing the volume available for the adsorbed molecules. This volume reduction restricts the

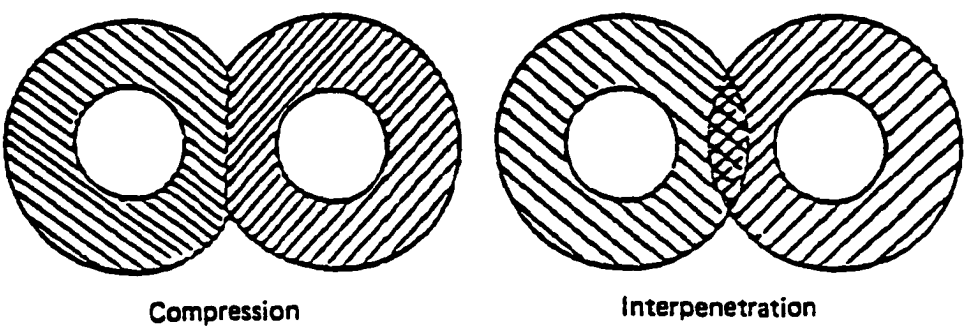

Figure 3.5. Two possible repulsive interactions of adsorbed polymer layers in sterically stabilized colloidal systems (Gregory, 1978)

polymer movement and causes the repulsion between the particles. Second, when the two polymer-coated particles collide and polymer tails interpenetrate, increasing the polymer concentration in overlapped region, a strong hydrophilic action of extended polymer sections leads to repulsion. Natural organic materials such as humic substances are common in water supplies. They are anionic polyelectrolytes, adsorb at interfaces, can be surface active and may contribute to particle stability by steric effects (Amirtharajah and O'Melia, 1990).

4. Solvation forces: These forces result from the changes in the local arrangement of molecules (solvent structure) near a surface or interface. These are strong repulsive forces acting over a very short distance range, i.e., under 1 to 3 nm and may dominate over both electrostatic repulsion and van der Waals-London forces for small separation distances between the particles or surfaces, but they do not contribute significantly to the long range tail of forces (Israelachvili, 1985). **Figure 3.6** (Israelachvili, 1985), shown on page 23, is the illustration of the variation of solvation forces as two particles or surfaces approach. Sigma(σ) in this figure is the incremental change of separation distance between two surfaces corresponding to the period exhibited by the pressure fluctuation (oscillation) shown in **Figure 3.6b**. As seen form **Figure 3.6b**, the solvation force becomes significant when the separation distance between two particles equals sigma. As a result, the density of the solvent also changes radically within this separation distance. Sigma is material specific and has different values for different solvents. For water, sigma has a value of 0.25 nm. Since both ε and n of the Hamaker's constant depend on density of solvent (ρ), Hamaker's constant (A) is also influenced by

the solvation forces. So oscillatory solvation forces are often thought of as van der Waals forces at small separation distances with the molecular properties of the liquid taken into account (Hanson, 1989).

5. Born repulsion: This repulsion is caused by the overlapping of electron clouds as the particles approach each other on a molecular scale. This force is difficult to distinguish from other forces and may not be active in an aqueous system, because of the solvation forces.

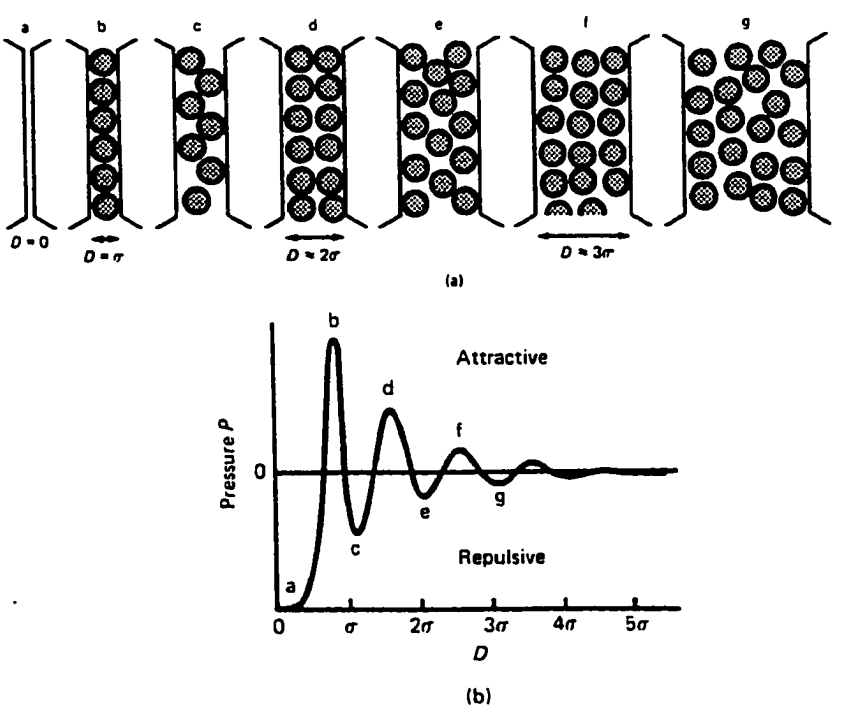

Figure 3.6. **Structural changes in a liquid as two surfaces approach; (a) the molecular ordering of water at the surface changes as the separation distance D changes. The density of liquid molecules in contact with the surfaces varies between maxima and minima. σ = 0.25 nm for water; (b) corresponding solvation pressure (Israelachvili, 1985)**

3.3 Destabilization of Colloids

3.3.1. General

As mentioned earlier, like particles of lyophobic colloids are thermodynamically unstable and have a tendency to lump together. But the particles are kinetically stable because of several interacting forces, and are prevented from colliding with each other. Although four or five different forces are found responsible for this kinetic stability, two among them (electrostatic repulsion and van der Waals attraction) are the most important. As shown in **Figure3.4c and d**, these two forces create a resulting energy barrier that prevents the particles from colliding and sticking together. There is nothing that can be done to increase the attractive force of the system. Thus, if one desires to decrease the stability (or energy barrier) of a colloidal suspension, it is necessary to reduce the repulsive forces. The repulsive portion of the curve is a function of surface charge and solution chemistry. In the water treatment field, the surface charge is usually modified. If we reduce or eliminate the surface charge, the barrier to flocculation is reduced or eliminated. This reduction of the barrier to flocculation is called destabilization and can be achieved in several ways discussed in the following paragraphs.

3.3.2. Adsorption and charge neutralization (A/D)

This is also called coagulation by potential control. In this process, the surface charge of particles are altered by adsorption of counterions from the coagulant chemical,

reducing the net charge on the particle surface, thereby reducing the repulsive energy barrier and encouraging rapid coagulation. If this process of charge reduction on the particle surface is continued to a limit, either by coagulant chemical addition at a particular pH or by the pH adjustment at a particular coagulant dose, where the electric charge on the particles is actually zero, the state is referred to as the point of zero charge (pzc) for that colloid. If the process is continued further, restabilization of colloids can take place and colloids again become kinetically stable. Metal coagulants like alum and ferric salts display such coagulation properties at specific pH levels and are used in destabilization of colloids in water treatment operations (Benefield et al., 1982; Hunter, 1987; and O'Melia, 1972).

The extent of adsorption, and hence, the destabilization capacity of coagulants depends on the chemical structure, the presence of certain functional groups, and the degree of hydration of coagulants. Polyvalent hydrolyzed metal ions are much more efficient in adsorption on colloidal surfaces than monovalent or unhydrolyzed ions. According to Stumm and Morgan (1981) the predominant adsorbable species are polynuclear compounds such as $Al_8(OH)_{20}^{4+}$ or $Al_6(OH)_{12}^{6+}$. Preformed iron coagulants, containing large portion of highly charged polymeric species are readily adsorbed on particles and neutralize their negative charge strongly (Tang and Stumm, 1987).

Stumm and Morgan (1981) proposed that hydrolysis increases the adsorption tendency of the Al complex by making it more hydrophobic. This can be done by reducing the effective charge of the center ion or ions and hence decreasing the interaction between the central Al atom and the remaining peripheral aqua groups

(ligands). As a result a covalent bond is produced between the hydrolyzed Al ion and specific sites on the solid surface by reducing the energy necessary to displace water molecules from the coordination sheath around the Al ions. Also, ion-solvent interactions present an energy barrier to close approach of highly charged ions to the interface between a low dielectric constant solid (e.g., kaolinite and SiO_2) and water (James and Healy, 1972c). When the ionic charge is lowered by hydrolysis, the ion-solvent interaction is decreased lowering the energy barrier. The ions then approach closer to the interface which results in greater coulombic and short-range interaction energies, that are more favorable to adsorption.

Matijevic and Kolak (1967) observed, in a study of coagulation of lyophobic colloids by metal chelates, that hydration alone is not the only factor influencing the absorbability of complex ions. They found that similar metal chelates (i.e., $Co(en)_3^{3+}$ and $Cr(en)_3^{3+}$, which have different metal centers, but same organic ligand (ethylene-diamine) and net charge) exert very different destabilizing effects. The central metal ion influences the distribution of electrons in the ligands and also the specific chemical groups of the ligand affecting the adsorption capacity of the chelate at the colloid surface. Since work is required to remove the hydration layer of an adsorbing ion, the more hydrated an ion, the less it adsorbs.

James and Healy (1972a) showed a relationship between adsorption of hydrolyzed cobalt ions on silica and pH. The fractional adsorption of Co(II) on silica is low at lower pH range (1 to 5) where cobalt is present entirely as Co^{2+}; the adsorption then increases sharply and free Co^{2+} decreases rapidly in the pH range 6.5 to 8.0 and the

predominant cobalt species become the adsorbable hydroxo cobalt(II) complexes ($CoOH^+$ and $Co(OH)_2$). Therefore there is a qualitative correlation of the pH of abrupt increase in adsorption with hydrolysis. James and Healy (1972c) proposed that the delay in adsorption is due to the large change in solvation energy contribution that opposes the coulombic and specific interactions. When the solvation energy is lowered by increasing the lower charged hydrolysis products as the pH increases, adsorption also increases. This abrupt change in adsorption capacity within a short pH range is a characteristic of the most metal ions used as coagulants. There is a range of 1 to 2 pH units where the extent of adsorption rises from 0% to almost 100%. James and Healy (1972c) also postulated that the adsorption of metal ions on the silica surface occurs when the solution conditions are suitable for some hydrolysis of a particular metal ion.

Using measured OH:Al ratios and residual aluminum concentrations, Dentel and Gossett (1988) indicated that destabilization by adsorption is brought about by precipitation of positively charged aluminum hydroxide on to the original particle surfaces. James and Healy (1972b) also presented similar evidence which indicates that the adsorption of hydrolysis products leads to the formation of a layer or a partial layer (depending on the amount of aluminum, hydrogen ion, Al-complexing ligands, etc., in the system) of amorphous hydroxide precipitate on the particle surface. They concluded that this results from a lowered stability of the precipitate at the surface caused by the interfacial electrical field and they referred to this as surface nucleation or precipitation. An approximate stoichiometric relationship is usually observed between coagulant dose and the surface area of the colloid for an adsorptive interaction, in which, a certain

fractional coverage of the particle surface has to be achieved to produce optimum coagulation. Beyond that coverage particles may tend toward restabilization and coagulation efficiency may be lowered.

3.3.3. Double layer compression

If someone adds to the colloidal suspension an "indifferent electrolyte" whose ions enjoy no special relationship with the surface (like adsorption), have no chemical characteristics in coagulation such as hydrolysis and act as point charge, the presence of these added counterions results in a smaller diffuse layer surrounding the particles. High concentration of such electrolytes in solution produce correspondingly high concentrations of counterions in the diffuse layer simply following the electrostatic rule; ions of similar charge to the primary charge of the colloid are repelled and counterions are attracted. The volume of the diffuse layer necessary to maintain electroneutrality is reduced, and the effective thickness of the diffuse layer is reduced correspondingly. As a result the distance between the repelling colloidal particles decreases, the attractive van der Waals interaction can dominate at all separations, the energy barrier can disappear, and electrostatic stabilization can be eliminated.

In 1900, Hardy summarized the results of the use of such electrolytes as coagulant in the Schulze-Hardy rule, which states that the destabilization of colloid by an indifferent electrolyte is brought about by ions of opposite charge to the colloid and that the coagulation effectiveness of the ions increases significantly with ion charge. For example, the concentrations of Na^{+}, Ca^{2+}, and Al^{3+} required to destabilize a negative

colloid are observed to vary about in the ratio of 1:(1/100):(1/1000) (Amirtharajah and O'Melia, 1990). This destabilization mechanism is of limited interest to the people concerned with coagulation in potable water treatment systems. Usually coagulants used in water industry are not "indifferent electrolytes" and they undergo many and more important reactions in addition to electrostatic ones. One such reaction was discussed in the previous section.

3.3.4. Enmeshment in a precipitate

This mechanism can not be thought of as a pure "colloidal destabilization" method, but merely as a physical means of colloidal removal. Here metal coagulants such as aluminum and ferric salts are added, at the appropriate pH, to the water greatly in excess of their solubility in water to cause precipitation of a metal hydroxide [e.g., $Al(OH)_{3(s)}$ or $Fe(OH)_{3(s)}$. The colloidal particles serve as nuclei around which precipitation occurs, causing the enmeshment of the particles, which eventually settle out. These precipitates enmesh the particles as they grow and can also collide with the other particles later on (Amirtharajah and O'Melia, 1990). This process is referred to as "sweep floc" removal.

Not just the oversaturation of the solutions by the metal coagulants, but some degree of supersaturation must be exceeded for rapid precipitation to cause "sweep floc". This critical supersaturation depends on several parameters, including temperature and the concentration of solid particles already present in the solution. This "sweep floc" mechanism is not stoichiometric, moreover the critical supersaturation necessary for

rapid precipitation could in fact decrease with increasing surface concentration, with colloidal particles providing interfaces for localized oversaturation (Stumm and O'Melia, 1968). The rate of precipitation is also increased by the presence of certain anions in the solution.

Heterocoagulation is another phenomenon in the sweep floc mechanism observed by Dentel and Gossett (1988), in which an additional possible removal mechanism is that the metal hydroxide first attains a solid state in solution and then heterocoagulates (collide with particles of different kind) with the particulates in the water. In the treatment of low but objectionable concentrations of colloidal particles, sweep floc with high coagulant dosages where gelatinous metal hydroxide precipitates are produced rapidly can be effective, and is used in order to enhance flocculation kinetics.

In low turbid water, particle aggregation is limited by the number of collisions or contact opportunities that exist in the suspension. High concentrations of rapidly formed precipitates increase the floc volume, enhance collision opportunities, and produce settleable floc. In typical water treatment practice under sweep floc conditions, water is supersaturated three to four orders of magnitude above the solubility of the metal to precipitate metal hydroxide in 1 to 7 seconds (AWWA Committee report, 1989).

3.3.5. Adsorption and interparticle bridging

This mechanism is observed in polymer coagulation. In coagulation with metal salt this phenomenon does not take place. When long-chain polymers with high molecular weight are added to a colloidal dispersion, polymers may adsorb on particles

at many points along the chain and also a single polymer molecule becomes attached to more than one particle. In that case particles are bridged together, in which polymer serves as a bridge. For effective bridging, the polymer needs to adsorb in such a way that a significant fraction of segment is not in contact with the surface of the particle, but extend some distance into the aqueous phase. Also adsorbed amount should not be too great, so that a significant fraction of the surface remains free of adsorbed polymer. As a result, contacts can occur between unoccupied areas of a particle surface and extended segments of chains adsorbed on other particles as shown in Figure **Figure 3.7a** (Gregory, 1989; and Amirtharajah and O'Melia, 1990).

If polymer is added in excess amount and the excess is adsorbed onto the particle surface, bridging is prevented because of inadequate free particle surface for bridging contacts to occur and particles are restabilized by surface saturation and can be sterically stabilized as shown in **Figure 3.7b** (Gregory, 1989). That is why an "optimum dosage" of polymer is required to achieve good bridging flocculation and that dose is usually found to depend on particle concentration.

3.4. Flocculation and Flocculation Models

3.4.1. General

Once the particles are destabilized by one or more of the mechanisms previously discussed, then those destabilized particles must be brought into contact with one another for aggregation to occur. This process is called flocculation and the starting

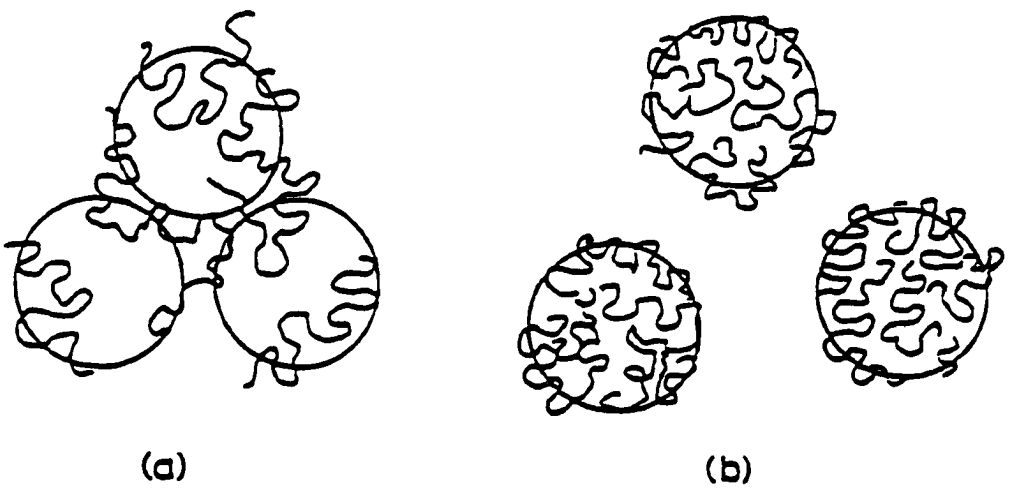

Figure 3.7. Schematic illustration of (a) bridging flocculation and (b) restabilization by excess adsorbed polymer (Gregory, 1989)

point for a discussion of flocculation kinetics is the classic work of Smoluchowski in 1917. This work dealt with aggregation of micron-sized particles by Brownian motion and laminar shear and did not consider turbulent flocculation. Ernst (1986) gives the Smoluchowski flocculation kinetic equation in the following form:

$$dn_k/dt = (1/2)[\Sigma K_{ij} n_i n_j] - n_k[\Sigma K_{ik} n_i] \qquad 3.3$$

The term in the left hand side represents the rate of change of concentration of k-fold aggregates, where k=i+j, and variable n represents number concentration of particles. K_{ij} and K_{ik} are referred to as collision kernels (rate coefficients). Equation 3.3 represents the irreversible aggregation without any consideration of breakup of aggregates, which would require a third term on the right hand side.

Above equation represents aggregation driven by two different mechanisms. First, particles collide from time to time due to differential thermal energy of the system and the mechanism is called Brownian motion or perikinetic flocculation. Second, fluid shear causes velocity gradients and particles follow the motion of suspending fluid resulting in interparticle contacts, and this is called orthokinetic flocculation. Other than these two, there is another mechanism which is called differential settling. All these three will be discussed in the following sections.

3.4.2. Perikinetic flocculation

If the particles are compact and the driving mechanism is Brownian motion the kernel in the Smoluchowski's equation is $K_{ij} = 4\pi D_{ij}(a_i + a_j)$, where $D_{ij} = (D_i + D_j)$ is the combined diffusion coefficient for particles i and j. The variables a_i and a_j are the radii

of the colliding spheres. For diffusion coefficients, the Stokes-Einstein expression is used which is $D_i = kT/(6\pi a_i \mu)$, where k is the Boltzmann's constant, T is the absolute temperature and μ is the dynamic viscosity of the fluid.

Upon substituting the values of K_{ij} and D_i in Equation 3.3, the discrete form of the equation results:

$$dn_k/dt = [kT/3\mu][\Sigma R_{ij} n_i n_j - 2n_k \Sigma R_{ik} n_i] \qquad 3.4$$

The term $R_{ij} = (a_i + a_j)^2/(a_i a_j)$ represents the collision sphere of the interacting particles i and j. The first term represents particle growing out of the i and j classes into the k class. The second term represents particles growing out of the k class into some other class.

The Smoluchowski treatment for this type of flocculation is based on the collision of spheres, in which, as the particle size increases, the diffusion coefficient decreases but the collision radius increases. These have opposing effects on the collision rate and for similar, equal size, particles, they balance exactly. This assumption is questionable in case of aggregates. Two colliding solid spheres must form a dumbbell shaped aggregate and, with higher order aggregates, many different shapes become possible as shown in **Figure 3.8** (Gregory, 1989). The collision rate of such aggregates are likely to differ from those for spheres. Moreover, the effects of size on collision radius and the diffusion coefficient can not be expected to balance each other in the same way as monodisperse spheres. For a monodisperse suspension Equation 3.4 assumes very simple size-independent form of collision rate constant as follows:

$$-dn_T/dt = (4kT/3\mu)n_T^2 = k_p n_T^2 \qquad 3.5$$

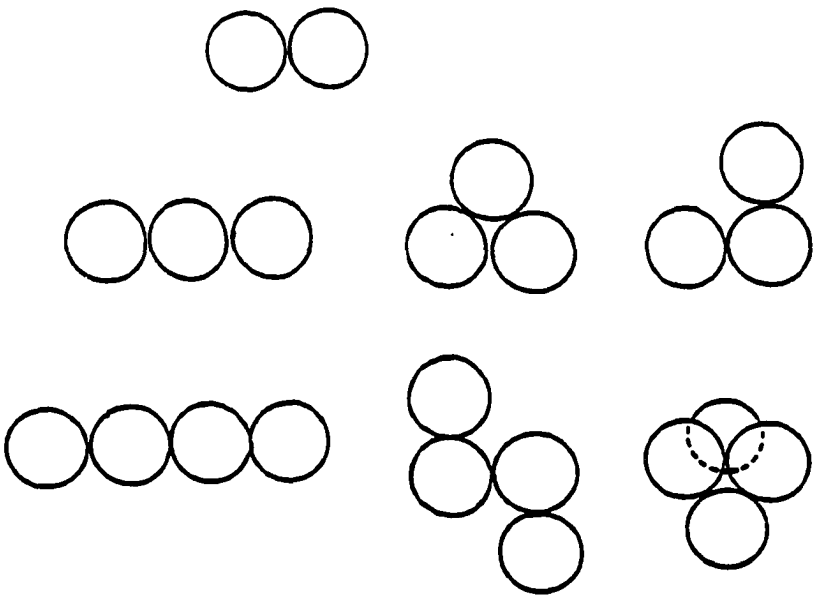

Figure 3.8. Possible shapes of aggregate upto four fold (Gregory, 1989)

$k_p = 4kT/3\mu$ is known as the flocculation rate constant and has a value of $6.13X10^{-18}$ m^3s^{-1}, for aqueous dispersion at 25° C. Equation 3.5 results from Equation 3.4 for monodispersed suspension of spherical particles where $a_i = a_j$ and $n_i = n_j = n_T$. For monodispersed suspension and at the beginning of the flocculation, two terms of Equation 3.4 collapse into one term. This time the equation was written in terms of the rate of change of the primary particles instead of some intermediate size particle. Rate constants determined experimentally for rapid flocculation of latex particles by Lichtenbelt et al. (1974) are about half of the value given by Equation 3.5. This reduction in rate is known to be a result of hydrodynamic interaction between approaching particles (Gregory, 1989).

3.4.3. Orthokinetic flocculation

The second process of Smoluchowski treatment is the orthokinetic flocculation where particles are assumed to follow fluid streamlines (with velocity u) and the collision frequency depends on the size of the particles and on the velocity gradient (perpendicular to the flow direction, z) or shear rate. The flow is laminar with a constant velocity on a streamline. If the particles are compact and the driving mechanism is a laminar shear field, the kernel for Smoluchowski model is $K_{ij} = 4/3(du/dz)A_{ij}^3$. The shear gradient, du/dz, is also called the velocity gradient and is symbolized by G. $A_{ij} = (a_i + a_j)$ is the collision radius for particles i and j. With this value of K_{ij} Equation 3.3 assumes the form for laminar shear flocculation as follows:

$$dn_k/dt = (2G/3)[\Sigma(a_i + a_j)^3 n_i n_j - 2\Sigma(a_i + a_k)^3 n_i n_k] \qquad 3.6$$

The first term represents particle growing into the k size class, and second term represents particles growing out of the k class into another size class. So as the time approaches infinity, all the particles will form a single macro-floc since there is no breakup term in the model. But in reality, the floc will reach a maximum size and will break during flocculation due to the fluid motion. The maximum size of the floc will be determined by the strength of particle bonds in the floc and the stress exerted by the fluid motion. The breakup terms will assume the same form as the two terms just presented in Equation 3.6 except the sign on them will be opposite. That is, particles will be growing into the class size due to breakage of larger floc, and particles will be leaving the class size due to breakup to smaller floc (Hanson, 1989).

For a monodisperse suspension the initial rate of decline of the total particle concentration, n_T due to orthokinetic flocculation can be derived from Equation 3.6 as follows:

$$-dn_T/dt = (16/3)Ga^3n_T^2 = k_on_T^2 \qquad 3.7$$

Since $a_i = a_j$ and $n_i = n_j = n_T$. This expression makes it clear why fluid motion is effective in promoting collisions, especially for larger particles. The third power of the particle size dependence is in marked contrast to the perikinetic case. By comparing Equations 3.5 and 3.7, the ratio of collision rate constants for early stages of ortho and perikinetic flocculation is given as $k_o/k_p = 4G\mu a^3/kT$. For a shear rate of only $10s^{-1}$ in aqueous dispersions at room temperature, the ratio is unity for a particle radius of about 0.5 μm. For larger particles and higher shear rates, the orthokinetic rate becomes much greater implying the need for fluid motion for flocculation (Gregory, 1989).

The above expressions from Smoluchowski's treatment are for laminar flow and can not be applied to turbulent flocculation. But there are several possible alternative approaches. An early attempt to treat flocculation in turbulent flow was made by Camp and Stein in 1943. They took Smoluchowski's solution for well defined laminar shear flow, and replaced the velocity gradient (du/dz) with a root mean square velocity gradient and called it rms velocity gradient G for the turbulent flow field. According to their formulation, the absolute velocity gradient at a point p is given as:

$$G_p=[\{(du/dy)+(dv/dx)\}^2+ \{(du/dz)+(dw/dx)\}^2+ \{(dv/dz)+(dw/dy)\}^2]^{1/2} \qquad 3.8$$

where u, v, and w are the velocity components in x, y, and z directions respectively. For a Newtonian fluid, this can be reduced to $G=(\varepsilon/\upsilon)^{1/2}$, where ε is the total energy dissipated per unit mass, and υ is the kinematic viscosity. This expression of G is then directly inserted into Smoluchowski's model for laminar shear flocculation to yield a model for turbulent flocculation (Hanson, 1989).

The main problem with this model of Camp and Stein (1943) is that, it does not specifically include many important phenomena associated with the turbulent flocculation. Some of them are

- eddy size distribution and the relationship between eddy size and the transport of floc of various sizes,
- effect of coagulant chemistry and precipitate surface chemistry,
- effect of coagulant and system chemistry on floc strength,
- non-isotropic, non-homogeneous nature of the flow field (i.e., spatial variation in the flow field),

- mechanisms involved in breakup (surface erosion vs. fracture), and the dependence of the dominant breakup mechanism on floc size and flow field characteristics,
- particle and floc size distribution are usually polydispersed and frequently multi-nodal,
- particle and floc strength and hydrodynamic forces.

Since these effects are not included explicitly in the model, they are all lumped together into whatever parameters are used to fit the model to the observed data. Many attempts have been made to improve Camp and Stein's generalization of Smoluchowski's model.

Saffman and Turner (1956) developed a model for orthokinetic turbulent flocculation of rain drops in a cloud based on two assumptions: (1) the turbulent flow field was homogeneous and isotropic, which is an idealization with the turbulence independent of position and direction, and (2) the particles were small compared to the Kolmogorov microscale. This microscale approximately defines size of the eddies below which the energy is dissipated primarily by viscous effects (Amirtharajah and O'Melia, 1990). This Kolmogorov microscale has been derived as $\eta_k=[\upsilon^3/\varepsilon]^{1/4}$ (Tatterson, 1991). Saffman and Turner's model is given as:

$$N_{ij}= 1.294n_in_j(a_i+ a_j)^3G \qquad 3.9$$

where N_{ij} is the number of collisions per unit time per unit volume and other variables were defined previously.

Even though their model was rigorously derived, it differed from that of Camp and Stein (1943) only by the value of the constant. The constants differ only by 5% (Camp and Stein's 1.333 to Saffman and Turner's 1.294); all the other variables in the

expression were exactly the same for two models. Based on their second assumption, the particles must meet the criteria shown in **Table 3.3** at 25^0 C for the model to be valid (Hanson, 1989).

Table 3.3. G-value and the corresponding limiting particle size for the Saffman and Turner model; this size is the Kolmogorov Microscale of turbulence (Hanson, 1989)

G-value	Limiting size in μm
10 /sec	300
50/sec	134
100/sec	77

In the water treatment industry, the flocculation energy is usually tapered from G value of 100 to $20s^{-1}$ and the floc can easily be larger than the corresponding microscale. But the number of flocs larger than microscale may not be high and may appear only at a considerable time after the start of flocculation. The primary particles found in water treatment are generally less than 10 μm and will fulfill these criteria. So this model has a broad region of applicability, before too large flocs have been formed in the reactor.

Delichatsios and Probstein (1975) theoretically derived kinetic models for orthokinetic flocculation in isotropic turbulent flow for two conditions where the radius of collision spheres is smaller than or greater than the Kolmogorov microscale. Their two models are given as follows:

For viscous subrange i.e. $(a_i + a_j) << \eta$

$$N_{ij} = 0.408 n_i n_j (a_i + a_j)^3 G \qquad 3.10$$

For inertial subrange i.e., $(a_i + a_j) > > \eta$

$$N_{ij} = 2.152 n_i n_j (a_i + a_j)^{7/3} \varepsilon^{1/3} \qquad 3.11$$

For the collision sphere smaller than the microscale, the equation was similar in the form to Saffman and Turner's equation, except their constant was about one third of the Saffman and Turner's constant. For collision sphere larger than the microscale their expression differed from that of Saffman and Turner. Also their expression did not have any viscosity term implying that for the particles larger than microscale, the collision frequency is independent of viscosity.

All the above mentioned turbulent flocculation models differ a bit from the original Smoluchowski model in the sense that these models estimates the number of collisions in a suspension at the beginning of flocculation where Smoluchowski's model expresses the rate of change of some intermediate size particles after some progression of flocculation. Thus the second term on the right hand side in Smoluchowski's model is absent in these turbulent models.

Delichatsios and Probstein (1975) also compared theoretical flocculation rates for monodispersed and polydispersed suspensions with the same floc volumes, and showed that the polydisperseness results in a decrease in the flocculation rate. These authors did not include the differential sedimentation in polydispersed suspension which may question the validity of their results.

By investigating the difference in treatment plant efficiency between monodispersed and polydispersed systems with the same floc volume, Lawler et al.

(1980) concluded that the process performance was worse for the homogeneous suspension than for the suspension with a broad particle size distribution. They performed a simulation type model assuming additivity of Brownian and shear flocculation.

Hudson (1965) derived a model relating total particle reduction and floc volume as follows:

$$n_T/n_o = e^{-VGt\phi/\pi} \qquad 3.12$$

V = volume of floc per unit volume of water

ϕ = sticking factor

n_o= suspended particle number originally present

n_T= free or unflocculated particle number at time "t".

This model was developed based on Camp and Stein's work (1943) with the assumption that the diameter of the flocs is so large that the primary particle diameter can be safely ignored in the mathematical analysis, i.e., $d_{floc} \rangle\rangle d_{primary}$ so $d_{floc} + d_{primary} = d_{floc}$. Argaman and Kaufman (1968 and 1970) also adopted the above mentioned assumption in deriving their flocculation model including breakup (will be discussed later).

The above equation is similar to the integral form of Equation 3.7 with a sticking factor ϕ and a volume fraction $V=4\pi a^3 n_T/3$ inserted into it before integration. The above form also shows that the rate of entrapment of suspended particles in flocs is depended upon the volume of the floc, not on the number or size of the particles. This assumption of very large floc diameter compared to the primary particle appears to produce good agreement with experimental results for flocculation in the "sweep floc" region. In this

region, large metal hydroxide precipitates form early in the flocculation process. However, for flocculation in A/D region, the fundamental assumptions upon which this model is based are violated for a significant length of time during the progress of flocculation. For the early portion of the flocculation process, the number concentration of larger floc is too small to have an impact on flocculation kinetics.

3.4.4. Differential settling

Flocculation also occurs when faster settling particles overtake slower settling particles. Assuming linear particle motion up to contact with another particle and that Stoke's law applies in settling of particles, the collision frequency for spherical particles of equal density can be given by (Gregory, 1989)

$$N_{ij}= (2\pi g/9\mu)(\rho_s- \rho)(a_i+ a_j)^3(a_i- a_j)n_i n_j \qquad 3.13$$

where the collision kernel can be given as

$K_{ij}=(2\pi g/9\mu)(\rho_s- \rho)(a_i+ a_j)^3(a_i- a_j)$

g = acceleration due to gravity

ρ_s and ρ = density of the particles and the fluid respectively.

This mechanism can be very important in promoting flocculation when particles are fairly large and dense.

3.4.5. Comparison of different flocculation models

It is useful to compare different flocculation models. In the most simple way, the kernel for different flocculation models of early stage flocculation can be given as

(Gregory, 1989):

Perikinetic (Brownian Motion) : $\beta_{ij(Br)} = (2KT/3\mu)(a_i + a_j)^2/a_i a_j$

Orthokinetic (Fluid shear) : $\beta_{ij(Sh)} = (4/3)G(a_i + a_j)^3$

Differential settling : $\beta_{ij(DS)} = (2\pi g/9\mu)(\rho_s - \rho)(a_i + a_j)^3(a_i - a_j)$.

At the early stages of flocculation, very few k-fold (i+j) particles are present, so that the second term on the right hand side of both Perikinetic and Orthokinetic models can be dropped. **Figures 3.9a** and **3.9b** (Han and Lawler, 1992) shows the relative importance of different flocculation mechanisms for different initial particle size on the initial rate of flocculation. **Figure 3.9a** was drawn using the above expressions of kernel for different mechanisms based on one particle of fixed size and computing the various rate constants as a function of the size of the second particle. The fixed particle diameter was taken as 2 μm and the diameter of the second particle varied from 0.1 to 100 μm. The fluid is assumed to be water at 20°C and the specific gravity of the particle is taken as 2.65. For the Orthokinetic case, a shear rate of 32 s^{-1} has been assumed.

In deriving the flocculation models in **Figure 3.9a**, it has been assumed that the particles follow a rectilinear path (straight line) while approaching each other before collision. But, the actual path of particle motion is curvilinear and requires trajectory analysis due to following reasons (Han and Lawler, 1992):

> First, water between the particles must move out of the way; this water movement influences particle, and considerations of this phenomena are termed hydrodynamic interactions. These interactions tend to prevent particle collisions. Second, van der Waals attractive forces exist between any two particles and become significant at small separation distances; these forces tend to promote particle collisions. Third, if the particles have charged surfaces, a diffuse layer of ions rich in those with the charge opposite to that of the surfaces is induced in

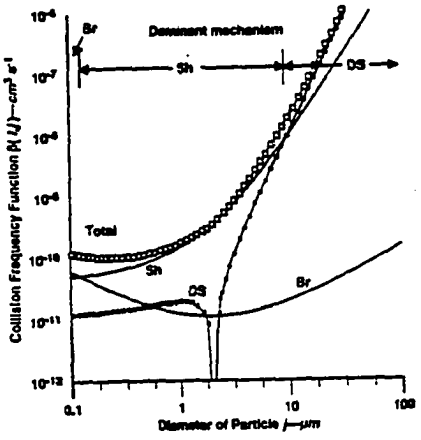

(a)

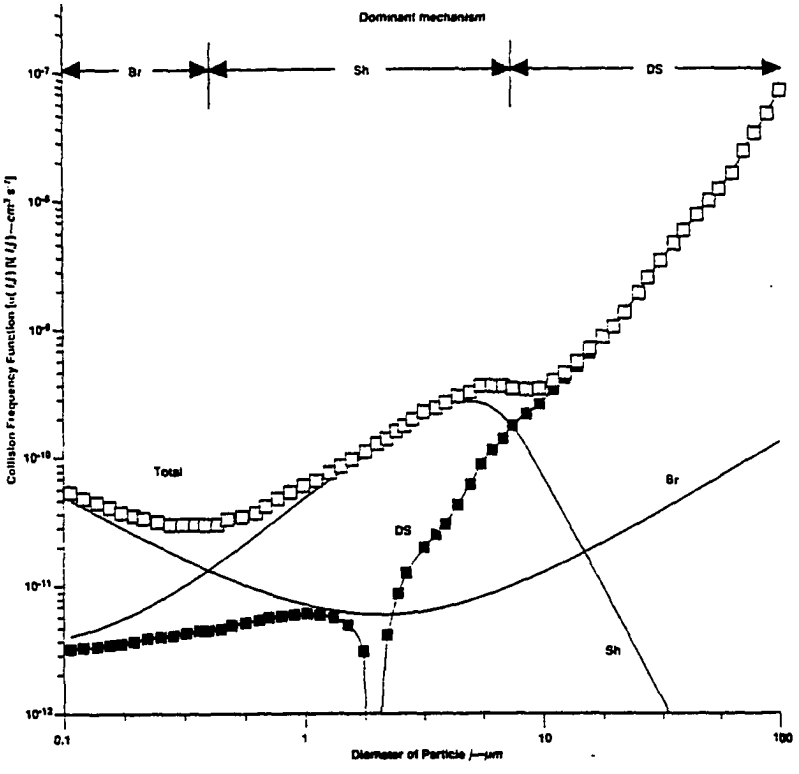

(b)

Figure 3.9a. Collision frequency functions in a) rectilinear model and b) curvilinear model (DS-differential sedimentation, Sh-fluid shear, Br-Brownianmotion; d_i - 2 μm; ρ_p -2.65 gm/cm^3; T-20° C; G-32 s^{-1}) (Han and Lawler, 1992)

> the fluid surrounding each particle. The resulting electric fields of two approaching particles of similar charge cause an electrostatic repulsion and thereby tend to inhibit particle collisions. (p. 82)

Considering the above factors Han and Lawler (1992) proposed that the above collision kernels need to be multiplied by a parameter called the collision frequency factor, α_{ij} , which has a value always less than unity in a curvilinear flow. For rectilinear flow the value is 1. Han and Lawler (1992) proposed the following expressions of α_{ij} for those three collision mechanisms:

1. Perikinetic : $\alpha_{ij(Br)} = a + b\lambda + c\lambda^2 + d\lambda^3$
2. Orthokinetic : $\alpha_{ij(Sh)} = 8(10^{a + b\lambda + c\lambda + d\lambda})/(1+\lambda)^3$
3. Differential sedimentation : $\alpha_{ij\ (DS)} = 10^{a + b\lambda + c\lambda + d\lambda}$

Where λ is the size ratio of small particle to larger particle ($0 < \lambda < 1$) and a, b, c, and d are constants which depend on various factors in different collision mechanisms. In perikinetic mechanism, the constants change with either particle diameter. In orthokinetic mechanism the constants are dependent on Hamakar constant (A), fluid viscosity (μ), rms velocity gradient (G), and diameter of the larger particle. In differential settling the constants depend on Hamaker constant, diameter of large particle, and both particle and fluid density. Using the above correction factors, Han and Lawler (1992) modified **Figure 3.9a** to obtain **Figure 3.9b**. The total collision kernel was calculated as follows:

$$\beta = \beta_{ij(Br)}\alpha_{ij(Br)} + \beta_{ij(Sh)}\alpha_{ij(Sh)} + \beta_{ij(DS)}\alpha_{ij(DS)}$$

When **Figures 3.9a and 3.9b** are compared, the following phenomena are

observed (Han and Lawler, 1992):

1. The shapes of the curves for Brownian motion and differential settling in the curvilinear case are similar to those in the rectilinear case, but the collision frequencies in the curvilinear model are dramatically reduced in magnitude.

2. The above phenomenon is also observed in collisions for fluid shear for particles smaller than the constant size (2 μm), but the two models yield dramatically different results when the second particle is substantially larger than the fixed size (2 μm) particle. As the larger particle increases in size, the collision frequency reaches a maximum and then is reduced in curvilinear case, where as, it increases gradually in the rectilinear case.

3. The regions of dominance for Brownian motion and differential settling are significantly expanded in **Figure 3.9b** compared to those in **Figure 3.9a**, but the region in which fluid shear is dominant is reduced.

3.4.6. Floc strength and break-up

Floc break-up usually occurs in orthokinetic flocculation due to application of fluid shear to increase the collision rate. This follows the "hierarchical" nature of flocculation in which small flocs, composed of primary particles, are distinguished from "aggregates" of these flocs. Only "aggregates" are considered to break under shear, giving smaller "flocs" which are more resistant to break-up. Under given shear conditions, it is generally found that flocs grow only to a certain limiting size, beyond which breakage to smaller units occurs (Tambo and Hozumi, 1979). Camp (1955)

stated: "There is a limiting size corresponding to each value of the mean velocity gradient, G; and the size is greater, the smaller the velocity gradient" (p. 14). Ives and Bhole (1973) stated that other researchers such as Ritchie (1956), Michaels and Bolger, (1962a and b), Argaman and Kaufman (1970) and Lavankar and Gemmell (1968) observed the same fact. So the results of the above practical experiences and the laboratory investigations have proved one fact beyond a doubt, that the maximum limiting size of the floc changes inversely with respect to velocity gradient and this remains one of the most effective empirical indications of floc strength.

Hanson (1989) cited Hinze's (1955) work which dealt with the fundamental mechanisms involved in the splitting of a liquid droplet in a dispersion process as follows:

> Three types of deformation mechanisms proposed by Hinze are as follows: (1) lenticular, (2) cigar-shaped and (3) bulgy deformation. In lenticular deformation the droplet is flattened forming the shape of a contact lens. The break-up depends on the magnitude and duration of force applied to the drop. If the magnitude and duration are sufficient, the drop forms a torus which then breaks into many small drops. Cigar-shaped deformation forms a prolate ellipsoid, then a long cylinder thread, and finally the structure breaks up into droplets. When the surface of the droplet is deformed locally, due to pressure differences at the interface, the deformation is called bulgy deformation. Bulges and protuberances occur, and parts of the drop finally separate. In droplet break-up, the effect of surface tension is important. If the deformation is not too large, the surface tension restores the drop to its original spherical shape; but this mechanism is not ubiquitous in a floc. So Hinze's work should be viewed critically in case of floc break-up. But his work is important in the sense, that it provides the basis for much of the work that followed. His work, somewhat similar in floc deformation,is that the dominant mechanism in droplet break-up in a turbulent flow field is droplet size dependent. For droplets equal to and larger than Kolmogorov microscale, the dynamic pressure forces of the turbulent motion are the cause for droplet break-up. For droplets smaller than microscale, the viscous stress will be the dominant break-up mechanism, which is true for floc break-up too. But this last idea was not explicitly stated by Hinze. (p. 216)

Several researchers, later on, tried to investigate the break-up mechanism of clay flocs. Michaels and Bolger (1962b) worked with kaolinite suspensions, and found that floc yield stress was a function of solids concentration. In their study they found a direct relationship (one increases as the other increases) between yield stress and the square of solids concentration below 5% solid concentration by weight. For higher solids concentration this relationship was even more dramatic.

The strength of kaolinite floc with alum was measured by Hannah, Cohen, and Robeck (1967a) in a sweep floc region (pH=7.6 and alum dose=15 mg/l). They performed the floc strength test with three clay concentrations; 5, 15, and 50 mg/l. They used distilled water buffered with 50 mg/l sodium bicarbonate for making suspensions and used a G value of 50 s^{-1} for flocculation speed. The floc strength was measured by passing the flocculated suspension through the Coulter counter orifice and counting the number and size of the particles at the outlet. The results showed that both the modal and maximum floc size increased with the increase of clay concentration. But they observed the opposite relationship between floc size and alum dose for a constant clay concentration. Three alum dosages were used; 5, 15, and 25 mg/l. They found that largest number of large and sturdy flocs were formed for 5 mg/l dose (the lowest alum to solid ratio that was tested). But the flocculation rate was very slow. A similar trend was also seen with pH variation (tests were done at 7.2, 7.6, and 8.1). The flocs grown at 7.2 were the strongest, but the slowest to grow; but they did not mention anything about the size at different pH levels.

Tambo and Hozumi (1979) observed a direct relationship between floc size and

pH over a pH range 6.5 to 8.0 in a clay-alum floc system. They also found a linear relationship with negative slope between the log of maximum floc diameter and the log of energy dissipation over that pH range. The ALT ratio (mg Al/mg clay) seemed to influence the maximum size only at pH 6.5 (**Figure 3.10**). At all the pH levels, the maximum floc size was close to or below Kolmogorov microscale indicating that the particle break-up occurred due to viscous forces.

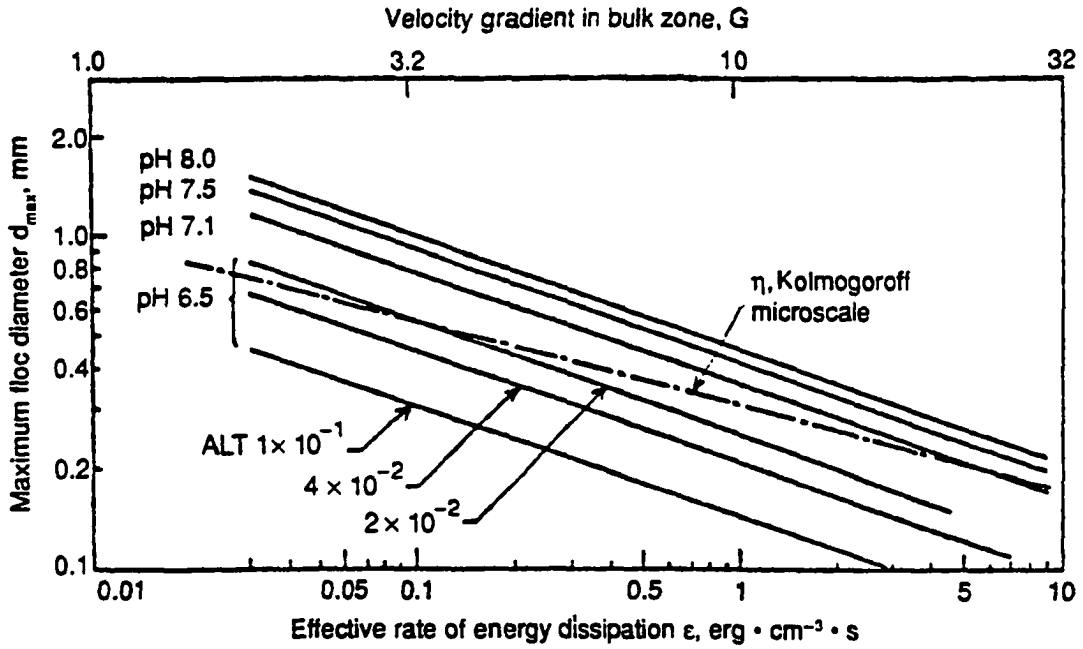

Figure 3.10. Relationship between maximum floc diameter and the effective rate of energy dissipation of clay-aluminum flocs (Tambo and Hozumi, 1979b)

A very useful study was performed by Glasgow and Hsu (1984) using kaolinite clay and a polyacrylamide. The system was first flocculated at G=53 s^{-1} for 20 minutes and then the suspension was subjected to much higher G value, 224 s^{-1} for 3 minutes with the intention for floc break-up. They observed that this hike in mixing intensity did not increase the number of primary particles, but caused a decrease in number of large flocs. So they concluded that the floc has a multi-level structure, and rather than being broken down to primary particles it is being reduced to first or second level aggregates.

Working with alum-kaolinite system, Francois and van Haute (1983) clearly determined the levels of floc structure. They determined that the floc had a four level structure. The structure consisted of primary particles, flocculi (small floc), flocs (made of aggregate flocculi), and floc aggregates. Each level above the primary particles is a little bit weaker. With the increasing mixing intensity in the reactor, the flocculated material will continue to break until a floc structure is reached which has sufficient strength to stand the stress.

Tambo and Watanabe (1979a) derived an expression relating terminal settling velocity to floc density as follows:

$$U = [(4g/3)(R_e/45)\{(\rho_f-\rho_w)/\rho_w\}d_f]^{1/2} = (g/34\mu)(\rho_f-\rho_w)d_f^2 \qquad 3.14$$

U = terminal settling velocity (cm s^{-1})

g = gravitational acceleration (cm s^{-2})

R_e = Reynold's number = $\rho_w U d_f/\mu$

ρ_f and ρ_w = Density of floc and water respectively (gm cm^{-3})

d_f = floc diameter (cm) and μ = dynamic viscosity (gm cm^{-1} s^{-1})

The above expression was developed simply by putting $C_D=45/R_e$ in the settling velocity expression for discrete particle where C_D is the drag coefficient. The above value of C_D corresponds to sphericity (ψ) of 0.8 near Reynold's number 1 (**Figure 3.11**). The sphericity of ordinary floc was assumed to be around 0.8 based on photograph of flocs and on several sphericity data in literature. The authors have defined the floc effective density as $\rho_e = (\rho_f - \rho_w)$ (buoyant density of floc) and plotted this effective density against floc diameter under varying conditions of pH, stirring speed, alkalinity etc.

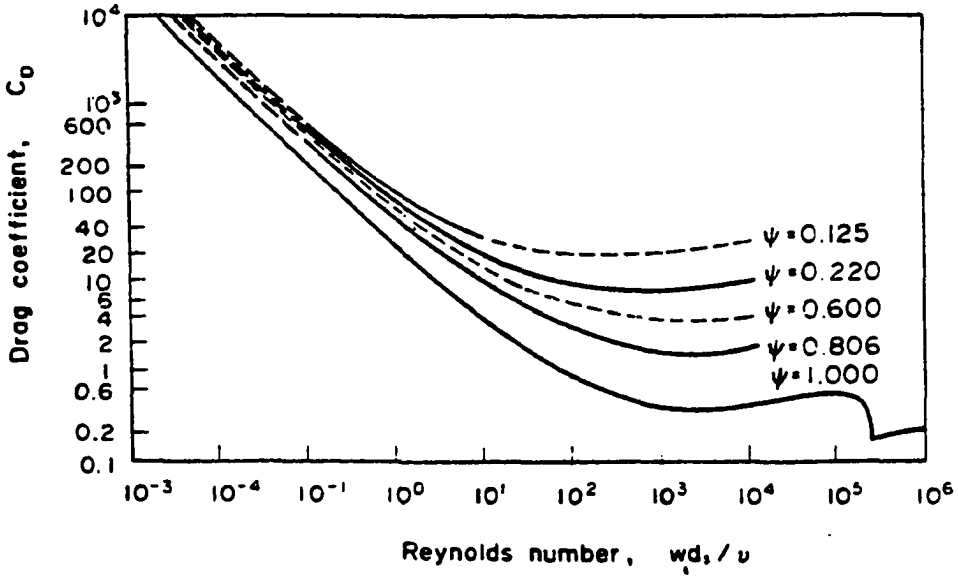

Figure 3.11. Relationship between Reynolds number and drag coefficient (Tambo and Watanabe, 1979a)

When they plotted floc effective density versus floc diameter in a log-log paper they found a linear relationship with a negative slope under all experimental conditions. From their experimental results they found that effective density of floc is not much influenced by agitation intensity between 40 to 80 rpm (no energy input information was provided) and concluded that with more intense agitation, smaller flocs are produced which are inherently denser (higher ρ_f). It appears from their result that the smaller flocs have less number of water molecules in their structure than the larger flocs. The effective density (which can also be considered as buoyant density) is the same for both large and small flocs. They also found that at the fixed floc size, the floc density increases as the ALT ratio decreases and that the effect of raw water alkalinity on the floc density is negligible in the alkalinity range of usual surface waters (50 to 200 mg/l as $CaCO_3$).

Based on the theoretical considerations on turbulent flow field, Tomi and Bagster (1977) noted that floc rupture by instantaneous pressure difference on opposite sides of the floc is only theoretically valid for floc in the size range where inertial effects dominate, i.e., for flocs larger than kolmogorov microscale. But viscous effects are significant for smaller flocs and local velocity gradient at the floc surface may break up these flocs.

Based on the difference of the dynamic force exerted on the unit area of opposites sites of a floc, Tambo and Hozumi (1979) developed the expression for maximum floc size in two size ranges as follows:

$$d_{max} = K^{*}\varepsilon_o^{-1/(1+Kp)} \quad \text{for} \quad d_f \rangle\rangle \lambda_o$$

$$d_{max} = K\varepsilon^{-3/\{2(3+Kp)\}} \text{ for } d_f \ll \lambda_o \qquad 3.15$$

where $K^* = k^*(\sigma/\rho_w)^{3/\{2(1+Kp)\}}$, $K = k(\sigma\mu/\rho_w)^{3/\{2(3+Kp)\}}$ and $\lambda_o = (\upsilon^3\rho_w/\varepsilon_o)^{1/4}$

ε_o = the mean rate of energy dissipation per unit volume in a basin (erg $cm^{-3}s^{-1}$), σ = binding strength (gm cm^{-1} s^{-2}),

μ = the absolute viscosity (gm $cm^{-1}s^{-1}$),

υ = the kinematic viscosity (cm^2s^{-1}), k and k^* = constants,

ρ_w = density of water (gm cm^{-3}) and

Kp = floc density function (dimensionless)

λ_o is the Kolmogorov microscale, where the energy input in the expression was per unit volume rather than per unit mass. Under a given coagulation condition Kp and σ are constant. Tambo and Watanabe (1979a) reported the value of Kp in the range of 1.0 to 1.5 and the expressions for d_{max} become:

$$d_{max} = K^*\varepsilon_o^{-(0.5 \text{ to } 0.4)} \quad \text{for} \quad d_f \gg \lambda_o$$

$$d_{max} = K\varepsilon_o^{-(0.38 \text{ to } 0.33)} \quad \text{for} \quad d_f \ll \lambda_o$$

Since under the turbulent flow conditions, the effective energy dissipation rate is proportional to the third power of the rotational speed of the flocculator blade, N (rps), and to the second power of G then the expression for d_{max} in terms of N and G is as follows:

$$d_{max} \propto N^{-(1.5 \text{ to } 1.2)} \propto G^{-(1.0 \text{ to } 0.8)} \text{ for } d_f \gg \lambda_o$$

$$d_{max} \propto N^{-(1.5 \text{ to } 1.2)} \propto G^{-(0.76 \text{ to } 0.66)} \text{ for } d_f \ll \lambda_o \qquad 3.16$$

Working with alum and clay, Boadway (1978) noted that if the strength of the bonds between particle is independent of size, and the equilibrium floc size is shear rate

dependent, then there must be structural differences in the larger flocs. Their photographic evidence shows that the larger the floc, the more tenuous the bonds become, with evidence of weak spots.

3.4.7. Models including break-up

Introducing several hypotheses in von Smoluchowski's theory to make it applicable to the turbulent regime, Argaman and Kaufman (1970) proposed the following expression for flocculation kinetics:

$$dn_1/dt = - 4\pi\alpha\, K_S R_F^3\, n_F n_1\, K_P G + B\,(R_F/R_1)^2\, n_F\, K_P G \qquad 3.17$$

They also defined the following terms

$K_F = 3\alpha\phi$ = flocculation constant

ϕ = floc volume fraction = $(4/3)\,\pi\, n_F\, R_F^3$

R_F = radius of floc = $K_1/(K_P G)$

R_1= radius of primary particles

B = floc break-up constant and a characteristic of a particular kind of floc

α = fraction of collisions producing aggregation, called collision efficiency

K_P= paddle performance coefficient

K_S= proportionality coefficient expressing the effect of turbulence energy spectrum on the diffusion coefficient.

K_1= constant relating the average floc diameter to the rms velocity gradient in the tank.

n_F = number of flocs per unit volume at time t

$$K_B = (3B\phi K_P^2)/(4\pi n_o R_1^2 K_1) \qquad 3.18$$

Using the above defined terms in Equation 3.17 Ayesa et al. (1991) rewrote the model in the following form:

$$dn_1/dt = -K_A n_1 G + K_B n_o G^2 \qquad 3.19$$

n_1= number of primary particles per unit volume at time t

n_o= number of primary particles per unit volume at time t = 0

K_A= floc aggregation coefficient (dimensionless)

K_B= floc break-up coefficient (s)

K_A indicates the ease of aggregation and has the following expression

$$K_A = K_F K_P K_S$$

K_B indicates the floc fragility under hydraulic shear and has the expression as given in Equation 3.18.

Bratby et al. (1977) integrated Equation 3.19 for the time interval that a stirred batch reactor experiment lasts, t, as follows:

$$n_1/n_o = (K_B/K_A)G + \text{Exp}\,(-K_A Gt)\{1-(K_B/K_A)G\} \qquad 3.20$$

In the above expression G, t, and n_1/n_o are known experimental data, while K_B and K_A are unknown parameters to be determined by an adjustment procedure. Argaman and Kaufman (1970) and later, Odegaard (1985) published the values for K_A and K_B for the usual range of G and t in wastewater treatment as follows:

$K_A = 3.0 \times 10^{-4}$ (dimensionless) and $K_B = 5.0 \times 10^{-6}$ s for

$5s^{-1} < G < 50s^{-1}$ and $0 < t < 2000s$

Ayesa et al. (1991) developed a computer based numerical technique to estimate the values for K_A and K_B. When they generated ideal data using Equation 3.20 with the above reported values of K_A and K_B, they observed high percentage of error with respect to real experimental data as shown in **Table 3.4**. When they fitted Equation 3.20 to real data, they found different values of K_A and K_B than the above suggested values, which are also shown in **Table 3.4**. Based on the results of fitting Equation 3.20 to sets of real experimental data, they also found an inverse dependence of K_B/K_A on G. They ascribed this dependence of K_B/K_A on G exclusively to the break-up coefficient K_B based on several considerations found in various literature sources, especially the observation of an inverse relation of maximum stable floc diameter with G. They used their rigorous numerical technique to compare three models with three different expressions of K_B. These three expression of K_B are as follows:

Model 1: K_B constant

Model 2: $K_B = K_1 \ln G + K_2$ suggested by Bratby (1980)

Model 3: $K_B = K_1 G^n + K_2$ suggested by Ayesa et al. (1991)

Table 3.4. Results of application of the numerical method by Ayesa et al. (1991) to three groups of data.

Data	K_A	$K_B(s)$	Error (%)
Turbidity (Bratby, 1977)	2.10×10^{-4}	3.35×10^{-7}	23.60
Color (Bratby, 1980)	4.05×10^{-4}	7.93×10^{-6}	21.48
Color (Margeli and Garcia-Heras, 1987)	2.83×10^{-4}	1.96×10^{-6}	29.61

The results of adjustment with the above models are shown in **Table 3.5**. From these results it is clear that introduction of this type of dependence between breakup coefficient (K_B) on G in the expression describing the flocculation process (Equation 3.20) leads to an appreciable decrease in the final relative error. In all the cases model 3 performed best. The significant improvement was observed when model 3 was applied to color data of Margeli and Garcia-Heras (1987) with regard to model 2, but the marginal improvement in the relative error when Bratby's data were adjusted suggest that the way in which K_B changes with G is greatly dependent on the kind and concentration of the flocs generated in each particular process (Ayesa et al. 1991). But Ayesa et al. (1991) did not give any explanation about the negative exponent (n = -2.1) that was obtained when they fit their model to the color data of Margeli and Garcia-Heras (1987). The inverse relation between K_B and G in this case raises the question about the applicability of their model.

Letterman et al. (1979) used the kinetic model by Parker et al. (1970) in determining the effect of bicarbonate ion concentration on flocculation with aluminum

Table 3.5. Results of adjustments of real experimental data using the three models of flocculation (Ayesa et al., 1991)

Data	Model	$K_A \times 10^4$	K_B (s)	K_1	K_2	n	Error (%)
Turbidity	1	2.15	3.35×10^{-7}				23.60
(Bratby,	2	2.87		-1.87×10^{-7}	1.37×10^{-6}		14.81
1980)	3	2.99		-2.05×10^{-15}	5.37×10^{-7}	3.4	13.68
Color	1	4.05	7.93×10^{-6}				21.48
(Bratby,	2	4.15		-4.42×10^{-6}	2.16×10^{-5}		14.66
1980)	3	4.01		-2.53×10^{-11}	1.01×10^{-5}	3.5	13.87
Color	1	2.83	1.96×10^{-6}				29.61
(Margeli &	2	3.62		-2.13×10^{-6}	1.05×10^{-5}		26.48
Garcia-Heras,	3	6.11		2.25×10^{-6}	3.92×10^{-6}	-2.1	20.19
1987)							

sulfate. The model is given as

$$dN/dt = -k_1N + k_2 \qquad 3.21$$

in which N is the concentration of unflocculated primary particles; k_1 is an agglomeration rate constant; and k_2 is a floc break-up or erosion rate constant. If the residual turbidity n is assumed to be proportional to N, then Equation 3.21 can be integrated from time, t = 0 and residual turbidity = n_o to time, t = t and residual turbidity = n to yield

$$\ln[(n-k_2/k_1)/(n_o-k_2/k_1)] = -k_1t \qquad 3.22$$

Plot of n vs. t yields a concave curve where n decreases with length of flocculation period and gradually approaches asymptote $n = k_2/k_1$ (**Figure 3.12**). The quantity k_2/k_1 is obtained by plotting n vs. t and then locating the asymptote. The magnitude of k_1 is determined by measuring the slope of the best-fit line obtained when the left hand side of Equation 3.22 is plotted against the length of flocculation period (t). The magnitude of k_2 is determined by multiplying the quantity k_2/k_1 by k_1. They performed a series of jar tests in determining the residual turbidity for various periods of flocculation followed by a 30 minute sedimentation.

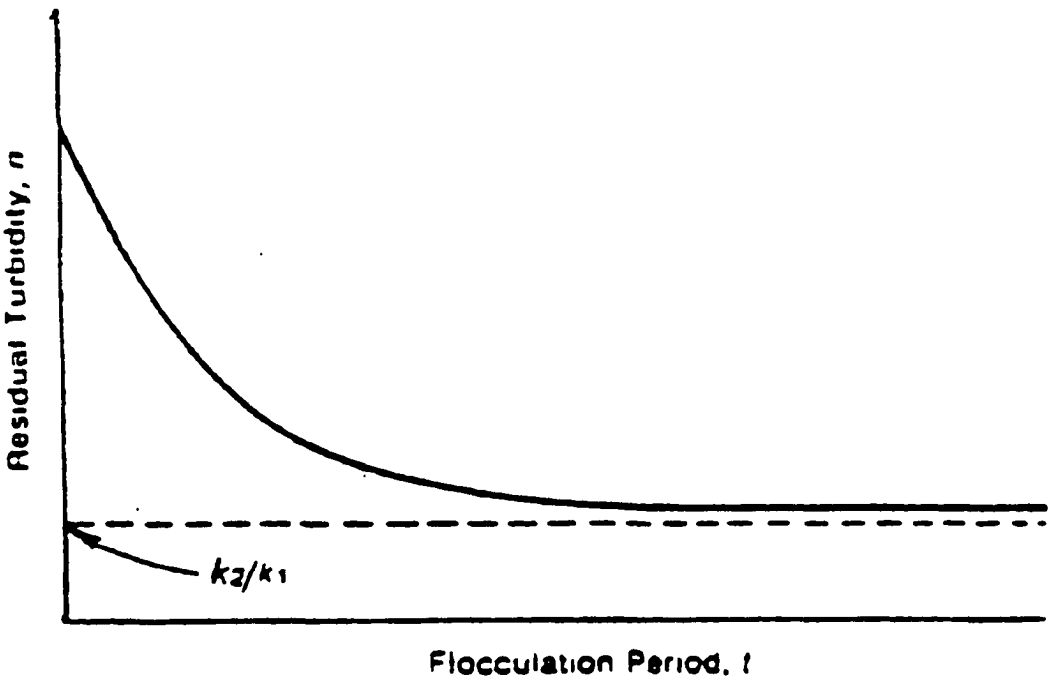

Figure 3.12. Residual turbidity versus flocculation period (Letterman et al., 1979)

3.5 Coagulants

We have seen previously that coagulants or flocculating agents are added to a particular suspension to destabilize the lyophobic colloids from their kinetic stability. There are two major categories of primary coagulants being used in the water treatment industry: metal salts, and organic polymers. The metal salts of aluminum and iron, particularly alum [$Al_2(SO_4)_3.18H_2O$], are the most widely used coagulants (Sricharaenchaikit and Letterman, 1987). They are relatively inexpensive and can be easily prepared by the operators. Recently synthetic organic cationic polymers are gaining popularity because of their high efficiency in turbidity removal. But they are expensive and we do not know a great deal about them. Since all the work in this project was performed with metal salts the discussion will be confined to metal salt coagulants only.

Metal salt coagulants are available in a number of chemical forms, all of which are salts of aluminum or iron. The following are the metal coagulants that are commonly used (Hanson, 1989):

- alum or aluminum sulfate [$Al_2(SO_4)_3.nH_2O$]
- polyaluminum chloride [$Al(OH)_xCl_y$]
- ferric sulfate [$Fe_2(SO_4)_3$] and ferrous sulfate [$Fe(SO_4)$]
- ferric chloride [$FeCl_3$]
- ferric nitrate [$Fe(NO_3)_3.9H_2O$] for research studies only

Many researchers, in discussing metal salts, deal with aluminum and iron salts

simultaneously because of their identical solution chemistry. Since the work reported herein was done with alum and ferric nitrate, the same format will be followed with the distinct differences noted where necessary. The general mechanisms of particle destabilization are the same for both metals. But because of differences in reaction kinetics, solution speciation, and electron structure, these two types of metal salts may respond differently in the destabilization process, especially due to temperature changes.

When a metal salt is added to clay suspension, the solution chemistry of metal ions is the prime concern and the speciation of the ion influences the destabilization of colloidal particles. The influence of the associated anion is often negligible, especially when the anions have single charge (e.g., Cl^-, NO_3^- etc.). Sulfate (SO_4^{2-}) ions influence the destabilization nature of primary particles when they are present in appreciable concentration, but their influence at the low concentration contributed by the alum dose is not significant and can be negligible. So mainly the discussion will emphasize Al(III) and Fe(III) ions. The scope of discussion about the chemistry of these two coagulants is enormous, but the discussion will be limited mainly to that part which is important for coagulation-flocculation process.

When a metal salt coagulant is added to a colloidal suspension, different monomeric and polymeric species are formed at different pH and concentrations, following a sequence of steps called hydrolysis, which represents the progressive replacement of water molecules in the hydration shell of metal ion by hydroxyl groups. Taking aluminum as an example, the following sequence of hydrolysis steps can be

written for increasing pH (Gregory, 1989):

$$Al^{3+} \rightarrow Al(OH)^{2+} \rightarrow Al(OH)_3 \rightarrow Al(OH)_4^-$$

Hydrolysis involves a loss of positive charge until the uncharged hydroxide is formed (at sufficient concentration). This is practically insoluble in water and so forms a precipitate, which is initially amorphous, but may slowly form crystalline gibbsite.

Baes and Mesmer (1976) provided an excellent discussion of the hydrolysis of cations, the soluble species formed as a consequence of hydrolysis and the importance of soluble metal hydrolysis products as follows:

> Most cations from one or more hydrolysis products. ... Because of the number of diversity of the hydroxide complexes which can be formed in solution, the resulting chemical behavior of a given metal can be a complicated function of pH and concentration and ... if the identity and stability of the hydrolysis products are not known ... quite unpredictable.
>
> The determination of the identity of dissolved hydrolysis products has proven to be a difficult and challenging task primarily for two reasons:
>
> 1. The hydrolysis complexes formed are often polynuclear, that is, they contain more than one metal ion. It can be readily perceived that this can result in the formation of a far greater variety of species than would be the case if only mononuclear species were formed during the hydrolysis of a cation. Less obvious, perhaps, is that this can also allow more hydrolysis products to be present simultaneously in appreciable amounts. The diversity of possible species and the number which can appear more or less simultaneously greatly complicate the problem of identifying them and determining their stability.
> 2. The range of pH over which the formation of soluble hydrolysis products can be studied is often limited by the precipitation of the hydroxide or the oxide of the metal cation. While the range of conditions studied usually can be extended to quite supersaturated solutions, the limitations imposed by hydrolytic precipitation are often severe, rendering the problem of characterizing the hydrolysis products formed in solution even more difficult than would otherwise be the case.

> Soluble hydrolysis products are specially important in systems where the cation concentrations are relatively low. The formulas and charges of the hydrolysis products formed in such systems can control such important aspects of chemical behavior as
>
> 1. adsorption of the dissolved metal on the surface of mineral and soil particles,
> 2. the tendency of the metal species to coagulate colloidal particles,
> 3. the solubility of the hydroxide or oxide of the metal,
> 4. the oxidizability or reducibility of the metal to another valence state .... (pp. 2-3)

Figure 3.13 (Amirtharajah and O'Melia, 1990) is the solubility diagram for aluminum in water which was drawn using thermodynamic data based on **Table 3.6.** **Figure 3.13a** shows the different hydrolysis products at equilibrium with crystalline aluminum hydroxide [gibbsite, $Al(OH)_{3(c)}$, log K=-33.5, i.e. solubility product is $10^{-33.5}$) and Figure 3.13b shows the equilibrium diagram of different hydrolysis products with amorphous $Al(OH)_{3(am)}$ (logK=-31.5). In this diagram three polymeric species [$Al_2(OH)_2^{4+}$, $Al_3(OH)_4^{5+}$ and $Al_{13}O_4(OH)_{24}^{7+}$] and five monomers [Al^{3+}, $Al(OH)^{2+}$, $Al(OH)_2^+$, $Al(OH)_3$, and $Al(OH)_4^-$] are in equilibrium with freshly precipitated $Al(OH)_{3(am)}$. Lines for the $Al(OH)_2^+$ and $Al(OH)_3$ species are dashed to indicate that their concentrations are uncertain because of doubtful thermodynamic data. In both the diagrams, at alkaline pH values (pH $\rangle$ 8.0), the principal soluble species present at equilibrium is the monomeric anion $Al(OH)_4^-$ (Amirtharajah and O'Melia, 1990).

Figures 3.14 and 3.15 (Baes and Mesmer, 1976) demonstrate the complexity of the metal speciation with regard to both concentration and pH. The dashed lines in the figures represent the percent of the metal present as a specific species and the number label in the lines (x,y) indicates, the number of aluminum ions in the species (x), and

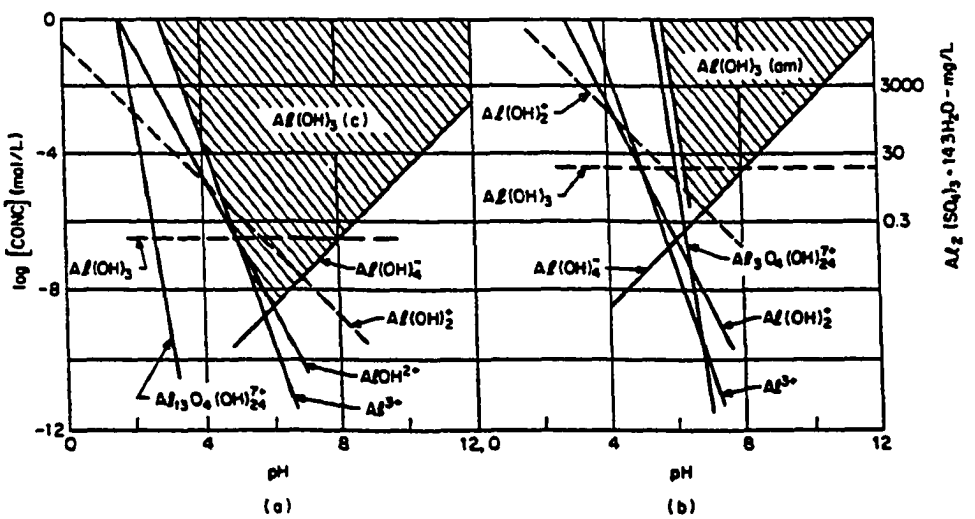

Figure 3.13. Solubility of aluminum at equilibrium with (a) gibbsite and (b) amorphous $Al(OH)_3$. Thermodynamic data were taken from Table 3.6 (Amirtharajah and O'Melia, 1990)

Table 3.6. Silicate, Iron (III), and Aluminum Equilibria (Amirtharajah and O'Melia, 1990)

Reaction	log K(25°C)
1. $SiO_2(am) + 2H_2O = Si(OH)_4$	−2.7
2. $Si(OH)_4 = SiO(OH)_3^- + H^+$	−9.46
3. $SiO(OH)_3^- = SiO_2(OH)_2^- + H^+$	−12.56
4. $4Si(OH)_4 = Si_4O_6(OH)_6^- + 2H^+ + 4H_2O$	−12.57
5. $Fe^{3+} + H_2O = FeOH^{2+} + H^+$	−2.2
6. $FeOH^{2+} + H_2O = Fe(OH)_2^+ + H^+$	−3.5
7. $Fe(OH)_2^+ + H_2O = Fe(OH)_3 + H^+$	−6
8. $Fe(OH)_3 + H_2O = Fe(OH)_4^- + H^+$	−10
9. $2Fe^{3+} + 2H_2O = Fe_2(OH)_2^{4+} + 2H^+$	−2.9
10. $3Fe^{3+} + 4H_2O = Fe_3(OH)_4^{5+} + 4H^+$	−6.3
11. $Fe(OH)_3(am) = Fe^{3+} + 3OH^-$	−38.7 (estimated)
12. $\alpha - FeO(OH) + H_2O = Fe^{3+} + 3OH^-$	−41.7
13. $Al^{3+} + H_2O = AlOH^{2+} + H^+$	−4.97
14. $AlOH^{2+} + H_2O = Al(OH)_2 + H^+$	−4.3
15. $Al(OH)_2^+ + H_2O = Al(OH)_3 + H^+$	−5.7
16. $Al(OH)_3 + H_2O = Al(OH)_4^- + H^+$	−8.0
17. $2Al^{3+} + 2H_2O = Al_2(OH)_2^{4+} + 2H^+$	−7.7
18. $3Al^{3+} + 4H_2O = Al_3(OH)_4^{5+} + 4H^+$	−13.94
19. $13Al^{3+} + 28H_2O = Al_{13}O_4(OH)_{24}^{7+} + 32H^+$	−98.73
20. $Al(OH)_3(am) = Al^{3+} + 3OH^-$	−31.5
21. $Al(OH)_3(c) = Al^{3+} + 3OH^-$	−33.5

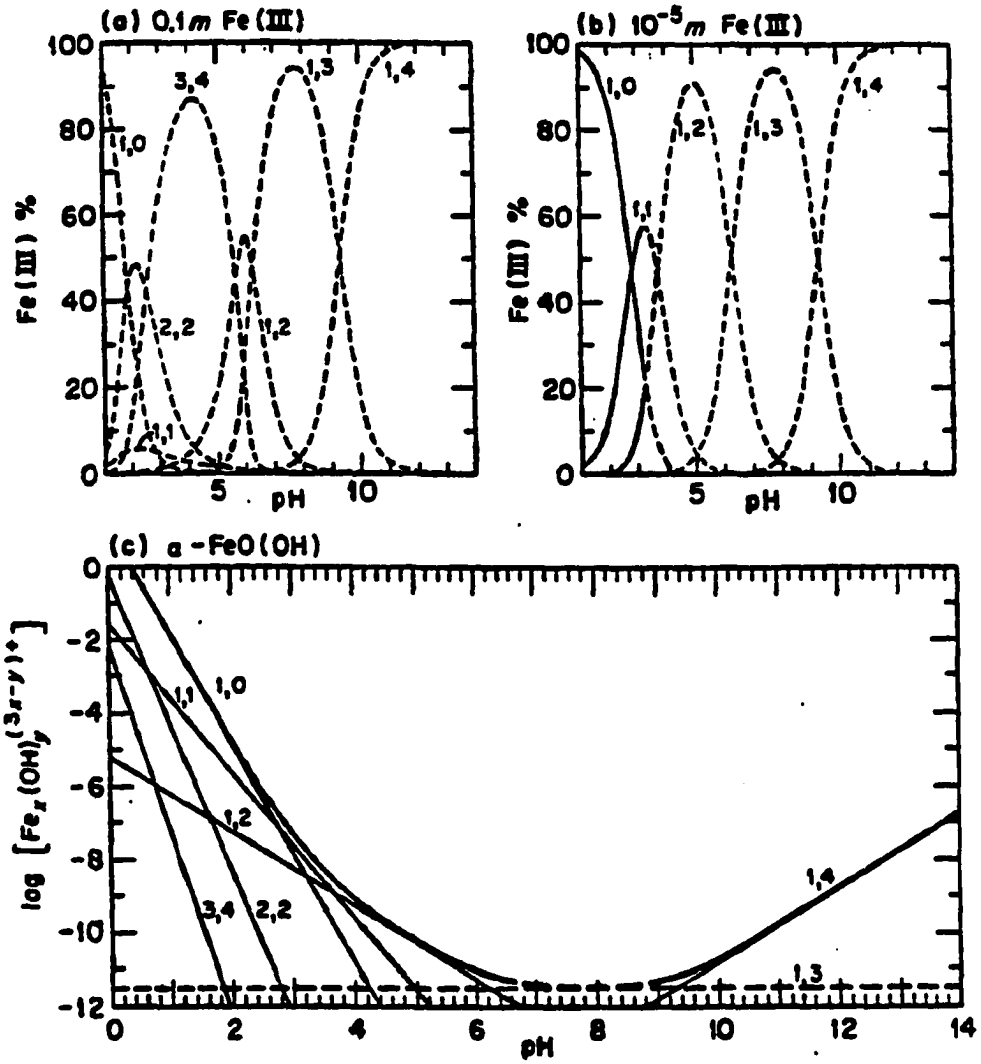

Figure 3.14. Distribution of hydrolysis products (x,y) at I = 1M and 25°C in (a) 0.1M Fe(III), (b) 10^{-5}M Fe(III), and (c) solutions saturated with α-FeO(OH). The dashed curves in (a) and (b) denote regions supersatuarted with respect to α-FeO(OH); the heavy curve in c is total concentration of Fe(III) (Baes and Mesmer, 1976)

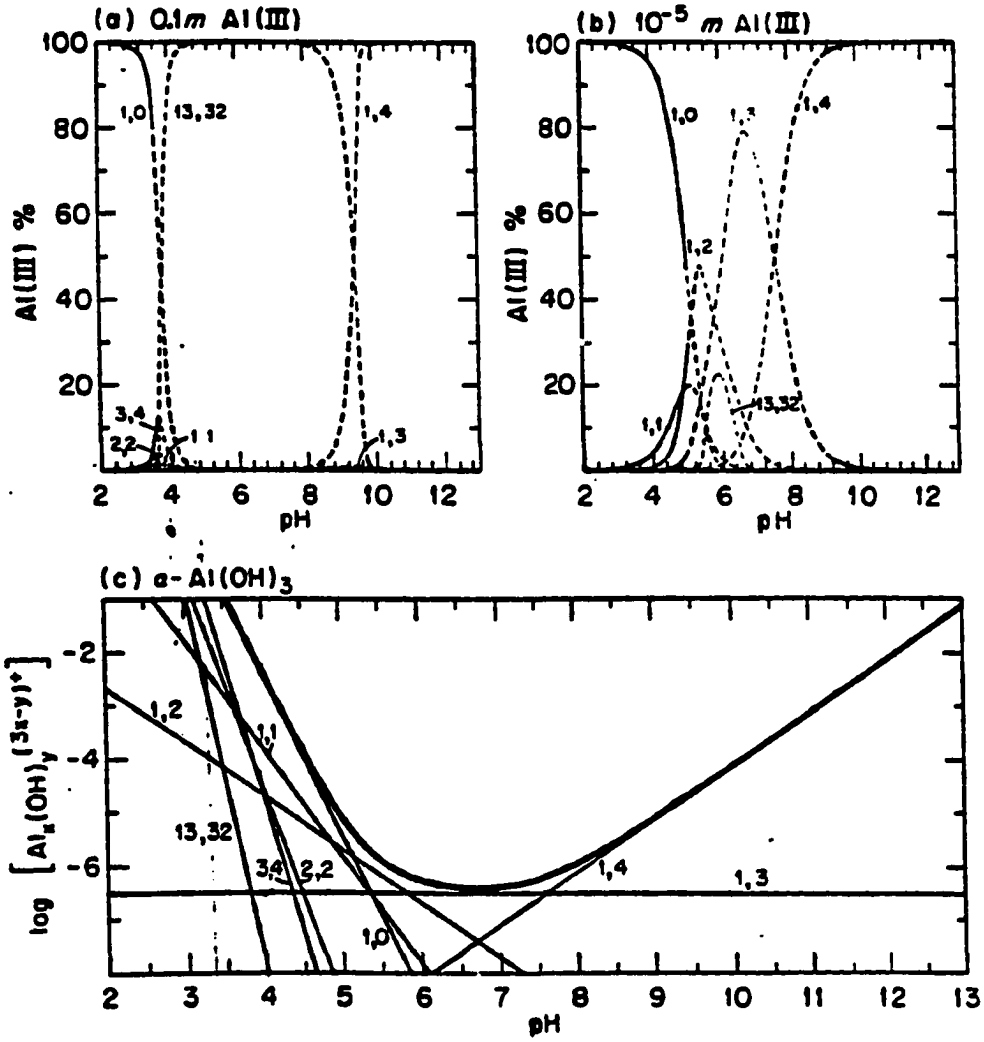

Figure 3.15. Distribution of hydrolysis products (x,y) at I = 1M and 25°C in (a) 0.1M Al(III), (b) 10^{-5}M Al(III), and (c) solutions saturated with α-$Al(OH)_3$. The dashed curves in (a) and (b) denote regions supersatuarted with respect to α-$Al(OH)_3$; the heavy curve in c is total concentration of Al(III) (Baes and Mesmer, 1976)

the number of hydroxide ions present in the species (y). Similar information on the pH dependence of aluminum speciation is shown in **Figure 3.16** (Hayden and Rubin, 1974). Moreover, the concentration dependence of metal speciation for aluminum sulfate, ferric chloride and ferric sulfate solutions is shown in **Figures 3.17, 3.18, and 3.19** respectively. From all the figures and discussion stated above, it is clear that distribution of different species in aqueous solution of metal coagulants is dependent on the concentration of metal coagulants and the solution pH.

From the above figures we can also visualize the distinct differences between alum and ferric coagulants. From **Figure 3.14c** we can see that the minimum solubility of iron(III) is $10^{-11.5}$ and that occurs at pH between 7 and 9. On the other hand least solubility of alum is $10^{-6.5}$M and that occurs at pH between 6 and 7. Also from **Figure 3.20** (Burgess, 1988) we see (from the right hand axis) that the mean residence time for a water molecule in the primary hydration shell for iron(III) is in the micro second (μsec) range, while for aluminum(III), it is in the second range. Based on these time-scales it appears reasonable that the iron(III) will come to equilibrium much quicker than aluminum(III) (Hanson, 1989).

Figures 3.21 and 3.22 represent turbidity coagulation diagram for aluminum and iron respectively (Amirtharajah and Mills, 1982 and Johnson and Amirtharajah, 1983). These figures were developed based on the data obtained from major coagulation results of several researchers. The coagulation data were plotted on a single diagram of log [Metal species] in moles per liter versus the pH of the mixed solution, and superimposed on the thermodynamic solubility diagram that formed the framework for

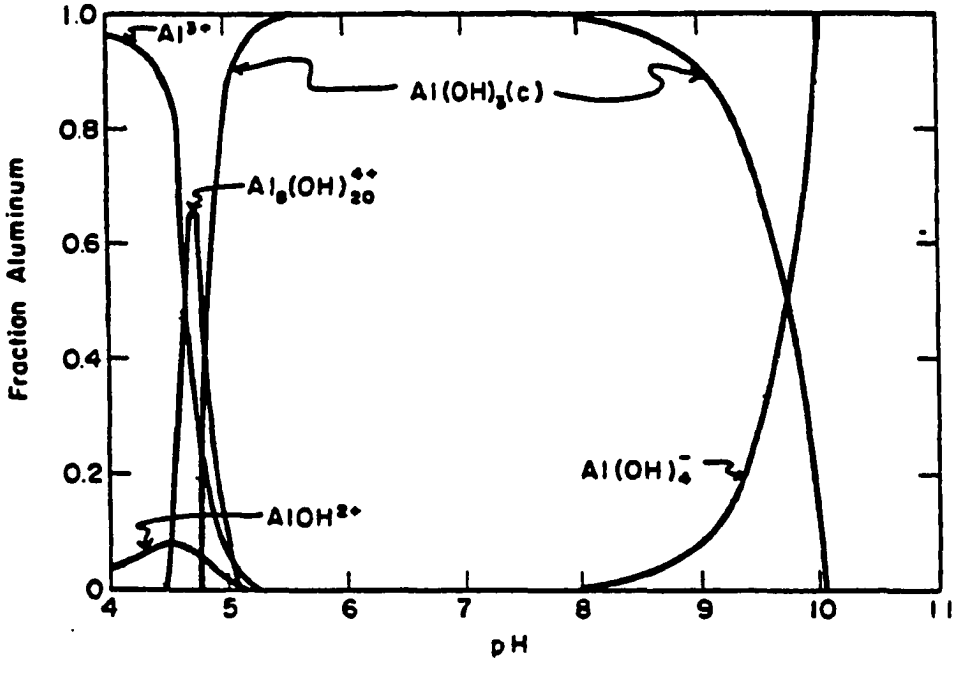

Figure 3.16. Distribution of 5.0×10^{-4} M hydrolyzed aluminum (III) as a function of pH (Hayden and Rubin, 1974)

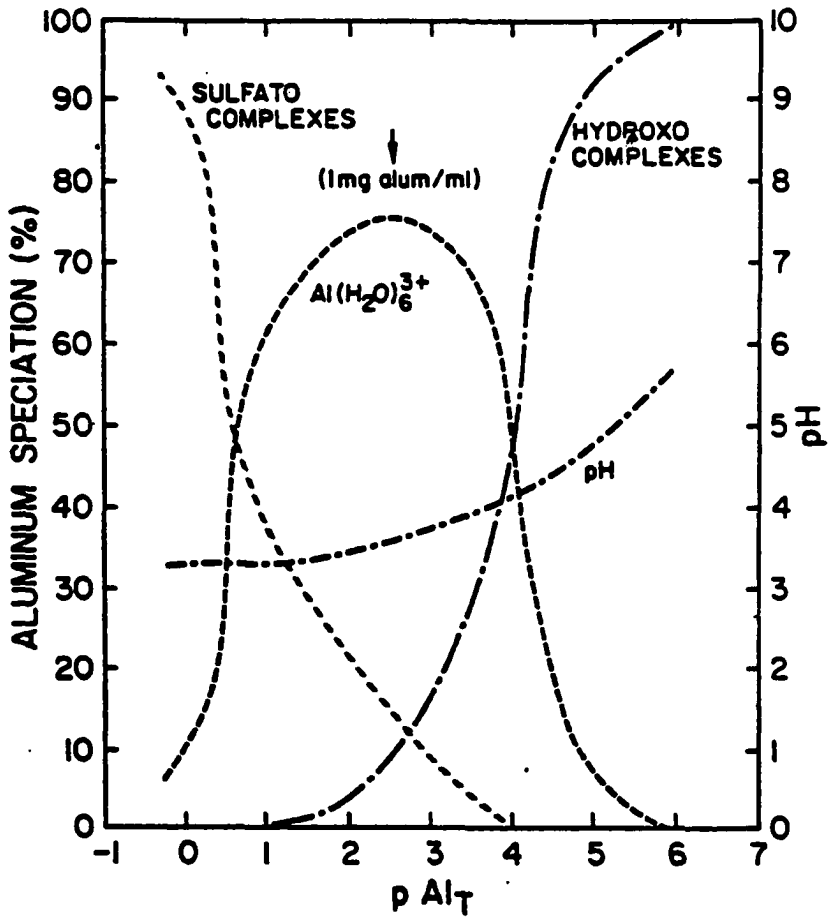

Figure 3.17. Species composition of aluminum sulfate solutions (O'Melia, 1978)

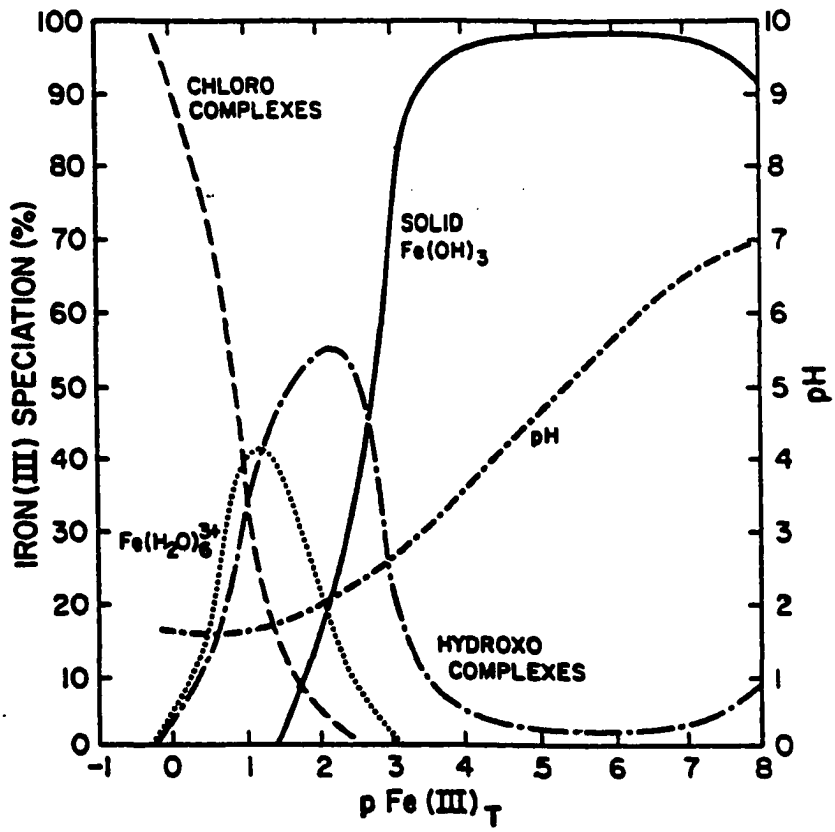

Figure 3.18. Species composition of ferric chloride solutions (O'Melia, 1978)

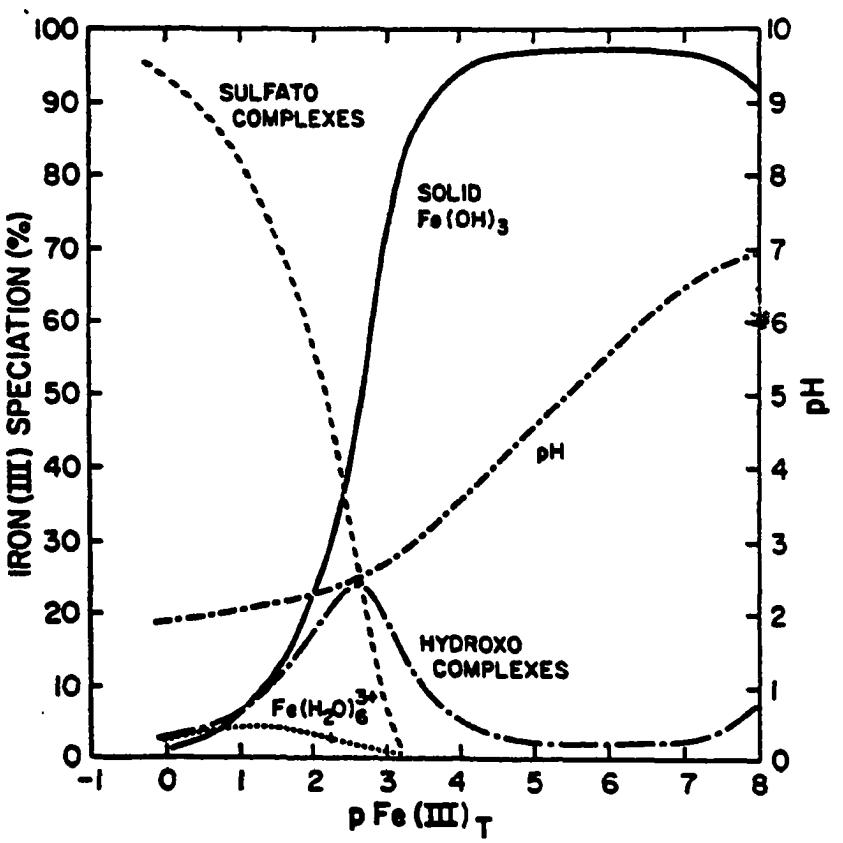

Figure 3.19. Species composition of ferric sulfate solutions (O'Melia, 1978)

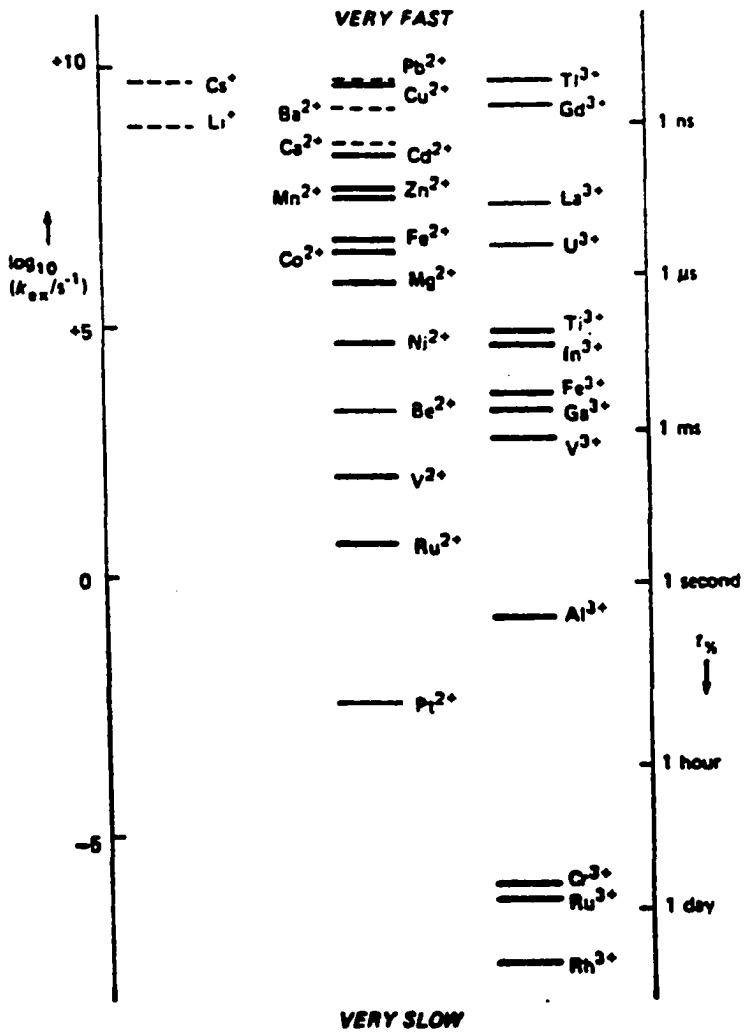

Figure 3.20. Rate constants for water exchange, and mean residence times for water molecules in primary hydration shells, for 2+ and 3+ metal ions, at 298°K. Octahedral species are indicated by thick lines, non-octahedral species by thin lines. Dashed lines denote estimates arrived from rate constants for complex formation (Burgess, 1988)

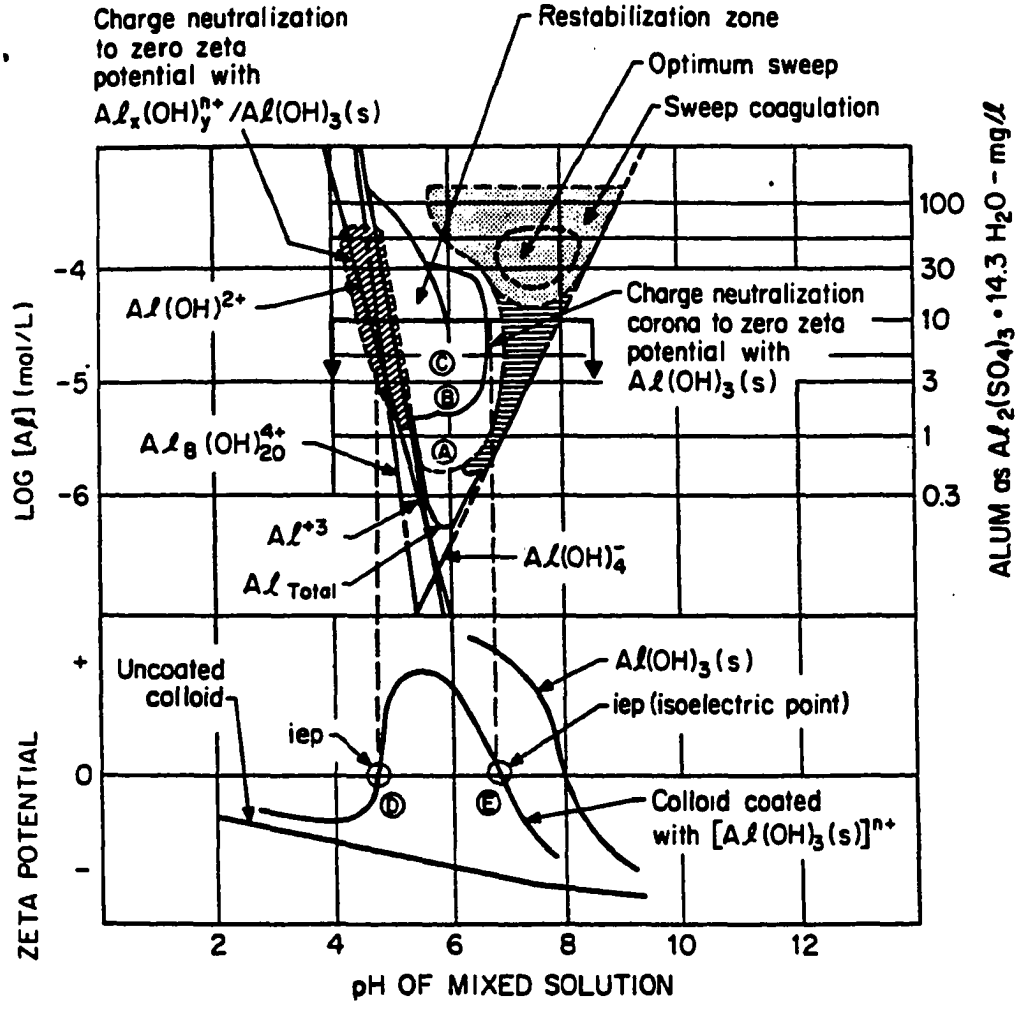

Figure 3.21. The alum coagulation diagram and its relationship to zeta potential (Amirtharajah and O'Melia, 1990)

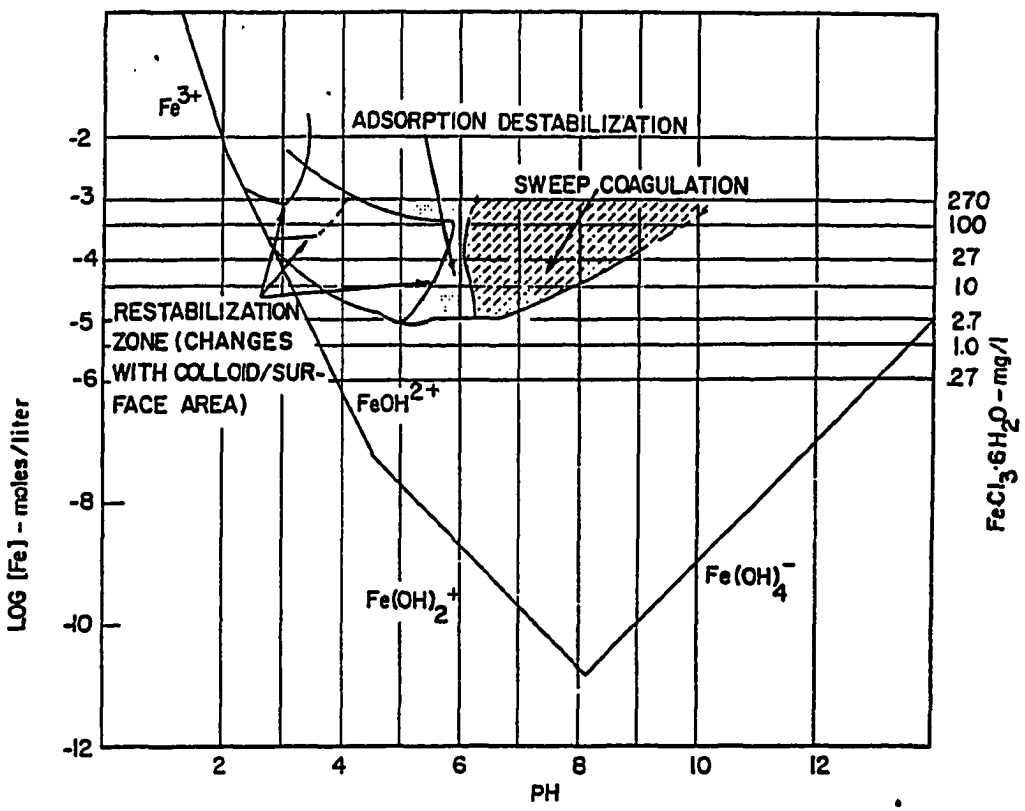

Figure 3.22. The ferric chloride coagulation diagram for turbidity removal (Johnson and Amirtharajah, 1983)

the coagulation results. The interaction between the colloid and aluminum hydroxide and the relationship of the zeta potential to the coagulation diagram are shown in the lower portion of the alum coagulation diagram.

In the next few paragraphs an attempt will be made to explore the coagulation diagrams in understanding the coagulation process, i.e., how the system will react at different coagulant dosages and pH conditions. For the sake of simplicity alum will be considered in detail and difference between aluminum and ferric salts will be illustrated in some aspects.

Coagulation occurs when soluble hydrolysis species (e.g., $AlOH^{2+}$) or solid aluminum hydroxide (which can itself be charged because of surface complexes) interact with colloidal particles (Amirtharajah and O'Melia, 1990). From the lower portion of **Figure 3.21** it can be seen that the surface charge of the solid $Al(OH)_3$ is pH dependent. At low pH it is very positive, and as the pH increases, the charge decreases. At the isoelectric point (iep) or at the point of zero charge (pzc), the surface charge of aluminum hydroxide precipitate is zero. The isoelectric point (iep) for aluminum hydroxide is in the pH range of 7.0 to 9.0, depending on the ions in the solution, especially the anions. **Table 3.7** lists representative values for the pzc of $Al(OH)_3$ and $Fe(OH)_3$ precipitates.

The data shown in **Figure 3.21** were based on the assumption that aluminum hydroxide has a pzc (i.e., isoelectric point) of 8.0. The interaction of the positively charged colloids produces two points of zero zeta potential at pH values of 4.8 and 6.8 at points D and E of **Figure 3.21**. Favorable coagulation can be expected at both these

conditions of pH. Between these two values, the coated colloid is restabilized because of

Table 3.7. Typical pH values resulting in the zero point of charge (zpc) for hydroxide precipitates

Aluminum Hydroxide	Ferric Hydroxide	Source
	6.7	Stumm and Morgan, 1962
	8.0	O'Melia, 1978
	6.8	Hong-Xia and Stumm, 1987a
7.0		Hayden and Rubin, 1974
9.0		Letterman and Vanderbrook, 1983
8.0		Amirtharajah, 1984 and Hall, 1965

excess adsorption of positively charged species. **Figure 3.23** (Hall, 1965) and **Figure 3.24** (Hong-Xia and Stumm, 1987b) illustrate the zeta potential-pH relationship for alum and iron coagulants respectively.

Hanson (1989) presented two examples in order to demonstrate:

- the complexity of the metal salt system,
- the difference between the adsorption/destabilization (A/D) and the sweep floc mechanisms, and
- the importance of coagulant precipitation kinetics in determining the flocculation mode.

The first example was for a high dose of alum (30mg/l as alum). This is an optimal sweep floc dosage. The second example was for a low dose (5 mg/l as alum), typical of

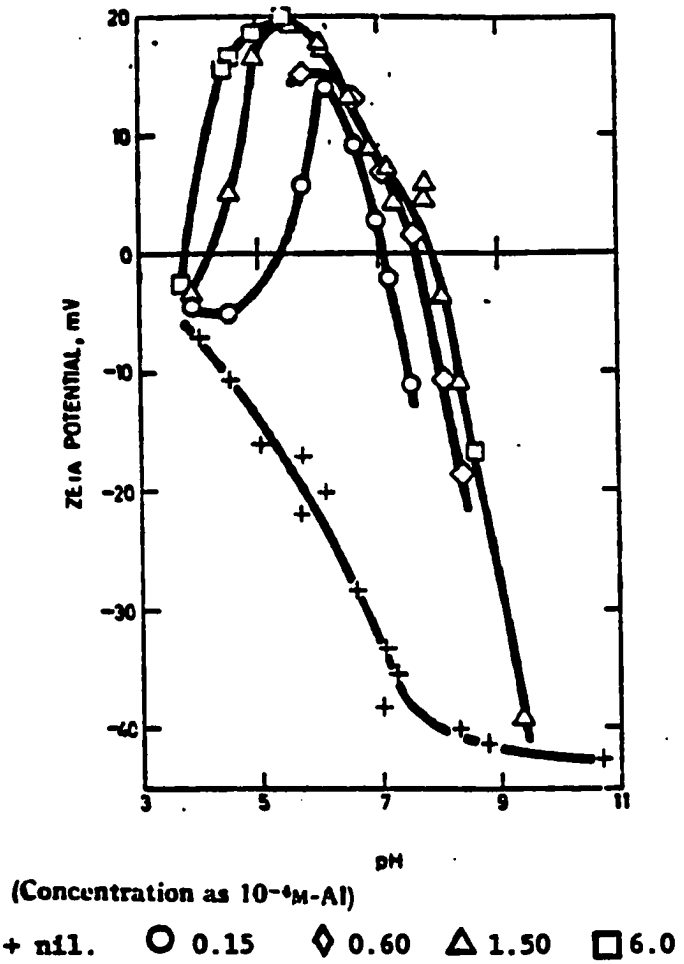

Figure 3.23. Zeta potential of kaolinite in aluminum sulfate solutions (Hall, 1965)

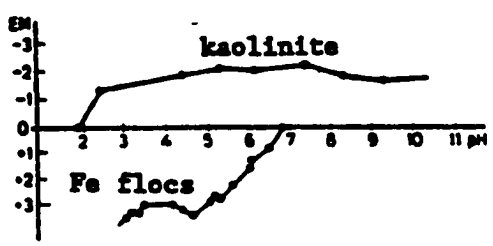

Figure 3.24. Micrelectrophoresis mobility of kaolinite and Fe flocs (Hong-Xia and Stumm, 1987b)

A/D coagulation.

Considering a dose of 30 mg/l and refering to **Figure 3.21** Hanson (1989) stated as follows:

> Remember, these conditions represent the final coagulant concentration and pH in the reactor. As we start at pH of 4.0 we are outside the precipitation boundary in a region where all of the aluminum exists in a soluble Al^{3+} state. At a pH of 4.5 two things happen:
>
> - the solubility limit is reached,
> - the soluble species are dominated by the hydrolyzed polymeric aluminum species [$Al_x(OH)_y^{n+}$; $Al_8(OH)_{20}^{4+}$, as seen in **Figure 3.16**].
>
> The hydrolyzed polymeric species actually becomes the dominant species just prior to precipitation, and are only present in the appreciable amounts over a narrow pH range (Hayden and Rubin, 1974). The narrow pH range in which these polymeric species dominate, appears to coincide with the first charge neutralization range in **Figure 3.21**.
>
> Small hydroxy complexes are reasonably soluble and easily adsorbed on to the colloid particles, making these complexes extremely effective coagulants (Eilbeck and Mattock, 1987).
>
> As we continue across the diagram to a pH of 5.0, the hydrolyzed polymeric species disappear, and are replaced by $Al(OH)_3$ as the dominant species. This is the restabilization range. The surface charge of solid $Al(OH)_3$ is pH dependent (Stumm and Morgan, 1981). At low pH it is very positive, and as the pH increases, the charge decreases. At zero point of charge (ZPC), or the isoelectric point, the surface charge of aluminum hydroxide precipitate is zero. ... In the restabilization area the surface charge on the precipitate is so high that the particles with adsorbed precipitate experience charge reversal, and become positively charged. It is noted that if the primary particle concentration is high enough, the restabilization zone may disappear entirely, because there will not be enough precipitate to reverse the original charge.
>
> As the pH is raised, the surface charge of aluminum precipitate becomes lower and lower, and somewhere near pH of 6.0, the typical water is once more destabilized and will coagulate. ... Again, note how sensitive the surface chemistry of these hydroxide precipitates is to shifts in pH. At a pH of 6.5 the adsorption/ destabilization mechanism ceases to dominate the flocculation and sweep floc becomes the dominant mode of coagulation. In sweep floc large quantities of aluminum hydroxide precipitate are formed. These precipitates sweep up the particles as they move through the water.
>
> ... When the pH is low enough so that adsorption followed by precipitation on the surface is favored, there will not be sufficient aluminum in solution to form the large quantities of precipitate needed for sweep floc to

> occur. However, as the adsorption step becomes less and less favorable, the soluble aluminum is in solution long enough for the sweep floc to form. Sweep floc dominates from pH of 6.5 to 8.4. At a pH of 8.4 the hydroxide species once more become more soluble. (pp. 117-119)

From **Figure 3.22**, it appears that for a ferric chloride dose of 30 mg/l, the restabilization will prevail over a broad range of pH about 2.8 to 5.6 for low colloid concentration (this range narrows at higher colloid concentration) followed by a much narrower A/D region (pH range is about 5.6 to 6.0). Again a much broader sweep floc region exists beyond pH 6.0 until a pH of about 9.0. A combination of **Figures 3.21 and 3.22** is shown in **Figure 3.25** (Johnson and Amirtharajah, 1983).

Water treatment engineers and researchers are interested in two main mechanisms of flocculation; adsorption/destabilization and sweep floc mechanisms. The interaction between the two mechanisms and the metal salts is shown schematically in **Figure 3.26** (Dentel, 1987). The formation time of different aluminum hydrolysis species is shown in **Table 3.8** (Amirtharajah, 1987) which will help understand the shift from one mechanism to another.

Table 3.8. Formation time of aluminum hydrolysis species (Amirtharajah, 1987)

Hydrolysis species	Time scale (sec)
Al (III) monomers	< 0.1
Al (III) polymers	0.1 to 1
Aluminum hydroxide precipitates	1 to 7

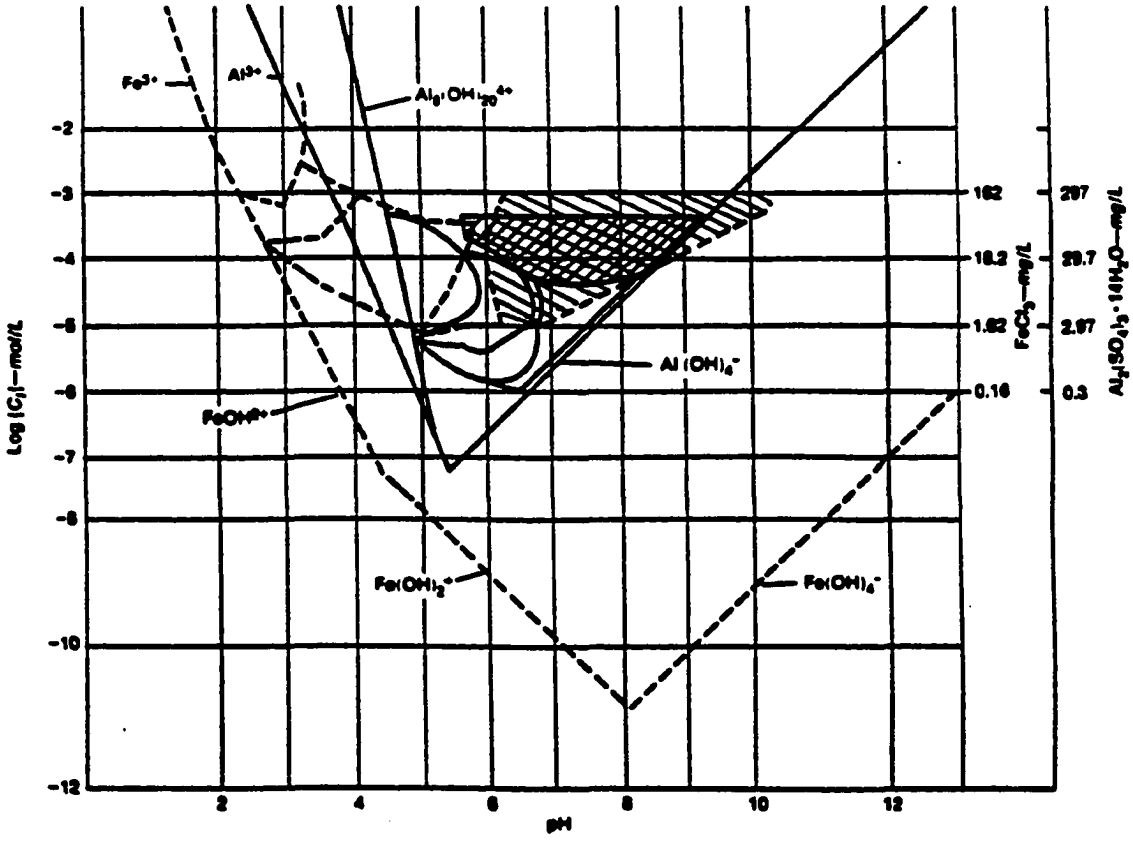

Figure 3.25. Ferric chloride and alum coagulation diagrams [hatched areas represent sweep floc zones for ferric chloride (\\\) and alum (///)] (Johnson and Amirtharajah, 1983)

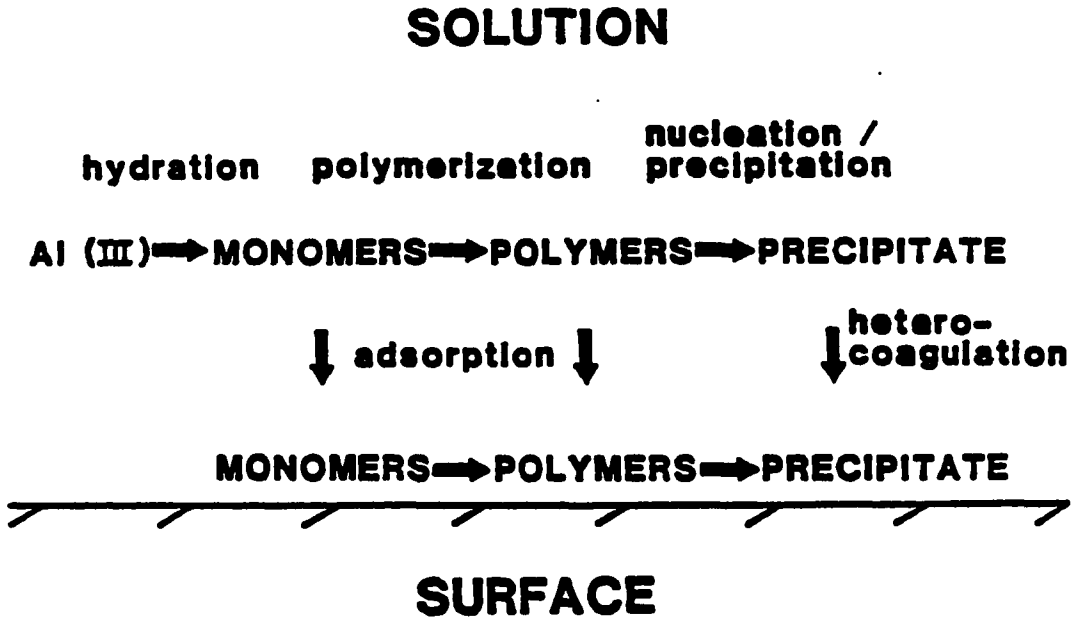

Figure 3.26. Schematic representation of the various pathways followed by aluminum hydroxide species in solution or at a surface in contact with the solution (Dentel, 1987)

All the discussion above was for high coagulant dose, i.e., 30 mg/l. If a low coagulant dose, i.e., 5 mg/l, is considered the first change in alum coagulation diagram is that all of the regions previously described shift to the right. The other change is the disappearance of the sweep floc region. With the low dose of alum the A/D mechanism will be effective, but there is not enough aluminum added to the system to form a good sweep floc even if the pH is favorable (Hanson, 1989). When the ferric chloride coagulation diagram is considered at this dose of 5 mg/l, the first change evident is that both the restabilization and sweep floc regions shrink at low dose whereas the A/D region expands in both the pH directions (← →). Many researchers such as Morris and Knocke (1984) and Dann (1988) have found that sweep floc formed with iron (III) is denser and probably stronger than the floc formed with aluminum (III). So from all the discussions made in this section, it is clear that the hydrolysis reactions, metal hydrolysis product speciation, and the mode of coagulation depend on pH and the concentration of the coagulants.

Bicarbonate ion has been used as a buffer system by several researchers (Letterman et al., 1979; Letterman and Vanderbrook, 1983; Hanson and Cleasby, 1990; Hanson, 1989; Amirtharajah and Mills, 1982 etc.) in coagulation flocculation research. The main purpose of using this ion is to maintain a constant pH during the coagulation flocculation process. Since pH is the one of the parameters that controls the metal hydrolysis product speciation, hydrolysis reaction and the mode of flocculation, the rapid drop in pH with the addition of coagulant might alter the intended mechanism. Letterman and Vanderbrook (1983) showed rather dramatically the importance of pH in

the flocculation process, by flocculating a colloidal suspension at a pH of 6 and 8 with alum. At pH=8, the aluminum concentration required for charge neutralization was almost 10 times greater than that needed at a pH=6.

Hanson (1989) demonstrated the importance of the buffer. He showed that the pH of Ames, IA tap water became 8.0 after it was allowed to stay overnight. When 15 mg/l of alum was added to this unbuffered tap water, the pH dropped form 8.0 to 6.7. Hanson (1989) further indicated that at this dose of 15 mg/l as alum, the shift in pH is likely to move the coagulation mode from the sweep floc region to A/D region and if someone intends to work in A/D region, it is best to control the system pH so that the entire experiment can be done in the A/D region. He also stated that A/D region exists close to a pH of 7 (**Figure 3.21**) which suggests the need of carbonate as the buffer system of choice since its buffer intensity shows a peak (change in pH per unit of strong acid is minimum) between a pH range of 5 to 8. In the pH range of 7 to 8.3 it can be assumed that almost the total carbonate carbon concentration is equal to the bicarbonate ion concentration.

Miller (1925) and Letterman et al. (1979) indicated that addition of a carbonate buffer to the system would not only stabilize the pH, but would broaden the range for good flocculation. Using a method of analysis based on a kinetic model of the flocculation process and series of jar tests, Letterman et al. (1979) showed that an increase in the initial bicarbonate ion concentration increased both the agglomeration and erosion rate constants. Overall performance improved with increasing initial bicarbonate ion concentration. They attributed this effect of bicarbonate ion on

flocculation efficiency to its ability to alter the physico-chemical characteristics of the aluminum hydroxide precipitate. They worked with 50 mg/l kaolin clay suspension which was prepared on the day of experiments at 23°C. They used 1% $Al_2(SO_4)_3.18H_2O$ stock solution for feeding without any dilution. All experiments were performed using 1-L volume of suspension. Two minutes rapid mix was done by a magnetic stirrer followed by variable period of flocculation on a Phipps and Bird jar test apparatus at 40 rpm (corresponds to $G=50s^{-1}$ at 23° C). Residual turbidity was measured after 30 minutes of sedimentation. Dosages used was between 10 to 40 mg/l as alum. No method was employed to control the pH; they recorded the pH (after rapid mixing) and it was variable depending upon the coagulant and buffer concentrations. But in their study they did not report any measurement of zeta potential which raises the question about the mode of flocculation (A/D or sweep floc) for each experiment.

3.6 Turbulence and Mixing

3.6.1. General

Turbulence and mixing are often discussed simultaneously in many literature sources. They are very much interrelated. Both of them are generated or caused by energy input or transfer in the system. In coagulation and flocculation processes both of them are very important to understand. In this section, the interrelation between mixing and turbulence and their importance in flocculation will be discussed. Before entering into the details of turbulence and mixing the complexity of turbulence, its extent and the

tussle among various researchers to explain this phenomenon need to be discussed.

The extent of both turbulence complexity and turbulence literature is next to infinity. It has many questions without answers; it has many surprises. The biggest surprise probably so far is as follows (Gleick, 1987):

> Turbulence was a problem with pedigree. The great physicists all thought about it, formally or informally. A smooth flow breaks up into whorls and eddies. Wild patterns disrupt the boundary between fluid and solid. Energy drains rapidly from large-scale motions to small. Why? ... It seemed almost unknowable. There was a story about the quantum theorist Werner Heisenberg, on his deathbed, declaring that he will have two questions for God: why relativity, and why turbulence. Heisenberg says, *I really think He may have an answer to the first question.* (p. 121)

In the last decade or two there has been a strong tussle between two groups of fluid dynamists based on the opposing approaches used to explain this phenomenon. One set of beliefs is advocated by the followers of the statistical approach. They attempt to explain the dynamics of the flow in terms of the averaged flow characteristics and according to Lesieur (1987), "This community, which has followed the glorious trail of Taylor and Kolmogorov, believes in the phenomenology of cascades and strongly disputes the possibility of any coherence or order associated to turbulence" (p. vii). The other set of beliefs are supported by an increasing number of scientists who identify themselves with the emerging theories, based on the philosophy of order within the chaos. These scientists consider "... turbulence from a purely deterministic point of view, by studying either the behavior of dynamical systems, or the stability of flows in various situations. To this community are also associated the experimentalists who seek to identify coherent structures in shear flows" (p. vii) (Lesieur, 1987).

The above are not the only theories, they were actually preceded by phenomenological theories of turbulence. Some of these phenomenological theories stated by Brodkey (1967) and Bird et al. (1960) are Boussinesque's Eddy viscosity theory, Prandtl's Mixing-length theory, Taylor's Viscosity transport theory, von Karmans's Similarity hypothesis, etc. These theories are semiempirical in nature and tried to achieve an expression for the turbulent momentum flux associated with the fluctuating components of velocity in a turbulent flow field.

Due to limitless complexity in deriving flow equations for turbulent flow and solving them, most of the studies of turbulent flow were empirical or semiempirical, based on many assumptions and numerous experimental results. Those studies, based on many assumptions, were adequate for prediction of the mean velocity profile necessary for solving many practical problems, but could not be much of help in trying to understand the true mechanism of turbulent flow. Uncountable numbers of studies are going on in various fields involving turbulent transport of various quantities (like momentum, mass, heat etc.). All those will not be discussed here; rather a portion will be discussed that will augment the understanding of the impact of turbulence on the flocculation process.

3.6.2. Definition of turbulence

Dictionary meaning of "turbulent" is stormy agitation or erratic in velocity. Hinze (1975) defined turbulent fluid motion as an irregular condition of flow in which the various quantities show a random variation with time and space coordinates, so that

statistically distinct average values can be discerned. He further states that turbulence can be thought of as a superpositioning of ever smaller periodic motions or eddies. Voke and Collins (1983) state: "The turbulent flow of viscous fluid is one of the most complex and beautiful macroscopic phenomena found in nature. It is essentially four dimensional, involving the time dependent interchange of energy and momentum between vortices of different sizes and lifetimes, ..., in three dimensional space" (p. 119).

Despite many debates and complexities in turbulence, it is accepted that most flow must display some salient characteristics before it can be christened as being turbulent. These characteristics include inherent disorder, enhanced mixing, presence of vorticity, and time dependency which distinguish turbulence from wave motion and two dimensional flows (Hinze, 1975; Lesieur, 1987; Panton, 1984; Shapiro, 1961; Stewart, 1969; Tennekes and Lumley, 1972; Gleick, 1987; and Voke and Collins, 1983).

Disorder: A turbulent flow is unpredictable in detail, i.e., the characteristics are irreproducible in its entire detail even if all the experimental conditions are reproduced in exactly the same details. But averages over suitably large intervals of space and time seem to be well-defined and stable. According to Gleick (1987), "It is a mess of disorder at all scales, small eddies within large ones. It is unstable. It is highly dissipative, meaning that turbulence drains energy and creates drag. It is motion turned random" (p. 122).

Figure 3.27 (Amirtharajah and O'Melia, 1990) shows a schematic diagram of a turbulent flow field which consists of the concepts of the intensity of turbulence, the

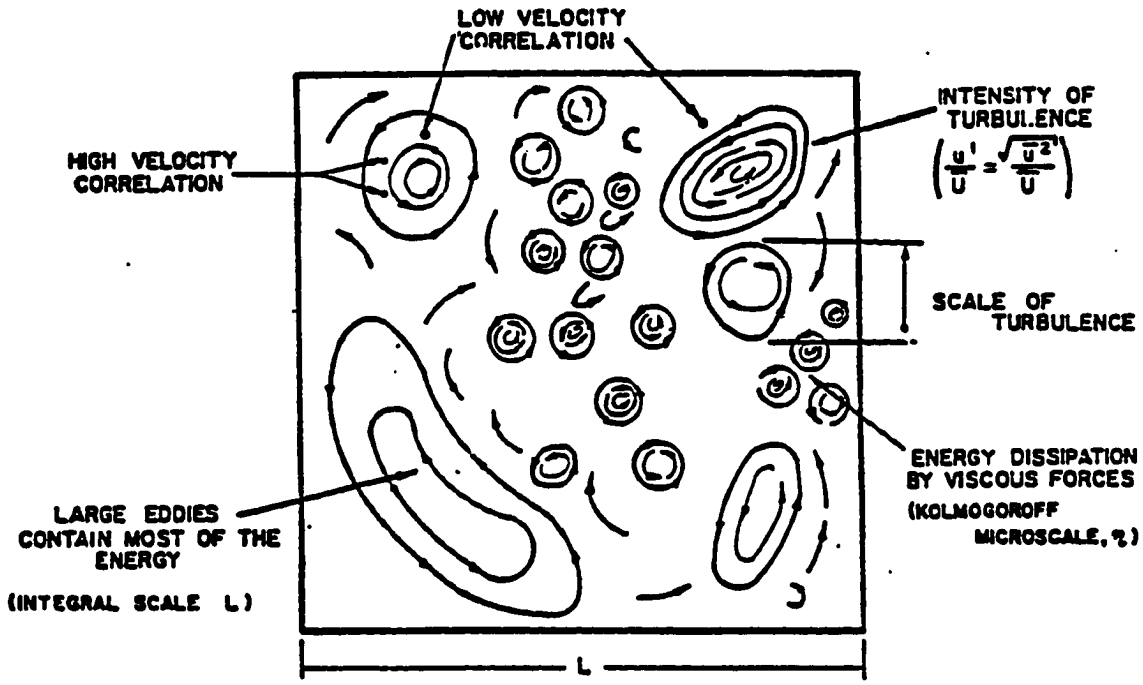

Figure 3.27. Schematic diagram of turbulent flow field (Amirtharajah and O'Melia, 1990)

scale of turbulence, and the correlation functions. The length scale of turbulence can be crudely interpreted as the average size of turbulent eddies or the size of the packet of fluid within which high correlation of fluid velocity exists. As shown in Figure 3.27, very large vortices or large eddies arise from the interaction of the mean flow with the boundary that have macroscale and contain a large fraction of turbulent energy of the system. These large eddies degenerate successively through energy cascade (or transfer) to the smallest eddies where they are dissipated by viscous effects into heat. The terms eddies and vortices are often used interchangeably in the turbulent literature, but vortices would be more appropriate term (Hanson, 1989).

Time dependency: In addition to the variation of velocity with respect to spatial coordinates, if we look microscopically at a point in the turbulent flow field, we will see a fluctuation of velocity with time with respect to an average velocity, $\overline{U}$. This fluctuation of velocity with time is illustrated in **Figure 3.28** (Amirtharajah and O'Melia, 1990) where an instantaneous velocity U at a point in a turbulent flow field can be represented by a time averaged value $\overline{U}$ and a superimposed fluctuating velocity u as: $U = \overline{U} + u$. The summation of the fluctuating velocity component is necessarily zero; but the root mean squared (rms) velocity of fluctuations, $(\overline{u^2})^{1/2}$ represents the variance of the velocity and is called the intensity of turbulence, u' (Amirtharajah and O'Melia, 1990). This intensity is often normalized by the time averaged velocity, $\overline{U}$ as $u'/\overline{U}$ and is called normalized turbulence intensity. The intensity of turbulence increases with the increasing value of $u'/\overline{U}$.

Energy cascade: In a very simple way, turbulence is frequently described as an

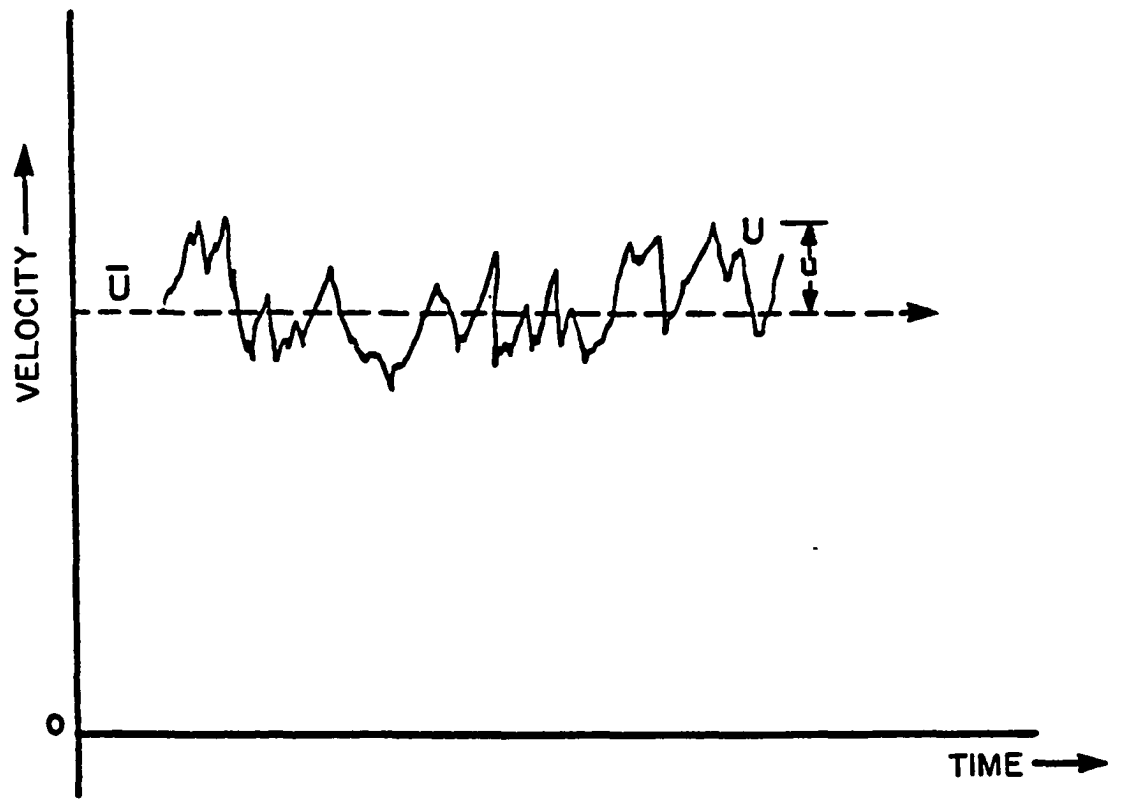

Figure 3.28. The instantaneous and fluctuating velocity in a turbulent flow field (Amirtharajah and O'Melia, 1990)

energy cascade (or eddy cascade); where the energy is put into the system at large length scales. The cascade of energy then takes place predominantly from neighboring eddies to neighboring eddies continuing to smaller and smaller length scales (larger and larger velocity gradients) through the mechanism of vortex stretching until viscosity finally dissipates the energy received by the smaller eddies (Frost and Bitte, 1977; and Voke and Collins, 1983).

The above idea of hierarchy of energy transfer from larger length scales to smaller length scales was the crop of Lewis F. Richardson's fertile brain. Monin and Yoglom (1971) describe the Richardson idea as follows:

> According to his assumption, developed turbulence consists of a hierarchy of 'eddies' (i.e., disturbances or non-homogeneities) of various orders. Here the 'eddies' of a given order arise as a result of the loss of stability of larger 'eddies' of the preceding order, borrowing their energy, and, in their own turn, losing their stability and generating smaller 'eddies' of the following order to which they transmit their energy. Thus arises a peculiar 'cascade process', of breaking down of eddies in which the energy of the overall flow is transmitted to motions of smaller and smaller scale, down to motion of the smallest possible scale, which is stable. To be stable, these extremely small-scale motions must be characterized by a sufficiently small Reynolds number. Thus it follows that viscosity will play an important role and, consequently, there will be considerable dissipation of kinetic energy into heat. The corresponding physical picture of developed turbulence is expressed in the following rhyme ... often quoted (usually without the exact reference and the last line):
>
> Big whorls have little whorls;
> Which feed on their velocity;
> And little whorls have lesser whorls,
> And so on to viscosity
> (in the molecular sense). (pp. 12-13)

Figures 3.29, 3.30, 3.31, and 3.32 sum up the entire energy picture of turbulent flow. **Figure 3.31** is the modification or enhancement of **Figure 3.30** for a stirred

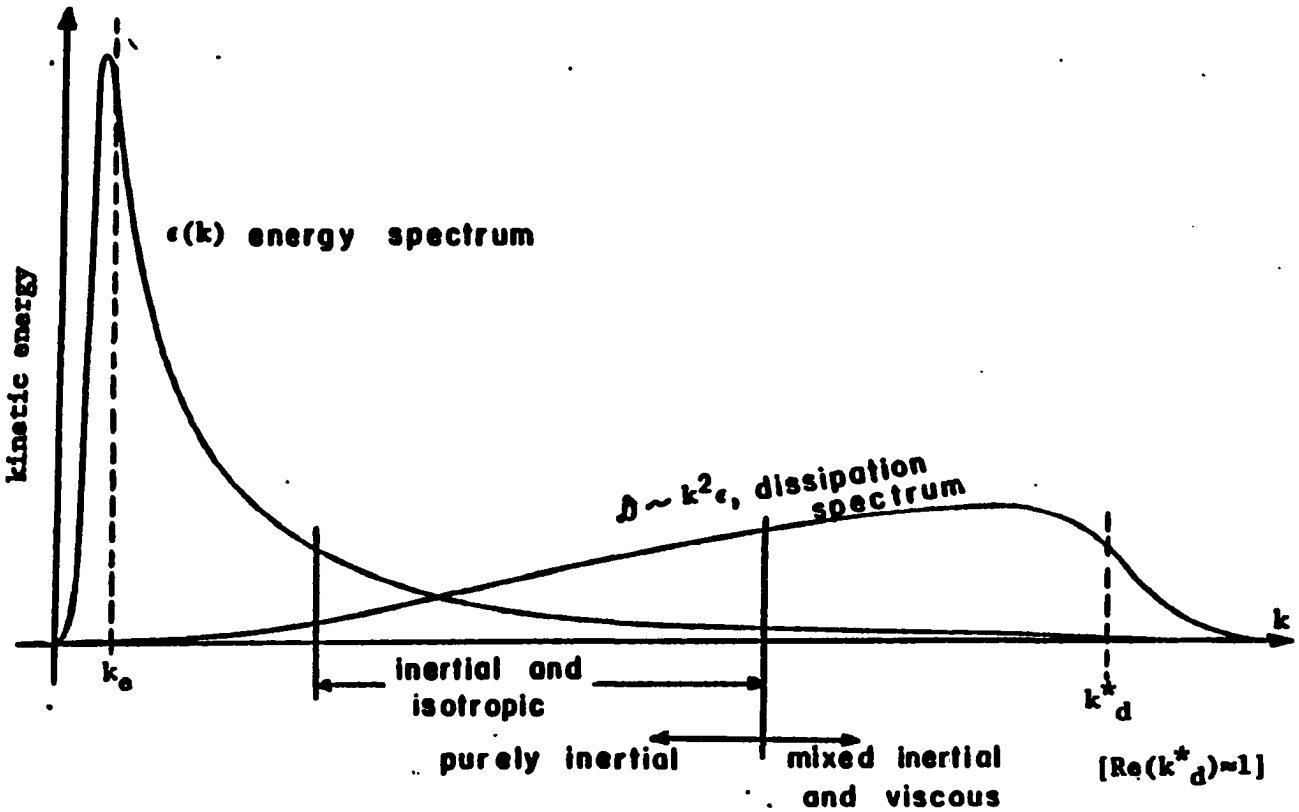

Figure 3.29. Spectral ranges in turbulence of moderate Reynolds number (Hanson and Cleasby, 1990)

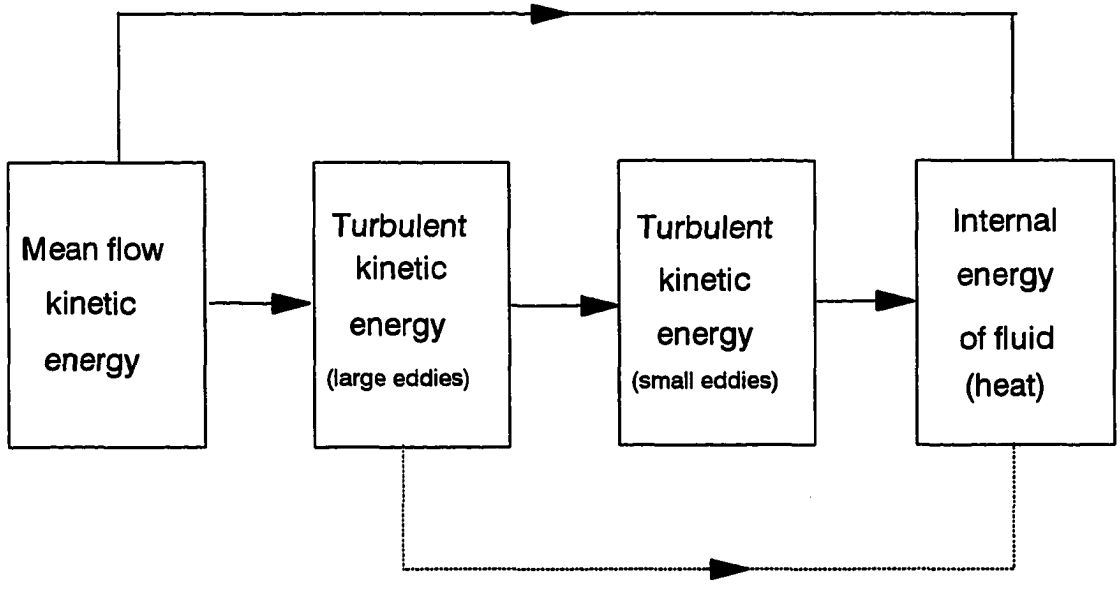

Figure 3.30. Crude representation of average energy degradation path (Corrsin, 1961)

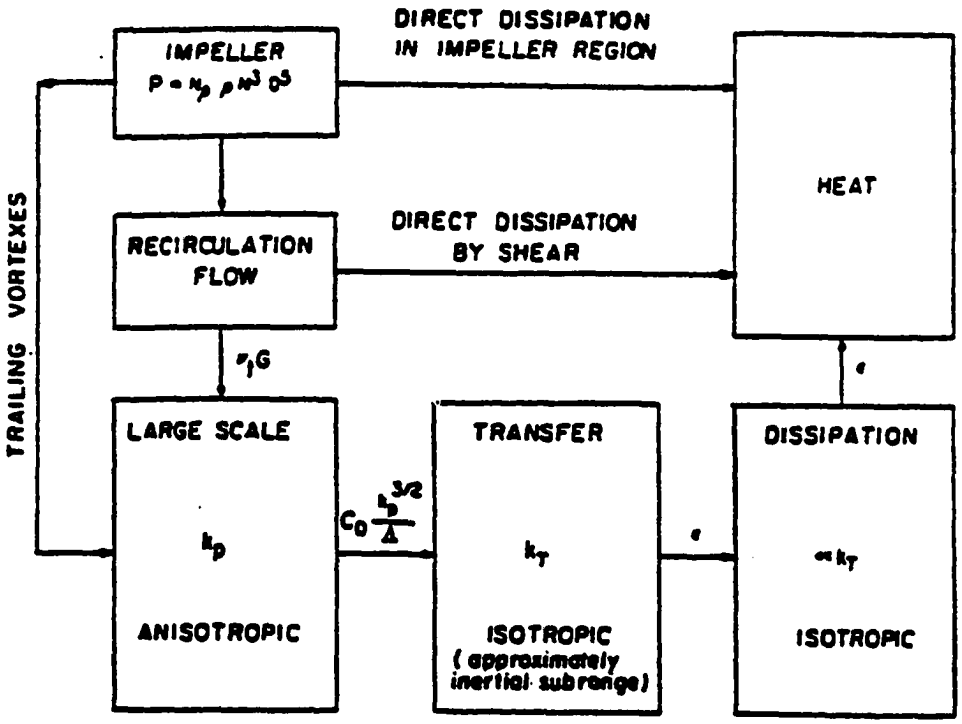

Figure 3.31. Model of dissipation of mechanical energy in an agitated vessel (Placek et al., 1986)

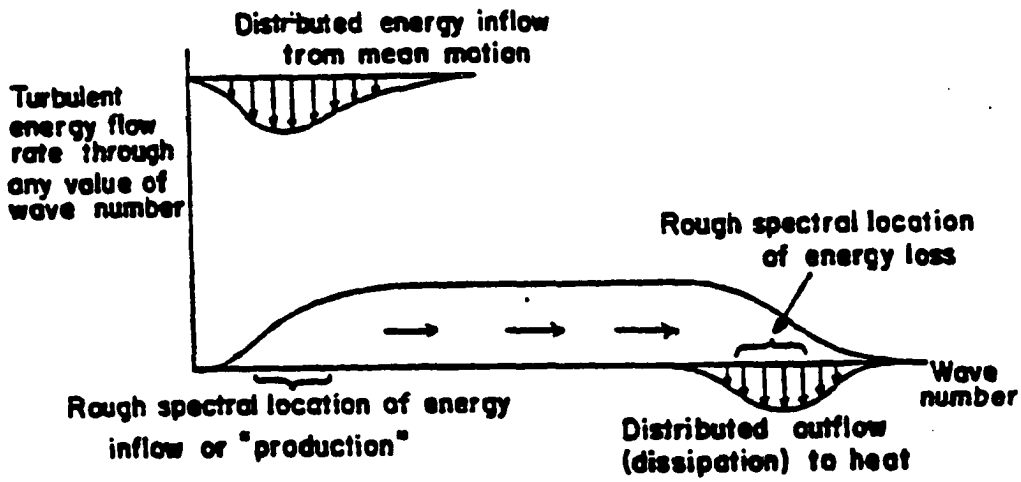

Figure 3.32. Schematic representation of average turbulent kinetic energy path in wave number space (Corrsin, 1961)

vessel. **Figure 3.29** is the three-dimensional turbulent energy spectrum and the dissipation spectrum. The y-axis is the kinetic energy contained in a specific eddy size at a fixed point in time which is a function of wavenumber and the x-axis is the wavenumber. The wavenumber described here is based on a concept from spectral theory and can be regarded as a "transform" (inverse of the vortex or eddy size, 1/d; d is the diameter of the vortex) such that small wavenumbers correspond to large eddy sizes which are fewer in number and large wavenumbers correspond to small eddy sizes - much larger in number (or frequency) (Bradshaw et al., 1981; Corrsin, 1961; Hinze, 1975).

The variables k_e and k_d represent the eddy sizes which contain majority of the energy and dissipate majority of energy respectively. As seen from the figure, the maximum energy is contained in the low wavenumbers (corresponding to large eddy sizes). These large eddies are inertia controlled and are very little affected by viscosity. Frost and Bitte (1977) called these "energy bearing anisotropic eddies". This range of eddies is most frequently referred to as the "production scale eddies". These eddies are produced directly by the velocity gradients induced by the mixing equipment. The introduction of kinetic energy by the mixing equipment in the system is shown schematically in **Figure 3.30**. The left most box represents the kinetic energy in the bulk flow. This bulk flow kinetic energy is responsible for direct production of the largest eddies in the second box.

In **Figure 3.29,** it has been shown that a peak occurs around k_e in the low wavenumber region. The eddies with wavenumbers around k_e represent the average size

of energy containing eddies. These large eddies then become smaller through mechanism of vortex stretching, and the energy of the large eddies is cascaded down to smaller and smaller eddies. Ultimately an eddy size is reached in which majority of energy dissipation takes place. This energy dissipation takes place in the eddies with wavenumber equal to or less than k_d. This range is frequently called the "dissipation subrange"and is often referred to as Kolmogorov microscale. Also shown in **Figure 3.29** is the dissipation spectrum with eddies of different sizes. It is also seen that most of the dissipation is associated with the smaller eddy sizes.

Figure 3.31 illustrates the approximate route taken by energy of the mean flow, to be dissipated as heat (or to be conserved as the internal energy of the fluid). Mean flow loses a part of its kinetic energy directly to viscosity (converted to heat, just like in laminar flow). The remaining fraction goes into the production of large eddies which, in turn, lose some energy directly to viscosity. The remaining part of the energy of large eddies goes into the energy of smaller eddies, which lose it to viscosity. **Figure 3.32** shows the above information in the same wavenumber space reference frame indicating the location of the region where energy of the mean flow is acquired by the eddies, the direction of energy transfer, and the region where the eddies lose their energy to viscosity. Kolmogorov speculated that small scale eddies, in a homogenous turbulent flow, lose the preferred orientation of the mean rate of strain, taking a universal structure of isotropy. Kolmogorov called it local isotropy. So he mentioned that true turbulent flow is homogenous and isotropic. Hinze (1975) states that even if the large scales of turbulence are strongly anisotropic, the small scale turbulence will tend to be

isotropic.

Voke and Collins (1983) provided the description of energy transfer or eddy cascade as follows:

> The largest 'eddy' of all is the gross mean flow whose energy arises from imposed shear, pressure gradients, buoyancy or other body forces, constrained by boundary conditions. The mean flow loses energy through vortex formation or other mechanisms to eddies of next smaller size; these are the largest true turbulent eddies. They in turn lose energy to smaller structures through vortex stretching or tilting. The interactions become increasingly random and hence isotropic as the causal link with the original imposed force and the boundary constraints become more extended and tenuous.
>
> The energy cascade may continue through many orders of magnitude in a high Reynolds number flow. The transfer is overwhelmingly in the direction form lower wavenumbers to higher wavenumbers. (This is not the case in two-dimensional turbulence - one key reason why true turbulence must be three-dimensional).
>
> The cascade peters out eventually because the smaller eddies, although they contain less energy and involve smaller vortical velocities, involve higher strain rates and vortices than the larger eddies. The velocities are lower but the velocity gradients are larger. As a result, molecular viscosity comes into play an increasingly important role at higher wavenumbers, until eventually a scale is reached where nearly all the energy extracted from large eddies is dissipated by friction, with none left to pass on down the cascade to smaller scales. At this point the energy spectrum start to fall increasingly rapidly towards zero. (p. 122)

Mixing: Mixing is the process by which a non uniform system is made uniform. An ideal mixture is generally conceived as having the condition where the concentration or other scalars are uniformly distributed throughout the system. Tatterson (1991) stated that mixing of one liquid into another liquid under turbulent flow conditions involves bulk motion or convective transport, turbulent diffusion, and molecular diffusion. He further cited the work of Beek and Miller (1959) who divided the mixing process up into three simultaneous and successive stages: (1) the distribution of one material into

another, (2) the breakup of this distribution into smaller portions, resulting in an increased surface area of contact, and (3) the molecular diffusion of materials into each other. Convective transport is usually considered macromixing, and turbulent and molecular diffusion is micromixing.

Perfect mixing occurs when a molecule of one species in a mixture of two or more species finds the molecules of other species in all its neighboring positions. This ultimately occurs due to molecular diffusion when molecules of "A" (in a mixture of two, A and B) from an A-rich region travel toward the B-rich region due to concentration gradients and the same amount of B-molecules from a B-rich region travel toward the A-rich region to satisfy mass conservation law. Ultimately a time is reached when a molecule of "A" finds molecules of "B" in all its neighboring positions. But this process is slow and depends on concentration gradient and interfacial area. Hydrodynamic conditions under turbulent flow greatly increase the speed with which mixing is achieved by increasing the interfacial area between the materials and by maintaining high concentration gradients. Turbulence breaks bigger clumps of molecules into smaller clumps.

Tatterson (1991) illustrated the concentration spectrum to describe the concept of micromixing mechanism in terms of statistical turbulence theory. In doing so, he mentioned two length scales: (1) Kolmogorov microscale which has been defined earlier and (2) Batchelor length scale (also called Batchelor's concentration length scale), $\eta_b = (\upsilon D_L^2/\varepsilon)^{1/4}$, where D_L is the diffusivity of the liquid ($cm^2\ s^{-1}$) and υ is the kinematic viscosity as defined earlier. In his interpretation, he divided the concentration spectrum

into an inertial-convective subrange, a viscous-convective subrange, and a viscous diffusive subrange. The concentration spectrum he described is almost similar to the energy spectrum. If the concentrations contained in different sized eddies are plotted against the wavenumbers of those eddies, a plot similar to the kinetic energy versus wavenumbers (**Figure 3.29**) could be obtained. At the beginning stages of mixing, distributive mixing occurs where specie-rich solutions break up into large- and intermediate-sized eddies to form a macroscopically uniform mixture (**Figure 3.33a, b** and **Figure 3.34**). This occurs at the smallest wave numbers (largest sized) eddies in the concentration spectrum and in the lowest portions of the inertial-convective subrange. The inertial convective subrange is characterized by the largest-scale eddies down to the Kolmogorov microscale. In this subrange, convection is primarily responsible for mass transfer, and diffusion is not considered important. The scale of the unmixed material is reduced by eddy motions. This stage is also called the dispersive mixing where the specie-rich eddies become smaller but high segregation still exists between species. The viscous-convective subrange exists between Kolmogorov microscale and the Batchelor's concentration length scale , η_b. The eddies are subject to laminar strain which causes further scale reduction into the viscous-diffusive subrange which begins at the Batchelor's concentration length scale. In this subrange, diffusion and laminar strain are equally important and diffusion dissipates the concentration differences. The eddies have reached the smallest scales, and diffusion occurs on molecular level.

Figures 3.33a through d (Baldyga and Bourne, 1984b) represent above steps of mixing schematically. **Figure 3.33a** refers to the relative movement of two points α and

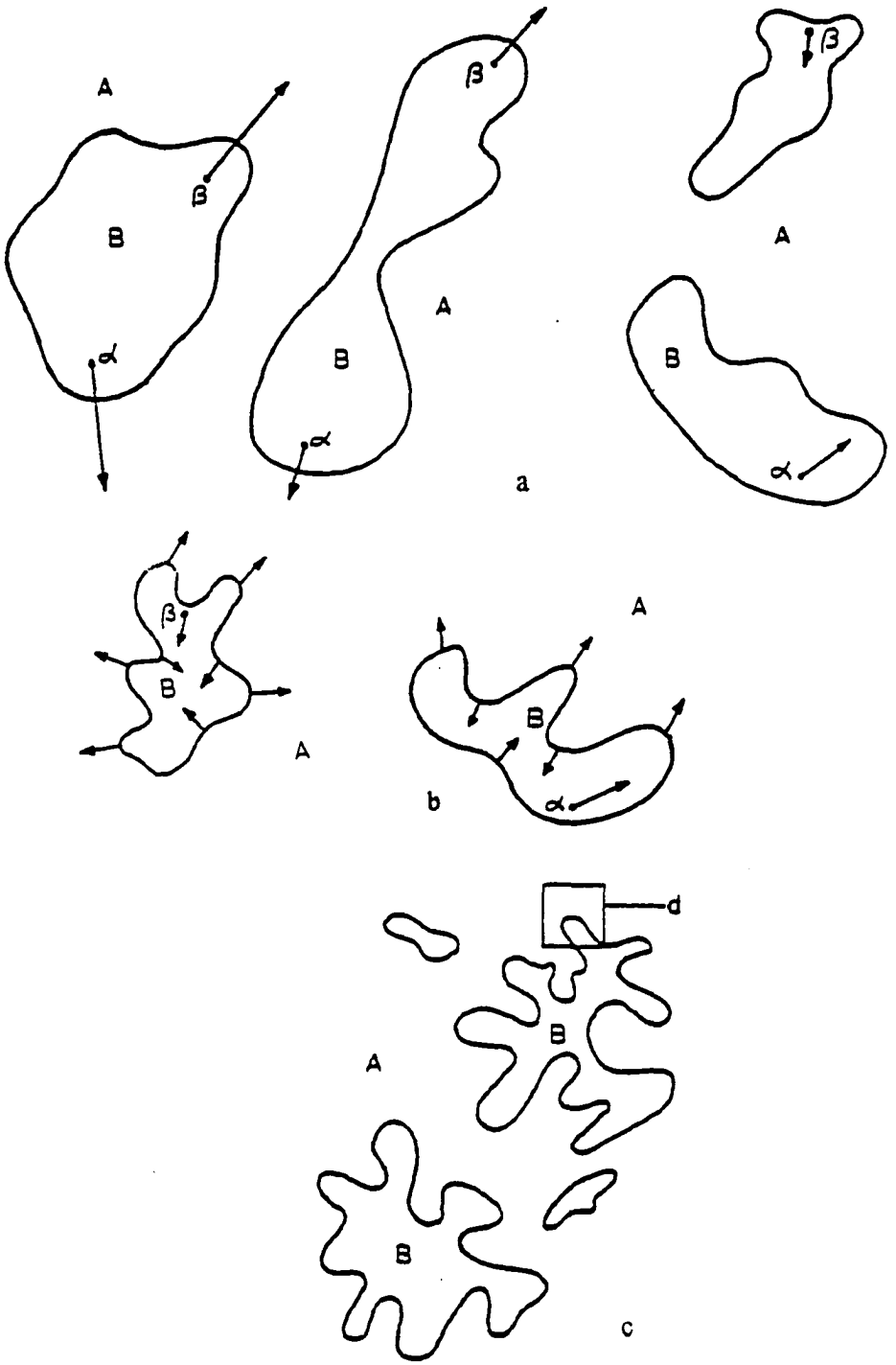

Figure 3.33. a,b) Large and small scale deformations within the inertial subrange; c) Fine scale, laminar deformations in viscous subrange (Baldyga and Bourne, 1984b)

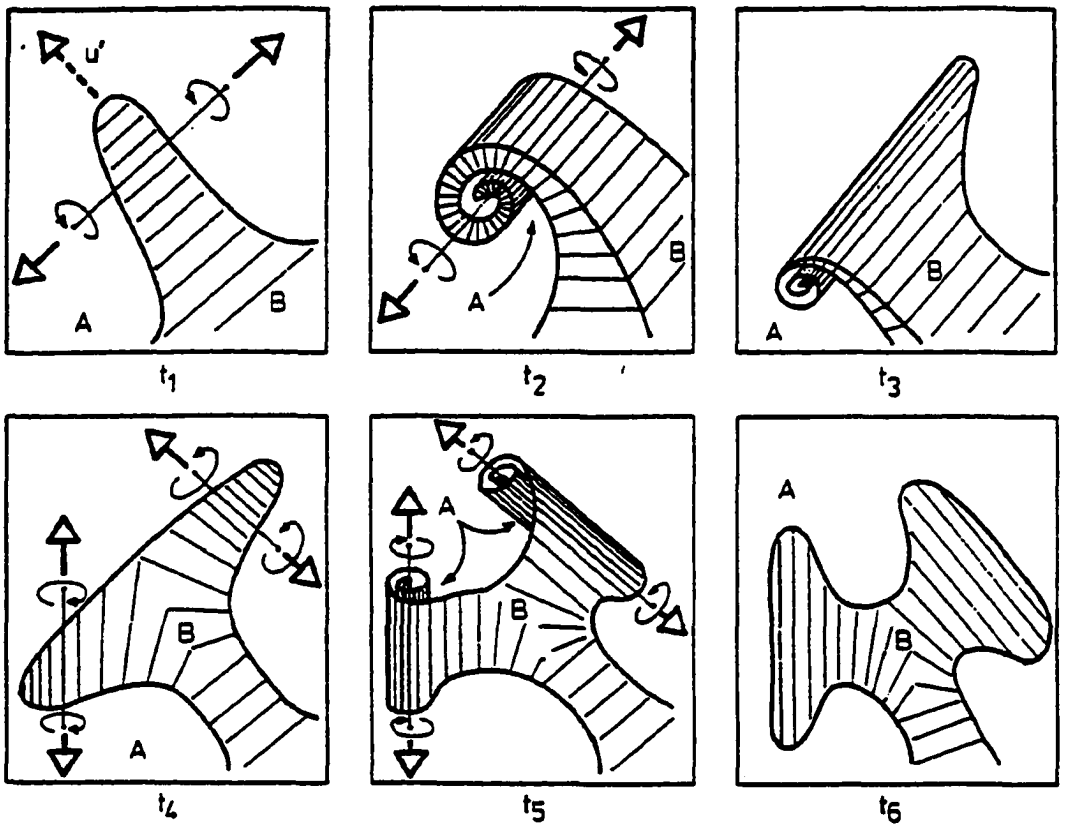

d

Figure 3.33. (continued) d) Action of vorticity acting on fluid elements whose initial thickness is on the order of Kolmogorov microscale, η_K (Baldyga and Bourne, 1984b)

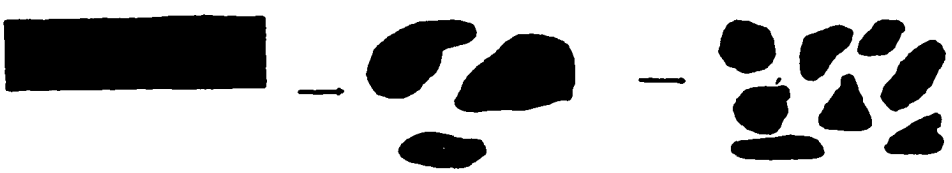

Figure 3.34. The process of dispersion (Brodkey, 1975)

β located far enough apart that their separation distance falls in the inertial subrange (left hand sketch). This relative movement of these two points far enough apart results in the deformation (middle sketch), so that the scale of the elements formed is reduced resulting in an independent movement of the elements (right hand sketch). **Figure 3.33b** depicts further deformation of a fluid element due to the action of inertial velocity fluctuations. **Figures 3.33a and b** refer to the inertial-convective subrange of the concentration distribution, where no micromixing occurs, but where the structures which will subsequently participate in micromixing are formed. **Figure 3.33c** indicates finer scale with the occurrence of laminar deformations within the viscous subrange, whilst **Figure 3.33d** concentrates on a small region and follows the development of the smallest, most energetic, and concentration dissipative vortices.

Amirtharajah and O'melia (1990) stated Danckwerts' (1958) definition of the scale of the segregation intensity, I_s, in an analogous fashion to the definition of normalized turbulence intensity. When the instantaneous concentration at a point in a turbulent flow field is given by the summation of the mean value C and a fluctuating value c, as $C = C + c$ and the rms concentration fluctuation is given as $c'=(c^2)^{1/2}$. Then the intensity of segregation can be given as

$$I_s = (c')^2/(c_o')^2 \qquad 3.23$$

where c_o' is the initial root mean square concentration fluctuation. The intensity of segregation defines the "goodness of mixing" and at unmixed condition $I_s = 1$, while at perfect micromixed condition $I_s = 0$.

Brodkey (1975) illustrated pictorially in **Figures 3.34 and 3.35** the effect of

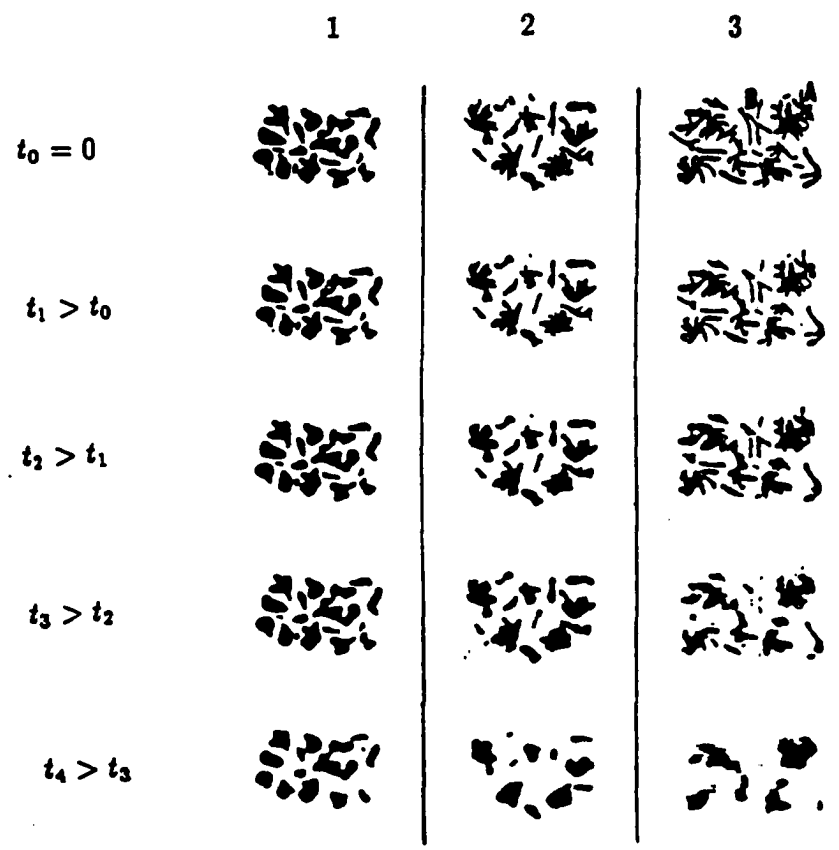

Figure 3.35. Influence of increased surface area and reduced dimensions on mixing (Brodkey, 1975)

turbulent dispersion on the mixing process. In these two figures he wanted to show how dispersion breaks down and substantially reduces the size of "solute fluid" (e.g., dye solution) particles in order to increase the area "exposed" to the solvent (e.g., water) and to increase the concentration gradients. **Figure 3.35** depicts the impact of size reduction on the overall rate of diffusion. The topmost row shows three different levels of dispersion of a dye, with increasing levels of dispersion from left to right. As can be seen from the figure, the filamentous structure of the solute elements in the third column provides them with much greater surface area and a greater dye concentration gradient than that of the elements in the first column. The elements in the middle column show an intermediate level of dispersion between the left and the right columns.

The topmost row of pictures can be regarded as time '0' = t_o for diffusion. Pictures in subsequent rows can be considered the result of diffusion at times t_1, t_2, t_3, and t_4 respectively where $t_4 > t_3 > t_2 > t_1 > t_o$. This picture illustrates that the "solute fluid" elements in third column diffuse much faster than the elements in the first or second columns, causing the system to achieve a higher level of homogeneity within the same time period than the elements in first and second columns.

Vortex stretching: In the above subsection, it has been seen that energy is transferred in a turbulent flow field from large eddies to small eddies through the mechanism of vortex stretching.

Srivastava (1988) illustrated the phenomenon of conservation of vorticity in **Figure 3.36** which shows a cylindrical vortex filament (much elongated form) before

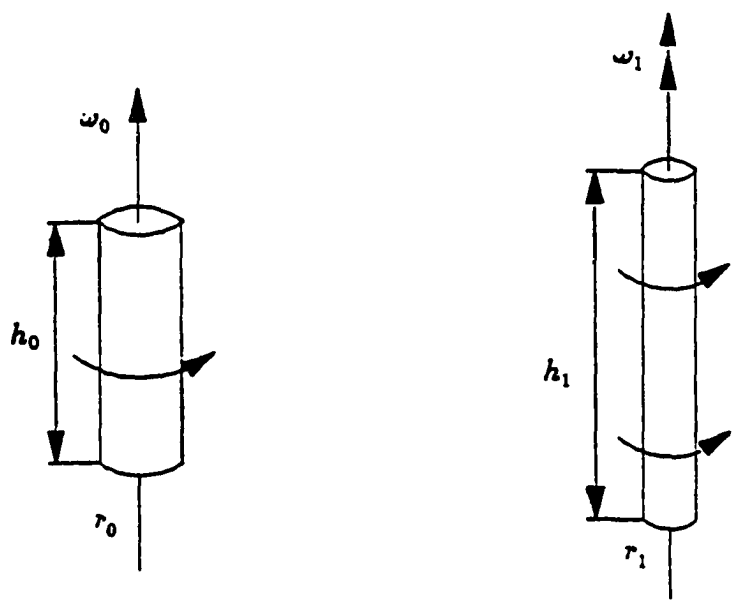

Figure 3.36. Principle behind energy transfer from large eddies to small eddies (Srivastava, 1988)

and after stretching. Before stretching, the diameter, height, and angular velocity were r_o, h_o, and ω_o respectively and the same were r_1, h_1, and ω_1 respectively after stretching. Since the filament is stretched in height, $h_1 = (\pi r_o^2 h_o)/(\pi r_1^2) = h_o(r_o/r_1)^2 > h_o$, as a result $r_o > r_1$. The angular momentum (the moment of the momentum about the axis of rotation) of the cylinder (before stretching), L_o, is given as

$$L_o = \int_0 (2\pi r h_o dr)(\omega_o r)r = (1/2)\pi h_o \rho \omega_o r_o^4 = I_o \omega_o \qquad 3.24$$

Where I_o is the moment of inertia.

After stretching, the angular moment of filament, L_1 is given as

$$L_1 = (1/2)\pi h_1 \rho \omega_1 r_1^4 = I_1 \omega_1 \qquad 3.25$$

From the principle of conservation of angular momentum, $L_o = L_1$ i.e.

$$(1/2)\pi h_o \rho \omega_o r_o^4 = (1/2)\pi h_1 \rho \omega_1 r_1^4$$

$$\Rightarrow (1/2)\pi h_o \rho \omega_o r_o^4 = (1/2)\pi h_o (r_o/r_1)^2 \omega_1 r_1^4 \text{ since, } h_1 = h_o(r_o/r_1)^2$$

After cancelling the like terms and rearranging

$$\omega_1 = (r_o/r_1)^2 \omega_o \qquad 3.26$$

Since $r_o > r_1$, $\omega_1 > \omega_o$.

Now if we consider the kinetic energy; this can be given before stretching as

$$K_o = (1/2)I_o \omega_o^2 = (1/2)L_o \omega_o \qquad 3.27$$

and after stretching the kinetic energy is given as

$$K_1 = (1/2)I_1 \omega_1^2 = (1/2)L_1 \omega_1 \qquad 3.28$$

Since $L_o = L_1$ and $\omega_1 > \omega_o$, it implies that $K_1 > K_o$ or, the process of stretching has resulted an increased kinetic energy of the rotating cylindrical vortex filament.

The concepts of vortex stretching have been shown in **Figure 3.37** (Tennekes

and Lumley, 1972) and **Figure 3.38** (Frost and Bitte, 1977). By establishing relation between the time rate of change of the vorticity (angular velocity in a vortex or eddy) fluctuation and the fluctuating rate of strain, they developed the expressions as follows:

$$\omega_1 = \omega_o e^{st}, \ \omega_2 = \omega_o e^{-st} \qquad 3.29$$

$$\omega_1^2 + \omega_2^2 = 2\omega_o^2 \cosh 2st \qquad 3.30$$

where s is the strain in the direction of vorticity and t is the time. This is for two dimensional strain and for the sake of simplicity, it has been assumed $s_{11} = -s_{22} = s$ and $s_{12} = s_{21} = 0$. Positive strain for expansion and negative strain for compression. t is the time. From the above expression in Equation 3.30, it is seen that the total amount of vorticity increases for all positive values of st. That is when a vortex is expanded or stretched, its angular velocity and kinetic energy increase. The vorticity component in the direction of stretching, ω_1, increases rapidly and that in the direction of compression, ω_2, decreases slowly at large st.

Figure 3.38 (Frost and Bitte, 1977) illustrates the action of vortex stretching which causes the upper vortex segment (which is larger) to stretch and the lower vortex segment to compress, causing a net transfer of energy from the bottom vortex segment to the top segment. This top vortex segment, in turn, does the same thing to another vortex segment of lower size and so on. Moreover an extension in one direction decreases the length scales and increases the velocity in other two directions, which stretch other elements of fluid with vorticity components in these directions as illustrated in **Figure 3.39** (Frost and Bitte, 1977). This figure shows that two parallel vortices stretched in the x_1 direction result in an increase in u_2 in the positive x_2 direction in an

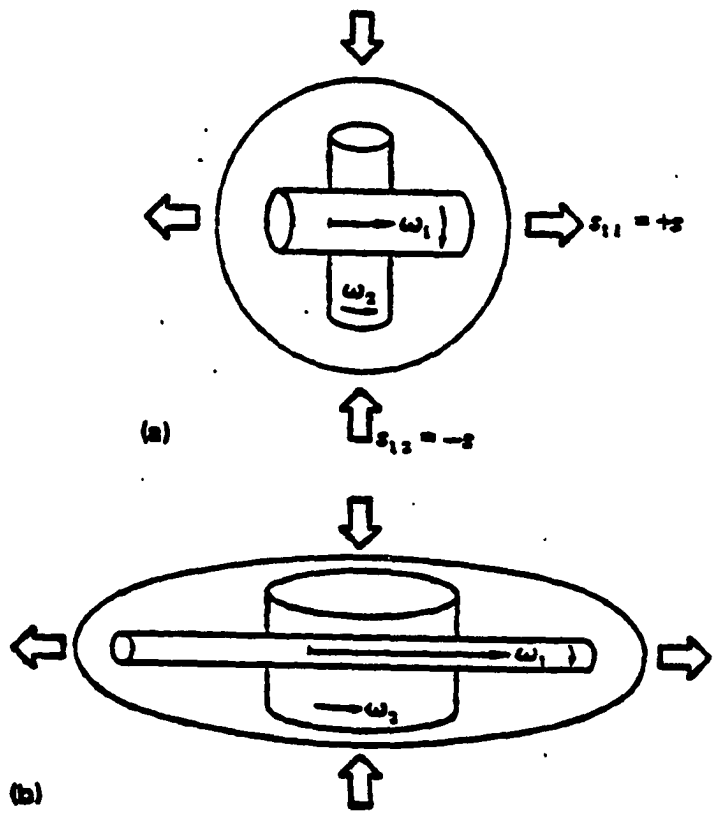

Figure 3.37. Vortex stretching in a strain-rate field: (a) before stretching, (b) after stretching (Tennekes and Lumley, 1972)

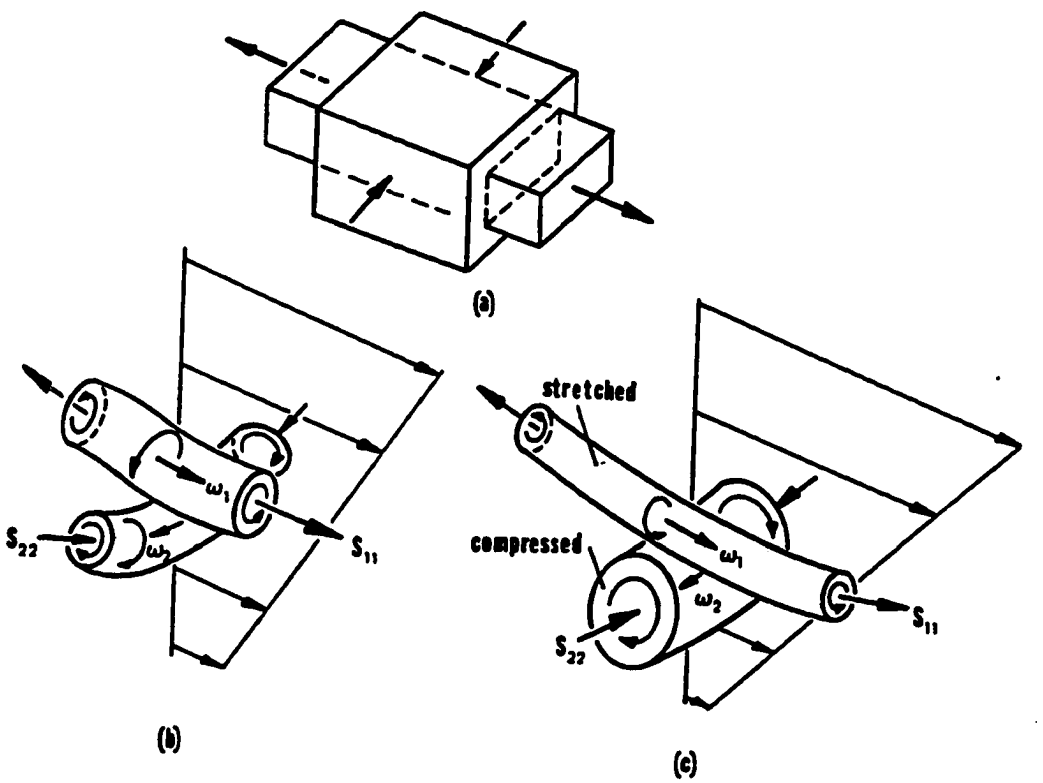

Figure 3.38. Concept of vortex stretching (Frost and Bitte, 1977)

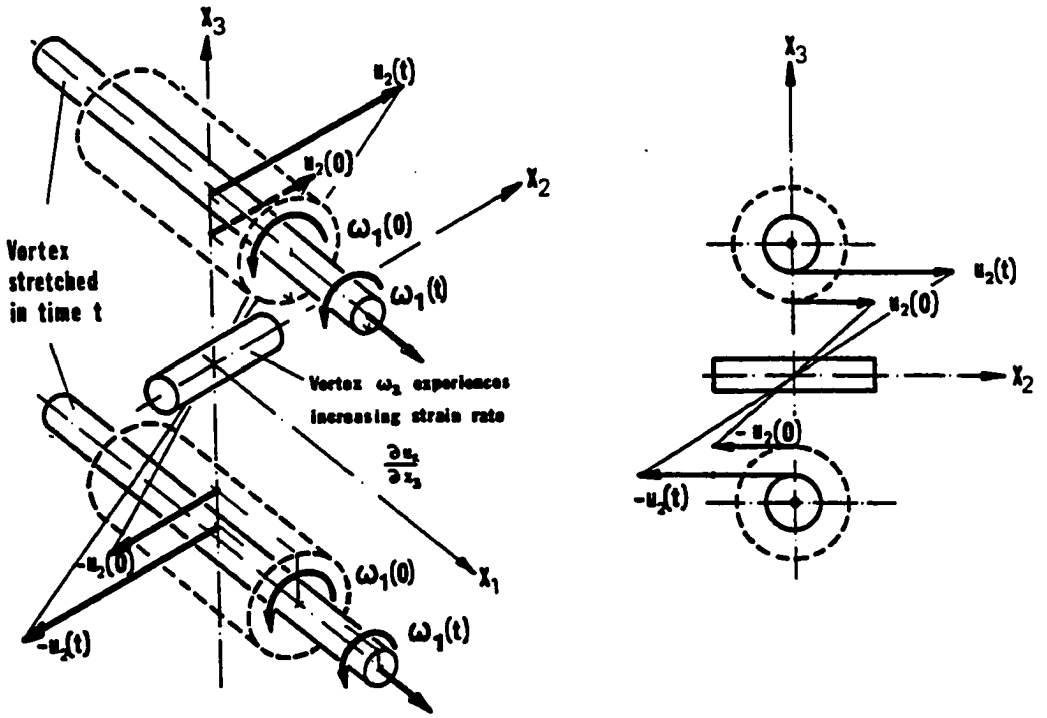

Figure 3.39. Vortices stretched in the x_1 direction increase the strain rate $\delta u_2/\delta x_3$ (Frost and Bitte, 1977)

upper plane and in the negative x_2 direction in lower plane. Thus an increasing strain-rate field is generated which is experienced by vortex, ω_2, causing it to stretch. As it stretches, a new strain field is created, which in turn stretches other vortices, and so on. This process continues, with the length scale of the augmented motion getting smaller at each stage, with the energy transfer from higher scale to lower scale (Frost and Bitte, 1977).

3.6.3. Turbulent mixing

As it has been seen earlier that mixing is one of the features that takes place in a turbulent flow field. Bourne (1982) describes mixing of two components (A and B) in a turbulent flow field as follows:

1. The B-rich solution stream breaks up into large B-rich eddies, which exchange position with A-rich eddies to form a uniform mixture macroscopically. This process is referred to as distributive mixing and at a scale much smaller than this eddy size, no mixing occurs.

2. The large eddies of step 1 decay in size and form a finer grained dispersion through the effect of turbulent shear. Yet the mixture remains highly segregated at the molecular level, although some diffusion and reaction start at the boundaries of large eddies. The mixing in this phase is termed dispersive.

3. Diffusion within the finely dispersed structure of step 2 operates over short distances and proceeds to randomize the substances at the molecular scale. The result of diffusive mixing is termed a homogenous mixture.

The above three steps may occur simultaneously to some extent. Steps 1 and 2 are often termed by the researchers as convective mixing (macromixing) or turbulent diffusion, and being brought about by flow, turbulence, and eddy diffusion, whereas mixing at molecular scale or micromixing belongs to step 3. As shown in **Figure 3.35** (Brodkey, 1975), turbulence takes us from the first column to the third column and in this column, molecular diffusion takes us from top row to the bottom row. All in all, the combination of turbulence with molecular diffusion yields a much better mixing in a much shorter time than would have been possible with just molecular diffusion.

Scale of segregation, L_s and intensity of segregation, I_s have been defined earlier. The former is a measure of the size of unmixed clumps of pure components. This is a measure of some average size. As the clumps are pulled and contorted, the scale of segregation is reduced; this would be going form left to right along the top of **Figure 3.35**. The intensity of segregation describes the effect of molecular diffusion on the mixing process. It is a measure of the difference in the concentration between neighboring clumps of fluid (Brodkey, 1975). Thus moving down the columns in **Figure 3.35**, the concentration difference between the clumps and the inter-clump region decreases as molecules of the dye diffuse out of the clumps. This corresponds to a decreasing intensity of segregation. So while a decrease in the intensity of segregation (i.e., a more uniform and non-clumpy mixture) can only be created by molecular diffusion, turbulence is required to help speed up the process by very rapidly reducing the scale segregation (smaller clumps of fluid).

Tennekes and Lumley (1972) have shown that time taken by molecular diffusion

alone to disperse a transported quantity (e.g., heat) uniformly through a space, t_m, is much longer than the time, t_t, that would be required to disperse the same quantity through the same space by turbulent diffusion. For a gaseous substance, they showed that the ratio of t_t/t_m is inversely proportional to the Reynolds number R_e, which is an indicative of the intensity of turbulence. So when R_e is high, t_t/t_m is low and vice versa; implying that at high Reynolds number, the time scale for "turbulent diffusion" of a substance over a given length scale is much smaller than the time scale for molecular diffusion alone.

The mechanisms involved in turbulent flow field which enhance mixing are as follows (Patterson, 1985; Frost and Bitte, 1977; Srivastava, 1988 and Chakrabarti, 1991):

1. Shear: The process of continuous distortion (stretching in one direction and contraction in the other) of fluid elements by shear speeds up the overall process of diffusion resulting in an enhanced time rate of mixing. **Figure 3.40** illustrates the thinning of two different shapes of fluid element (rectangular and circular). Part(b) of the figure shows the fate of a dye spot in a viscous fluid subjected to a rectilinear flow, in the absence of molecular diffusion. With increasing time, the circular spot is transformed first into an ellipse, then into a thin long finger, similar to the behavior of the thinning of rectangular fluid element shown in part(a). The spot, in this finger-shaped form, possesses a much larger interfacial surface area than the circle (at time = 0). As a result of the distortion process the blob shrunk in one direction which increased the probability for the fluid element at the center of the circle to diffuse out of the blob

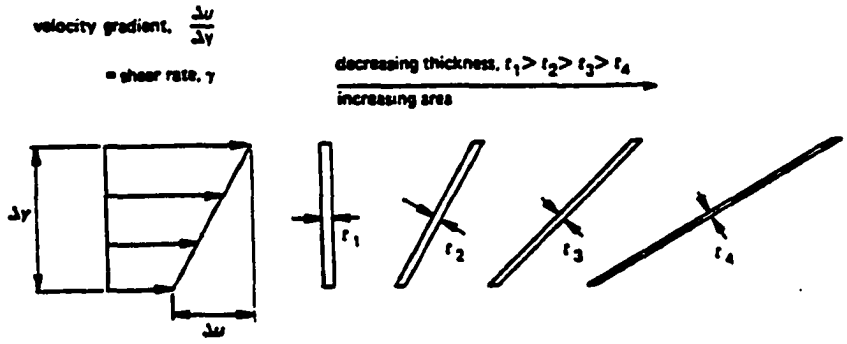

(a)

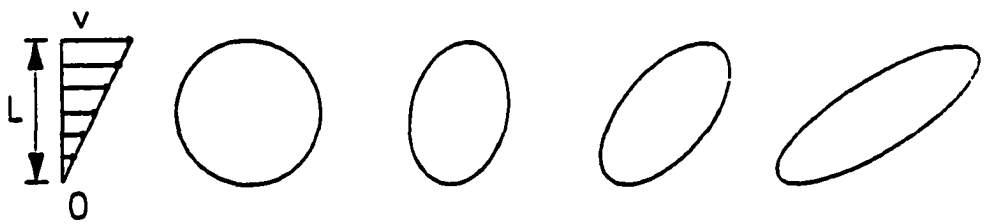

(b)

Figure 3.40. Role of shear in turbulent mixing. (a): Thinning of a rectangular fluid element in a rectilinear shear flow field (Harnby et al., 1985). (b): Distortion of a spot of dye (in the absence of molecular diffusion) in a viscous fluid subjected to a rectilinear shear flow field (Srivastava, 1988)

into the bulk fluid through that direction - making the overall process of diffusion much faster. So it is clear that the process of distorting a dye spot by shear can enhance the time rate of mixing.

2. Elongation and vortex stretching: As has been mentioned earlier that energy is constantly being transferred from large eddies to smaller ones through the process of vortex stretching. From **Figure 3.39** it can be seen that a new strain field is created due to stretching of one vortex, which in turn, stretches other vortices, and so on. This process continues, with the length scale of the augmented motion getting smaller at each stage, with the energy being transferred from large scale to smaller scale. Also from **Figure 3.36** it can be seen that thinner and longer vortex tubes are constantly being formed and dissipated. If a blob of dye is inserted in a turbulent flow field, some of it is likely to be trapped in a vortex tube which gets elongated and thinned. The deformation of the vortex tube containing this dye will increase the interfacial surface area and reduce the distances which the molecules must travel before mixing with the surrounding fluid. As a result an increase in the time rate of mixing of the dye with the bulk solution via molecular diffusion occurs.

The process of elongation, mentioned above, continues to distort the fluid elements to dimensions of the order of the Kolmogorov microscale. As the vortex tube is dissipated by the viscous forces, it has a much lower Reynolds number than before, and thus the time scale for transport of the dye (over a given length scale) by molecular diffusion is smaller than the transport by fluid motion. A shear field exists in a dissipating eddy which distorts the dye element as shown in **Figure 3.40**. Besides, the

flow has very low Reynolds number indicating that transport by diffusion continues to dominate as the eddy gets smaller in size.

Both the above mentioned mechanisms act simultaneously in a turbulent flow field, resulting in an enhanced time rate of mixing of dye with the bulk fluid. The fluid elements get engulfed in eddies and go through the process of elongation, shear, and molecular diffusion over and over again. Even though the eddies containing the fluid elements get dissipated, the fluid elements don't come to rest, the fluid elements become the part of the bulk flow and other eddies for the next distortion process.

3. Bulk flow and the velocity gradients in the bulk flow: Bulk flow is considered to be the largest possible eddy and represents the length scale at which the energy is being fed into the system (Hanson, 1989). This bulk flow generates the spatial velocity gradients in a turbulent flow field which in turn cause the particles initially close together to become dispersed and separated. The mixing by bulk flow can be considered as the largest macroscale mixing.

3.6.4. Turbulent mixing and chemical reactions

So far we have talked about the mixing of a dye into the surrounding fluid under a turbulent flow field in a non-reacting system. If the chemical reaction takes place as the fluids mix, then the scenario is much more complicated. The rate at which a reaction between A and B proceeds depends on how rapidly encounters between A and B molecules take place. In general, chemical reactions can be divided into two categories. Slow reactions and fast reactions. Slow reactions are chemically controlled and the rate

depends on the probability that an encounter between reacting molecules will lead to chemical reaction. Turbulent mixing may not be all that important as the reaction kinetics dictate the outcome of the process. So, even if the reactants molecules in a slow reaction are uniformly distributed throughout the system, the speed of the reaction would not change radically because the rate is controlled by the thermodynamic condition (energy barrier) which prevents reactants molecules from reacting with each other. That is, it will take a longer time for the reactants to react and form the products than the time needed to mix the reactants uniformly throughout the system. Diffusion time is much shorter than the reaction time. The rate of these reactions can only be enhanced by changing the thermodynamic conditions (changing the temperature or reducing the energy barrier through the use of a catalyst).

Fast chemical reactions are fast relative to mixing, e.g., neutralization, precipitation, combustion and hydrolysis (as in coagulation), and are characterized by steep concentration gradients on the molecular scale, which ensure that the rate of reagent diffusion matches the high consumption rate due to the reaction. Reactions occur almost with every encounter between reactant molecules and are said to be diffusion controlled. The turbulence and the resulting mixing play as important a role as the reaction kinetics in these reactions where the rate at which reactant molecules can come together is governing the overall speed and outcome of the reaction.

O'Brien (1975) quotes Toor's analysis to better understand how the role of turbulence changes with the inherent kinetics of a given chemical reaction as follows:

> From a practical point of view, the most useful single parameter for

describing the role of turbulence on chemical reactions is a ratio of time scales (a time scale τ_k characteristic of the kinetic scheme to a time scale τ_m characteristic of turbulent mixing). In a single-step, irreversible reaction, the inverse of the reaction rate constant in conjunction with characteristic concentration can represent the chemical reaction time; whereas, the time for the decay of fluctuations of a scalar field in the turbulence might represent the mixing time adequately. Three regimes suggest themselves:

1. $\tau_k/\tau_m >> 1$, The slow reaction,
2. $\tau_k/\tau_m \sim O(1)$, The moderate reaction,
3. $\tau_k/\tau_m << 1$, The very rapid reaction.

In case one, it is abundantly clear, at least when approximate statistical homogeneity applies, that turbulence will induce chemical homogeneity before any significant reaction will occur and the fluctuations in concentration of any species at a point will generally be negligible compared to the mean concentration in determining the rate of reaction.

In the second case, complex coupling between the turbulence and the reaction is to be expected even under statistically homogenous conditions.

In the third case, the behavior depends crucially on the nature of the reaction, as we shall see later. In particular, for multispecies reactions in which the species are not uniformly distributed in space, the progress of the reaction will be diffusion limited since molecules must first diffuse to the same point before they can react. It is rate of molecular diffusion, enhanced by turbulence through stretching of isoconcentration lines, which must control the rate of progress of the reaction. (pp. 23-24)

The effect of turbulent mixing on chemical reactions will be illustrated in following few paragraphs. Based on the direction of reaction, chemical reactions are divided into two categories; reversible and irreversible. The main chemical reaction (hydrolysis) that occurs in a coagulation-flocculation process is considered to be irreversible in nature by most researchers. The irreversible reactions can be divided into following types:

1. Simple reaction: When two reactants A and B react to give products as $A + B \rightarrow$ products, is simplest in nature. The speed of product formation depends on how fast the encounter could be made between the reactant molecules by breaking the solvent cage as shown in **Figure 3.41**. If thermodynamic conditions do not restrict the

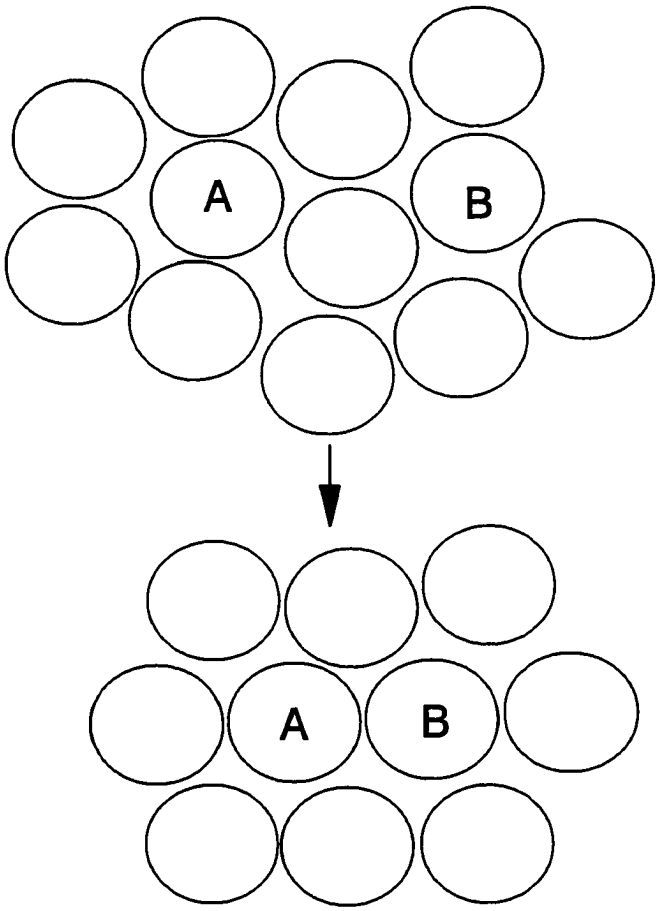

Figure 3.41. Diffusional encounter between reacting solutes A and B in a solvent (Adamson, 1979)

reaction to occur, it is the rate of encounters which governs the net rate of a reaction. This is where the diffusion ability of the solute molecules in a given solvent comes into picture. Solute molecules having a larger coefficient of diffusion, D, will be able to have more encounters in a given time period than the molecules with smaller D. Also for reacting molecules with fixed D, the diffusion ability can be increased by reducing the size of the solvent cage, the packets of reacting materials, thereby increasing interfacial surface area. All this can be done by higher turbulence induced by intense mixing.

2. Parallel reaction: In parallel reactions, reactants can undergo two or more reactions independently and concurrently where two or more species may react through alternative paths to give two or more different product species (simple parallel reactions) as shown below:

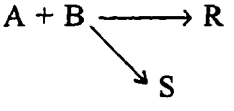

When two or more reactant species compete for another reactant, the reaction is called competitive parallel reaction and can be illustrated as follows (Hill, 1977):

$$A + B \rightarrow R$$

$$A + C \rightarrow S$$

Mixing is important for the competitive parallel reaction. If the reaction ($A + B \rightarrow R$) is faster than the reaction ($A + C \rightarrow S$) and R is the desired product, then high intensity mixing will favor the formation of R over S.

3. Series reaction: In this type of reaction, one or more of the products formed initially undergoes a subsequent reaction to give yet another product. Significant

amounts of both the intermediate and the final product species will be present during the normal course of the reaction. The general scheme for these reactions may be represented as

$$[A...] \rightarrow [B...] \rightarrow [C...]$$

where the quantities in brackets may denote more than one molecular species (Hill, 1977). Often the ultimate product formation depends on the type and relative distribution of the reactants. The relative distribution of reactants depends on the mixing intensity or how widely the reactants are distributed in the system. So mixing ultimately determines the nature and speed of the ultimate product formation. These reactions include condensation polymerization reactions, partial oxidation reactions, and reactions in which it is possible to effect multiple substitutions of a particular functional group on the parent species (mono-, di-, tri-, etc. substituted products) (Hill, 1977).

4. Series-parallel or competitive-consecutive reaction: These types of reactions may be represented in general form as:

$A + B \rightarrow R$ the reaction rate constant k_1

$R + B \rightarrow S$ the reaction rate constant k_2

A and B react to produce R. R, however, competes with A in reacting with B to form S. Also, since it is necessary for the first reaction to occur and form R before the second reaction can take place, the reactions are consecutive. Thus, overall, these two reactions are called competitive-consecutive reactions. This reaction set may be regarded as parallel reactions with respect to consumption of species B and as a series reaction with respect to species A, R, and S. Overall they are also called series-parallel reaction.

Common examples include the nitration and halogenation of benzene and other organic compounds to form polysubstituted compounds (Srivastava, 1988 and Hill, 1977).

In a well mixed A system, where B is in limited supply (i.e., B is the limiting reagent), the first reaction is favored since B will react with A and R will be formed. Once R is formed, then in a well-mixed A system, R will only be with A since, all the B has already reacted with A to form R. But in a poorly mixed system, after R has been formed, B will still be available to react and a portion of available B will react with R to form S.

Srivastava (1988) performed a thought experiment to illustrate the effect of the mixing intensity on the product distribution of the above reaction set. He considered two cases:

1. Case with no mechanical mixing: If a blob of B is introduced in a vessel full of A, the interfaces of blob B are the only places where A and B molecules can react, because that is the only place from where molecules of B can diffuse into the bulk solution of A, meet them and react. So any R formed in the first step of this reaction sequence is very likely to diffuse equally in all directions (including towards the blob of pure B), resulting in a fraction of the total R reacting with B through the second step of the competitive-consecutive reaction set to form S.

2. Case with extremely intense mixing: In this case, turbulence breaks down the blob of pure B into smaller elements. As the blobs are reduced in size, diffusion spreads B molecules into A in a much shorter time period than in the previous case, resulting in a relatively better (more uniform, as compared to previous case) spatial distribution of A

and B. Thus, any R formed by the reaction of A and B has much less B to react with than in the earlier, unmixed case. Therefore, compared to first case, more R will be formed and very little S. In the above discussion the relative speed of the reaction steps was not considered. When one reaction is much faster than another, the presence of turbulence and its diffusive action complicates the situation even more by tilting the balance in favor of the faster reaction - particularly if the time scale of reaction is comparable to the time scale of turbulent diffusion.

Baldyga and Bourne (1984a,b, and c), Belevi et al. (1981), Bourne et al. (1981a and b), Bourne and Dell'ava (1987), and Rice and Baud (1990) performed several theoretical and experimental studies on mixing and fast chemical reactions. In doing so, they employed the above mentioned competitive-consecutive reaction. They defined a term called the product distribution parameter, which is a measure of the degree of segregation in the reaction zone and can be defined as follows:

X_s = moles of B consumed forming S/total moles of B consumed

$= 2C_{Sf}/(2C_{Sf} + C_{Rf})$

C_{Sf} = final concentration of product S,

C_{Rf} = final concentration of product R.

So a well mixed system will form more and more R and less and less S and product distribution parameter, X_s, will approach '0' where in a poorly mixed system the opposite thing will happen and X_s will approach '1'. All the above mentioned researchers have found that this product distribution parameter is a function of several dimensionless group such as, stoichiometric ratio of the reactants, N_{Ao}/N_{Bo}; the ratio of

the reaction rate constants, k_1/k_2; Schmidt number, S_c, the volume ratio, $\alpha = V_A/V_B$; the mixing modulus, M; and the stretching parameter, β. It also depends on some physical factors such as, impeller speed, diameter and width of the impeller, location of feed point in the reactor, mode of operation, etc. M and β can be defined as follows (Bourne, 1982; Bourne and Dell'ava, 1987; Rice and Baud, 1990; and Chakrabarti, 1991)

$$M = k_2 C_{Bo} \delta_o^2/D \text{ and } \beta = \gamma \delta_o^2/D$$

C_{Bo} = Initial concentration of reactant B (mol cm^{-3}),

δ_o = the size of the laminae through which the diffusion and reaction take place (cm). It is also called the initial half thickness of the fluid layer or the radius of a spherical reaction zone and defined as $(1/2)\eta_k$, where η_k is the Kolmogorov microscale (Rice and Baud, 1990 and Baldyga and Bourne, 1984c and Bourne et al., 1981b),

D = diffusivity of reactant B into A ($cm^2\ s^{-1}$), and

γ = the shear rate experienced by the laminae (s^{-1}).

Before discussing the effect of the above factors on product distribution parameter, different regimes in which chemical reactions take place will be discussed briefly as follows (Bourne et al., 1981a and b, and Belevi et al., 1981):

Molecular diffusional regime: This is the regime where the reaction rate is independent of the rate constant (k) and controlled by the molecular diffusion. This occurs in extremely fast and instantaneous reactions. In the molecular diffusional regime, diffusion entirely determines the reaction rate, the reaction zone shrinks from the whole vessel to a plane where A and B can not coexist, i.e., their concentrations sink to zero. The yield of the intermediate R in a competitive consecutive reaction is

zero under these circumstances and therefore $X_s = 1$.

Chemical regime: In the chemical regime, reaction rate is dependent on the reaction rate constants and the reagent solutions mix completely before the reaction has occurred to any significant extent. Reactions occur in the entire vessel and for a given set of reaction conditions, the smallest amount of secondary product (S) is formed and the minimum value of X_s is found in this regime for competitive consecutive reactions.

Mixed regime: In the mixed regime, the product distribution parameter (X_s) of a competitive consecutive reaction depends partly on the chemical reactions (e.g., rate constants) and partly on diffusional (e.g., agitation, viscosity and diffusivity of reactants in the solutions etc.) factors. The quantity of the secondary product (S) formed falls between the values for the chemical and the diffusional regimes. Thus in the mixed regime, X_s falls in an interval from a little more than zero to little less than unity (Bourne et al., 1981a and b, and Belevi et al., 1981).

The factors affecting the product distribution parameter (X_s) are described as follows:

1. N_{Ao}/N_{Bo}: This is the initial stoichiometric ratio of A to B. An increase in stoichiometric ratio suppresses the formation of secondary product, S, and thus decreases X_s. Chakrabarti (1991) mentioned that to form significant quantities of R, and dramatically reduce X_s, the initial stoichiometric ratio should be higher than 0.5 e.g., around 1. This value may change for different reactants. Ratios greatly in excess of 1 cause little 'S' to form and smaller X_s value, the price being a smaller conversion of A. This change of X_s with N_{Ao}/N_{Bo} is fully suppressed in the molecular diffusional regime,

where X_s is always 1, as mentioned before.

2. k_1/k_2: An increase in this ratio of rate constants promotes the formation of R over S. The trend is, however, greatest in the chemical regime, weaker in the mixed regime and entirely disappears in the diffusional regime, where a reaction plane forms. For a given pair of competitive-consecutive reactions, k_1/k_2 is controlled by thermodynamic conditions and can only be varied slightly by changing the temperature over the normal operation range.

3. Volumetric ratio α (V_A/V_B): In the chemical regime the volume ratio of the reactant solutions has no effect on product distribution; only the stoichiometric ratio is relevant. However, α plays a significant role in the mixed regime where volumetrically smaller feed stream is supposed to be dispersed in a turbulent and well-mixed environment. The assumption of better dispersion with lower α agreed well with experimental results. Thus the effect of increasing α in the mixed regime raises the value of X_s. For a constant stoichiometric ratio, α increases with the decreasing volume of B-solution with higher concentration. The interfacial surface area for diffusion falls causing a steeper concentration gradients and thus more formation of the secondary product S.

4. Mixing modulus, M: This is proportional to the half life times for diffusion (time for reactants to diffuse through half the Kolmogorov microscale, $\sim\delta_o^2/D$) and second order reaction. Low values of M characterize the chemical regime, where no concentration gradients occur. Sufficiently high values of M correspond to diffusion regime, with a narrow reaction plane formed where A and B meet and react

instantaneously. The mix regime falls between these limits - concentration gradients extend over a finite regions and the reaction is influenced by chemical as well as physical factors. Belevi et al. (1981) showed that for a CSTR, the chemical regime corresponds to M = 0, the diffusional regime corresponds to values of $M > 10^4$ and the mixed regime extends approximately over the range $10^{-2} < M < 10^4$. Baldyga and Bourne (1984c) showed that X_s increases with increasing M in a semibatch reactor.

5. Stretching factor β: This dimensionless constant is proportional to the ratio of the half times for diffusion ($\sim \delta_o^2/D$) in the absence of chemical reaction and for shrinkage ($\sim \gamma^{-1}$). Physically, β is a stretching parameter, proportional to the time needed to mix the reaction zone by diffusion alone and inversely proportional to the time required to deform it. Stretching clearly reduces the formation of S relative to the unstretched case (i.e., the effect of inhomogeneity on product distribution is smaller), all other conditions being equal. Thus higher value of β gives lower value of X_s.

The physical factors that influence the product distribution parameter can be described as follows:

1. Stirring speed: Bourne et al. (1981b) and Bourne and Dell'ava (1987) showed from their experimental results that product distribution parameter X_s is inversely proportional to the impeller speed. Higher impeller speed generates higher turbulence which in turn, reduces the size of the diffusion reaction laminae, δ_o, and reduces the value of M. As a result less secondary product S is formed as well as a lower X_s. Bourne et al. (1981b) found that viscosity also influences the product distribution parameter, X_s, in a CSTR and stated,

> The improvement in mixedness ... with rising turbine speed is unlikely to reflect faster blending, in the sense of a shorter circulation or mixing time. If this were so, then in the turbulent region (R_e > 3900 here) a change in viscosity, which is known from many measurements not to influence the circulation time, would have had no effect on X_s. Macroscopic blending through convective (eddy) diffusion does not seem to be decisive for homogeneity at the molecular scale. (p. 1656)

Rice and Baud (1990) stated somewhat different results in this respect. Interestingly, they found reproducibly that X_s, as a function of stirring speed, N, went through a minimum (0.01) representative of nearly perfect mixing at N ≈ 500 rpm and then increased somewhat at N = 700 and 900 rpm. The reason behind this, they stated, is the extreme vortexing (lowering of free surface in the reactor) in this high N range causing the feed tube location to be nearly a surface feed point even though they injected B-solution in the impeller discharge stream. Location of feed point is also a physical factor that influences the product distribution. They used a Pfaudler-style (name comes form the arrangement of the baffle) batch reactor with three-blade retreat curve turbine impellers (**Figure 3.42**). **Figure 3.42** also shows the position of B-solution feed points into A solution already present in the reactor. In this figure z is the vertical distance from the reactor bottom and H is the height of the liquid inside the reactor. They also found that X_s decreases with increasing diameter and width of the impeller.

2. Location of feed point: Rice and Baud (1990) employed nine locations (combination of A, B, C and z/H = 1.0, 0.6, 0.2 in **Figure 3.42**) of feed point for injecting B-solution into A-solution already present in the reactor. They found that X_s was independent of lateral position but was highly dependent on vertical position.

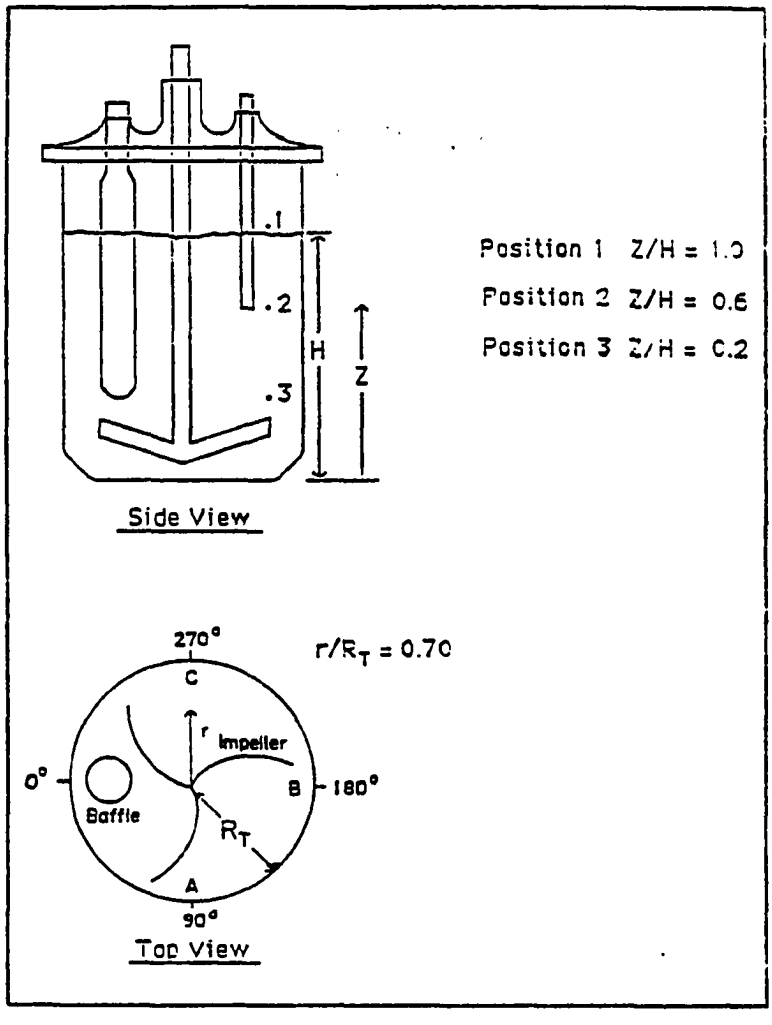

Figure 3.42. Impeller shape and B-solution feed point location (Rice and Baud, 1990)

Minimum X_s was obtained when feeding was done in location 3, near the impeller (z/H = 0.2)and the maximum was found when the feeding was done in location 1, near the surface (z/H = 1.0). Bourne et al. (1981b) observed that the maximum value of X_s was found when the feed was made near the surface (they designated this location position III; no figure is shown here), whereas the minimum was found not near the impeller (called position II), but somewhere below and inside the tip of the impeller (called position I). From their turbulence intensity measurement they attained the highest intensity in position II. Based on these experimental results they stated,

> The difficulty with injecting into the highly turbulent, radial jet leaving the turbine (position II) is probably that the time of exposure of the fresh feed to this turbulence level is short: the level falls rapidly as the jet hits the wall, is deflected axially and slows down. On the other hand, position I offers some chance of macromixing and formation of microeddies as the streams move axially and radially into and through the turbine, before reaching position II. (pp. 1658-1659)

The authors employed a CSTR mode of operation and introduced both A and B through two different feed pipes simultaneously. The feed pipes were located symmetrically on the opposite side of the impeller shaft for all positions (I, II and III).

David and Clark (1991) also illustrated that X_s is very much dependent on stirrer speed and the location of feed points (**Figure 3.43**). They worked with some basic-barium complex (A) and the HCl (B) in a competitive-consecutive reaction.

3. Type of injection: David and Clark (1991) showed that the type of injection of reactant B influences the product distribution parameter X_s (**Figure 3.44**). They indicated that the X_s varies inversely with the square root of the power input per unit

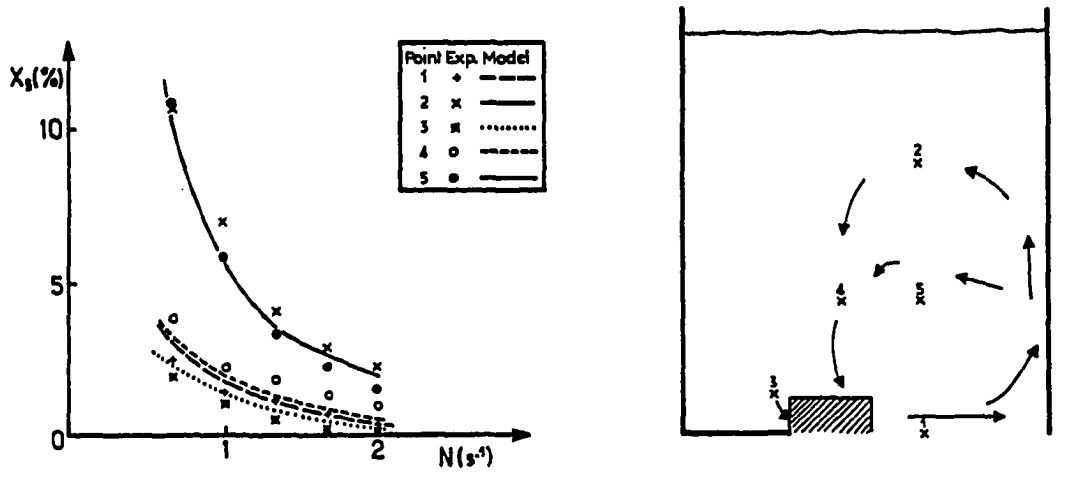

Figure 3.43. Product distribution parameter versus rotation speed in a stirred tank for five different points of addition of reactant B (HCl) (David and Clark, 1991)

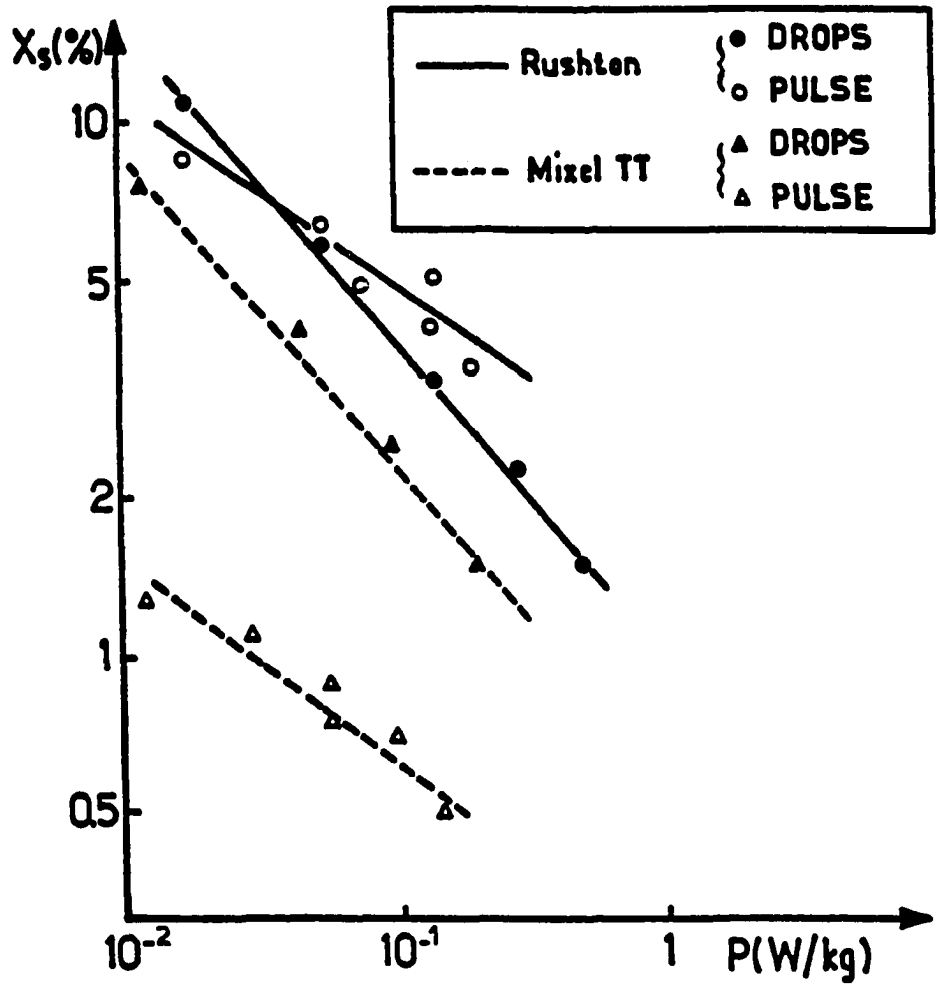

Figure 3.44. Product distribution parameter versus power delivered per unit mass of fluid for addition at point 5 (defined in Figure 3.43). Comparison of the performance of two types of impeller and two types of reactant B injection method (David and Clark, 1991)

mass in the case of dropwise addition (slow injection) and that X_s varies inversely with the one third power of the power input per unit mass for pulse addition. So for product selectivity and better mixing efficiency slow addition is better than the pulse addition.

3.6.5. Turbulent mixing and crystallization

Marcant and David (1991) working with calcium oxalate monohydrate batch precipitation have observed a significant impact of mixing on the crystallization process, especially the crystal size distribution (CSD). He also summarized some phenomena involved in the crystallization process and defined by various other researchers (Nyvlt et al., 1985; Marchal et al., 1988; Kulov et al., 1983; Matz, 1985 and Nyvlt and Karel, 1985). Those phenomena can be described as follows:

1. Nucleation: Solid formation starts with the appearance of very small crystals called nuclei. This process involves mainly homogenous primary nucleation during the first stage of precipitation where there are high values of supersaturation and heterogenous secondary nucleation when the molar concentration of crystals becomes significant.

2. Growth: Nuclei or small crystals grow by continuous collection of solute from solvent as long as supersaturation remains positive. It is often considered as a combination of two steps: mass transfer through crystal boundary layer and then integration to the crystal lattice.

3. Ostwald ripening: This is based on the Gibbs-Thomson-Oswald-Freundlich law, which states that crystals smaller than the certain limiting size of nuclei have

negative local supersaturation resulting in their dissolution (Kulov et al., 1983 and Matz, 1985).

4. Agglomeration and aggregation: Binary encounters of crystals and subsequent adhesion also lead to crystal growth (Nyvlt and Karel, 1985).

From their extensive study, Marcant and David (1991) observed that three factors are of prime concern in crystallization process. From their own experimental results and from the results of other researchers, they illustrated qualitatively the resulting effect of stirrer speed and feed point location in **Table 3.9**. The arrow in positive 45° (↗)indicates the enhancement of various crystal formation processes and the increase of crystal diameter and that in negative 45° (↘)indicates the rate decrease of the various crystal formation processes and the reduction of crystal diameter. Horizontal arrow indicates no influence and ? indicates undetermined influence. They also stated that changes in feed point location are much more important for micromixing effects and crystallization than modification of stirrer speed.

The other important factor that has had influence on crystallization process was the stirrer (impeller) type. They used two types of impeller: a Rushton turbine and a pitched blade impeller. The pitched blade impeller increased the overall crystallization rate and produced more crystalls of smaller size than the Rushton turbine. The pitched blade also achieved more conversion of solution phase into the crystalline phase. Conversion was determined by measuring the electrical conductivity of solution which decreased with the disappearance of solution (ionic) phase of the salt into the solid crystalline phase. Measured mass averaged diameter of the crystals was similar for both

Table 3.9. Influence of mixing variables on precipitation processes (Marcant and David, 1991).

	Rapid Local Process		Slow Processes Averaged over the Tank			Overall Effect
	Primary Nucleation	Secondary Nucleation	Growth by Integration	Diffusional Growth	Agglo-meration	N_c?
Same Feed Pt. Increasing Stirring Speed	Enhanced $N_c\nearrow$, $D\searrow$, $r\nearrow$	Enhanced $N_c\nearrow$, $D\searrow$, $r\nearrow$	No Influence $N_c\rightarrow$, $D\rightarrow$, $r\rightarrow$	Enhanced $N_c\rightarrow$, $D\nearrow$, $r\rightarrow$	Enhanced $N_c\searrow$, $D\nearrow$, r	D? $r\nearrow$
Same Stirring Speed, Addition in a more Tur--bulent Zone	Enhanced $N_c\nearrow$, $D\searrow$, $r\nearrow$	No Influence $N_c\rightarrow$, $D\rightarrow$, $r\rightarrow$	No Influence $N_c\rightarrow$, $D\rightarrow$, $r\rightarrow$	No Influence $N_c\rightarrow$, $D\rightarrow$, $r\rightarrow$	No Influence $N_c\rightarrow$, $D\rightarrow$, $r\rightarrow$	$N_c\nearrow$ $D\searrow$ $r\nearrow$

N_c = number of crystals per unit volume; D = crystal mean diameter; r = overall crystallization rate.

the stirrers until 5 minutes of mixing, but beyond that two-fold increase was observed for Rushton turbine over the pitched blade stirrer. It should be noted that both the impellers were stirred at the same speed (i.e. 400 rpm). So, energy input per unit mass of the solution was not the same for both the cases.

In determining the effect of mixing on the precipitation of barium sulfate from aqueous feedstreams of barium chloride and sodium sulfate in a mixed suspension mixed product removal (MSMPR) reactor, Fittchett and Tarbell (1990) observed that impeller speed and the feed concentration influenced the precipitation process. Growth rate (μm/s), mean particle length (μm) and mass transfer coefficient of materials from bulk solution onto the particle surface increased with impeller speed (ranged from 0 to 1200 rpm) and the shape of the particle varied with the feed concentration of one of the reactants. The reactor was operated in the steady state condition, and a two-blade pitched blade axial impeller with a pitch angle of 62 degree was used. The crystal morphology was studied using a scanning electron microscope (SEM) and a Hiac/Rayco model 4300 particle size distribution analysis system equipped with a Hiac/Rayco model ASAP aspirating sampler and a model CMH-150 high particle concentration sensor. The mixing was done for a very brief period (up to 38s maximum) during which only the primary nucleation was supposed to take place.

3.6.6. Turbulent mixing and coagulation

From the above discussions, it is understood that the fast chemical reactions are diffusion controlled and extremely sensitive to mixing. Previously it has also been seen

that based on pH and coagulant concentrations, different hydrolysis species are formed when metal coagulants are added to water. Also in water treatment, coagulation by metal salts occur predominantly by two mechanisms: (1) adsorption of hydrolysis species on the colloid surface, causing charge neutralization; and (2) sweep coagulation, where interactions occur between the colloids and the precipitating hydroxide. **Figure 3.45** (Amirtharajah and Tambo, 1991) illustrates the production of intermediate kinetic hydrolysis species of alum prior to formation of the aluminum hydroxide precipitate and the two mechanisms of coagulation that are dependent on the chemical species formed. The reactions that precede charge neutralization with alum are extremely fast; they occur within microseconds without the formation of Al(III) hydrolysis polymers and within 1s if polymers are formed. The formation of aluminum hydroxide precipitate before sweep floc coagulation is slower and occurs in the range of 1 to 7s.

It appears from **Figure 3.45** that the hydrolysis steps of metal coagulants are thus similar to multi-step consecutive (series) reactions and their competitive nature in distinguishing between two modes of coagulation made them susceptible to mixing. The speedy reaction times imply that for charge neutralization, it is imperative that the coagulants be dispersed in raw water stream as rapidly as possible (less than 1s) so that the hydrolysis products that develop in 0.01 to 1s will cause destabilization of colloid. In contrast, hydroxide precipitate formation, in sweep coagulation, is in the range of 1 to 7s and it is evident that extremely short dispersion times and high intensities of mixing are not as crucial as in charge neutralization.

Figure 3.46 (David and Clark, 1991) compares typical mixing, molecular

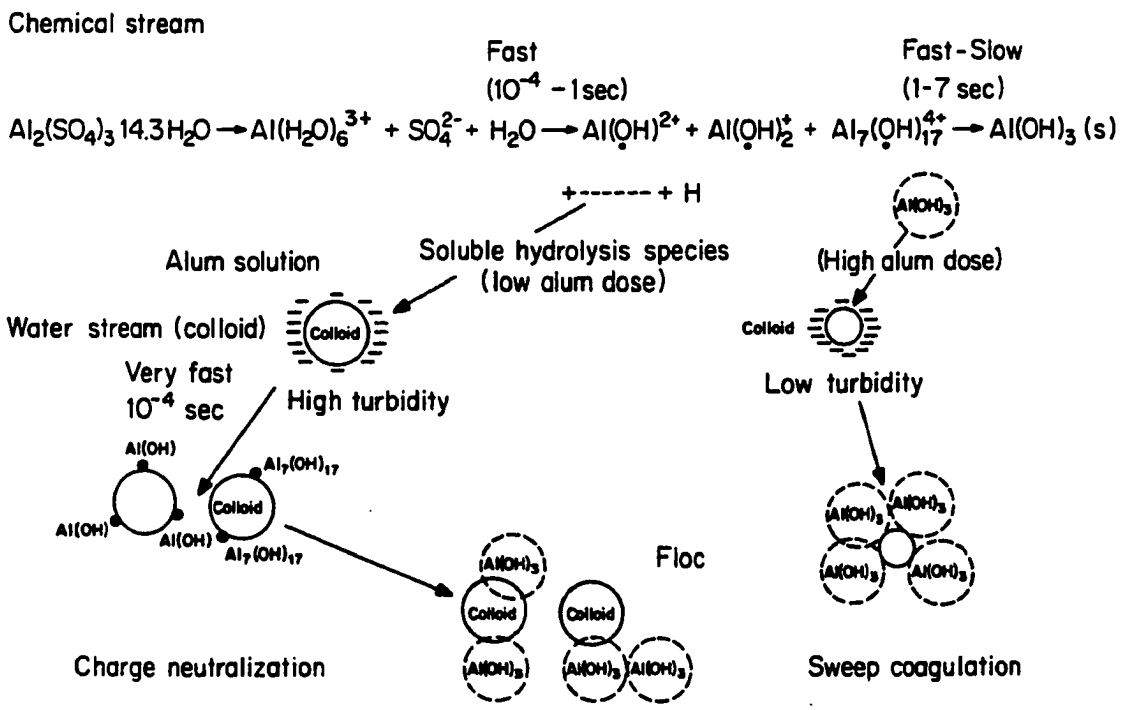

Figure 3.45. Reaction schematics of alum coagulation (Amirtharajah and Tambo, 1991)

diffusion, and metal ion hydrolysis characteristic times in a hypothetical 100-L reactor with a Rushton turbine over a range of energy dissipation conditions described by the velocity gradient, G. This figure incorporates both theoretical and experimental results of various research workers. In this figure $t_{turnover}$ is called the average turnover time of vessel contents due to impeller pumping and can be given as $t_{turnover} = V/Nd^3$. The $t_{Kolmogrov}$ is called the local Kolmogorov turnover time and can be given as $t_{Kolmogorov} = (\nu/\varepsilon)^{1/2}$. The $t_{Corrsin}$ is called the local mixing time in isotropic turbulence which falls between $t_{turnover}$ and $t_{Kolmogorov}$. The diffusive time scale is the time for the metal ions to diffuse over distance correspoonding to one-half the Kolmogorov microscale and can be given as $t_d = \eta_k^2/(2D)$.

V = volume of the suspension (cm^3)

N = impeller speed (rps)

d = impeller diameter (cm)

D = diffusivity of metal ion ($cm^2\ s^{-1}$)

other variables were defined earlier.

David and Clark (1991) called $t_{turnover}$, $t_{Kolmogorov}$, and $t_{Corrsin}$ the mixing time scales and t_d the diffusive time scale. From **Figure 3.46** it appears that all those time scales are a function of mixing intensity and almost all of them are in the order of seconds (except Kolmogorov time scale which about 0.1 s) for a wide range of G values, which span the typical values in practical water treatment. But the reactive time scales for aluminum and ferric hydrolysis reactions are independent of mixing intensity and are in the order of microseconds. It should be noted here that the ferric reactions shown here are for

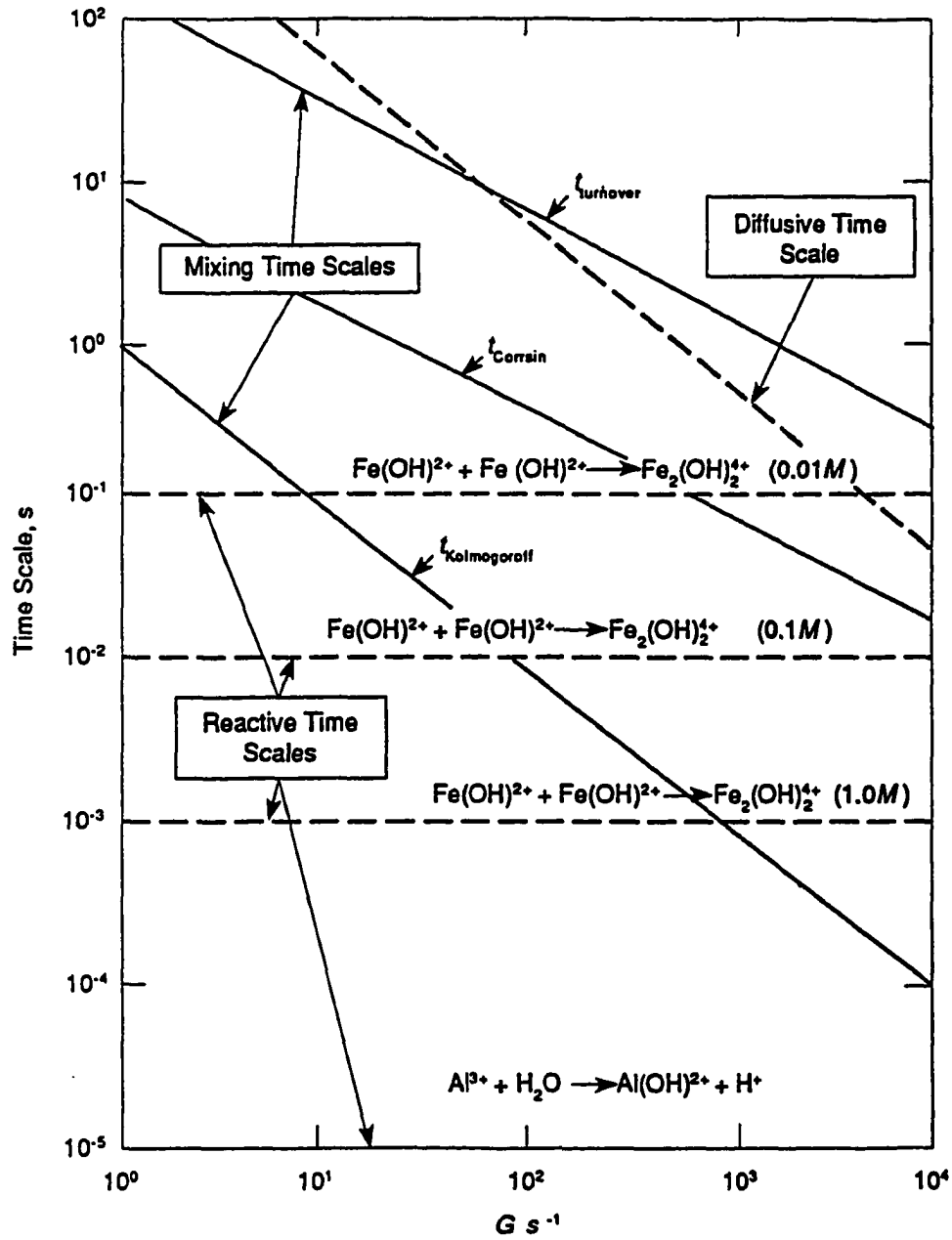

Figure 3.46. Comparison of mixing, diffusive, and reactive time scales in 100-dm^3 Rushton backmix reactor (David and Clark, 1991)

very high concentrations. Concentrations used for coagulation are usually much lower than these concentrations. The reactive time scales may be in the seconds region in those cases. It should also be noted that the ferric reactions shown in this figure are for two monomers combining to form a dimer. The time scale for the formation of monomer may not be comparable to these time scales. But the main purpose of this diagram is to indicate that the reactive time scales for hydrolysis reactions of metal coagulants are either much shorter than or comparable to mixing time scales. So coagulant hydrolysis reactions in typical mixers would be diffusion limited and very high intensity turbulent mixing (or micromixing) would be beneficial for the close contact of reactant molecules (here coagulant and water molecules) in order for the reaction to proceed. Also in fast, complex, consecutive hydrolysis reactions, it is expected that the mixing intensity will influence the final distribution of hydrolysis and precipitation products, e.g., the relative distribution of polymeric metal hydrolysis products and metal hydroxide (David and Clark, 1991).

3.6.7. Flow field homogeneity and flocculation

Figure 3.37 illustrates one image of vortex stretching. In part(a), there are two vortices of equal size. Each of these vortices could represent a volume of fluid containing a homogenous distribution of particles to be flocculated. Before stretching the particles are moving relative to the bulk flow, but are stationary with respect to each other. As one vortex undergoes stretching, a localized velocity gradient (i.e., shear gradient) is induced in the fluid contained in the vortex. This localized velocity gradient

induces particle collisions. The magnitude of the localized velocity gradient will be dictated by the diameter at which vortex tube stops stretching and becomes bound by viscous forces. The Kolmogorov microscale of turbulence is an approximate indicator of this lower size of eddy or vortex diameter.

The above picture and the entire discussion of energy cascade and dissipation have dealt with idealized turbulence. That is, turbulence is homogenous and isotropic and a simplified model of this turbulence was first proposed by Kolmogorov. The model proposed by Kolmogorov has given the following information regarding homogenous, isotropic turbulent flow and flocculation (Hanson, 1989):

- The largest eddies are strictly a function of reactor geometry, and only the largest eddies are a function of reactor geometry.
- In a homogenous turbulent flow field the smallest eddies will tend to be isotropic even if the larger eddies are anisotropic.
- At the energy input typical of flocculation, the inertial subrange probably does not exist.
- Turbulent eddies only interact effectively with features in the flow of nearly equal size, therefore even the smallest turbulent eddies do not interact with primary particles.
- Localized shear fields formed by the turbulent eddies do interact with the primary particles, and will cause flocculation.
- The smaller the Kolmogorov microscale of turbulence the more intense the localized velocity gradient.
- The energy dissipating spectrum is non-linear, and below the microscale of turbulence (η_k), the rate of dissipation is decreasing.

Many research studies based on dynamical system theory, i.e. chaos theory, depend on this simple and idealized intuitive picture of turbulence. This is encouraging to many researchers in flocculation because it indicates that, at

> least for intuitive purposes, this simple picture developed here is not to far from the mainstream of turbulence research. (pp. 71-72)

Now the deviations from above idealized model of turbulence will be discussed. Turbulence in an actual mixed tank reactor is far from homogenous and isotropic. Many researchers such as Cutter (1966), Rao and Brodkey (1972), Van't Reit et al. (1976), Okamoto et al. (1981), Clark (1985), Baldyga and Bourne (1984c), Bourne and Dell'ava (1987) and Rice and Baud (1990) found an order of magnitude spatial variation of energy dissipation in a circular tank with turbine type impeller. This significant variation was observed with baffled and unbaffled tanks as well as batch and continuous flow operations. **Figure 3.31** represents the energy pathways in an actual tank reactor and **Figure 3.47** shows a Rushton impeller and the flow near the impeller. The Rushton impeller is similar to the 2-blade turbine impeller used in this study, and it has been the subject of extensive experimental and theoretical works. From this Rushton impeller, some insight into the complexities inherent in the flow field of a stirred tank reactor will be gained.

From **Figure 3.31**, the first thing to notice that only a fraction of the energy per unit mass (ε) put into the reactor actually generates the turbulence. Some of the energy is dissipated directly by the impeller, and some is dissipated directly in the fluid shear. Clark (1985) indicated that about 30 percent of the total energy put into the reactor could be lost without producing any turbulence.

From the work of Van't Reit et al. (1976), it is understood that the impeller does not generate turbulence directly. It generates non-random pseudo-turbulent flows

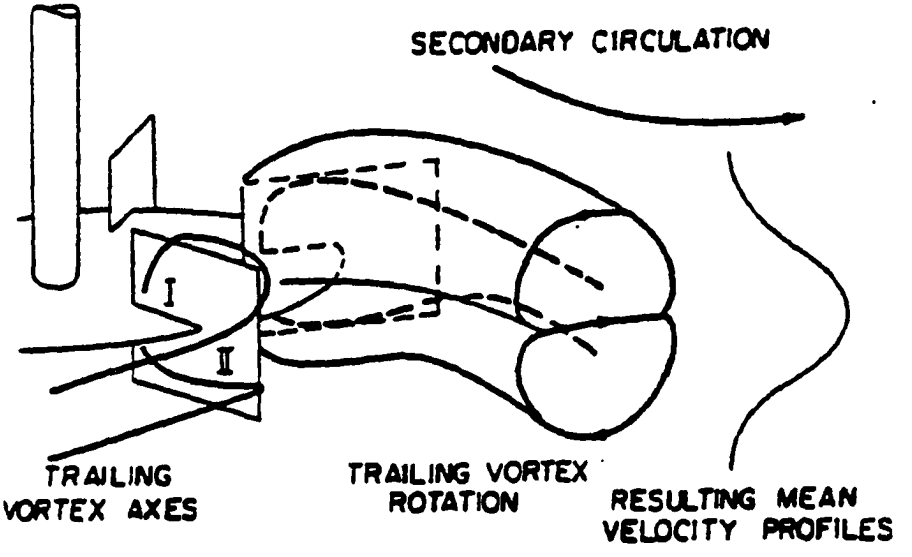

Figure 3.47. Trailing vortices behind a Rushton-type turbine impeller and resulting mean velocity profile (Hanson, 1989)

consisting of trailing vortices, impeller discharge flows, and recirculating flows, which in turn, generate turbulent flow. Although, these flows generated by the impeller exhibited intense fluctuations, they stated, "In the measurements in the impeller discharge, the following features have been noted: (a) there is a strong periodicity in the velocity near the blade as measured by the stationary probe, which is related to blade passage frequency; (b) turbulence intensity varies strongly with vertical distance from the agitator plane; and (c) the frequency-based energy spectra are inconsistent with isotropic turbulence theories" (p. 407).

Rao and Brodkey (1972) found in a continuous flow reactor that both the mean velocity (U) and the turbulence intensity (u') measured by hot-film anemometer were a function of radial and vertical distance. But relative intensity (u'/U) was almost independent of position. This implies the influence of trailing vortices and recirculating flow near the impeller (which was termed as pseudo-turbulence by Van't Reit et al., 1976). Rao and Brodkey (1972) also cited Batchelor's (1960) work which indicates that the probability density of the velocity fluctuations at a point for fully turbulent and nearly isotropic flow is close to the normal distribution as a consequence of central limit theorem. But in their work the authors found a significant deviation of that (probability density of velocity fluctuations) from normal distribution which indicated that the flow in their reactor was non-isotropic and intermittently turbulent. Their probability density distribution was skewed negatively, and the peak was shifted to the right of the mid-point indicating a non-turbulent region for a larger percent of time.

Okamoto et al. (1981) indicated that the rate of energy dissipation in the impeller

discharge region was 7 to 11 and 6 times greater than the bulk mean value for unbaffled and baffled circular vessels respectively. Also there was an overall 50-fold and 40-fold variation in value of ε from its maximum to minimum depending on positions within the vessel for unbaffled and baffled vessels respectively. The baffle slightly improved the uniformity of energy distribution.

Cutter (1966) showed that the ratio of local to average energy distribution rate (ε/ε') varies from about 70 near the tips of the blade to about 3.5 near the wall on the centerline of the impeller stream. Outside the impeller stream this ratio may attain a minimum value of 0.26 giving a 270-fold variation in the value of ε from its maximum to minimum. Rao and Brodkey (1972) found similar variations. Van't Reit et al. (1976) noted that such a high value of the ratio (ε/ε') is due to the large influence of pseudo turbulence created by blade passage and vortex rotation frequencies. Velocity measurements were made by either photographic technique (Cutter, 1966) or by stationary hot-film anemometer (Rao and Brodkey, 1972 and Van't Reit et al., 1976) in the above cases and both were influenced by the pseudo-turbulence. Van't Reit et al. indicated that real turbulence in the impeller discharge stream can only be measured reliably by means of a probe rotating with the stirrer. Cutter also estimated the following:

- 20% of the energy put into the reactor is dissipated in the impeller itself,
- about 50% of the total dissipation takes place in the impeller stream and
- about 30% of the energy is dissipated in the rest of the tank volume. (p. 44)

Figures 3.48 and 3.49 (Placek et al., 1986) show visually the energy generation and dissipation profiles for the upper right quadrant of the vessel stirred by a Rushton impeller. **Figure 3.48** shows the calculated energy profile and **Figure 3.49** shows the energy dissipation profile for the same region. These profiles were generated by solving a semiempirical energy transport differential equation with the help of a numerical technique after employing several assumptions and boundary conditions. These figures show the only the relative spatial variation, not the absolute values. These figures show that high kinetic energy and dissipation regions have almost overlapped.

By reviewing the works of several researchers Hanson (1989) concluded the following:

- It seems reasonable that mixer geometry may be an important variable in flocculator efficiency.
- It also seems that a mixer geometry which distributes the energy uniformly throughout the reactor vessel may have some advantages in flocculation where both growth and breakup are of concern.
- The areas of low energy in the recirculation region are areas which are less likely to be efficient in flocculation of small particles, and also less prone to causing floc breakup.
- The high energy regions are likely to efficiently flocculate small particles, and also breakup the floc which are formed in the less energetic regions.
- Is average ε or G, which is based on average ε, a reasonable parameter to use in quantifying a turbulent flow field which is obviously non-homogenous. (pp. 80-82)

Based on Cutter's (1966) work, Amirtharajah and O'Melia (1990) illustrates the energy dissipation and the corresponding G-values in the three zones relative to an arbitrary

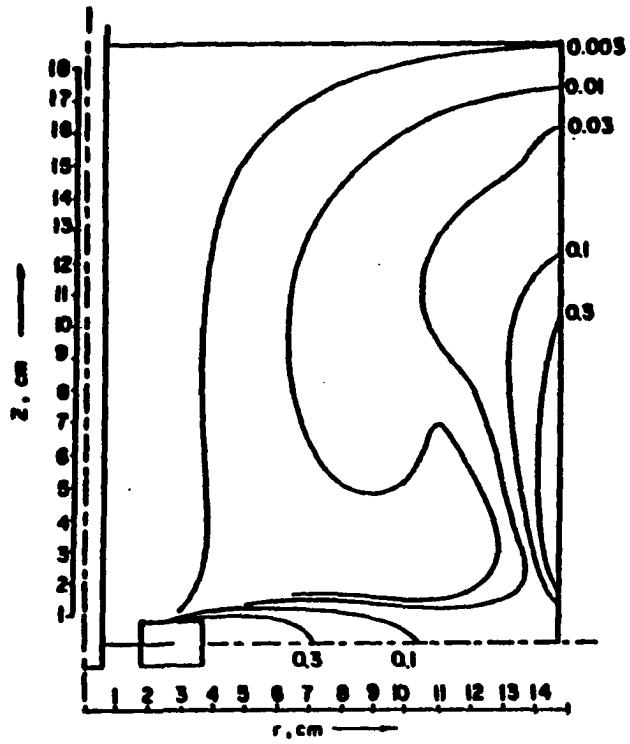

Figure 3.48. Calculated profiles of overall kinetic energy of turbulence for flow field around a Rushton-type impeller (Placek et al., 1986)

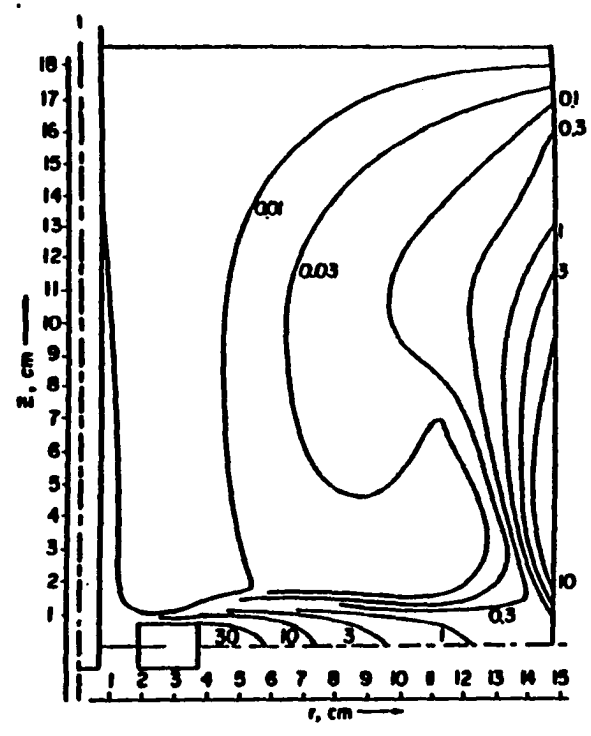

Figure 3.49. Calculated profiles of the dissipation rate of turbulence for flow field around a Rushton-type impeller (Placek et al., 1986)

average value of power and G for the entire tank equipped with a Rushton type impeller (**Figure 3.50**).

3.6.8. Flocculation experiments with alternative impellers

The researchers in water treatment flocculation have adopted a relatively simple method for determining the effect of mixing on flocculation. They employed different impellers either at constant G or constant power for comparison, and measured the outcome based on relative turbidity, filtration number or number of primary particles.

By comparing 30 geometric variations of a turbine impeller, Drobny (1963) concluded: "It appears definite that the flocculation process may be made more efficient with respect to power input by simple variations in the paddle designs" (p. 29). He flocculated Fullers earth with alum at a pH between 6 and 7. The alum dose was not reported, but based on the information presented, the flocculation mode was probably sweep floc. Flocculation efficiency was based on relative turbidity and the comparison was based on a constant power per unit volume for all of the impellers.

Argaman and Kaufman (1968 and 1970) and Hanson and Cleasby (1990) studied the two impeller designs shown in **Figure 3.51**, namely a 2-blade turbine impeller and a stake and stator (S&S) impeller. These two impellers represent the two extremes in the sense of energy input into the reactor. The turbine impeller delivers total energy in the centralized location and energy transfer takes place through pseudo turbulence and true turbulence (vortex stretching) into the bulk of the tank. The stake and stator on the other hand delivers power in a decentralized fashion into the whole tank volume.

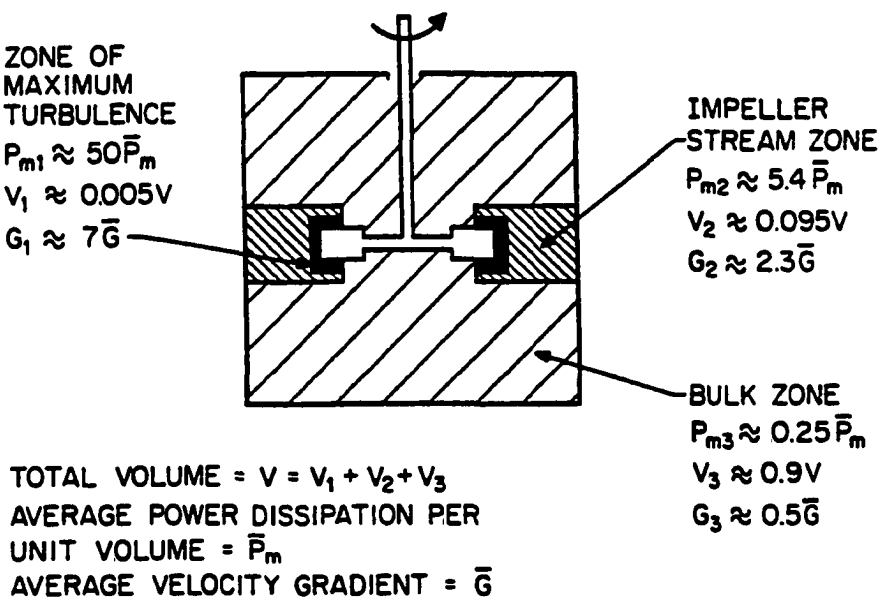

Figure 3.50. Partitioned energy dissipation in a stirred tank (Amirtharajah and O'Melia, 1990)

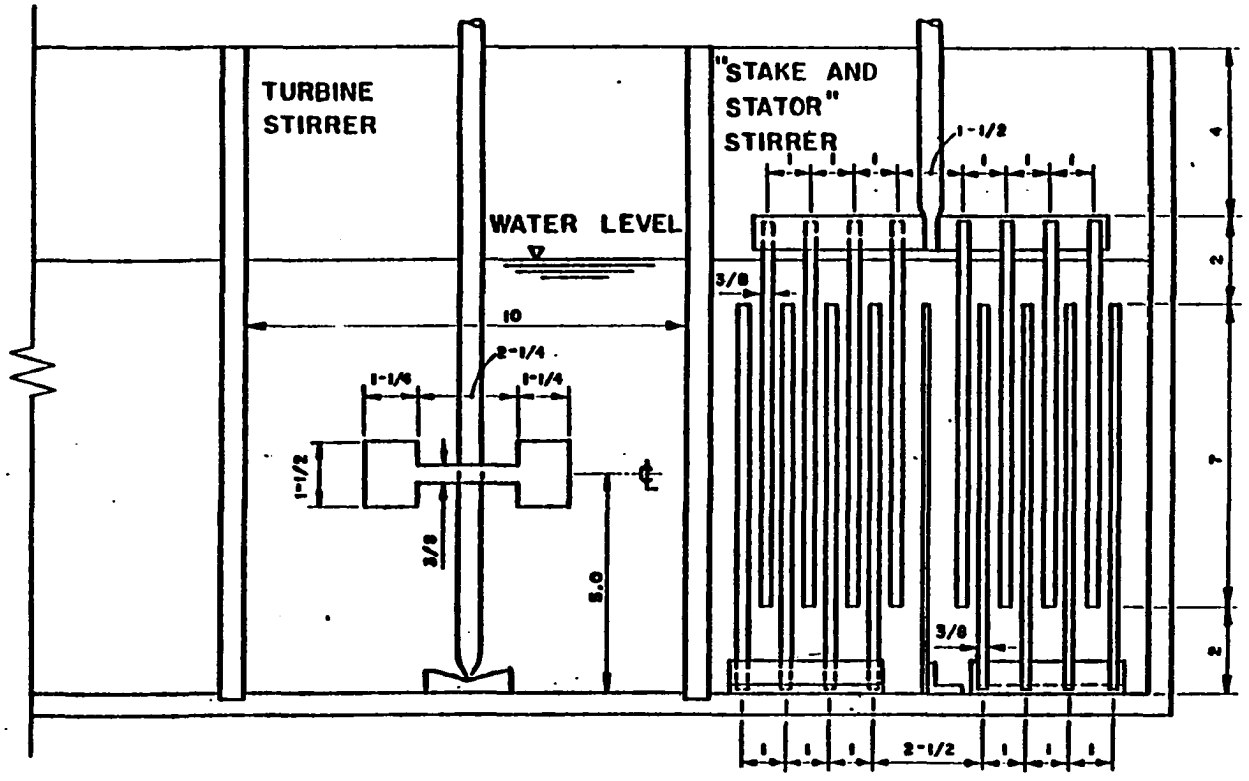

Figure 3.51. The turbine and stake and stator impellers used by Argaman and Kaufman (1968) and Hanson and Cleasby (1990); all dimensions are in inches

Argaman and Kaufman (1968) flocculated a 25 mg/l kaolinite suspension using 25 mg/l of alum as $Al_2(SO_4)_3.14H_2O$ at an unspecified pH. Based on such a high dose, it can be assumed that they were utilizing the sweep floc mode. The flocculation efficiency was based on the change in turbidity due to flocculation and sedimentation. They took two samples for every flocculation experiment; one immediately after the flocculation and the other was a supernatant sample taken at the end of 30 minutes settling. Before turbidity measurement, both samples were shaken vigorously to convert all the particles into primary particles. The percent difference between these two was considered the reduction of primary particles. It is very likely that all the flocs would not be reduced to primary particles simply by shaking, yielding a serious quantitative error. However this error did not invalidate the relative performance of the impellers in flocculation. They concluded that the performance of the S&S was superior to the turbine impeller. Their work was performed at 21° C. They also noted that G alone was not adequate for characterizing the flow field.

Hanson and Cleasby (1990) on the other hand worked in an A/D region at two different temperatures (20 and 5° C) with two energy levels (G=60/s and 22/s). They employed a direct approach in measuring flocculation efficiency. They measured the number of particles with an Automatic Image Analyzer (AIA) and related the flocculation efficiency to the speed of reduction of the total particle number during flocculation. From their extensive study they concluded:

- Stake and stator (S&S) and turbine impellers performed identically at both energy levels at 20°C and flocculation efficiency was better at higher

energy input.

- At 5°C the S&S started out at a slower rate of flocculation but eventually overtook the turbine. At higher energy level (G = 60/s) there was no time lag for turbine impeller, but a 10-min time lag was observed before the S&S impeller produced any noticeable change. At the end, this impeller produced better result than turbine impeller. At lower energy level both impellers showed a significant time lag, and time lag for S&S was larger than that of turbine impeller (20 min vs. 10 min).
- In the breakup study of flocculated sample with both the impellers at high intensity (that of rapid mix); they observed that turbine impeller generated many more primary particles than the S&S impeller. They concluded that the localized shear field produced by the turbine is much more intense than the localized shear fields produced by the S&S at the same G or same energy input.

Their study is not immune to flaw. For counting the particles they always obtained the samples from the discharge stream of turbine impeller which does not necessarily represent the true picture of the bulk of the tank. So the high initial flocculation rate and very high number of primary particles produced during breakup may have magnified the actual results to some extent.

Patwardham and Mirajgaonkar (1970) compared 6 impeller geometries, flocculating clay using alum at a pH of 7.6. Based on this pH it is probable that the work was performed in the sweep floc mode. Nothing was said about the dose and the

mode of coagulation. **Figure 3.52** shows the basic impeller geometries, experimental conditions, and results. All the paddles were submerged to a depth of 10 cm in the suspension water and water depth was 11.8 cm as indicated in **Figure 3.52**. The following definitions were given for the terms used in **Figure 3.52.**

A = area of the blade of the paddle (cm^2)

A_c = area of cross-section of the flocculation chamber (cm^2)

S = speed of the paddle (rps)

k = ratio of water speed to the speed of the paddle

F_N = flocculation number = $(\Sigma WL)/(Q\sqrt{A_c})$

L = paddle edge length (cm)

Q = flow of water through the chamber (liter/min)

W = The rate of water displaced by a blade of a paddle (liter/min) $= \int_{r_1}^{r_2} D\ dr\ 2\ \pi\ r\ S$

D = depth of paddle blades (cm)

r = distance of the center of blade from the paddle center line (cm)

r_1, r_2 = distance of blade edges from center of the paddle (cm)

S' was not defined. The calculated water displacements for impellers 1, 2, 3, 4, 5, and 6 in **Figure 3.52** were 22.6, 27.2, 29.1, 31.6, 51.0, and 36.5 liters/minute respectively.

Dimension of Ar^3 in the third column of **Figure 3.52** should be cm^5 instead of cm^4. No definition was given about the theoretical G_m and the paddle edge length (L). But from the information provided the paddle edge length can be viewed as wetted perimeter created by all the blades of the paddle and G_m can be considered as the average G defined earlier in this study.

Depth of water 11.8 cms
Surface Area 127 sq.in
Cross Area 157.5 sq.in.
Volume 1500 cc.

PADDLE DETAILS

Speed 40 r.p.m.
Stirring time 20 mins
Temp. 24 Deg. C
pH 7.6

S. No.	Paddle	A_r^3 cm^6	$\frac{Ax100}{A_c \times P}$ A	P	Paddle edge length cms	Theoretical S'	Theoretical 1-k	Theoretical G_M	Flocculation Number F_N	Settling velocity cm/min	Turbidity Residual p.p.m.	Width of blades / Width of opening	Efficiency of turbidity removal
1		1845	20	13.2	42	7.4	0.815	69.5	283	.3816	20	.25	82
2		1845	39.6	26.1	64	7.35	0.798	67	379	.4572	17	.6491	85
3		1845	39.2	25.9	84	9.45	0.764	64	570	.4826	16	.6485	85.5
4		1845	50	33	185	10.32	0.746	61.5	1103	.635	10	1.00	91
5		1841	52	34.3	234	12.5	0.686	57.5	1519	.762	7	1.082	94
6		1815	73.3	48.5	54	13.3	0.666	51.5	600	.635	11	1.987	90

Figure 3.52. Geometry of the paddles used by Patwardham and Mirajgaonkar (1970)

They also plotted power characteristics for different impellers and showed that power characteristics for impellers 1 through 5 were almost the same up to 40 rpm. No definition of power characteristics was given; also it was not explained how the theoretical G_m was different for those five impellers with same power characteristics. The impellers were rotated at 40 rpm with variable G_m for the different impellers. Settled turbidity was used as the measure of flocculation efficiency. The effect of impeller geometry was considered to be the main reason for the variation of flocculation efficiency. They also concluded that G_m is not adequate for deciding upon the best flow pattern to achieve effective flocculation, and that G_m needed to be supplemented by other suitable design criteria. They further stated that the impeller which provided the highest displacement of water by the blade (W) and the highest paddle edge length (L) for the same G_m, seemed to be the most beneficial.

Bhole and Limaye (1977) worked with five different container shapes of 1 liter containers and with five different impeller geometries, to determine the effects of container shape and impeller geometry on flocculation efficiency. The container shapes used in their study were circular, hexagonal, pentagonal, square, and triangular in horizontal cross-section. The horizontal cross sectional area of all the tanks were 78.5 cm^2 . The five impeller geometries used by them are shown in **Figure 3.53.** The area of each paddle was 19.354 cm^2. No information about paddle location inside the tank was given. The flocculation experiments were conducted using 25, 50, 75, and 100 mg/l Fuller's earth suspension at pH = 7.0 with alum dosages of 1, 5, 10, and 20 mg/l. The flocculation speeds were 20, 40, and 60 rpm for all the impellers. So it is likely that the

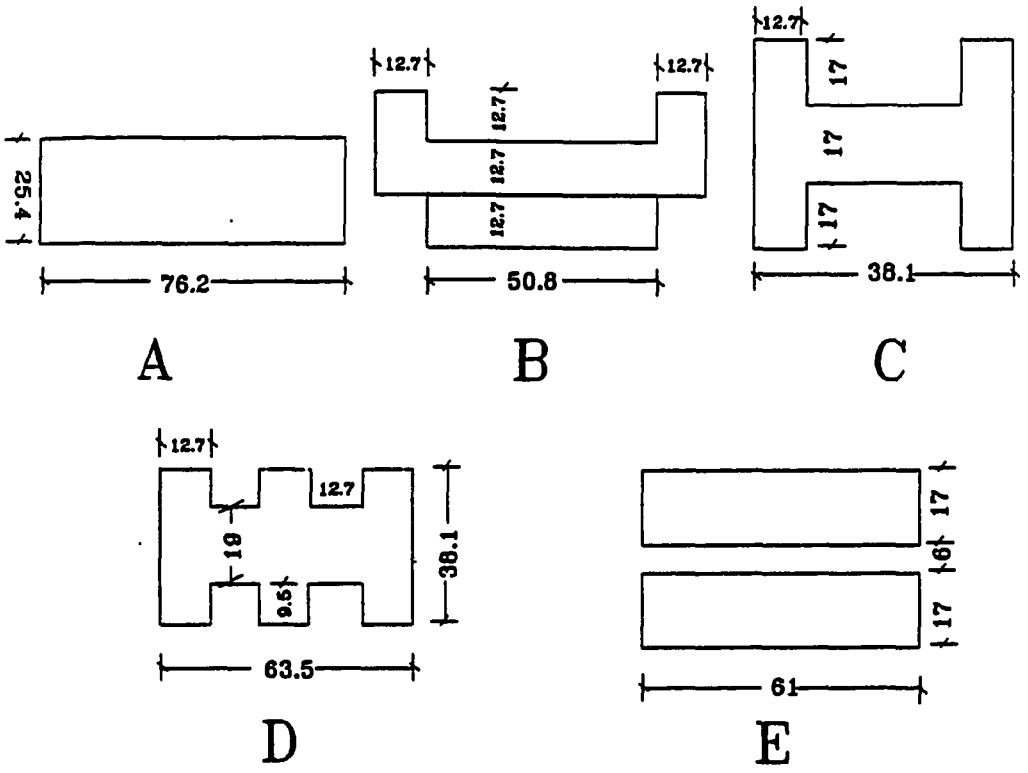

Figure 3.53. Geometry of the paddles used by Bhole and Limaye (1977). All dimensions are in mm

energy input was different for different impeller geometries. Flocculation efficiency was measured by the ratio of final turbidity to the initial turbidity. But no information was given about the final turbidity, whether it is at the end of flocculation or after some time of settling.

Working with flat blade impeller (shape A) and the five containers mentioned above (using all the Fullers earth concentrations and coagulant dosages), Bhole and Limaye (1977) found that pentagonal container gave the best result. Working with various combinations of impeller geometry and container shapes, they concluded that impeller D performed best with every container shape under all the conditions employed (combinations of Fullers earth concentration and coagulant dosages). The best flocculation results were obtained when impeller shape D was used with pentagonal container. The second best result was obtained with the same container and the impeller shape C.

Ives (1984), working in a 1-L reactor, compared nine impeller geometries as shown in **Figure 3.54**. A 16.7 mg/l kaolinite suspension was flocculated with $Al_2(SO_4)_3.16H_2O$ at unspecified pH and dose. Based on the information provided, it is likely that the work was performed in the sweep floc mode. He stated that the experiments were performed under the same conditions, but did not explicitly mentione what this meant. Based on the circumstances it is assumed either constant power input or constant G. Two measures of flocculation were used to evaluate those nine impellers: settled turbidity and filtration number (F) based on filtration of the flocculated water without settling. F can be defined as follows:

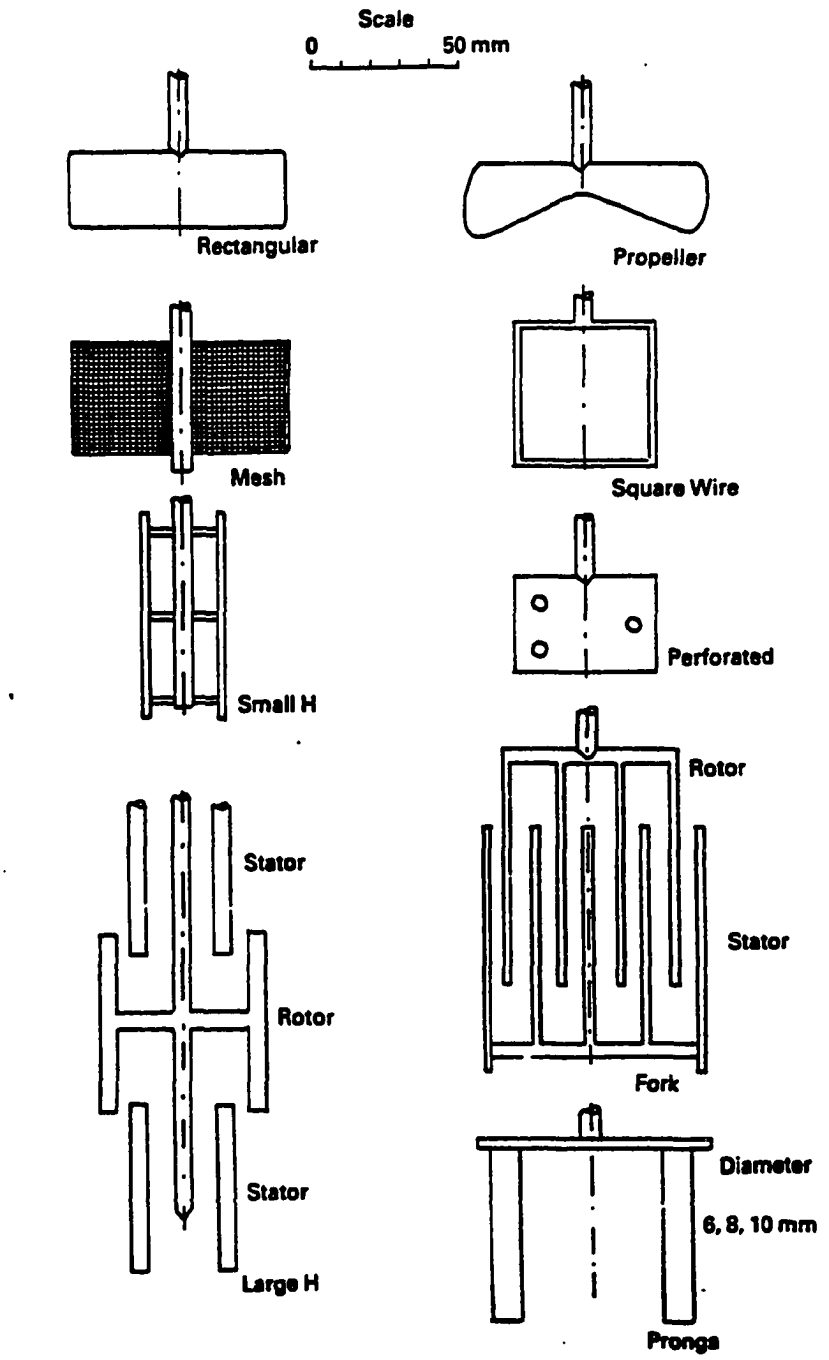

Figure 3.54. Geometry of the paddles used by Ives (1984)

$$F = (HC_F)/(V_aC_ot)$$

where, H = headloss, V_a = approach velocity, t = time of operation, C_o= inlet turbidity and C_F= outlet turbidity.

The lower the filtration number, the better the flocculation performance. He also showed a significant geometry effect on turbidity removal and filtration number. Although the performance order based on turbidity removal did not exactly match with that based on filtration number, the results indicated that the performance of the wire mesh was among the best three. The size of the mesh opening was not presented.

Koh and his colleagues (1984, 1987) addressed the non-homogenous nature of the turbulent flow field associated with turbine impeller in modelling orthokinetic flocculation. They used a fully destabilized suspension for flocculation modelling in a compartmentalized reactor which was divided into a number of regions (based on variable energy dissipation). Volume averaged shear rate, based on energy dissipation values from the literature was used to model the flocculation process. Comparing the results for various numbers of compartments, they concluded that there was little advantage in considering more than two compartments (impeller region and bulk flow region).

The above authors have also pointed out that the effective mean shear rate for flocculation is not the same as the mean value obtained from power dissipation per unit mass (ε), but is equal to the volume average value obtained from the first moment of the shear rate distribution. This quantity is highly independent of the system geometry. Experimental results indicated that the flocculation efficiency in a couette flow reactor

and in a stirred tank reactor are comparable if the effective mean shear rates are used.

Casson and Lawler (1990) studied the effect of small scale motions (micromixing) on flocculation or interparticle contact. They employed an oscillating grid impeller to generate small scale fluid motions directly. The flocculator was an acrylic cylinder into which a series of grid sections at even spacings was suspended horizontally and oscillated vertically (**Figure 3.55**). Each grid section was composed of an acrylic grid and two stainless steel grids. The acrylic grids had 1.25 inch (3.18 cm) squares (center to center) and were constructed of 0.25 inch (0.635 cm) square bars. A 4x4 mesh (16 grids per square inch) stainless steel grid with 0.125 inch (0.318 cm) round bars was placed on both sides of each acrylic grid. No information about reactor height and spacing of grid sections was provided. This type of oscillating grid impeller provided a well defined turbulent flow field for experimentation by directly generating small scale motions.

They stated that the two mixing conditions they used with this oscillating grid reactor had characteristic mixing time of only 12 seconds which is much less than that in a full scale flocculator (they mentioned 77 seconds for Davis Water Treatment Plant, Austin, Texas). The characteristic mixing time was defined as the time for the volume of a water in a given flocculator to be directly displaced by the mixing apparatus (i.e. the ratio of the total volume in the reactor to the volume of water per unit time "cut-through" by the mixing apparatus). The two mixing conditions used in the flocculation experiments were a grid oscillation frequency of 0.25 Hz with an amplitude of oscillation of 0.75 inch (1.91 cm) and a frequency of 0.75 Hz with an amplitude of

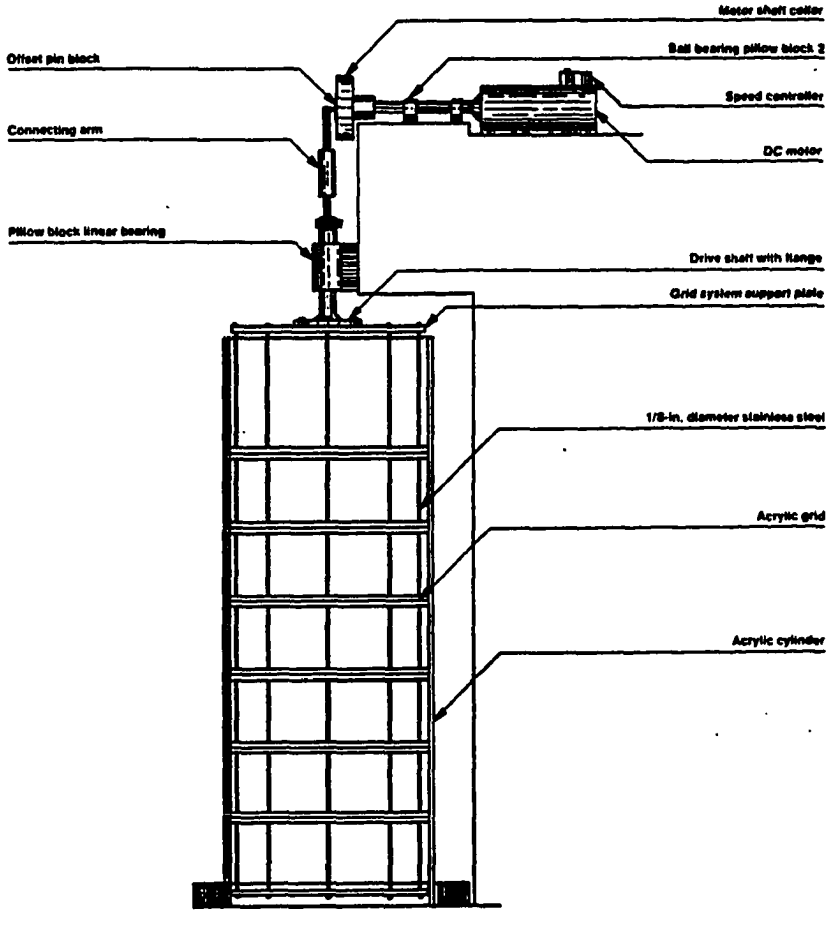

Figure 3.55. Schematic of the oscillating grid flocculator used by Casson and Lawler (1990)

oscillation of 0.25 inch (0.64 cm). The mean velocity of the grid was 1.91 cm/s in both of these operating conditions.

One dimensional time records of fluid velocity in the flocculator were measured by Laser Doppler Velocimeter (LDV) in both vertical (direction of the grid motion) and Horizontal (perpendicular to the direction of grid motion) planes at several locations in the reactor. From these measurements of velocity they obtained a power-spectral-density function. A similar power-spectral-density function was also used by Argaman and Kaufman (1968). The basic principle of the power-spectral-density analysis can be illustrated as follows (Frost, 1977):

> If the signal from a probe measuring, say, the u_1 (one velocity component) turbulence velocity fluctuations is processed directly through a root-mean-square meter, the reading will be proportional to the mean turbulence kinetic energy $\overline{u}^2_1$ and will include the contributions from the entire frequency range of eddies. However, if the signal is first processed through a spectrum analyzer, which is an arrangement of filters that permits only a small selected band of frequencies $\Delta\acute{\omega}$ to pass, then the root-mean-square meter reading will be proportional to the turbulence kinetic energy contained by eddies having frequencies only in this small bandwidth. Ideally the value of the energy spectral density function at the midpoint of the band would then be given by
>
> $$E_{ii}(\acute{\omega}) = \overline{u^2_i\ (\Delta\acute{\omega})}/\Delta\acute{\omega}$$
>
> where $\overline{u^2_i\ (\Delta\acute{\omega})}$ is the square of the root-mean-square reading. ... The energy spectrum curve established by plotting the value of $\overline{u^2_i\ (\Delta\acute{\omega})}$ versus frequency for each frequency band investigated would appear typically as illustrated in **Figure 3.56**. The function of frequency, $E_{11}(\acute{\omega})$, defined by the curve is called in addition to the energy spectrum density the one-dimensional energy spectrum function, the power spectral density function, or simply the spectral density. It follows that
>
> $$\overline{u}^2_1 = \int_0 E_{11}\ (\acute{\omega})\ d\acute{\omega}$$
>
> Similarly $\overline{u}^2_2$ and $\overline{u}^2_3$ are related to $E_{22}\ (\acute{\omega})$ and $E_{33}\ (\acute{\omega})$. (p. 109)

From their power-spectral-density analysis, Casson and Lawler (1990) found that the

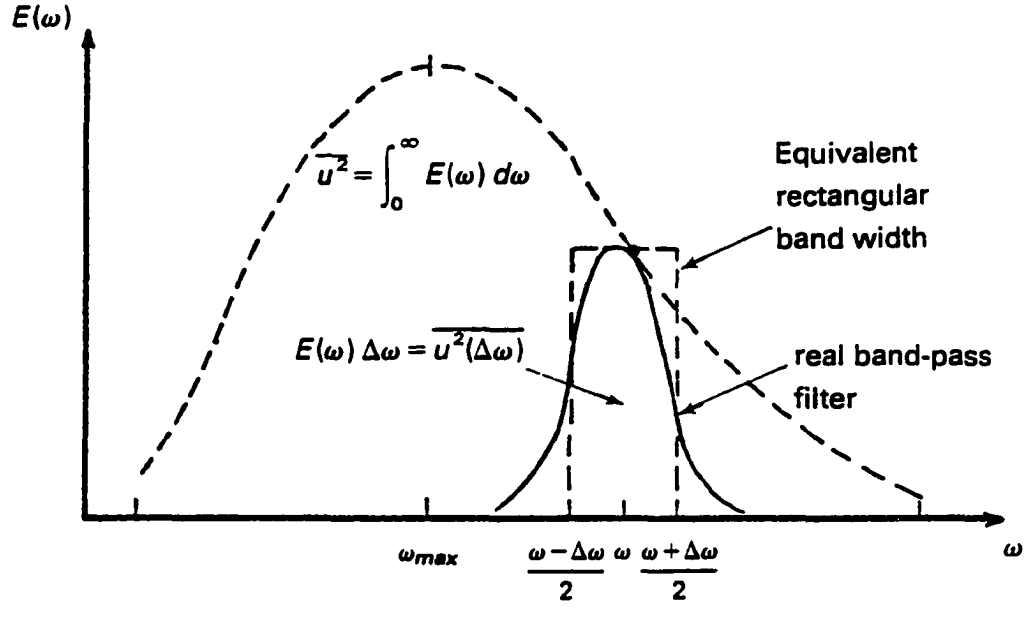

Figure 3.56. Energy spectrum and a typical frequency band E(ω) Δω (Frost, 1977)

two mixing conditions produced similar small scale motions and the difference between the two mixing conditions was found to lie in the larger scale motions (i.e. much larger than the particle sizes). These two mixing conditions produced similar flocculation rate of particles in suspension, indicating that the small eddies with length scale similar to the particle sizes in suspension were apparently responsible for their interparticle contact or flocculation. This result was confirmed with suspensions of monodispersed particles (single size particles), bimodal particles (two particle sizes), and trimodal particles (three particle sizes). Latex particles were used for making the suspensions, and were destabilized by changing the ionic strength with calcium nitrate along with nitric acid to maintain a constant pH of 2.0.

Arboleda-Valencia (1991) also reported some positive results for this type of mixing, tried in several Latin American locations. The concept of small scale turbulent motion generation was applied in both batch and continuous flow flocculation. In batch flocculation, the grid was operated in both circular rotating and vertical oscillatory patterns. His results indicated enhancement of flocculation kinetics due to this type of small scale turbulent motion. He worked with highly turbid water e.g., with 160 and 840 NTU turbidity. The details of the experiments (e.g., dose, pH, and the energy input) are missing in their report; probably they worked in the sweep floc mode. The following conclusions were drawn from their study:

1. In continuous channel flow flocculation, the grid sizes and spacings had a profound impact on the kinetics as well as on the extent of flocculation.
2. Flocculation time was an important parameter in grid flocculation. From several

experiments, it was found that the flocculation time could be reduced by an order of magnitude employing a continuous grid mixing pattern, and that long flocculation time had a deleterious effect (breakup of flocs) on flocculation. So every grid size and combination had a certain optimum flocculation time.

3. There was an optimum combination of screen size and number in batch flocculation for both operating modes (circular rotation and vertical oscillation).

McConnachie (1991) used three types of impeller in a 1-L square reactor in alum-kaolinite flocculation experiments. The geometry of the three impellers is shown in **Figure 3.57**. He measured the velocity and RMS of velocity fluctuations in both horizontal and vertical directions by Laser Doppler Anemometry (LDA), at different horizontal and vertical positions within the reactor. The mean velocity was calculated by taking the arithmetic mean of all the velocity readings (both horizontal and vertical components) on a particular horizontal plane. Then the overall mean velocity was calculated by taking the arithmetic mean of the five mean velocities determined for five horizontal planes (at five vertical locations). The overall mean of the RMS of velocity fluctuations was also calculated in a similar fashion. These were done with all the three impellers at four different speeds (16, 26, 42, and 60 rpm). From this study he showed that both the mean velocity and the overall mean velocity for the two paddle type (picket gate and branched) configurations, which effectively agitate the fluid by direct contact throughout the volume of the reactor, are independent of the paddle shape and directly proportional to paddle speed. The paddle stirrer (which is called turbine impeller in the current study) produced only 0.5 times the overall mean velocity of the other two

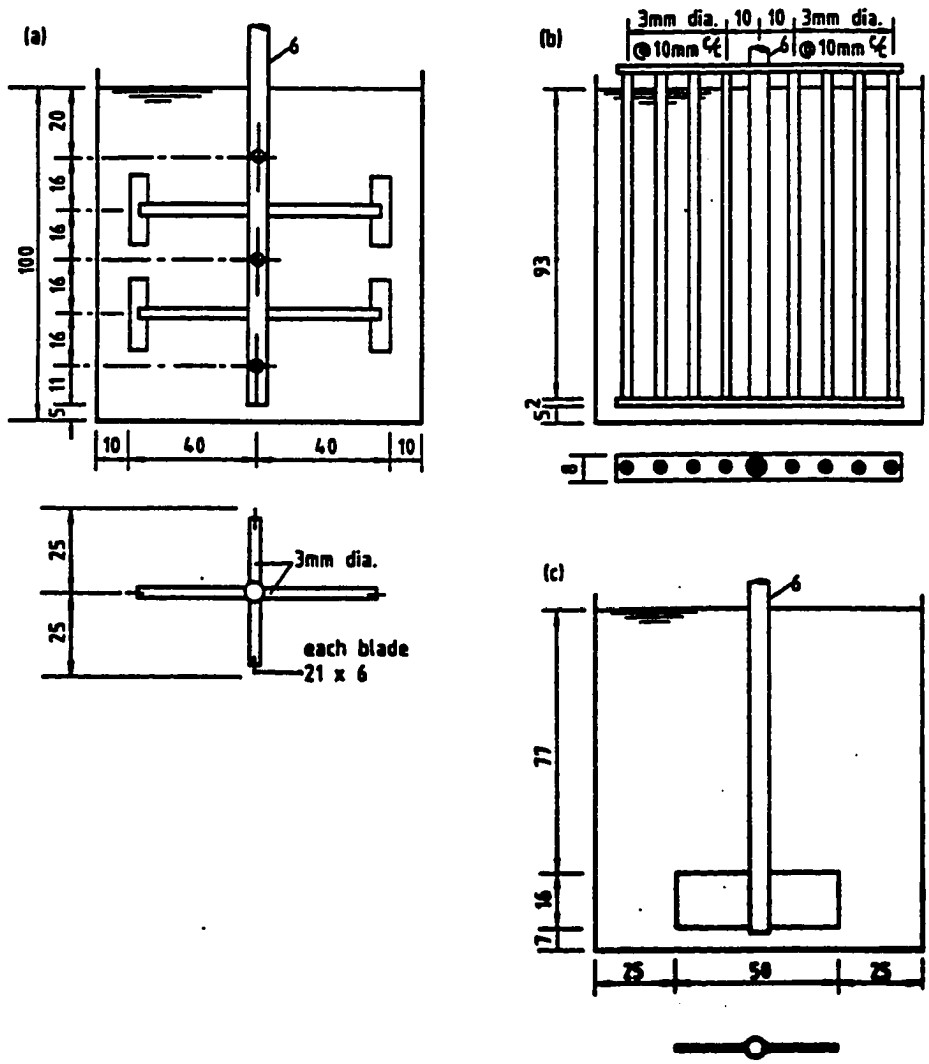

Figure 3.57. Details of stirrers used by McConnachie (1991): (a) Branched; (b) Picket Gate; (c) Paddle (Dimensions in mm)

with the same impeller speed. This was observed for all the four speeds employed in their study. He attributed this difference to the effective stirrer radius (the distance of the outer edge of each stirrer from the axis of its shaft). He also showed that the RMS of velocity fluctuations or turbulence intensity was different for all the impellers. He stated, ..."the branched one produced higher turbulent intensity than picket gate. This is probably due to the more severe vortex shedding from the edges of the thin plates than from the circular rods at any particular speed" (p. 745). The paddle mixer produced least turbulent intensity.

His flocculation experiments were probably performed in the sweep floc mode (pH = 7.0 and alum dose = 50 mg/l). Kaolin clay suspension used in the flocculation experiments was prepared in an unusual way. About 800 ml clay suspension of 6.25 gm/l was prepared with a series of vigorous mixing steps. This suspension was allowed to settle for 24 hours. Then, about 600 ml were decanted from the top to form the stock mixture. Later, 40 ml of stock were added to 950 ml distilled water to make the clay suspension. So, it is not possible to tell the clay concentration. The author did not provide any turbidity reading of the clay suspension.

His flocculation results did not show any noticeable geometry effect when compared with respect to constant power input per volume; and the power required to produce the lowest residual turbidities was within a close range for all the impellers tested here. The branched type was seen to be somewhat superior in producing relatively low turbidities over a wide range of power inputs. The author concluded that for a similar power input, a stirrer that extended throughout the volume of the reactor and had

sharp-edged blades was more versatile than the other types.

Clark et al. (1994) employed four different impeller geometries (rake, foil, pitched blade, and the Rushton turbine) in three different tank sizes (1 ft, 2.5 ft and 4 ft side dimension with square cross section) to investigate the effect of the four impeller geometris and scale on flocculation kinetics. In studies with different reactor size, the impeller diameter was increased with the tank size to keep the ratio of impeller diameter to tank width (D/T) constant. The results comparing different impellers were not conclusive although "there was a mild degradation in performance moving from the rake to the foil to the pitched blade to the Rushton impeller" (p. 125). The most highly reproducible response uncovered in the study when the tanks were operated at the same G was poorer performance as the scale was increased. They concluded, "... smaller flocculation systems tended to produce more large floc and fewer smaller floc than geometrically similar larger systems. This effect was observed regardless of the type of initial mixer, coagulant dose, initial mixing intensity, or flocculation impeller design" (p. 125).

4. MATERIALS, METHODS AND EQUIPMENT

4.1. Introduction

The work being reported here is an experimental investigation. The main objective is to determine the effect of various mixing variables on flocculation kinetics in a presumably turbulent flow field. Experiments were performed at two temperatures, 23° and 5° C; at two pH levels, 7.8 and 6.0 and several clay concentrations. The coagulant and the coagulant dosage were also varied in some cases. The flocculation experiments were performed in a bench scale batch reactor similar to the reactor used by Argaman and Kaufman (1968, 1970), Hanson (1989) and Hanson and Cleasby (1990) inside a walk-in constant temperature room. The temperature of the room was controlled and monitored using a personal computer (PC) based data acquisition and control system. Kaolinite clay similar to that used by above researchers was used in this study as the primary particle system. The suspension water was distilled water with added sodium nitrate to yield a 0.005M ionic strength. Alum and ferric nitrate were used as coagulants in this work. Five different types of mixing impellers as shown in **Figure 4.1** were used in this study. The physical and chemical conditions in the flocculation reactor were monitored using the aforementioned data acquisition system. The following control parameters were monitored:

- reactor pH,
- reactor temperature,

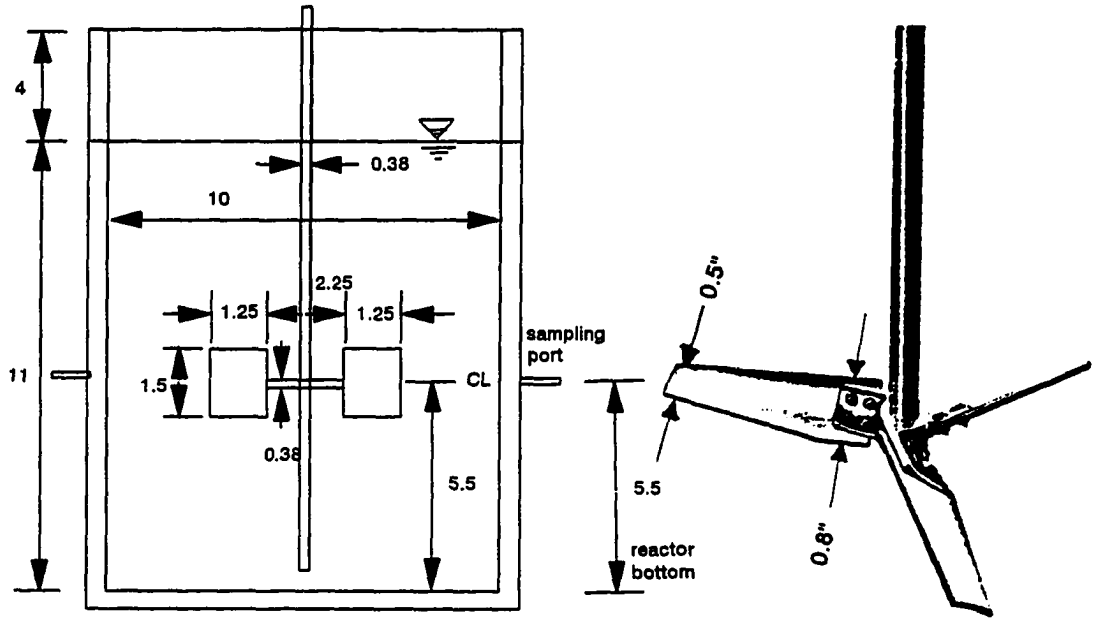

a: The 2-blade impeller and reactor

b: Lightnin A 310 fluidfoil impeller (Impeller radius is 2.6 inches and hub diameter is 1.3 inches)

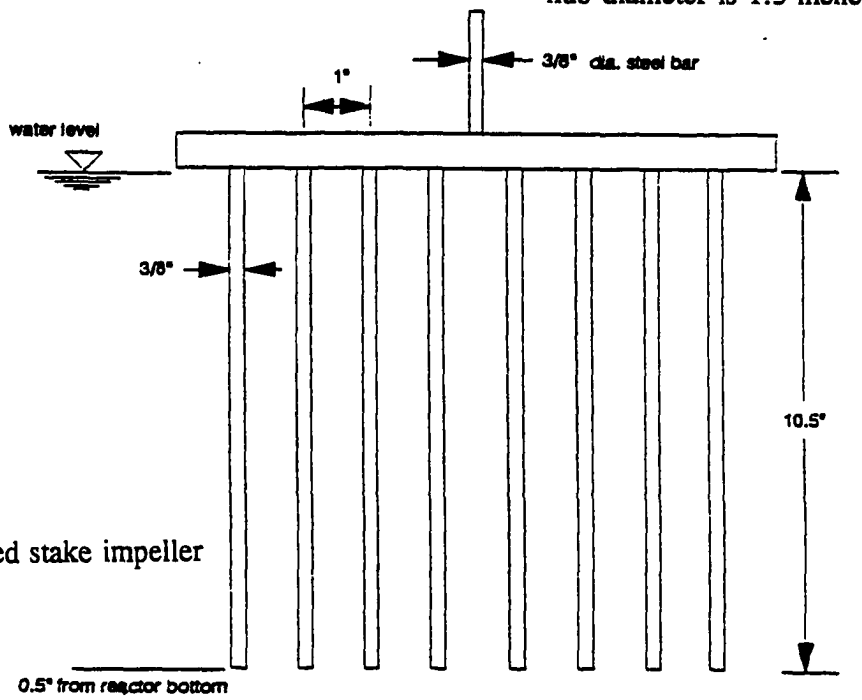

c: Modified stake impeller

4.1. Geometry of different impellers used in this study (all dimensions are in inches)

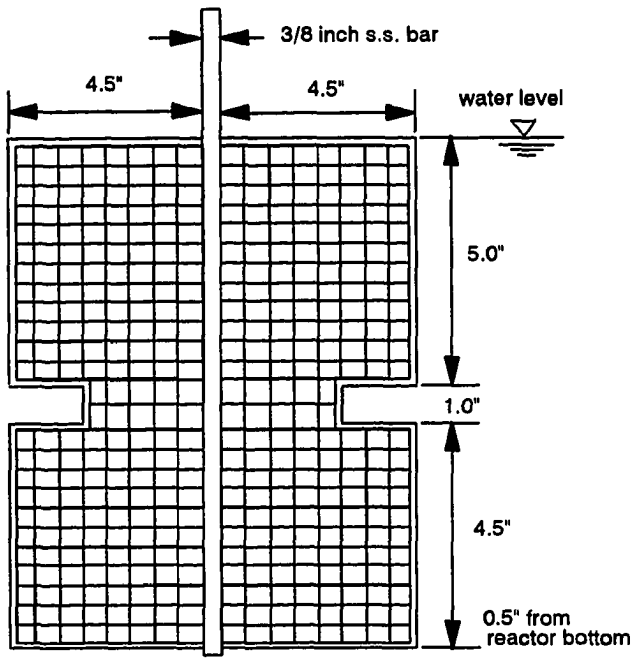

d: Wire mesh impeller

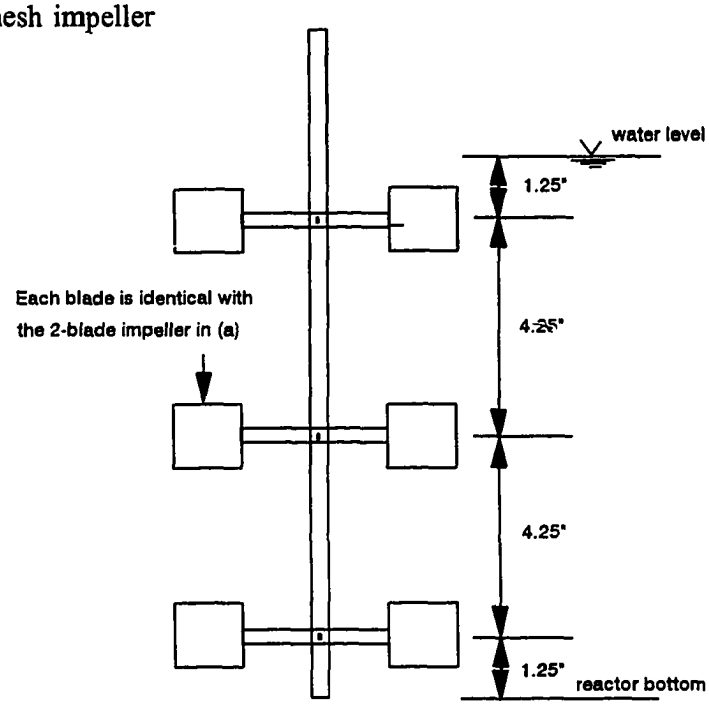

e: 2-blade vertical stack impeller

Figure 4.1. (continued)

- impeller rpm, and thereby, the energy input in the reactor,
- output from flocculation monitoring instrument,called Photometric Dispersion Analyzer (PDA).

The impeller rpm was used as the operational control parameter and was set to the desired value but was not recorded continuously. The other control parameters were recorded at 5 second intervals.

The kinetics were monitored by two different instruments. The first one was the Photometric Dispersion Analyzer, model 2000 (PDA 2000) which provided an on-line measure of flocculation kinetics. The PDA along with other components of the experimental set up is shown in **Figure 4.2.** The theory behind the PDA 2000 is that the ratio of the root mean square voltage of the fluctuating light intensity (V_{rms}) to the voltage corresponding to the mean transmitted light intensity (V_m) is found to increase substantially as the particle aggregation occurs during flocculation, and provides a sensitive measure of the extent of flocculation. This ratio value was termed as the "flocculation index" which was recorded at 5 second interval and was plotted as y-ordinate in all the figures containing results. The other instrument was the conventional Hach ratio turbidimeter that measured the homogenized turbidity and the supernatant turbidity after flocculation followed by various periods of sedimentation. The supernatant samples were collected at a depth of 14 cm from the reactor bottom for turbidity measurement, in most cases after 10, 20, and 30 minutes of settling . The turbidity values are shown in the parenthesis in all the figures containing results. The initial or homogenized turbidity, initial ratio value and zeta potential following rapid

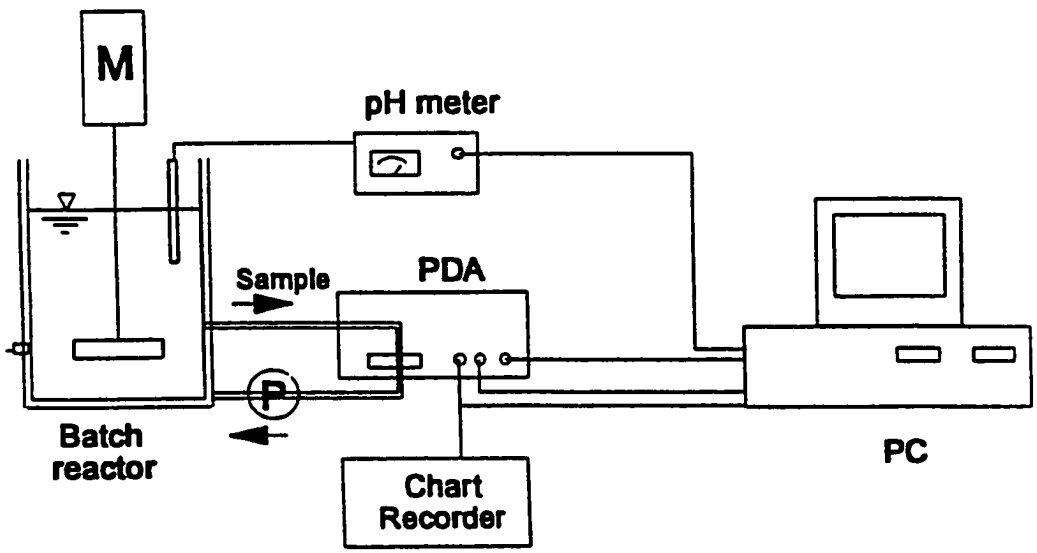

Figure 4.2. Schematic of the experimental setup

mixing were used as quality control parameters.

Initial suspension zeta potential was measured on a irregular basis to check the clay suspension characteristics. The following two subsections will discuss in detail about all the features described above. The first subsection will describe the materials preparation and the second will describe the methods and equipment.

4.2. Materials Preparation

4.2.1. Clay

Kaolinite clay was used as the primary particle system. Through a sophisticated particle counting technique, Hanson (1989) consistently counted a total around 7.1 million particles/ml of suspension containing 25 mg/l of kaolin clay, of which about 6.5 million are primary particles less than 2.5 μm in size. Assuming a spherical geometry with 1.8 μm diameter and a specific gravity (S.G.) of 2.65, one can calculate 3 million particles per ml. Hanson (1989) indicated that these clay particles are actually plate-like material rather than spheres. For clay dispersion, the best method among those three reported by Hanson (1989) was used. That is: "adding the clay to water circulating through a centrifugal pump, circulation was continued for at least an hour, and then repeated periodically (a total of 3-6 hours of circulation) prior to use". **Figure 4.3** is a schematic representation of clay dispersion and mixing system. According to Hanson (1989) this system has number of advantages, including:

- 45 liters of 800 mg/l suspension can be prepared at a time. This minimizes

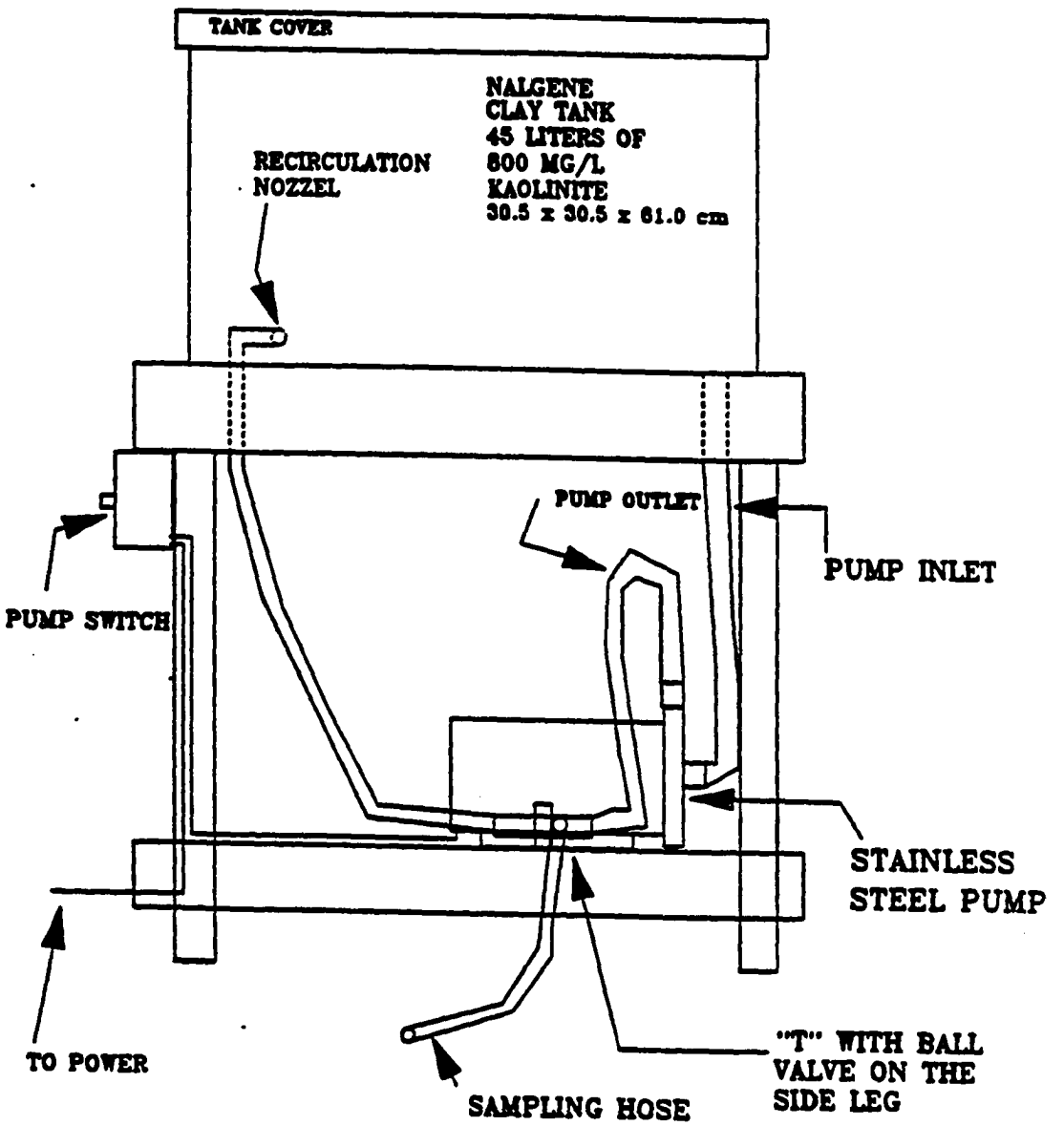

Figure 4.3. Schematic of the clay dispersion and mixing system

suspension variability. Errors due to measuring the clay and clay loss in simple transfer were reduced in significance because a fairly large amount of solid material (36 grams) is added to a large volume (45 liters) of distilled water,

- the 45 liters of stock suspension provided primary particles for a large number of experiments, providing continuity from one set of experimental conditions to another, and
- the circulation system made it easy to get a representative sample of the stock suspension.

But the system has some disadvantages. The disadvantages and the remedial measures taken to minimize them are described as follows:

1. The stock suspension lasted for a fair amount of time (four to six weeks). During this time frame, the pH of the stock suspension dropped gradually and particle aggregation occurred in the mixing tank. This resulted in successively lower numbers of primary particles in a series of measurements taken from a particular suspension. This was determined by particle counting with the Automatic Image Analyzer (AIA) and was also noticed by increased initial ratio value measured on the PDA instrument at the beginning of each experiment.

This aggregation was minimized by keeping the stock suspension pH near 7.0 by adding a small amount of 1N NaOH as needed, at regular intervals.

2. After almost eliminating the particle aggregation by pH adjustment as described above, there appeared another problem, the evaporation of moisture from the stock suspension. Before every experiment the stock suspension was mixed vigorously with

the pump for over 30 minutes which made suspension warmer and enhanced the evaporation rate of the moisture. This moisture condensed on the lid of the tank, and when the lid was opened for obtaining sample or for adding NaOH, some moisture dripped out of the lid and was lost. That is why, a gradual increase of turbidity was noticed for homogenized sample. For a 25 mg/l clay suspension, the homogenized turbidity reading was found to be around 22 at the earlier period when the stock suspension was near 45 liter mark and it was found to be around 26 when the stock suspension dropped below 20 liter mark. The mode was found near 24. This relative concentration change affected the initial PDA reading too, but did not show any noticeable change in zeta potential measurement.

This disadvantage was countered and minimized by adopting a practice of not using the entire volume of the clay suspension. When the volume in the stock tank dropped below the 15 liter mark, or when the 25 mg/l homogenized clay in the reactor showed a turbidity reading more than 26, then the suspension was discarded and a new suspension was prepared. The zeta potential of the homogenized sample did not show any noticeable change and was found around -30 mv in most cases. But, at the later period of this research the stock clay suspensions (after a number of stock suspensions had been prepared) showed a different flocculation tendency due to some unidentified reasons from the previous stock suspensions. The zeta potential reading of 25 mg/l homogenized sample was found around - 20 mv and the PDA reading of the homogenized sample in the reactor showed a marked increase. To minimize the impact of this problem, the stock suspension was discarded when the volume dropped below 25

liters or the PDA reading of the homogenized sample in the reactor increased significantly. It is also recommended that the results obtained with these stock suspensions not be quantitatively compared with the other results, as will be discussed in Chapter 6.

The following method was used to make a suspension of desired concentration in the reactor before an experiment. The reactor was filled up to the 14 liter mark with distilled water and a 90 ml of 1N $NaNO_3$ was added to it. The clay recirculation system was turned on before that and was run for 30+ minutes to insure complete homogeneity in the clay dispersion tank. During this time the PDA 2000 was warmed up and calibrated using the distilled water in the reactor. After 30+ minutes of mixing the clay dispersion tank, the required quantity of stock clay suspension was obtained from the surface near the discharge nozzle end of the recirculating system with a beaker. Immediately after that the correct amount was measured into either a 500 ml or 1 L graduated cylinder. The circulation was shut down immediately after the measured quantity was obtained. This measured quantity of stock clay was then added to the reactor and the volume of the liquid in the reactor was brought up to 18 liters.

4.2.2. Dilution water

The dilution water used in this study was distilled water added with required amount of 1N $NaNO_3$ to provide 0.005M ionic strength. This ionic strength was chosen based on the initial study which showed that this ionic strength facilitates stable and reproducible zeta potential measurement and does not induce any measurable

coagulation by double layer compression. A large nalgene plastic tank was filled up to the 400 liter mark from the distilled water supply using a rubber tube. This water was allowed to stay at least overnight to arrive at equilibrium with the atmosphere with respect to CO_2 transfer before conducting any experiments. The distilled water was drawn from the bottom of the tank with a sample hose into an 18 liter carboy and then transferred from the carboy into the reactor. For experiments at cold temperature the carboys filled with distilled water were placed inside the constant temperature room for about 48 hours to bring the water temperature near 5° C. Ninety ml of 1N $NaNO_3$ was added into the reactor. The stock solution of 1N $NaNO_3$ was kept inside the constant temperature room all the time.

4.2.3. Coagulant

Alum [$Al_2(SO_4)_3.18H_2O$] or Ferric nitrate [$Fe(NO_3)_3.9H_2O$] with molecular weights of 666.52 and 404.1 respectively both over 99% pure and in crystal form were used as coagulants in this study. All dosages in the results section are expressed as these molecules and these molecular weights. Both of these coagulants were obtained from Fisher Scientific, Fair Lawn, NJ with 500 gm net weight in plastic containers. The metal coagulants were stored as 0.25 molar stock solutions. The stock solution was always stored at room temperature and its pH was checked periodically to insure the stability and integrity of solution. The pH of alum and iron stock solutions always stayed near 3.2 and 1.3 respectively. The coagulant dosing solution was prepared fresh 24 hours before the experiments by diluting the appropriate amount of the stock solution with

deionized water in a 200 ml volumetric flask. Three concentrations of coagulant dosing solution (5 mg/ml, 10 mg/ml, and 20 mg/ml) were used in this study. The dosing solution was also stored at room temperature. No precipitates were observed in the dosing solution during this storage period. The required amount of coagulant dosing solution was loaded into a syringe equipped with #13 gauge needle and taken inside the constant temperature room just prior to injection into the reactor. The needle was about 4.5 inch long.

4.2.4. Base

All pH adjustments were made using reagent grade sodium hydroxide (NaOH) diluted volumetrically to 0.1N and 0.02N with deionized water. The base used for pH adjustment was not standardized in this study. It would be worth mentioning here that the distilled water from the building supply was used only to prepare the clay suspension; all the other chemicals were prepared with deionized water prepared in the laboratory using a Nanopure system in the Analytical Service Laboratory. The input water to the system is the building distilled water supply.

4.3. Equipment and Methods

4.3.1. Batch reactor and associated equipment

The work presented in this dissertation was carried out in a bench scale batch reactor similar to the reactor used by Argaman and Kaufman (1968, 1970), Hanson

(1989) and Hanson and Cleasby (1990). Essential features of the plexiglass reactor used in this study are shown in **Figure 4.4**. The electric mixing motor was mounted on a wooden support which was rigidly placed on the top of the reactor. Different impellers were attached to the motor via a 3/8 inch diameter steel rod, and a plexiglass coupler. The wooden support for the motor held the pH probe and the thermocouple for temperature measurement. The motor was controlled by a variable speed motor controller (Series H, G. K. Heller Corp., Floral Park, N.Y.). This motor controller was used to control the speed at which the motor was rotating as well as hold the rotational speed constant. The reactor had four ports on the four sides, 5.5 inch from the reactor bottom. This is the level of the impeller discharge stream inside the reactor. Two of these four ports were used to inject coagulant and base simultaneously and one was used to withdraw sample from the reactor and pass through the glass tube held by the PDA cell. The fourth one was sealed with a teflon septum. Two of the other three ports also had teflon septa covers and the chemicals were injected through the septa by piercing with the hypodermic needle. There were two ports near the bottom of the reactor. One was used to drain the entire contents of the reactor after each experiment and the other was used to recycle back the withdrawn sample from the PDA instrument during the experiment.

4.3.2. Photometric Dispersion Analyzer (PDA 2000) and flocculation monitoring

The flocculation rate was monitored qualitatively by a recently developed instrument throughout the entire duration of each experiment. This instrument is called

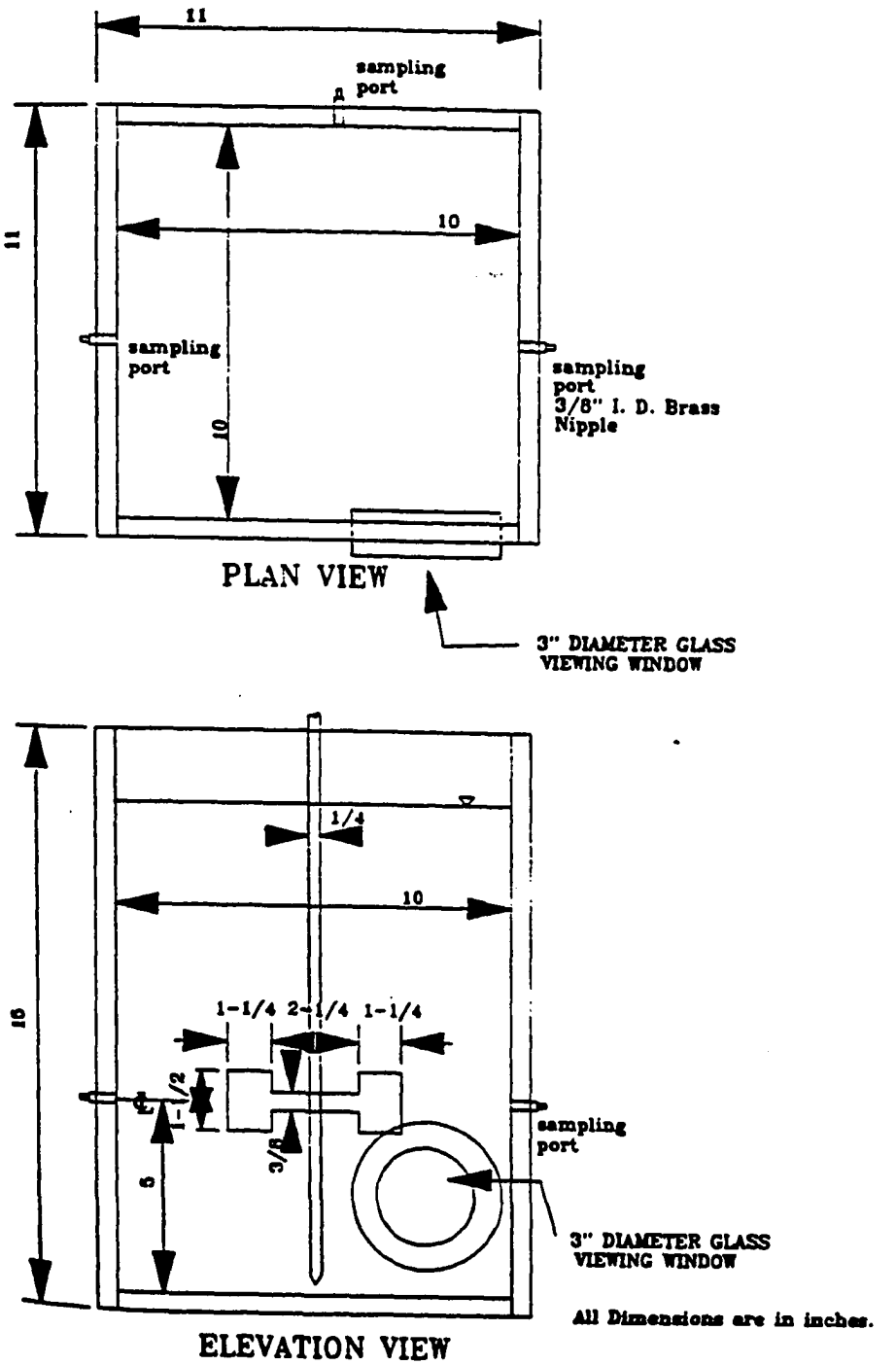

Figure 4.4. Schematic of the batch reactor (the 2-blade turbine impeller is shown within the reactor)

the Photometric Dispersion Analyzer, model 2000 (PDA 2000). This instrument is manufactured and distributed by Rank Brothers Ltd., Cambridge, England. The instrument is a sensitive on-line, flow-through detector, which gives a rapid indication of the state of aggregation of particles in a flowing suspension. The theory of the PDA was developed by Gregory (1985) and Gregory and Nelson (1984, 1986) based on Lambert-Beer law and assuming Poisson distribution of particle number in a flowing suspension. The Lambert-Beer law can be given as follows (Gregory and Nelson, 1986 and Ching et al., 1994):

$$I/I_o = V/V_o = \exp(-NCL) \qquad 4.1$$

where, I = transmitted light intensity; I_o = incident light intensity; N = number concentration of particles; C = scattering cross section of the suspended particles; and L = the optical path length. In practice the light intensity is converted at the detector to a proportional voltage. So mean voltage outputs V and V_o correspond to I and I_o respectively.

In a suspension illuminated by a light beam with cross sectional area A and length L, the average number of particles (n) contained in the illuminated volume equals NAL. As the suspension flows through the cell, the actual number of particles in the light beam will show a random variations about the mean value, n, as the sample is continually renewed by the flow (Gregory, 1985). This variation of particle number will follow a Poisson distribution so that the standard deviation about the mean equals the

square root of the mean (Std. dev. = $n^{1/2}$). It has also been shown by Gregory (1985) and Gregory and Nelson (1984, 1986) that the variation in the number of particles in the illuminated volume of a flowing suspension leads to corresponding fluctuations in transmitted light intensity and proportional voltage reading. The simplest measure of a fluctuating signal is its rms value, and for developing the theory of the PDA, they considered only the fluctuating component of the transmitted light intensity (or its corresponding ac voltage) after separating it from the mean (dc) value (**Figure 4.5**) and this V_{rms} can be given by

$$V_{rms} = V \text{ Sinh } (n^{1/2}C/A) \qquad 4.2$$

V = time averaged transmitted signal = $V_o \exp(-nC/A) = V_o\exp(-NCL)$

Even for very turbid suspensions, they mentioned, the quantity $n^{1/2}C/A$ will be much less than unity in which case, Sinh $(n^{1/2}C/A) \simeq (n^{1/2}C/A)$ and

$$V_{rms} = V (n^{1/2}C/A) \qquad 4.3$$

It is convenient to write the above expression in terms of the particle number concentration, N, rather than the average number in the illuminated beam, n, and to introduce a dimensionless term, R, which is the ratio of V_{rms} to the mean value V as:

$$R = (V_{rms}/V) = (L/A)^{1/2}N^{1/2}C \qquad 4.4$$

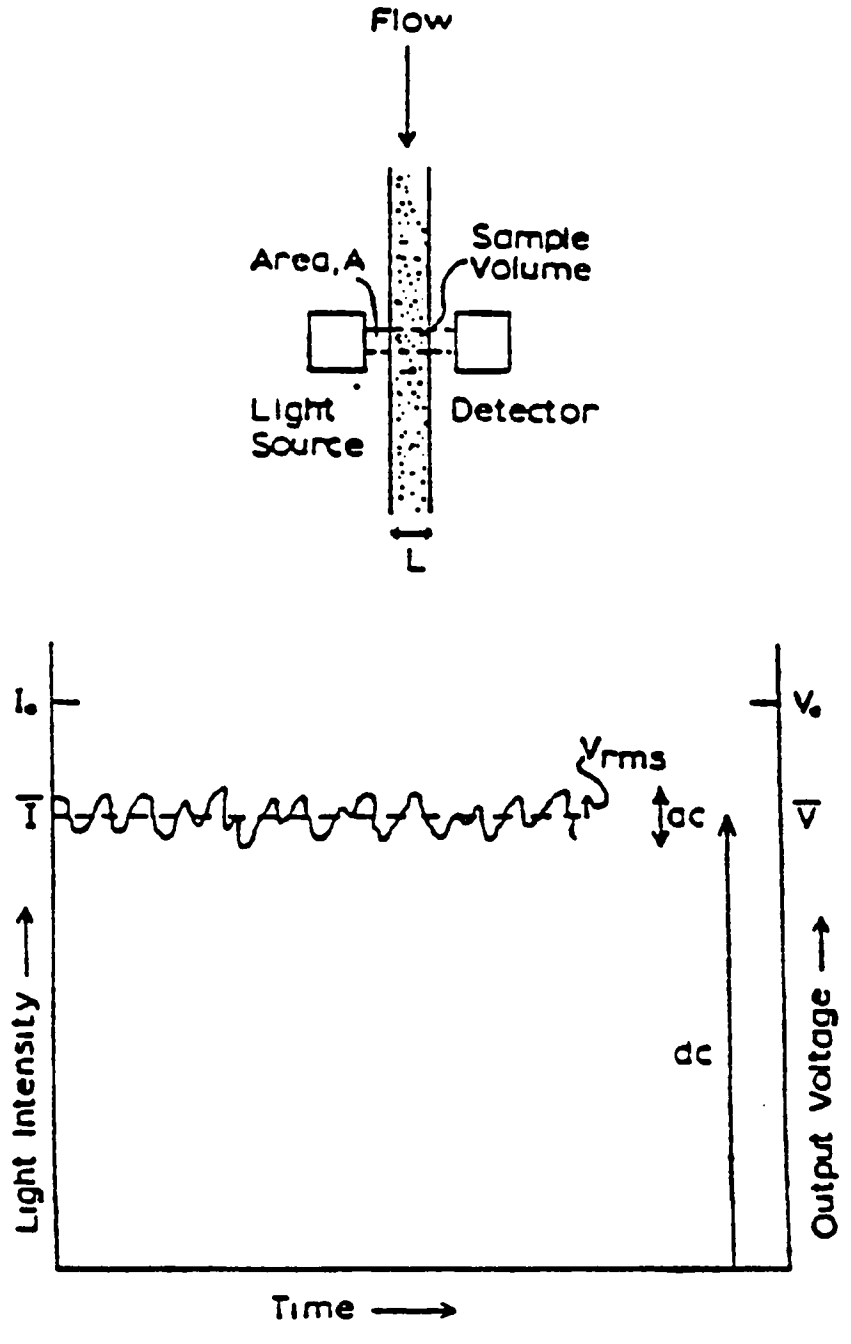

Figure 4.5. Turbidity and corresponding voltage fluctuations in a flowing suspension (Gregory, 1985)

When the particles aggregate, the rms or ratio value should change for two reasons:

(a) the number concentration decreases and

(b) the scattering cross section increases.

These have opposing effects on the ratio value, but one has less effect than the other, because from Equation 4.4, it can be seen that the ratio value depends on the square root of the particle concentration and on the first power of the scattering cross section. Thus, the net effect is a substantial increase in the fluctuations and in the measured ratio value as flocculation progresses. This has been observed by all the researchers working with the PDA. The scattering cross section at a given wavelength is dependent on the size and shape of the suspended particles. Gregory and Nelson (1984), from theoretical considerations, have shown that the rms value or the ratio value should vary as either the sixth root or the square root of the aggregation number, depending on whether coalesced spheres (**Figure 4.6a**) or extended aggregates (**Figure 4.6b**) are assumed. Real aggregates will be intermediate between these two extremes (**Figure 4.6c**). Extended aggregates will cause the maximum rms ratio value, but their mass density may be minimum.

Equation 4.4 was developed for monodispersed suspension; for a heterodispersed suspension, the expression can be modified to (Gregory and Nelson, 1986):

$$R = (L/A)^{1/2}(\Sigma N_i C_i^2)^{1/2} \qquad 4.5$$

where, N_i and C_i are the number concentration and scattering cross section of particles

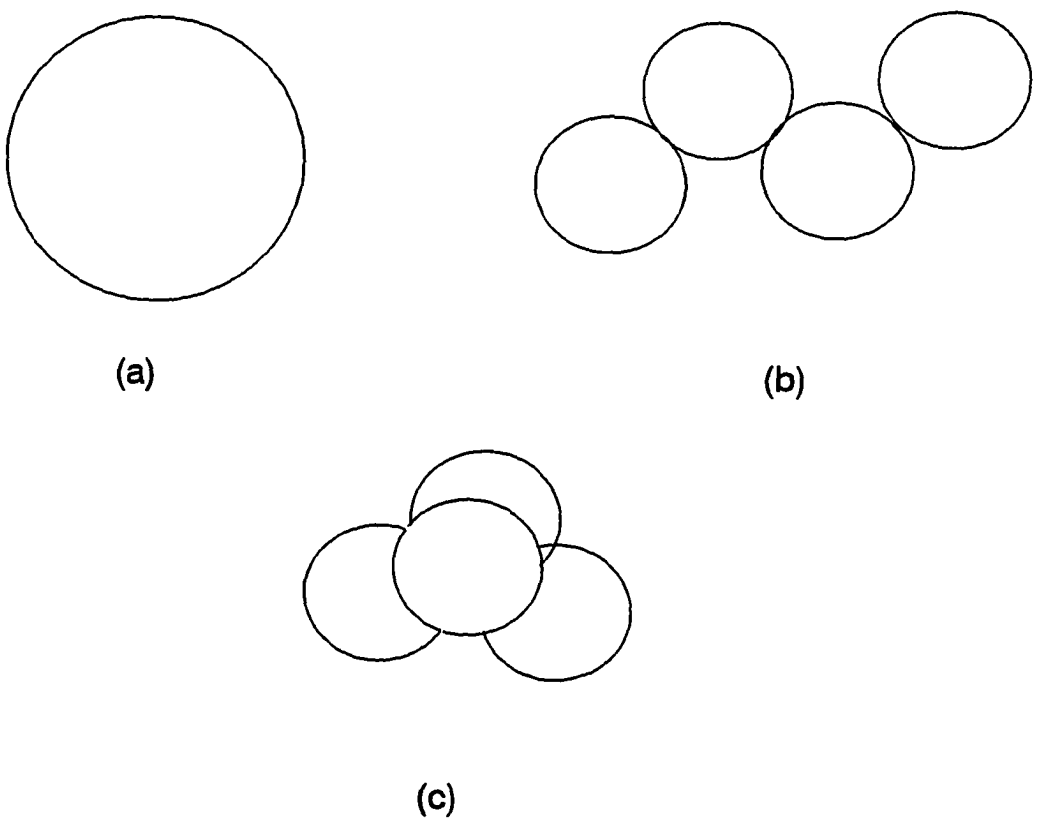

Figure 4.6. Forms of aggregates composed of four equal spheres. (a) Coalesced spheres, (b) Extended aggregate (e.g. aligned by flow), (c) Randomly oriented aggregate (Gregory and Nelson, 1984)

of size i, respectively. The above equation demonstrates that the fluctuating signal still depends on the square root of particle number concentration and on the first power of the scattering cross section. An analysis of the term ($\sum N_i C_i^2$) in Equation 4.5 reveals that smaller particles have a negligible effect on R, and that, in a coagulating suspension, the larger aggregates have a dramatic influence on R (Gregory and Nelson, 1986). Hence, the ratio R (or the value of V_{rms}) is a useful indicator of the degree of flocculation. For a given suspension, it can be assumed that larger values imply larger floc size. Ching et al. (1994) called this ratio value as the "coagulation index" in their study. In the current study this was called the "flocculation index" which is the more appropriate term because it represents the flocculation phase of the coagulation-flocculation process.

A "flocculation index" vs. time curve during a flocculation experiment may resemble one of the three curves shown in **Figure 4.7**. The rising limb of all the curves depicts the occurrence of flocculation where primary particles and small flocculi are growing into flocs. The rate of aggregation far outperforms the breakup rate and breakup can be assumed negligible in this region. The earlier portion of the rising limb represents the aggregation of primary particles into smaller flocs and later portion indicates the formation of larger flocs from the aggregation of smaller flocs or aggregation of flocs with primary particles. The plateau of the curves A and B indicates that flocculation has reached the equilibrium stage where flocs have grown to a limiting size in sheared suspensions, as a result of a competition between floc growth and breakup. The rates of aggregation and breakup are comparable. This has been pointed out by other researchers too (Gregory and Nelson, 1984 and Ching et al., 1994). The

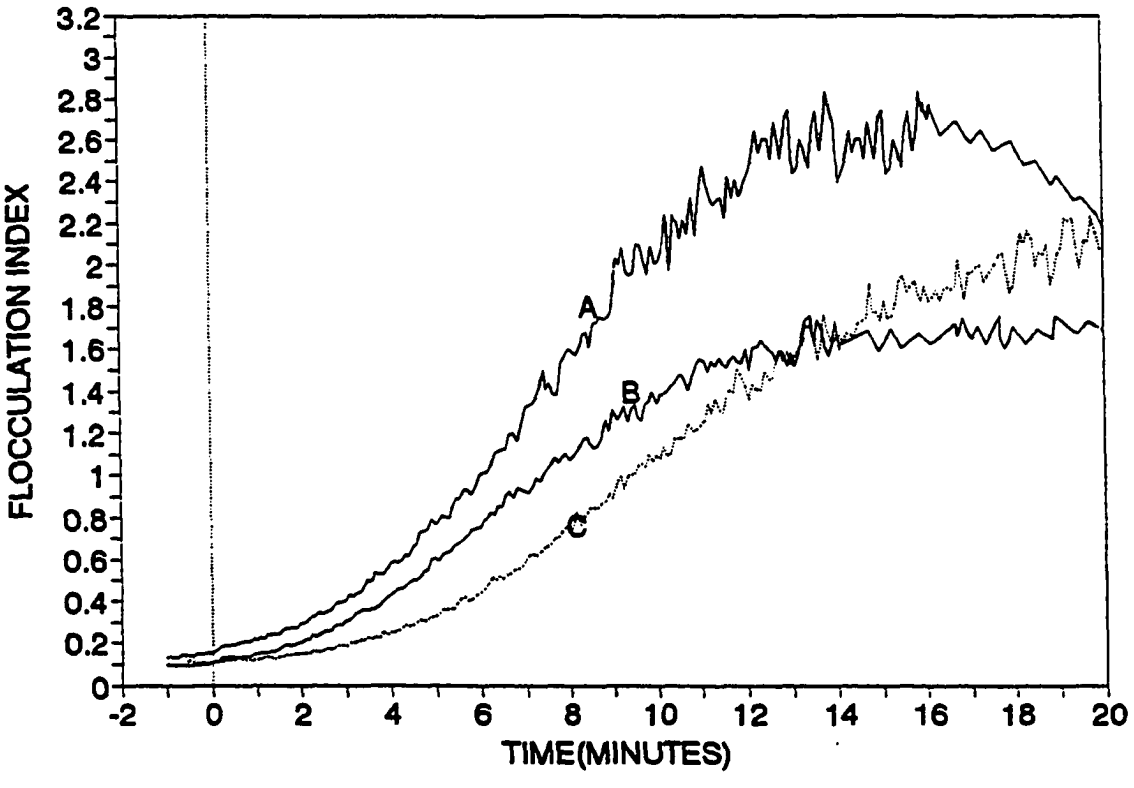

Figure 4.7. Typical flocculation index versus time curves for three different treatments during coagulation-flocculation process

falling limb of the curve A indicates the settling of much heavier floc particles during the later stage of flocculation resulting in a gradual decrease of the ratio value. This has been confirmed experimentally by Ching et al. (1994) and by the author.

During this research some flocculation performance phenomena were found to be predictable based on the relative shape of the flocculation index versus time curves illustrated in **Figure 4.7**:

1. A rising limb with higher slope always yielded better or comparable turbidity removal at the end of 30 minute settling following flocculation. For example, treatment A will produce better turbidity removal than B and B will be better than C.
2. When B and C are compared, it was seen in some cases that treatment C might have better turbidity removal at some intermediate periods (10 min and 20 min) of sedimentation following flocculation. Because curve C crossed curve B at the later period of flocculation, and it is possible that higher number of heavier particles were produced in treatment C during later period of flocculation, even though the initial flocculation rate was higher for treatment B. So higher initial flocculation rate removes more primary particles and very small flocs and results in better turbidity removal at the end of 30 minute settling. Later stage flocculation occurs predominantly between large flocs and results in better turbidity removal at early period of sedimentation.
3. If A and B are compared, it shows that flocculation is always better over the entire flocculation period in treatment A than treatment B. So turbidity removal in treatment A will be better than in treatment B after any period of sedimentation.
4. In some experiments, it was also observed that the turbidity readings after various

periods of settling were different for two experiments even though they produced similar "flocculation index" vs. time curve. This may be due to the effect of floc shape (see **Figure 4.6** for different floc shapes) on the flocculation index. Even though the particles in those two experiments created similar blockage to the light, it is possible that particles are more settleable in one experiment than the other.

The hardware and the operation of the instrument will be briefly discussed in the following paragraphs. During the flocculation process, a sample stream (flowing suspension in **Figure 4.8**) is withdrawn at a rate of 15 to 20 ml/min through a glass tube of 2 mm internal diameter by a peristaltic pump. The glass tube is held by the cell of the PDA which houses two precisely-aligned fiber-optic probes. The optical fibers carry the incident and transmitted light as shown in **Figure 4.8**. The light source is a high intensity light-emitting diode and the transmitted light is continuously monitored by a sensitive photodiode. The output from the photodiode is converted to a voltage which consists of a large dc component, corresponding to the average transmitted light intensity, together with a small ac component or ripple due to the fluctuations of particle number in the flowing suspension or of the transmitted light. The dc component is then eliminated by passing the signal though a suitable capacitor and can be seen as output on the display dial of the PDA by depressing the 'DC' switch. The ac component is then amplified by an ac amplifier and sent to an rms to dc converter. This converter converts the rms value to equivalent dc value which can also been seen on the display dial by depressing the 'RMS' switch. The PDA also calculates automatically the ratio of rms and dc values. This ratio can also been seen on the display dial of the PDA by

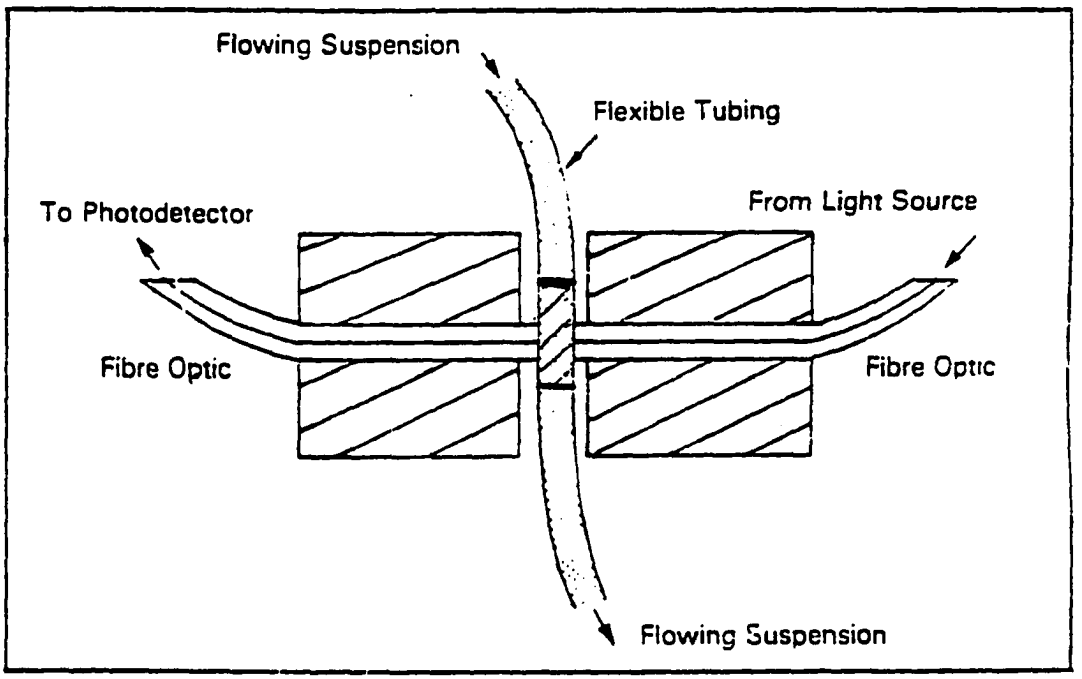

Figure 4.8. Schematic of the flow cell of PDA

depressing the 'RATIO' switch. All outputs can be smoothed by depressing the 'Filter' switch of the PDA. The display dial shows only the instantaneous value which existed when the switch was depressed. Both dc and rms readings can be adjusted by use of precision 10-turn gain controls, enabling a wide range of suspension concentrations and conditions to be monitored. The sensitivity of the machine can be increased by increasing the rms gain or decreasing the dc gain. Throughout the current study the PDA instrument was calibrated before each experiment using the distilled water in the reactor through a flow through recycle system with the help of a peristaltic pump. The rms gain was fixed at 50 and the dc gain was varied around 150 to set a dc voltage reading of 10 volt corresponding to the mean transmitted light intensity across the distilled water passing through the PDA cell with the help of a peristaltic pump. That means all the experiments were done with the same sensitivity of the machine.

The glass tube held by the PDA cell was connected with two ports of the reactor through a combination of tygon tubing and rubber stoppers. The sample was withdrawn at a rate of 20 ml/min from the upper port (5.5 inch from the reactor bottom), passed through the glass tube in the PDA cell and then recycled back to the reactor through the bottom port (1/2 inch from the reactor bottom). The connection of PDA with the reactor is shown in **Figure 4.2.**.

4.3.3. pH adjustment and monitoring

The initial pH of the homogenized clay suspension in the reactor was always found to vary between 5.6 to 5.8. At first, the pH of the clay suspension in the reactor

was always brought to the desired level (7.8 and 6.0) by adding base. Then, the required amount of coagulant and base was injected through two different ports into the impeller discharge stream. Immediately after that the two dosing syringes were removed from the ports; then, with another syringe, through one of the ports, a tiny amount of 0.02N NaOH was continuously added during the whole rapid mixing period to keep the pH near desired level. In most experiments this adjustment was continued until the end of flocculation. A typical pH vs. time curve is shown in **Figure 4.9**.

The base was added to the reactor using two syringes of 20 ml and 10 ml capacities respectively with #13 gauge needle. The base was added through the sample port on the side of the reactor simultaneously with the coagulant and was discharged into the impeller stream. The coagulant was injected in a similar fashion through another port. For a particular coagulant dose, a stoichiometric amount (equivalent to the coagulant dosage) of 0.1N NaOH was loaded in a 10 ml syringe, another syringe of 10 ml capacity was also loaded with 0.02N NaOH. From initial experiments, it was observed that base requirement during rapid mix at pH 7.8 was always higher than the stoichiometric amount required for neutralization of the coagulant. So after injecting the required amount of 0.1N NaOH simultaneously with the coagulant, some additional amount of base was always needed for fine tuning the pH. This fine tuning was done with more dilute solution (0.02N NaOH). Experiments at pH 7.8 always needed an additional 1 to 2 ml of 0.02N NaOH during rapid mix to prevent the downward pH drift. This was observed at both temperatures. The experiments at pH 6.0 did not require any additional amount of base for fine tuning the pH during rapid mix.

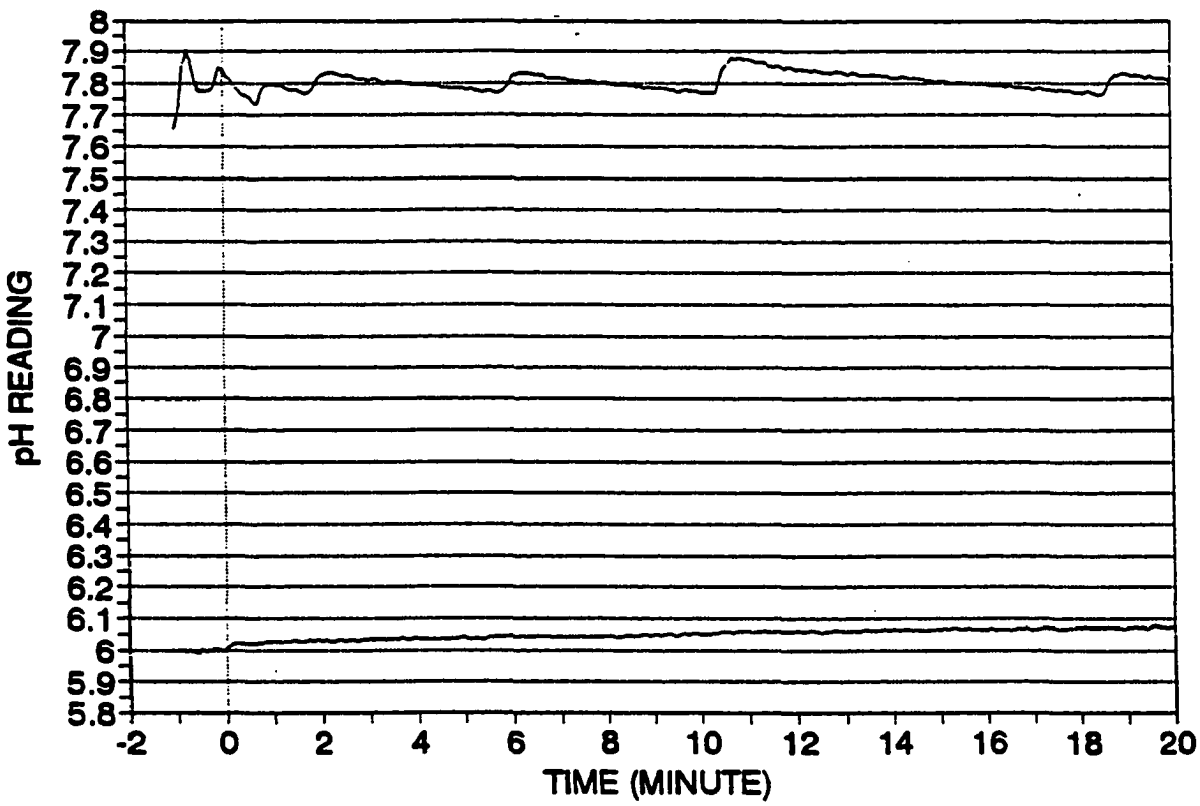

Figure 4.9. Typical pH versus time curves during coagulation-flocculation process for two experiments at different pH levels.

The pH of the system was continuously monitored using a 12 mm diameter pH probe, and a Fisher Scientific Accumet #610 pH meter. The pH meter was standardized using first a 7 buffer, and then a 4 buffer. It was checked again with the 7 buffer. The pH meter was checked at both the beginning and the end of each experiment. The tip of the pH probe was placed into the clay suspension through a port through the mounting support for the motor. The probe was connected to the pH meter and the output of the pH meter was connected to a personal computer outside the constant temperature room. This computer recorded pH values every 5 seconds throughout the duration of the experiment. In three sets of experiments with alum at pH = 7.8, buffer was added to obtain the pH control (43 mg/l of $NaHCO_3$ plus a small amount of NaOH as needed to reach pH 7.8, or 43 mg/l of $NaHCO_3$ plus 3 mg/l of Na_2CO_3 or 50 mg/l of $NaHCO_3$ plus 2 mg/l Na_2CO_3 respectively). After adding the required amount of buffer stock solution to the homogenized clay suspension in the reactor, the base was added (usually less than the amount needed for no buffer case) to the suspension to bring the initial pH near 7.8. In these experiments using buffer, the quantity of $NaNO_3$ added initially to the water was reduced correspondingly to keep the ionic strength at 0.005 M.

4.3.4. Temperature measurement

Routine temperature measurements were all performed using a type 'T' thermocouple. The thermocouple consisted of a pair of wires (copper/constantine), which form a bi-metallic junction. The junction produces a voltage which varies directly as the temperature varies. The data acquisition card was equipped with a cold block

(junction), and was internally calibrated to convert the voltage produced by thermocouple to a temperature reading. The thermocouple was encased in a glass sheath to prevent interference with the pH measurements. The glass sheath caused a minor lag in the response time of the probe, but it was not long enough to warrant concern (on the order of seconds). The temperature was also checked with the manual thermometer which gave same reading as that of thermocouple. Typical temperature profiles are shown in **Figure 4.10**.

4.3.5. Data acquisition and control

The data acquisition system was used to monitor the flocculation reactor. The following process control parameters were monitored:

- reactor pH,
- reactor temperature,
- outputs from PDA (dc, rms, and ratio).

The pH meter, the thermocouple for temperature measurement and the output ports of the PDA were connected to a terminal panel which was connected to the analog card of the ACPC-16 Analog Connection personal computer based data acquisition/control system (Strawberry Tree Computers; Sunnyvale, CA) (STC). The data acquisition and control card was housed in a z-159 Zenith Desktop Personal Computer System. During each experiment the STC collected the data and stored it to a file on a 5.25 inch floppy disk. The file was then retrieved in a Quatro Pro spreadsheet and graphs were drawn, saved and printed out to provide a permanent record of the flocculation conditions. The

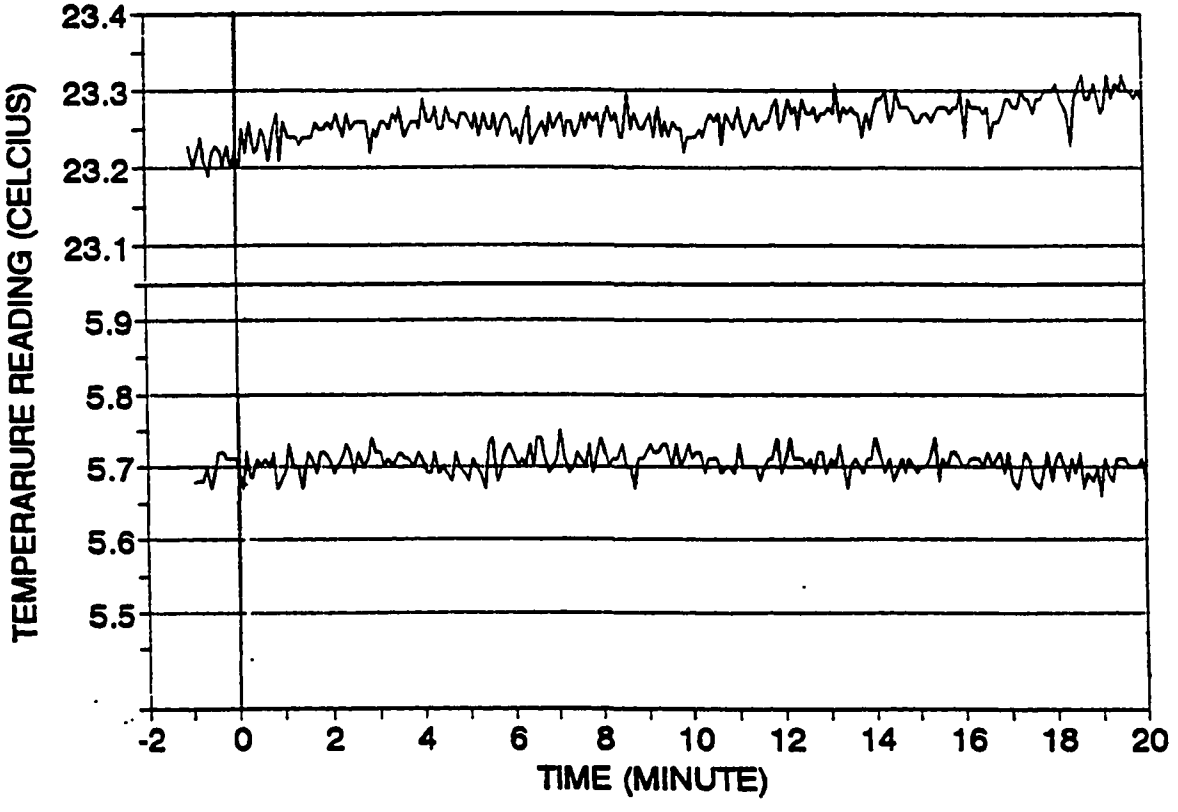

4.10. Typical temperature versus time curves during two experiments performed at different temperaturre

data acquisition system collected data on 5 seconds interval.

The constant temperature conditions were achieved using a walk-in constant temperature room. The temperature of the room was also monitored and controlled using the STC based data acquisition and control system. **Figure 4.2** illustrates the schematics of Experimental Setup, where M is the motor driving the impeller and PC is the z-159 Zenith Desktop Personal Computer System equipped with data acquisition system.

4.3.6. Turbidimeter and turbidity measurement

The turbidity of the initial suspension (homogenized) and samples taken at the end of different periods of sedimentation following flocculation was measured with a Hach Model 18900 Ratio Turbidimeter, manufactured and distributed by Hach Chemical Company, Loveland, CO. Turbidity was used as a quick surrogate check of kaolinite primary particle concentration. The turbidity of the settled water after flocculation is a common indicator of flocculation efficiency.

The turbidimeter was calibrated as per the manufacturers recommendations. The sample for turbidity measurement was drawn through the reactor sampling port from the impeller blade level which was 5.5 inch from the reactor bottom. It was taken with a 60 ml capacity syringe equipped with a #13 gauge needle. The homogenized (initial) sample was taken after intensely mixing the suspension (G = 450/s) for over a minute prior to coagulant addition. In addition, three more samples were collected at the end of 10, 20 and 30 minute sedimentation in the reactor with the mixer shut off following flocculation. The samples were loaded directly into a sample cuvette and the cuvette

was inverted gently several times before measurement. The outside of the cuvette was wiped clean with a tissue (Kimwipe) before placing the sample in the instrument. It was noted that all samples needed about a minute to produce stable reading.

4.3.7. Laser Zee Meter and Zeta potential measurement

A model 102 Lazer Zee Meter, manufactured by Pen-Kem Inc. of Croton-on-Hudson, NY, was used to measure zeta potential. The electronics in the zeta meter have been upgraded to model 104 electronics, but the optics were still original. Zeta potential (ZP) was used as a quality control parameter. ZP were measured on the coagulated sample immediately following rapid mix for all experiments. Zeta potential of the homogenized sample was measured irregularly to check consistency of the stock suspension. The measurement techniques detailed in the manufacturers literature were closely followed.

The calibration of the instrument was checked using a standard suspension provided by the instrument manufacturer. The instrument performed well measuring the standard colloid. The sample to be measured was drawn from the reactor and kept in the constant temperature room until before measurement. The measurement was done within half an hour after sample collection. The temperature of the cold sample changed gradually during measurement, but no temperature correction was applied to the reading, because, the correction provided by the manufacturer was negligible for a very large temperature change and was less than operator's error. A typical variation of ∓ 2 mv was observed for several readings of the same sample by a single operator. The variation

between operators was even greater.

4.3.8. Control of mixing intensity

The impeller rpm was used as the operational control parameter. The G for the reactor was estimated from G versus rpm curve generated from calculated power based on measured torque. The torque was measured by a rotating torque meter (Bex - O - Meter, Model 38, The Bex Company, San Fransisco, CA) using a photographic technique. The torque meter was connected between the motor and the impeller with the help of plexiglass coupling. The torque meter had two rotating parts. The top part had main torque scale and the bottom part had vernier scale. In standing (no motion) condition the two '0's aligned on the two scales. As the motor drove the impeller, torque meter rotated with the impeller and there was a twist between the two parts of the torque meter due to drag produced by the fluid on the impeller. But the reading produced by the torque meter through the relative displacement of the main and vernier scales could not be read by eye. Therefore the reading was obtained by photographing the scale with a 35 mm camera using high shutter speed (1000/s) and high speed black and white 'Kodak' film. The torque values were read out from the printed photographs later on. A series of pictures (at least three for each impeller rpm) were taken at different rotating speeds of each impeller, and the torque values were read from the printed photographs in oz-inch. The power was calculated from the following equation:

$$P = T.\omega \qquad 4.6$$

P = power in watts, T = torque in N-m, and ω = angular velocity = 2π(rps)

P = (N-m) x (2π x rps) = (2π/60) x (rpm) x (torque in N-m)

= 0.1047(rpm) x (torque in N-m)

= 0.1047(rpm) x 0.00706(torque in oz-inch)

= 0.0007391(rpm) x (torque in oz-inch)

The rms velocity gradient in the reactor (G) was calculated from the following equation:

$$G = [P/(V\mu)]^{1/2} \qquad 4.7$$

V = working volume of the liquid = 18 L = 1.8 x 10^{-2} m^3 and μ = dynamic viscosity in $N.s/m^2$ = 0.9608 x 10^{-3} at 23° C.

Therefore by putting these values of V and μ at room temperature (23^0 C),

$$G = [(0.0007391 \times rpm \times \text{torque in z-inch})/(1.8 \times 10^{-2} \times 0.9608 \times 10^{-3})]^{1/2}$$

$$= 6.54\,[NT]^{1/2} \qquad 4.8$$

N = rpm of impeller and T = corresponding torque reading in oz-inch.

The G versus rpm curves were plotted using Equation 4.8. The G versus rpm curves for the different impellers are shown in **Figures 4.11 and 4.12**. During the cold temperature experiments, in order to obtain desired mixing intensity, constant rpm was maintained. So the energy input was the same at both temperatures due to fully developed turbulence, but, the G values were less at cold temperature due to higher viscosity. This approach was also adopted by Hanson (1989) and Hanson and Cleasby (1990). Hanson

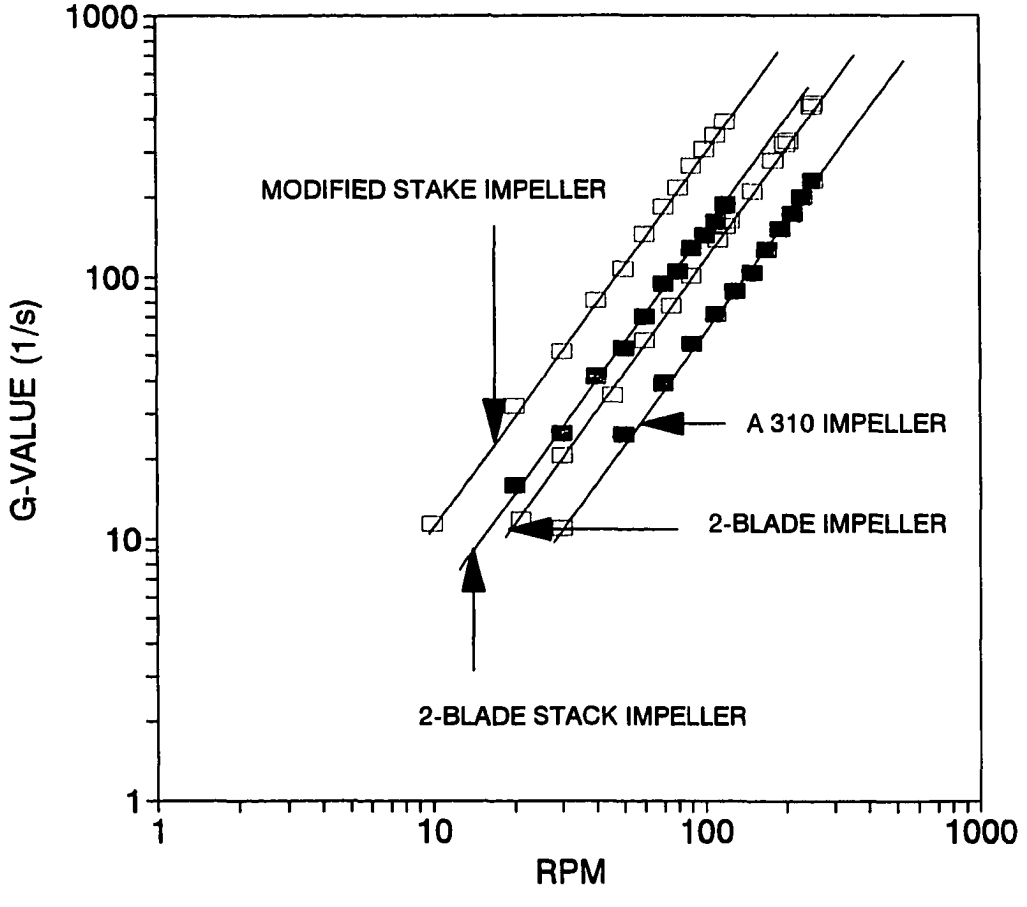

Figure 4.11. G versus rpm curves for different impellers at 23° C

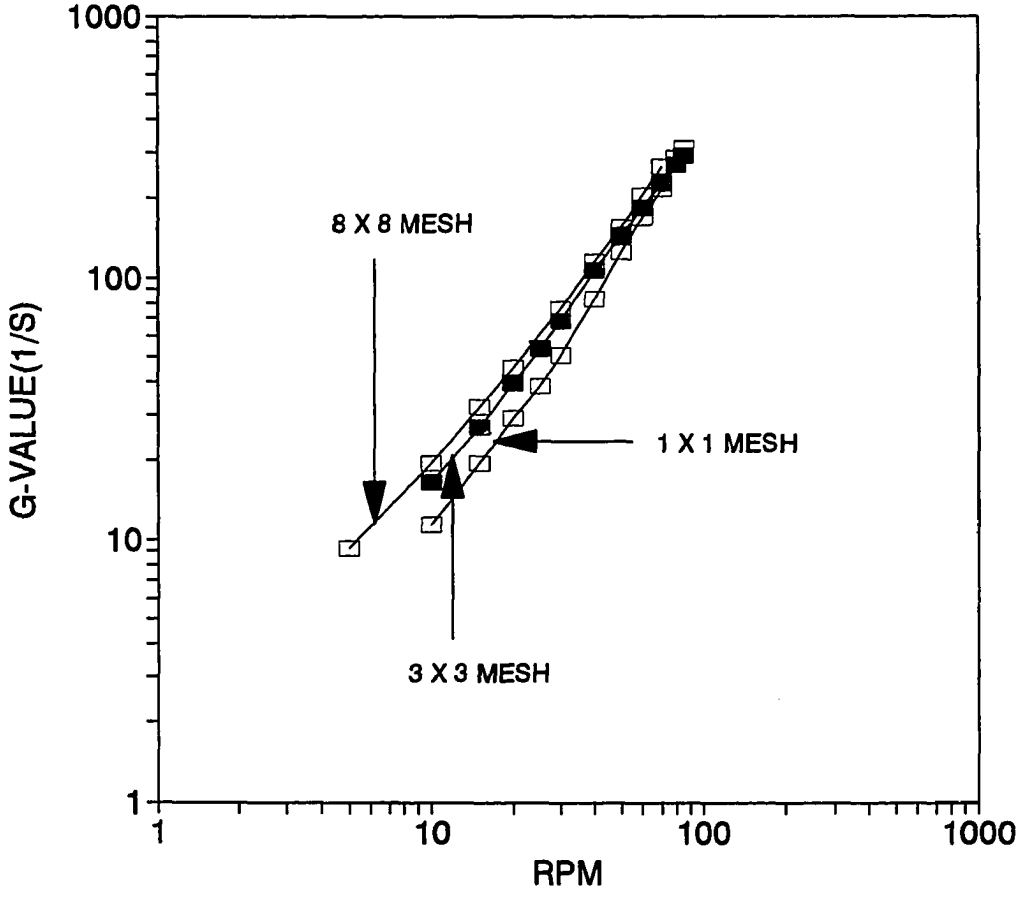

Figure 4.12. G versus rpm curves for wire mesh impellers at 23° C

(1989) gave the experimental evidence that the ε versus rpm was inertially controlled in his work (i.e., measured torque was the same at two different temperatures when the rpm was kept unchanged) using the same 2-blade impeller used in the current work. Hanson and Cleasby (1990) stated:

> It is noted that maintaining a constant rpm as the temperature varies is equivalent to maintaining a constant ε. This is because the system is inertially controlled, and the viscous forces can be neglected. This was verified experimentally. (p. 67)

It is assumed in the current work, that the same would be true for all of the impellers used in this study.

4.3.9. Mixing impellers

Five mixing impellers as shown in **Figure 4.1** were used in this study. A brief description of each of those impellers will be given in this subsection:

1. 2-blade impeller: This is a turbine impeller that generates radial flow in the reactor similar to that shown in **Figure 4.13a**. It has two circulating loops of flow at top and bottom of the impeller blade. This impeller was used by many researchers in flocculation studies, such as, Argaman and Kaufman (1968 and 1970), Hanson (1989), and Hanson and Cleasby (1990). **Figure 4.1a** shows the geometry of this impeller.

2. A 310 impeller: Figure 4.1b shows the geometry of this impeller. This is "fluidfoil" impeller, similar to a pitched blade turbine, that generates the flow in an axial pattern similar to that shown in Figure **4.13b**. This is designed and manufactured by LIGHTNIN, Rochester, NY, a unit of General Signal. The manufacturer claims it to be

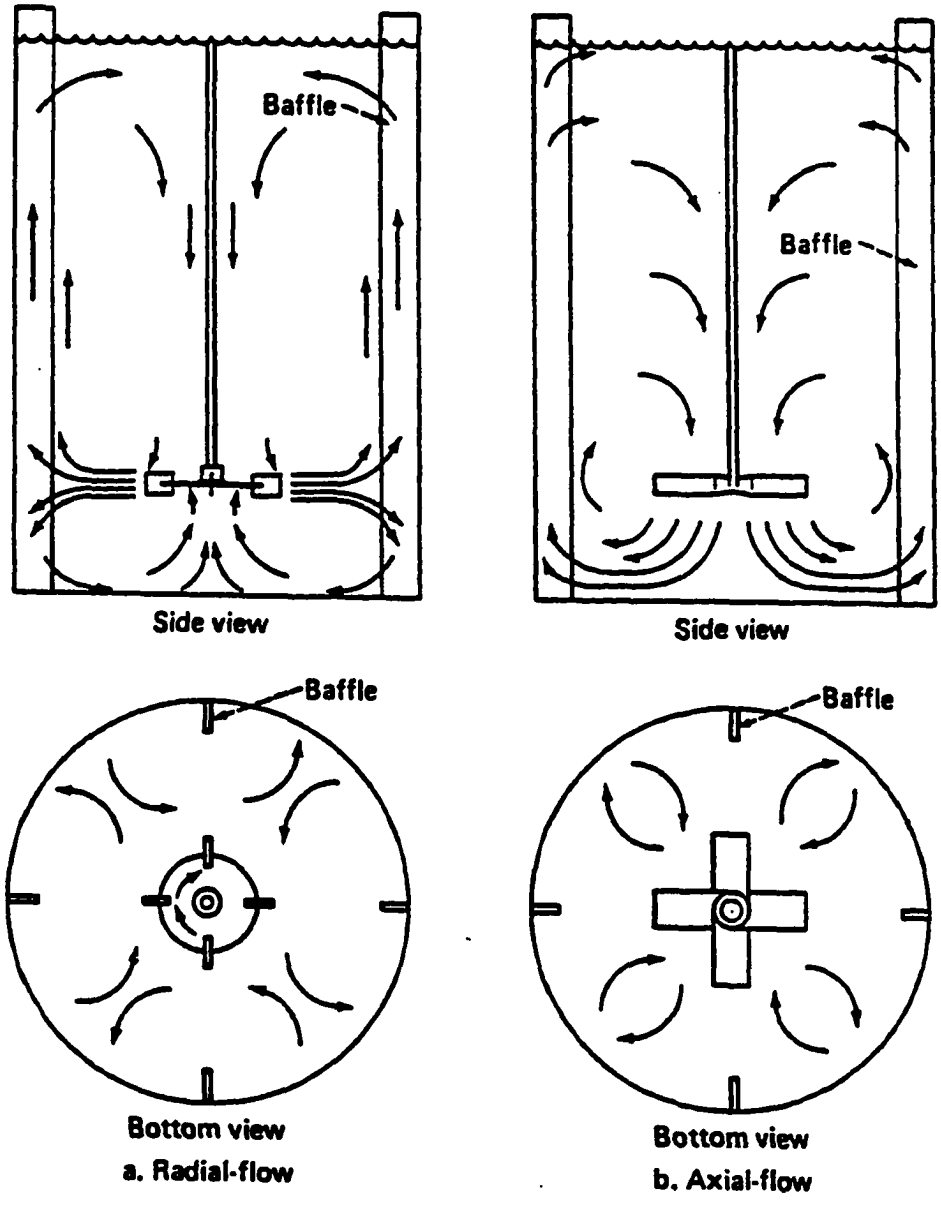

4.13. Flow patterns for radial and axial flow impellers (McDonough, 1992)

much more efficient with respect to flow generation and power consumption for keeping particles in suspension, than a pitched blade turbine (Manufacturer's advertising literature). The impeller used provided a D/T ratio (diameter of impeller/width of tank) of 0.52 which is near the maximum recommended by the supplier of 0.5. This impeller is a model of similar fluidfoil impellers used in full scale water treatment plants.

3. Modified stake impeller: This impeller geometry was obtained by modifying the stake impeller (without the stator) used by Hanson and Cleasby (1990) and Argaman and Kaufman (1970 and 1968). The number, width and the spacing of the arms were kept unchanged but the length of the arms were made longer to occupy almost the entire depth of the liquid. The arms are of stainless steel (3/8 inch wide by 10.5 inch long by 1/8 inch thick). The free end of the arms were 0.5 inch from the reactor bottom and the supporting arm was above the water surface. This impeller is opposite to the other two in the sense that it delivers power throughout the liquid volume and produces less pumping than the above two impellers for the same power input but requires lower speed to achieve the same torque. **Figure 4.1c** shows the geometry of this impeller.

4. Wire mesh impeller: This impeller was designed and manufactured by the author in the laboratory. The author believes that this impeller produces less pumping but generates high level velocity fluctuations throughout the reactor resulting in a small scale turbulent motions. No measurements were made of the velocity fluctuations but the theory of small scale motions produced by this impeller has been hypothesized based on the results of the work by Casson and Lawler (1990) and Arboleda-Valencia (1991). Three different mesh openings (8x8 openings, 3x3 openings, and 1x1 opening

per square inch) were studied in this study. The wires were thin (1 mm diameter) and are believed to produce much less drag than the flat long rectangular bars of the modified stake impeller. **Figure 4.1d** shows the geometry of these impellers.

5. The 2-blade stack impeller: Figure 4.1e shows the geometry of this impeller and **Figure 4.14** illustrates the flow pattern generated by this impeller inside a reactor. It has been manufactured by placing three 2-blade impellers with equal spacing on a vertical shaft. This impeller is believed to generate flow pattern intermediate between turbine types (both 2-blade and A 310) and the paddle types (modified stake and wire mesh) impellers.

The laminar to turbulent transition for an agitated tank with turbine impellers occurs at an impeller Reynold number (R_e), $\rho ND^2/\mu$ from 1 to 10,000, where N is the rotational speed in revolutions per time, D is the impeller diameter and μ is the dynamic viscosity (Tatterson, 1991). Above R_e = 10000, the mixing is fully turbulent. Most full scale water treatment plants use a flocculation G between 30 to 100/s. In the current study, the flocculation G values used were within this range. The impeller based Reynold's numbers for the 2-blade, A 310, 3 x 3 mesh, 2-blade stack, and modified stake impellers used in this study at lowest slow mixing intensity (G = 30/s at 23° C) were 10357, 19549, 17607, 8545, and 16582 respectively indicating that flocculation occurs under fully turbulent conditions in most situations. It should be noted that, under normal operating conditions, even though the impeller based Reynold's number indicates fully turbulent regime in the reactor for turbine impellers, it is probable that a good portion of the bulk fluid does flow under transitional regime due to flow field

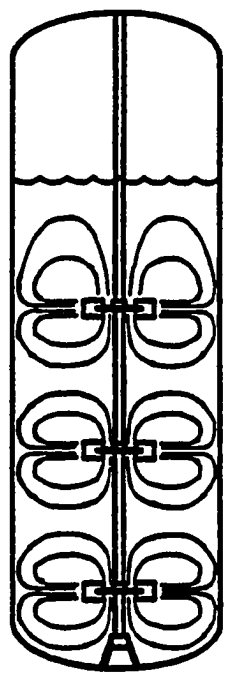

4.14. Flow pattern for vertical stacking radial flow impeller (McDonough, 1992)

inhomogeneity indicated by several researchers (Cutter, 1966; Okamoto et al., 1981; and Van't Reit et al., 1976). At cold temperature this becomes more certain.

4.3.10. Anatomy of a batch reactor experiment

The schematic of the experimental setup was shown earlier in **Figure 4.2**. The following sequence of steps will enable us to visualize the entire picture of how a batch reactor experiment was performed in this study:

1. On the day prior to the experiment, the dosing solution of desired concentration was prepared and stored at room temperature. On the day of experiment, the PDA instrument, clay mixing pump and turbidimeter were first turned on. The PDA instrument and the turbidimeter were warmed up for 30 minutes and for an hour respectively before use. The clay mixing was done for 40+ minutes to insure complete homogeneity in the tank.
2. During this time of equipment warm up and clay mixing, the reactor was connected to the PDA machine and the peristaltic pump, the syringes were loaded with the required amounts of coagulant and base, and pH meter was checked and calibrated
3. The reactor was then filled up to 12-L mark with distilled water and 90 ml of 1N $NaNO_3$ was added. The peristaltic pump was turned on to circulate this water through PDA cell. The 'DC' gain switch of the PDA was then adjusted to achieve a voltage gain of 10 volt using the clear water in the reactor. The RMS switch was set at 50 at this time. This calibration was checked for about 10 minutes.
4. After the clay suspension was mixed thoroughly, the required amount of stock clay

suspension was obtained with a beaker and measured into a graduated cylinder. This stock suspension was added into the reactor and the volume of suspension in the reactor was then brought up to 18 L. The peristaltic pump was turned off just before adding the clay into the reactor.

5.The wooden support equipped with impeller and electric motor was placed on the reactor and both pH and temperature probes were inserted into the holes through the support. The motor controller and the pH meter was turned on and the impeller speed was set corresponding to mixing G = 450/s in order to achieve a homogeneous clay suspension of kaolinite clay in the reactor.

6. After two minutes of mixing at this high speed, the homogenized sample was drawn from the reactor through sampling port by using 60-ml syringe with a needle to be used for turbidity and zeta potential measurement. The peristaltic pump was turned on again to circulate this homogenized sample through the PDA cell. High intensity mixing was continued for another two minutes before coagulant injection. During this whole period of high intensity mixing, base was added into the reactor through a sampling port with a rubber septum to set the pH at the desired level. The data acquisition system was instructed immediately after setting the target pH, to start recording data at 5 second intervals, directly to a floppy disk. The initial flocculation index value was recorded at this time.

7. Coagulant and base were then injected together through two ports into the reactor and the stop watch was turned on. After one or two minutes of rapid mixing at desired intensity, the impeller speed was reduced, set at desired slow mixing intensity and a

sample was drawn with 60-ml syringe for zeta potential measurement. During the whole period of this rapid mixing, the pH was maintained near the target value by the addition of 0.02N NaOH.

8. Flocculation was performed for 20 or 30 minutes. During this period, pH was maintained near the desired value by adding 0.02N NaOH. Flocculation index was observed visually and recorded manually at 5 minute intervals.

9. At the end of flocculation, the acquisition system was instructed to stop recording data on the floppy disk and the flocs were allowed to settle for 30 minute period. Samples were collected at a depth of 14 cm from the reactor bottom through the sample port at 10 minute intervals and turbidity of these samples was measured and recorded. The zeta potential measurement of the rapid mixed sample was also done during this settling period.

10. At the end of settling period, the batch reactor was drained into the drain pipe, was disconnected from the PDA and the peristaltic pump, and the reactor was washed thoroughly several times with warm and cold waters. The reactor was then placed inverted on paper towels to drain all the loose moisture from the reactor wall and allowed to dry off before the next experiment. At the end of the day the reactor was cleaned with soap and water. Usually two to three experiments were performed in a single day.

5. EXPERIMENTAL DESIGN

5.1. General

This section has been designed to direct or to act as a road map for the next chapter which contains the results of the experimental study. Since mixing was the prime concern of this study, the mixing variables were isolated from other physico-chemical variables. The variables were divided into two broad classes: mixing variables and physico-chemical variables. Mixing variables include:

- Impeller geometry
- Rapid mixing intensity
- Rapid mixing pattern
- Coagulation injection pattern
- Concentration of dosing solution
- Number of coagulation injection ports
- Slow mixing intensity
- Slow mixing pattern
- Mesh opening size
- Combination of impellers

The physico-chemical variables include:

- Type of coagulant
- pH

- Coagulant dose
- Temperature
- Clay concentration

It should be kept in mind that for evaluating the effect of a particular mixing variable, only that variable was varied and all the other mixing variables were kept unchanged. All the above mentioned mixing variables were tested using ferric nitrate as the coagulant. In addition, a number of experiments were done with alum to observe the effect of impeller geometry, rapid mixing intensity and slow mixing pattern. The following sections describe the experimental plans for evaluating the effect of different mixing variables under various sets of physico-chemical conditions. The physico-chemical conditions for each set of experiments are designated as 'treatment sets' in the following sections.

5.2. Experimental Plans

5.2.1. Experimental plan to observe the effects of impeller geometry

Figures 5.1a through e illustrate the experimental plans for evaluating the performance of different impeller geometries on flocculation efficiency. Five different impellers as shown earlier in **Figure 4.1** were tested for this purpose. In most of the flocculation experiments with ferric nitrate, three impellers (A 310, 2-blade and 3x3 mesh) were used. In two sets of experiments (see **Figure 5.1c**), four impellers were employed to observe their performance, and in two other sets of experiments, only two

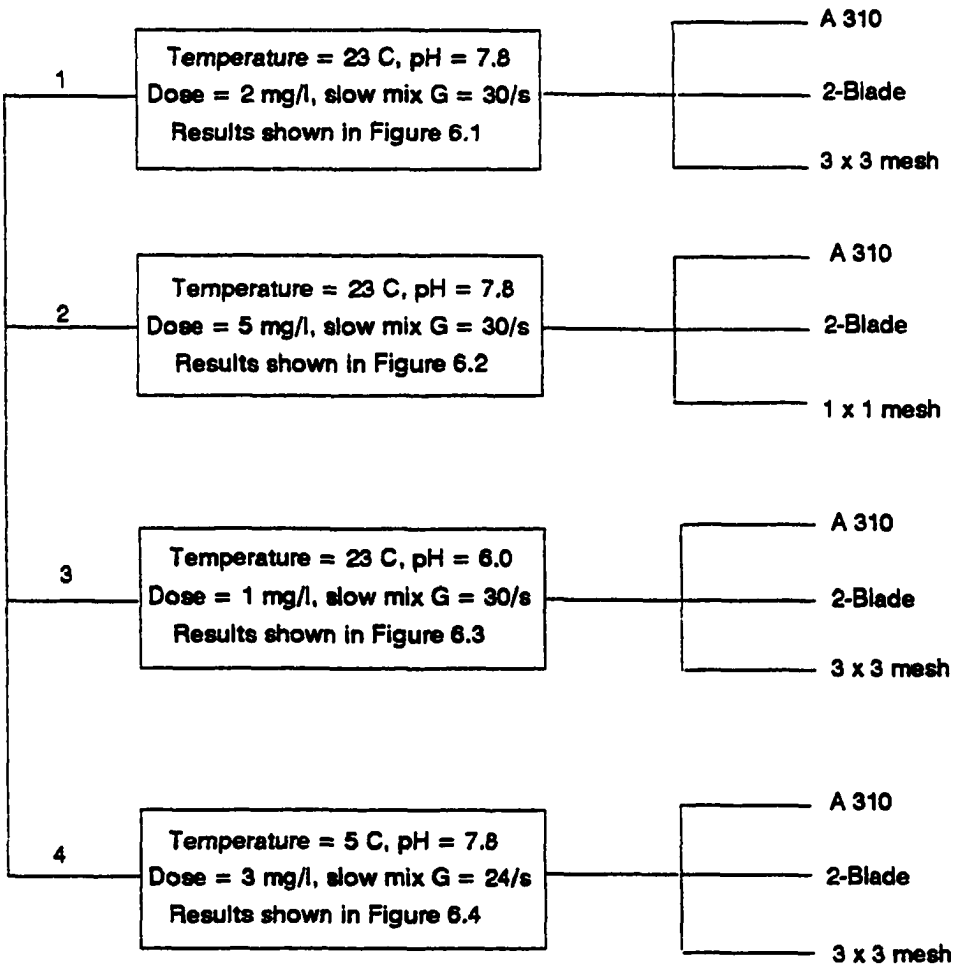

(a)

Figure 5.1. Experimental plan for evaluating the effect of impeller geometry on flocculation kinetics a) with ferric nitrate as coagulant under varying conditions; clay suspension concentration is 25 mg/l and rapid mix G values are 450/s at 23° C and 360/s at 5° C

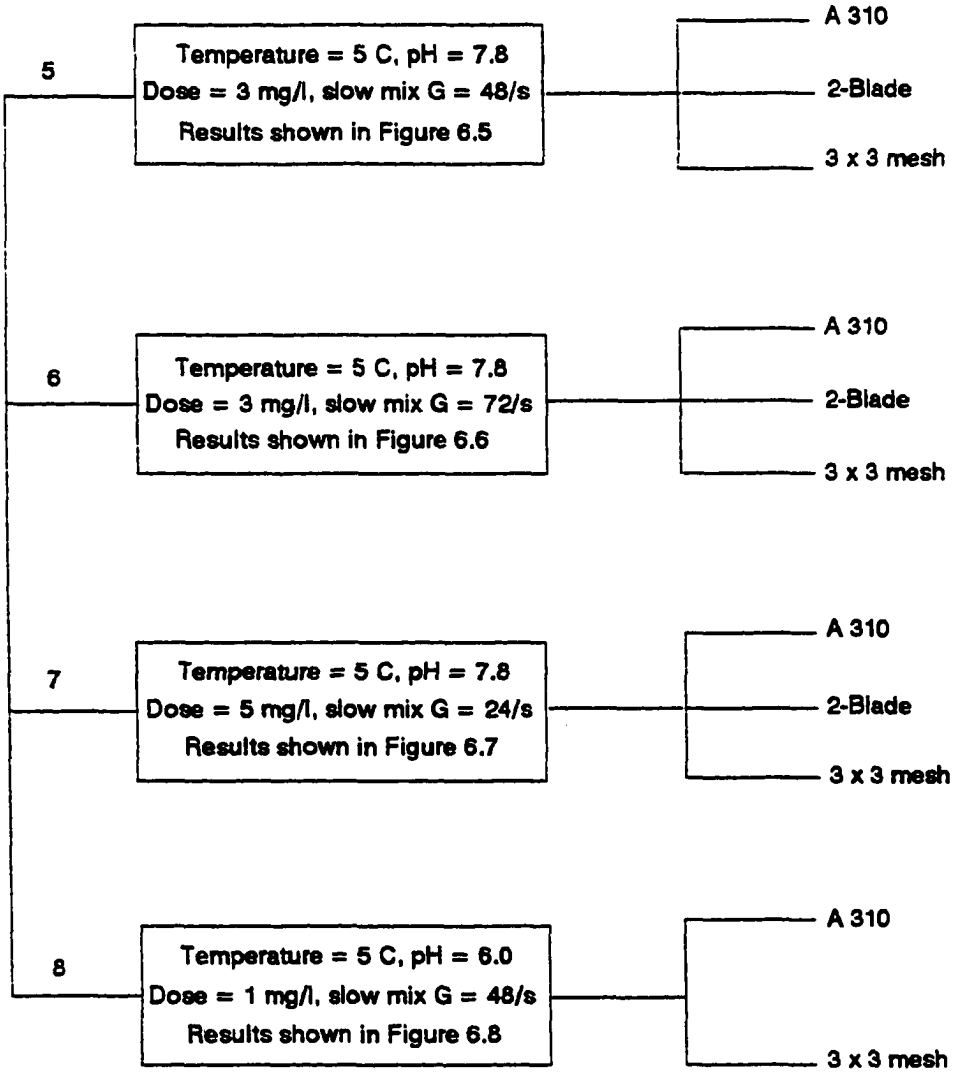

(b)

Figure 5.1. (continued) b) with ferric nitrate as coagulant under varying conditions; clay suspension concentration is 25 mg/l and rapid mix G = 360/s

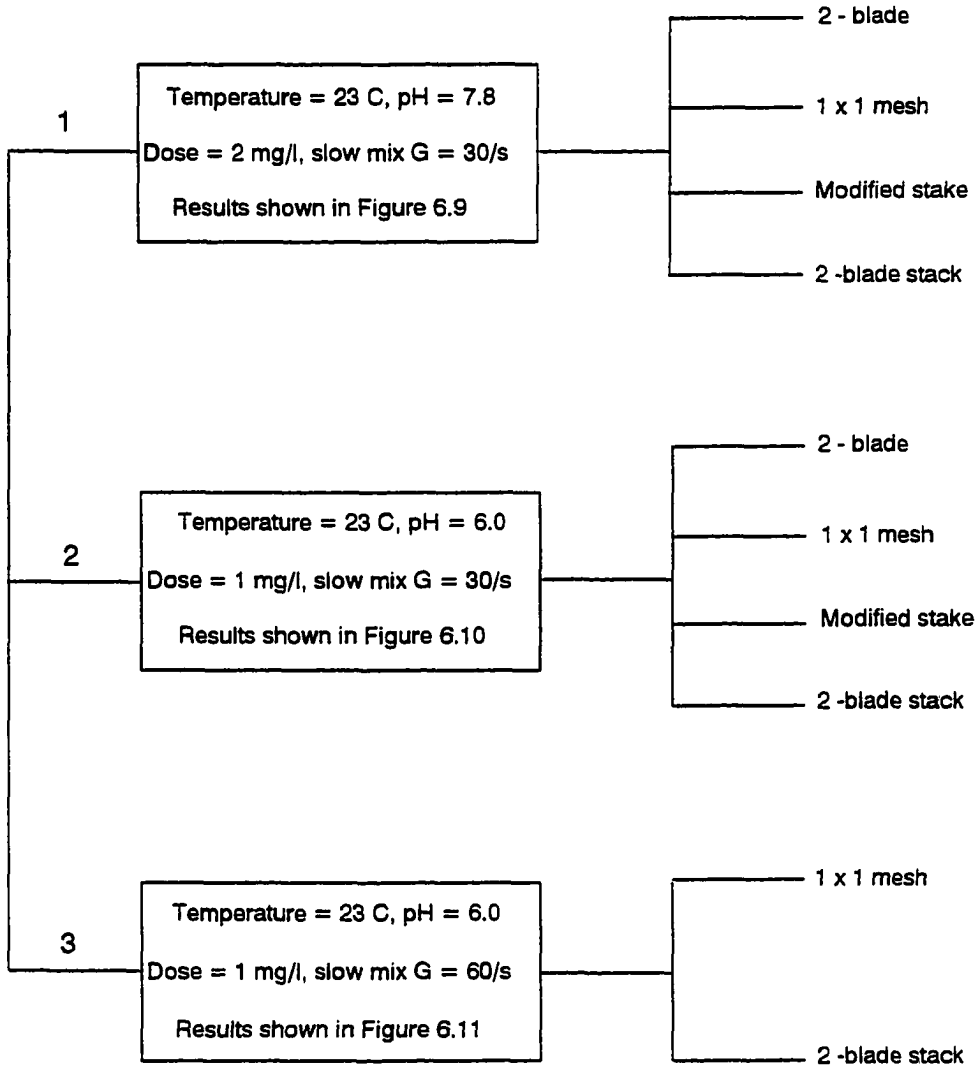

(c)

Figure 5.1. (continued) c) with ferric nitrate as coagulant under varying conditions; clay suspension concentration is 25 mg/l and rapid mix G = 325/s

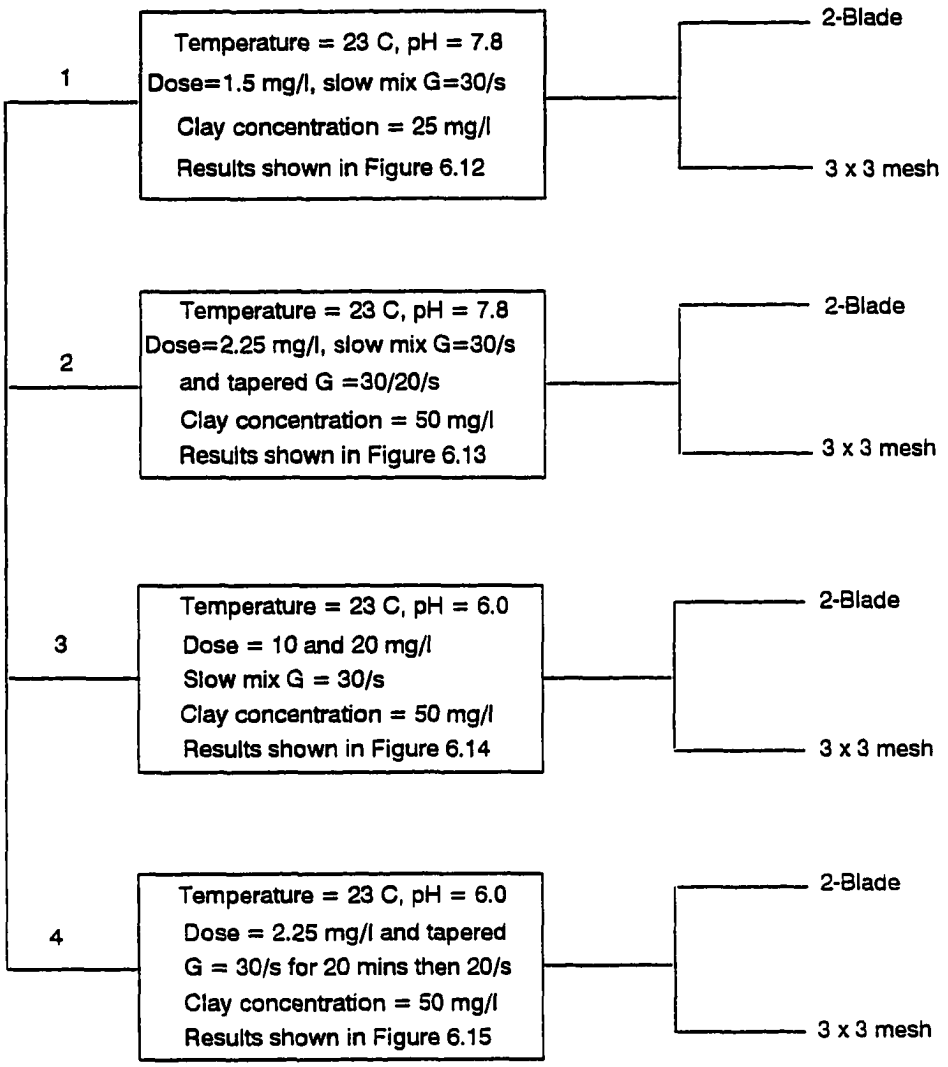

(d)

Figure 5.1. (continued) d) with alum as coagulant under varying conditions; rapid mix G = 325/s

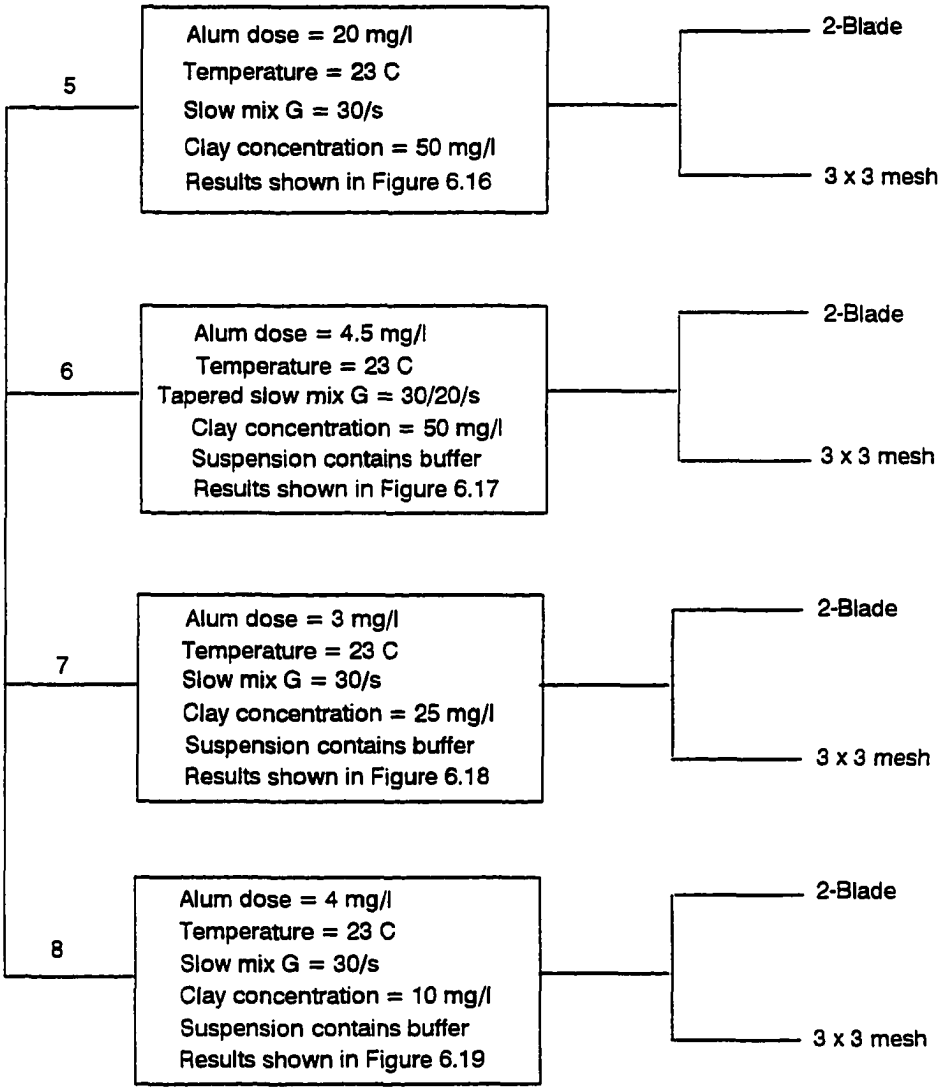

(e)

Figure 5.1. (continued) e) with alum as coagulant under varying conditions; rapid mix G = 325/s

impellers were used. **Figures 5.1a through c** show the experimental plans to evaluate the effect of impeller geometry on flocculation kinetics with ferric nitrate as the coagulant. **Figures 5.1d and 5.1e** illustrate the experimental plans to evaluate the effect of impeller geometry on flocculation kinetics using alum as the coagulant. Only two impeller geometries (2-blade and 3x3 mesh) were tested in this case under eight different sets of physico-chemical conditions.

5.2.2. Experimental plan for evaluating the effect of rapid mixing intensity

Figure 5.2 illustrates the experimental plan for evaluating the effect of rapid mixing intensity. Different rapid mixing intensities were used under varying conditions. In treatment set 1 (box 1 in **Figure 5.2**) five rapid mixing intensities (G = 200, 325, 450, 575, 700/s) were used. For treatment sets 2 and 3, three rapid mixing intensities were used and in treatment set 4, four rapid mixing intensities were used. In three cases (sets 1, 2 and 4) ferric nitrate was used as the coagulant and in case of treatment set 3 alum was used as the coagulant.

5.2.3. Experimental plan for evaluating the effect of rapid mixing pattern

Figure 5.3 illustrates the experimental plan for evaluating the effect of rapid mixing pattern. Ferric nitrate was used as the coagulant in all the cases. A constant Gt value of 27000 was arbitrarily chosen to vary the mixing pattern. Two patterns were tested: low intensity (G = 225/s) with long duration (2 minutes), and high intensity (G = 450/s) with short duration (1 minute). Three impellers were used in four different sets of

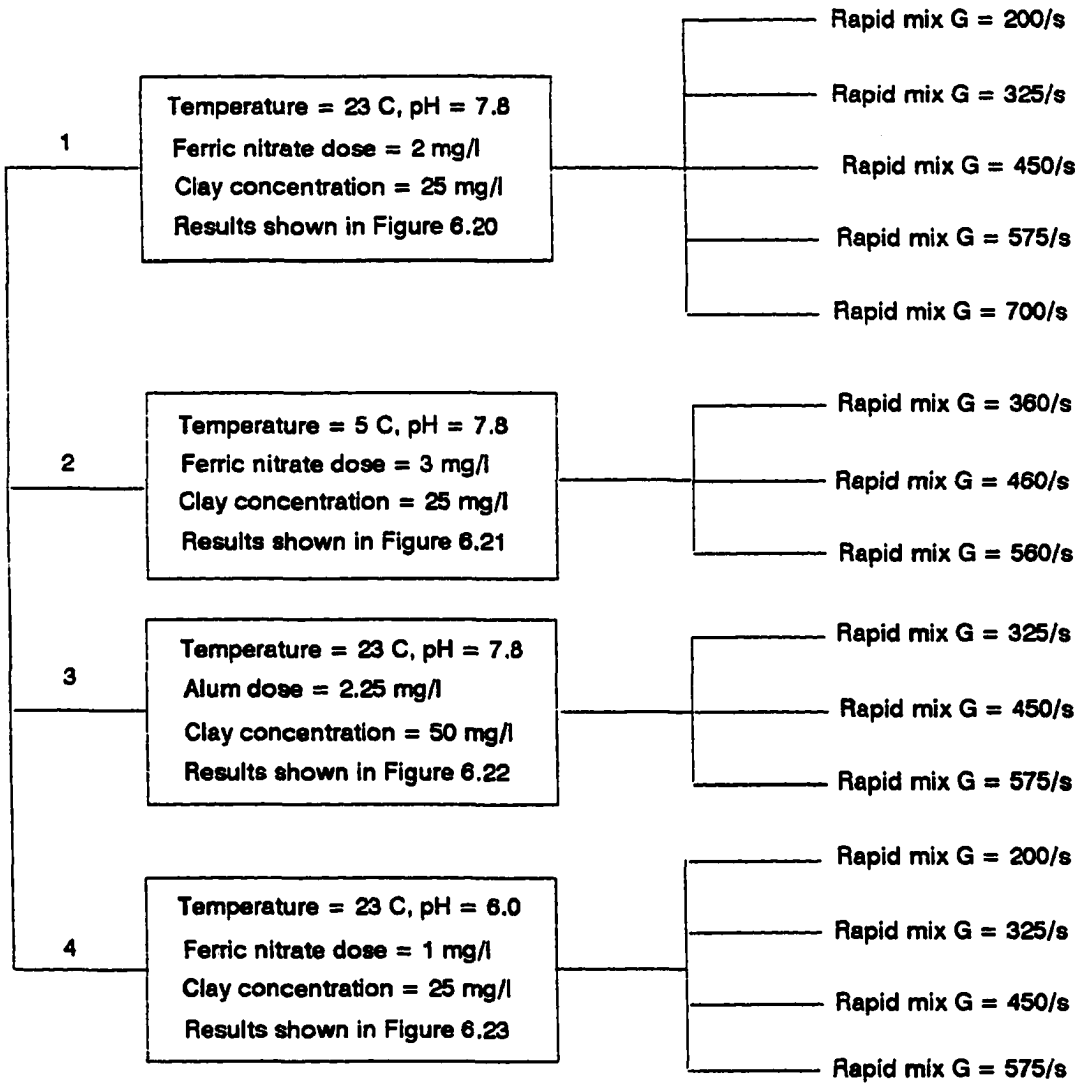

Figure 5.2. Experimental plan for evaluating the effect of rapid mixing intensity on flocculation kinetics with metal salts as the coagulant under varying conditions. 2-blade impeller was used and slow mix G values were 30/s at 23° C and 24/s at 5° C

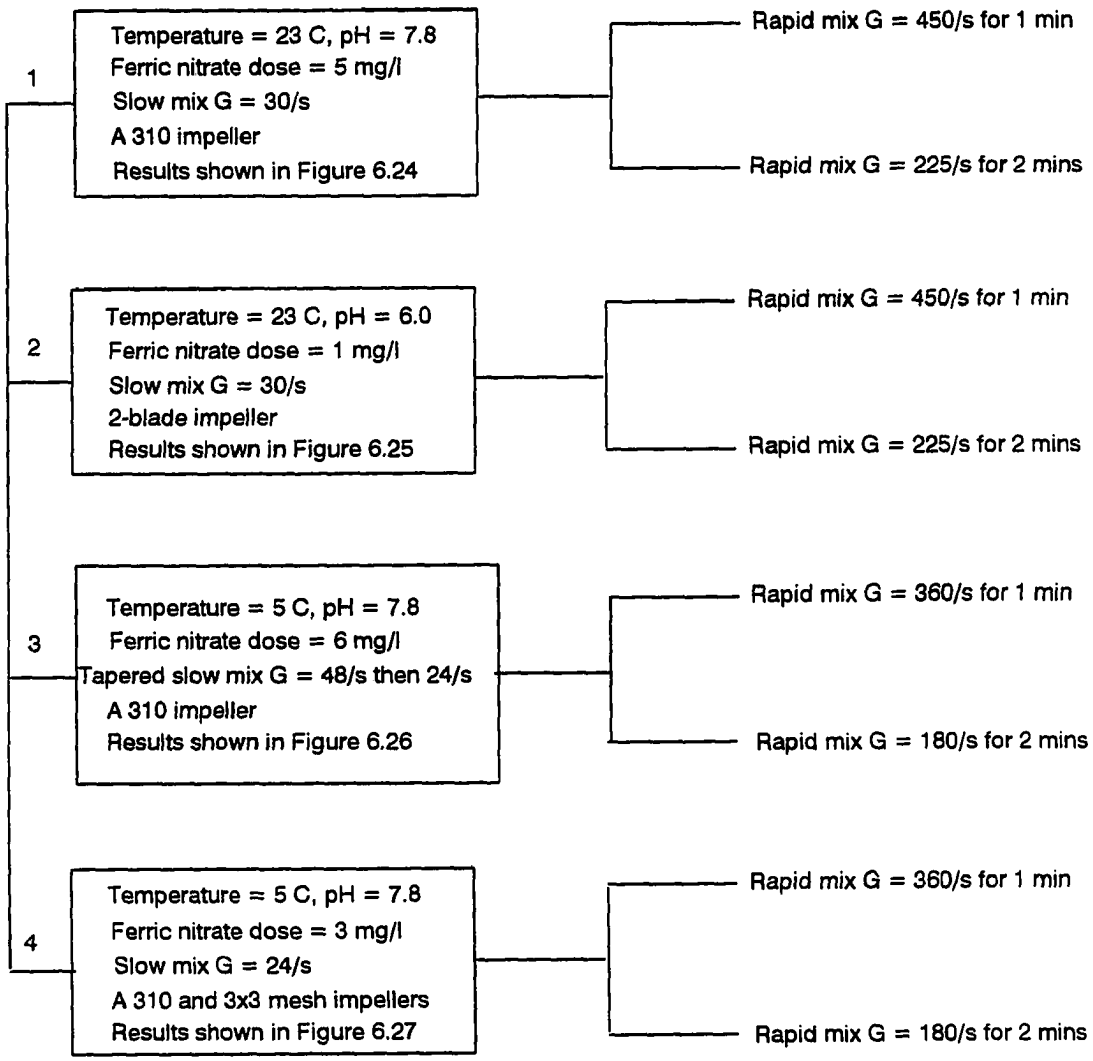

Figure 5.3. Experimental plan for evaluating the effect of rapid mixing pattern on flocculation kinetics with ferric nitrate as the coagulant under varying conditions. Clay concentration was 25 mg/l

physico-chemical conditions to observe the effect of these two rapid mixing patterns.

5.2.4. Experimental plan for evaluating the effect of coagulation injection pattern

Figure 5.4 depicts the experimental plan for observing the effect of coagulation injection pattern. Two patterns were used: slow injection (gradually over 10 seconds duration) and pulse injection (within a second) with a syringe equipped with #13 gauge needle. These patterns were tested with ferric nitrate coagulant and 2-blade impeller at two different temperatures.

5.2.5. Experimental plan for evaluating the effect of dosing solution concentration

Figure 5.5 shows the experimental plan for evaluating the effect of dosing solution concentration. Coagulant dose in the suspension was kept constant, only the concentration of the dosing solution was changed. That means, when the dosing solution concentration was half the previous concentration, twice the previous volume was injected into the reactor to keep the dose constant. Three dosing solution concentrations (5 mg/ml, 10 mg/ml, and 20 mg/ml) were used in treatment sets 1 and 2 and two concentrations (10 mg/ml and 20 mg/ml) were used in treatment set 3.

5.2.6. Experimental plan for evaluating the effect of number of coagulant injection ports

Figure 5.6 shows the experimental plan for determining the difference in performance between 1-point and 2-point injections of coagulant. In 1-point injection,

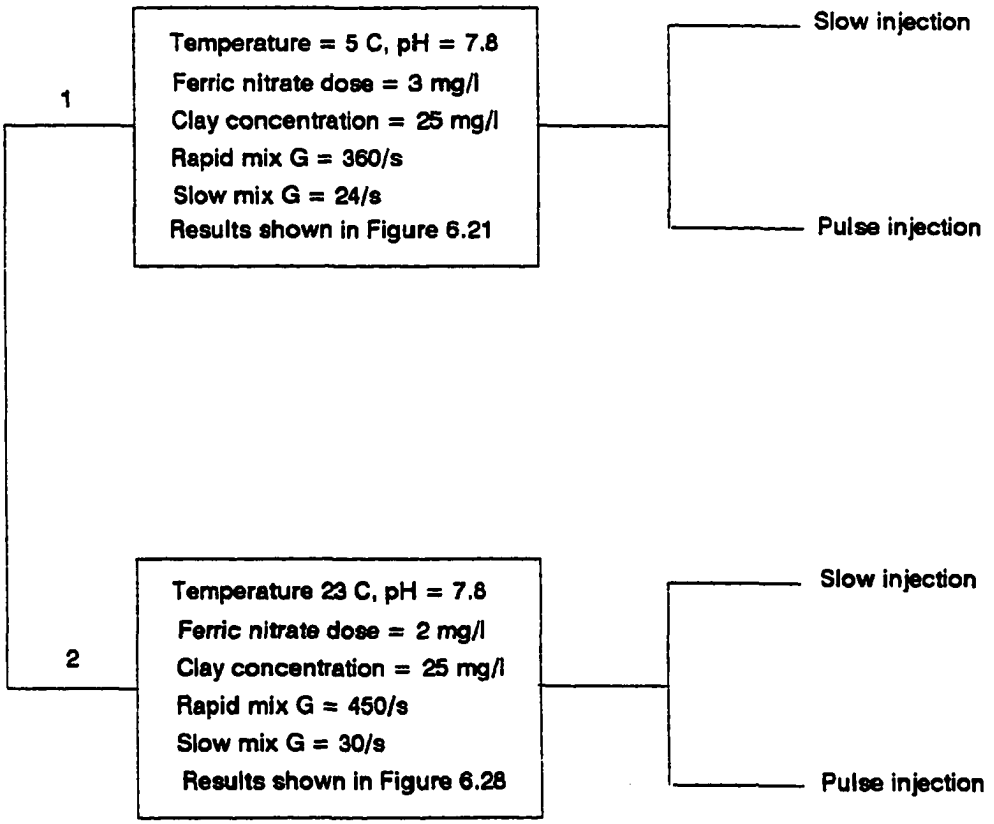

Figure 5.4. Experimental plan for evaluating the effect of coagulation injection pattern on flocculation kinetics with ferric nitrate as the coagulant under two different conditions. 2-blade impeller was used

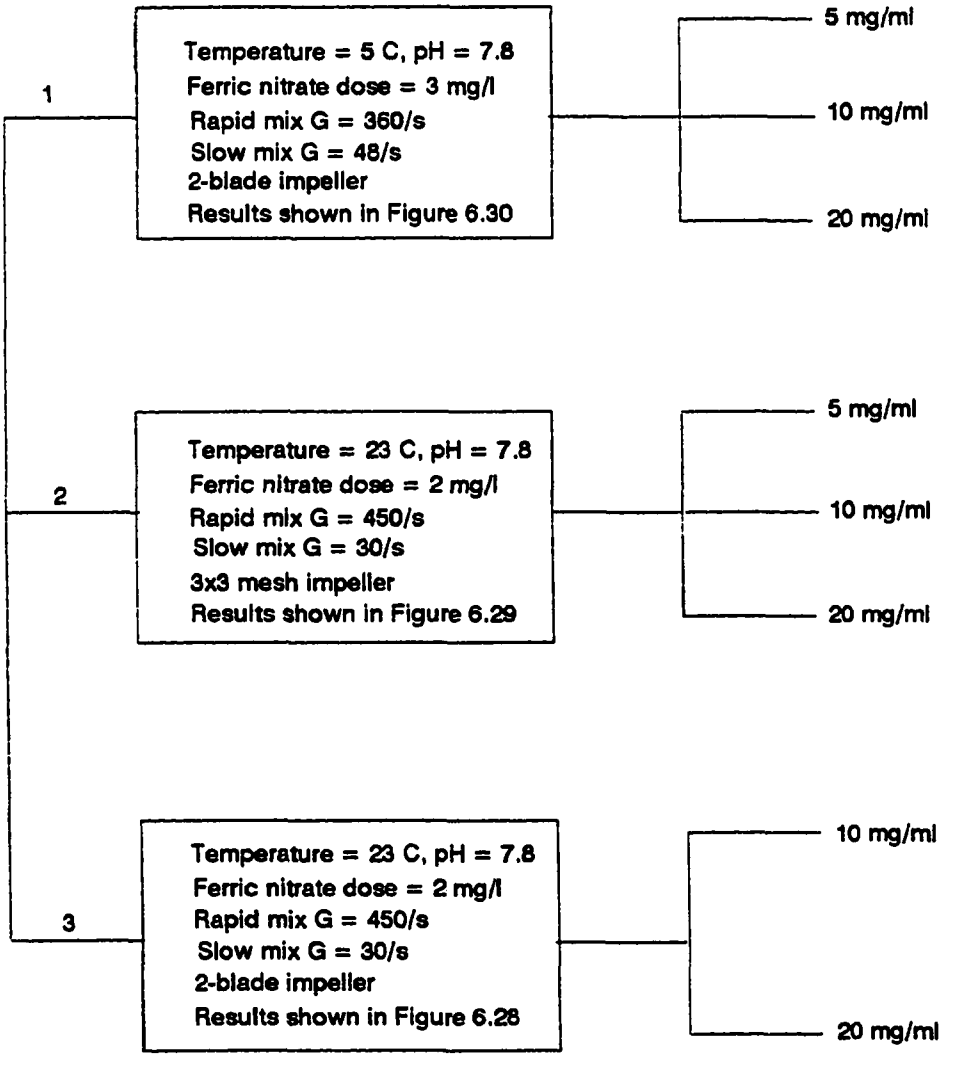

Figure 5.5. Experimental plan for evaluating the effect of the concentration of dosing solution on flocculation kinetics under three different conditions with ferric nitrate as the coagulant. Clay concentration was 25 mg/l

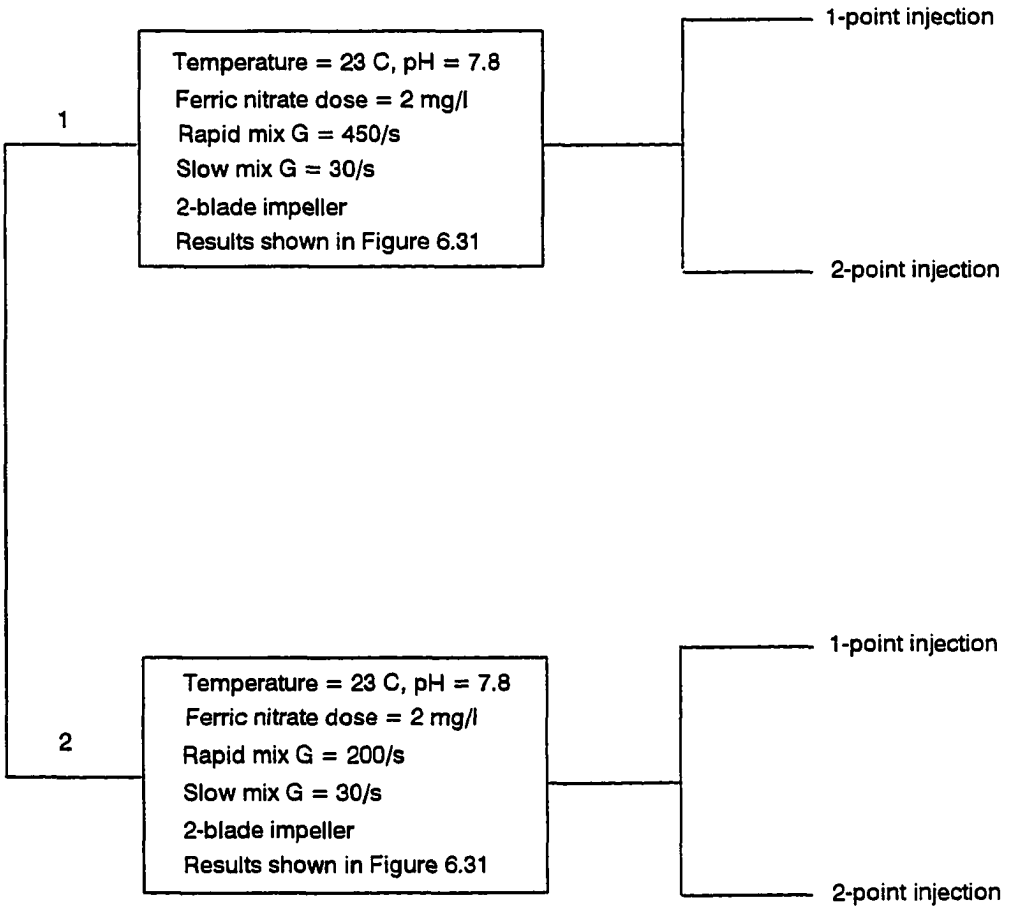

Figure 5.6. Experimental plan for illustrating the performance difference between 1-point injection and 2-point injection of coagulant on flocculation efficiency with ferric nitrate as the coagulant and at two rapid mixing intensities. Clay concentration was 25 mg/l

the entire volume of coagulant was injected through one port of the reactor by a syringe equipped with #13 gauge needle. In 2-point injection, the entire volume was divided equally into two syringes and then injected through two ports on opposite walls of the reactor.

5.2.7. Experimental plan for evaluating the effect of slow mixing intensity

Figure 5.7a illustrates the plan for experiments performed in cold water (5° C) at pH = 7.8. At cold temperature three slow mixing intensities (G = 24, 48, and 72/s) were tested with three different impellers (A 310, 2-blade and 3x3 mesh). **Figure 5.7b** illustrates the plan for experiments performed at warm temperature (23° C) at pH = 6.0. In this case, two intensities (G = 30 and 60/s) were tested with two other impellers (1x1 mesh and 2-blade stack).

5.2.8. Experimental plan for evaluating the effect of slow mixing pattern

Figures 5.8a and b illustrate the experimental plans for evaluating the effect of slow mixing pattern. **Figure 5.8a** is the plan for the experiments performed with ferric nitrate coagulant and **Figure 5.8b** is the plan for experiments done with alum coagulant. Two patterns were used: constant G, where mixing intensity was unchanged throughout the slow mixing period, and tapered G, where mixing intensity was lowered during the latter period of slow mixing, to reduce particle breakup as the particles grew in size. This reduction of slow mixing intensity was made at different time intervals for different treatment sets (physico-chemical conditions) as shown in the experimental plan.

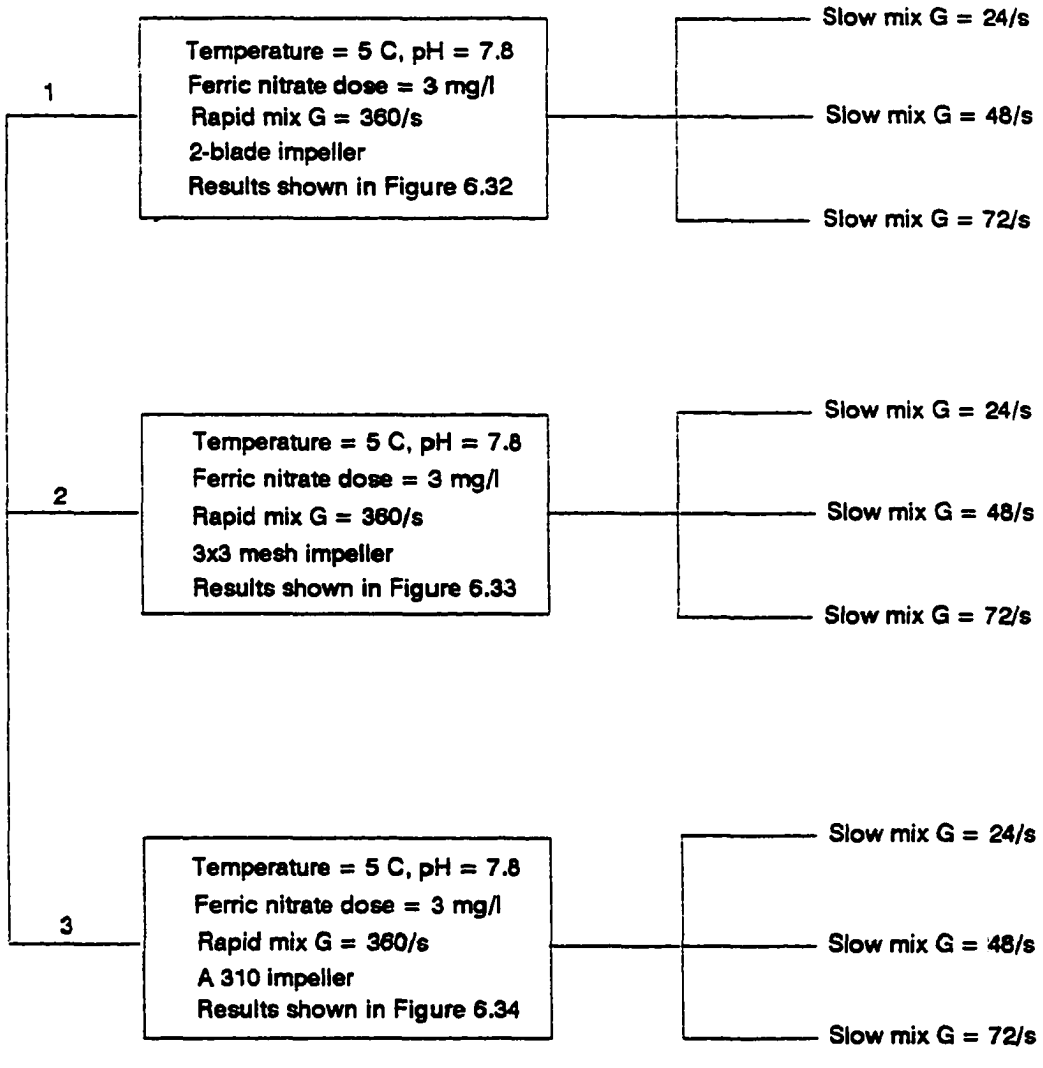

(a)

Figure 5.7. a) experimental plan for evaluating the effect slow mixing intensity on flocculation kinetics with ferric nitrate as the coagulant under varying conditions; clay concentration was 25 mg/l

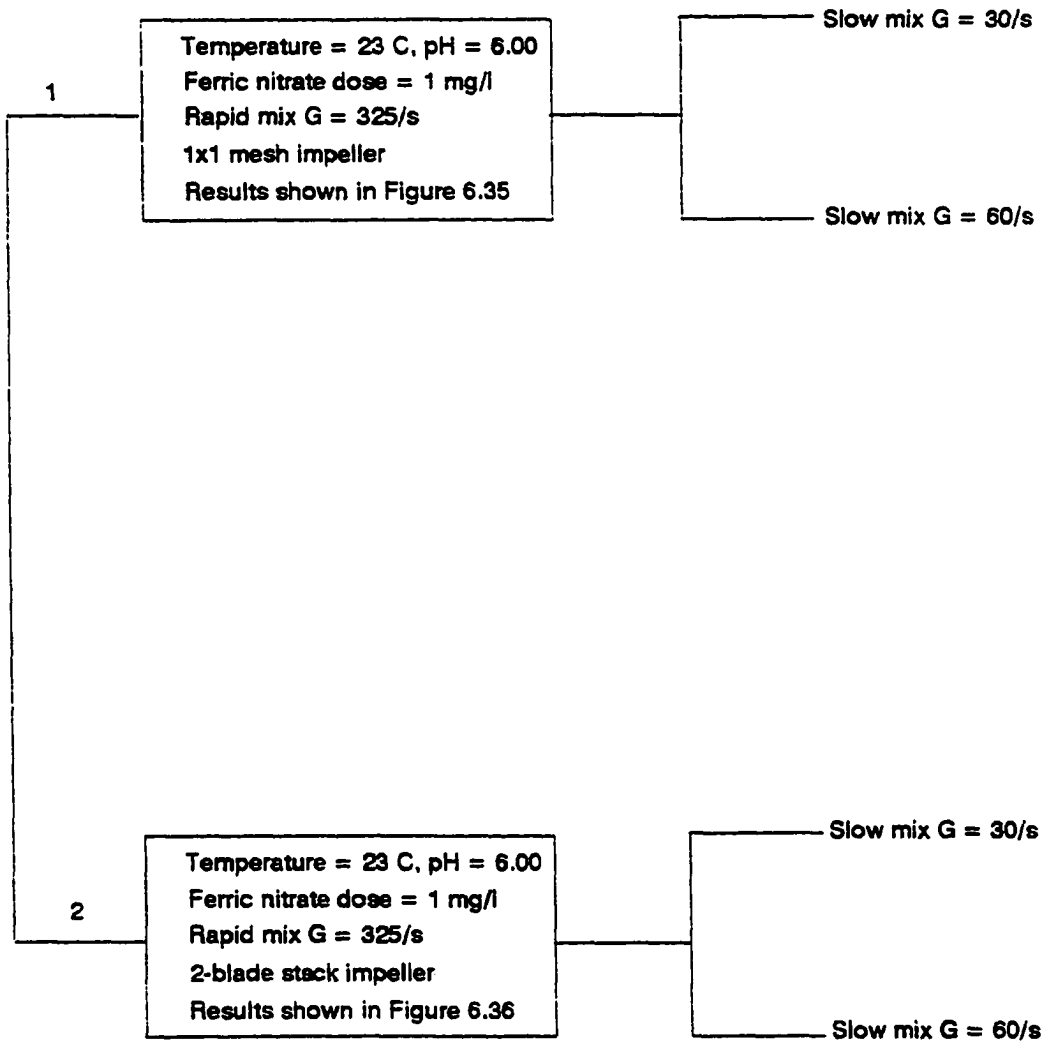

(b)

Figure 5.7. (continued) b)

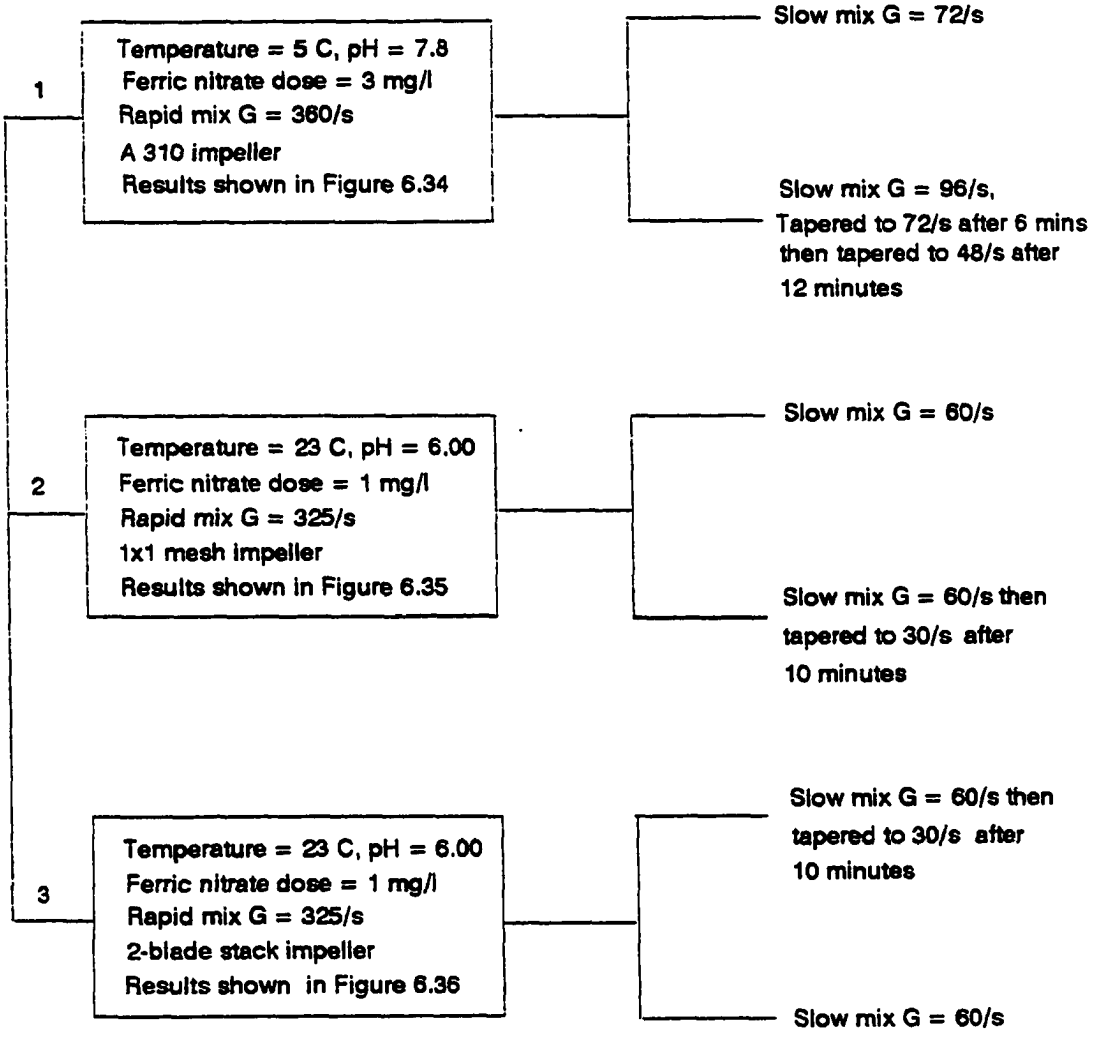

(a)

Figure 5.8. Experimental plan for evaluating the effect of slow mixing pattern on flocculating kaolin suspension with a) ferric nitrate as the coagulant under varying conditions; clay concentration was 25 mg/l

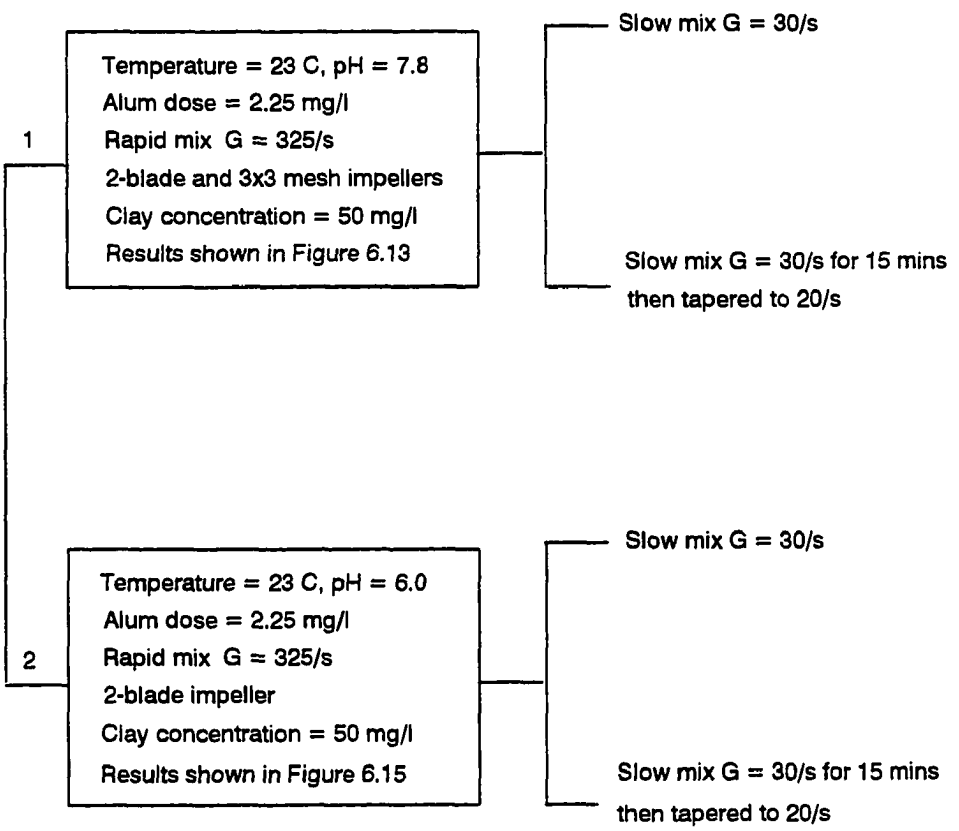

(b)

Figure 5.8. (continued) b) alum as the coagulant under two different conditions

5.2.9. Experimental plan for evaluating the effect of mesh size of the wire mesh impeller

Figure 5.9 illustrates the experimental plan for evaluating the effect of mesh size of the wire mesh impeller. Three mesh sizes, 1x1 mesh, 3x3 mesh, and 8x8 mesh corresponding to one, nine and sixty four square openings per square inch respectively, were used in treatment set 1. In treatment set 2, two mesh sizes, 1x1 and 3x3 mesh, were used.

5.2.10. Experimental plan for evaluating the effect of impeller combination

Figure 5.10 shows the experimental plan to determine the performance of impeller combination. Two impellers, A 310 and 3x3 mesh, were used for this purpose. Keeping all the other physico-chemical conditions constant, only the pattern of impeller use was varied in different phases of mixing (rapid and slow) as shown in the experimental plan. In two experiments, rapid mixing was performed with one impeller and slow mixing was performed with another one. The results of these experiments were compared with those for experiments performed with the same impeller throughout.

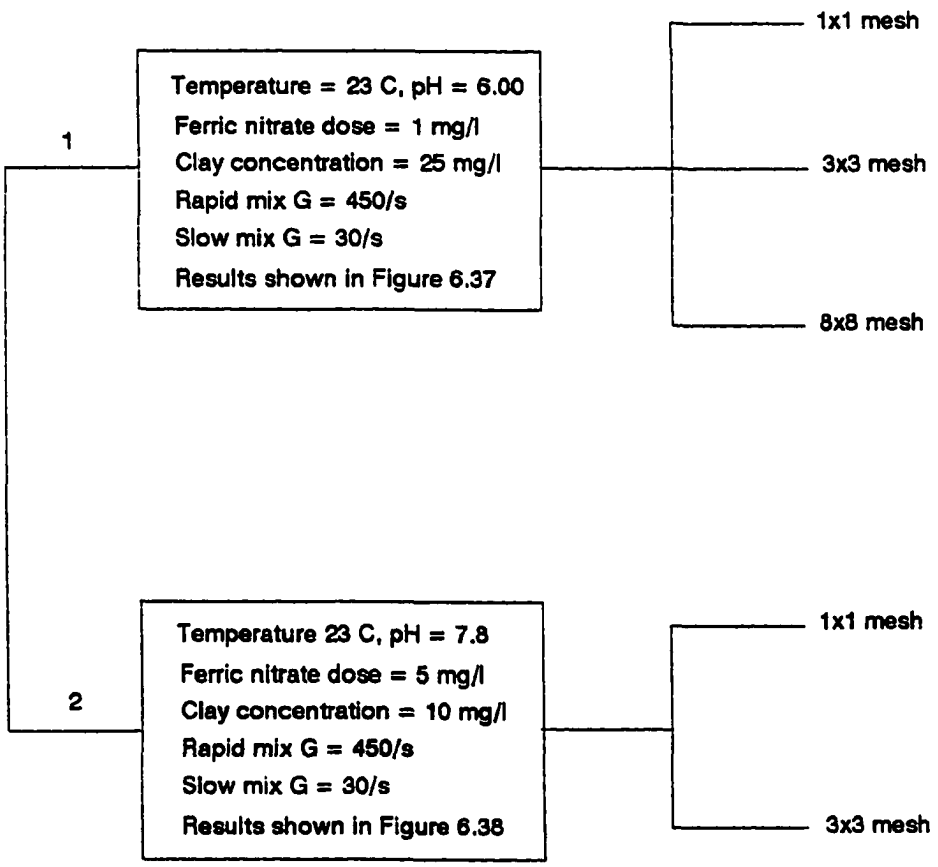

Figure 5.9. Experimental plan for determining the effect of mesh opening size of the wire mesh impeller on flocculation efficiency under two different conditions with ferric nitrate as the coagulant

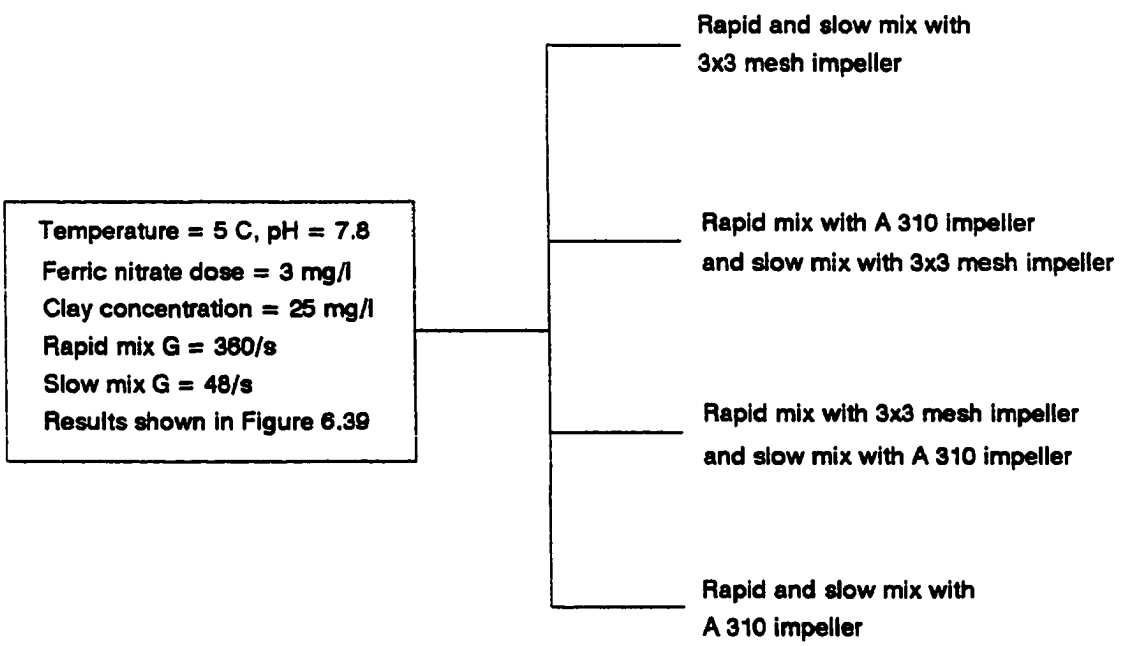

Figure 5.10. Experimental plan for evaluating the performance of two different impellers in both rapid and slow mixing stages

6. RESULTS, DISCUSSION AND CONCLUSIONS

6.1. Results

6.1.1. General

This chapter presents the results of the experimental investigations of this research. Experimental investigations were conducted to evaluate the impact of different mixing variables according to the plans outlined in the previous chapter. The results of the experiments are presented in graphical format where "flocculation index" (or PDA reading) is plotted against time (minutes). It should be noted that the ordinate scales are not the same in all figures. The scale was allowed to vary to present the data with the most sensitivity. A curve generated by an experiment corresponding to a particular mixing variable is marked with an arrow. The mixing variable is written at the tail of the arrow in all figures. The numbers in parenthesis with the arrow, represent the homogenized turbidity and the 10 minute, 20 minute and 30 minute settled turbidity respectively, following flocculation. In some experiments with alum, 40 minute turbidity was also measured and presented within the parenthesis.

Time "0" on the x axis represents the start of flocculation and acts as the demarkation line between rapid and slow mixing processes. Negative time indicates the rapid mixing duration. The rising limb of the curve corresponds to the growth of particle aggregates or flocs. The plateau and the falling limb correspond to equilibrium of growth and settling of heavier floc particles respectively. A steeper slope of the rising

limb means better kinetics in a particular treatment set (physico-chemical conditions). All the physico-chemical variables are mentioned at the top left corner of the figure. **Figure 6.1** is an example of a typical figure illustrating the results.

Some of the experiments were duplicated and some were triplicated. Due to change in clay characteristics and the random nature of flow through the PDA cell, it was not always possible to generate the exact quantitative "flocculation index" and turbidity readings. But qualitatively the results remained unchanged in all the replications. For example, if an impeller performed better once, it always performed better than the others in all the replicate experiments, even though it was not always possible to trace the exact same curve. The spread between replicates could be minimized by performing the experiments back to back with the same stock clay suspension. It was also found that two different clay suspensions with the same initial "flocculation index" and turbidity produced minimum departure between replicates. To minimize the replication error, the experiments performed to evaluate the effect of a particular mixing variable were conducted with the same stock clay suspension and in close proximity of time (usually in the same day or within two to three days).

The experiments to generate Figures 6.1, 6.2, 6.3, 6.9, 6.10, 6.11, 6.23, 6.24, 6.25, 6.35, 6.36, 6.37, 6.38 were performed at the latest part of this research. The stock clay suspension used in these experiments showed a significant variation in flocculation tendency as was evidenced by increased initial "flocculation index" value and less negative zeta potential (-20 mv as opposed to -30 mv in other figures not listed above) of the homogenized sample. The source of this erratic behavior was unidentified, but the

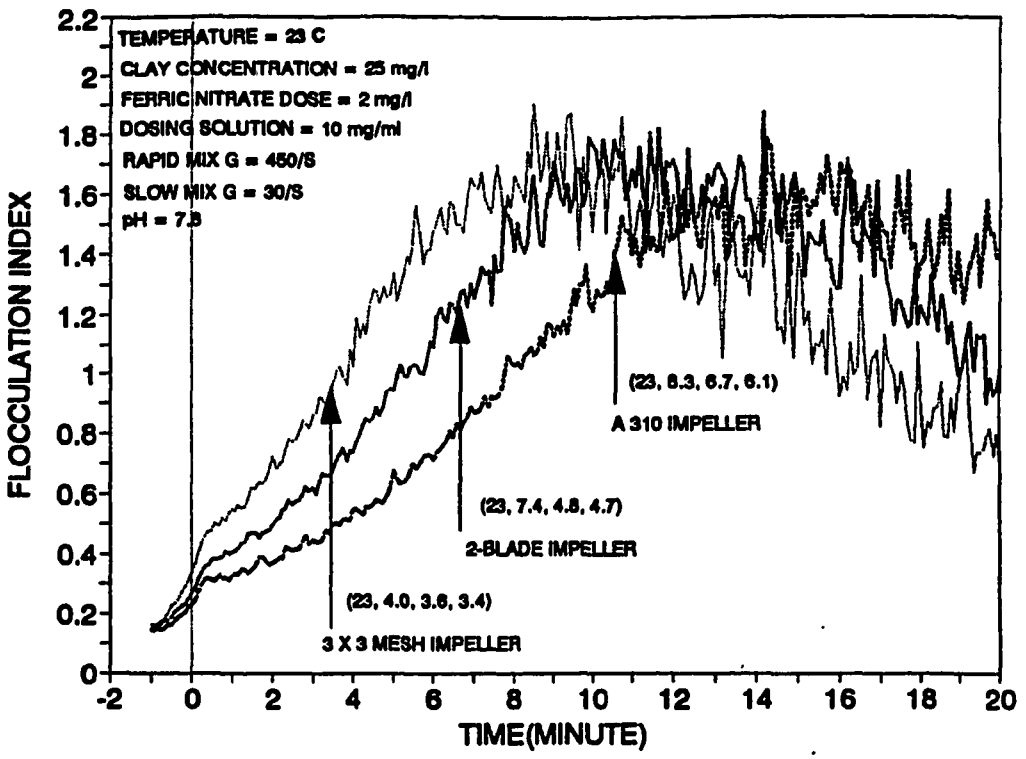

Figure 6.1. Effect of impeller geometry on flocculation kinetics at pH = 7.8 and temperature = 23° C with ferric nitrate as the coagulant. The G value of 450/s corresponds to 493, 248, and 112 rpm for A 310, 2-blade and the 3x3 mesh impellers respectively. The G value of 30/s corresponds to 63, 40, and 17 rpm for A 310, 2-blade, and 3x3 mesh impellers respectively. Numbers in parenthesis represent the homogenized turbidity and 10, 20, and 30 minute settled turbidity respectively following flocculation

error was minimized by more intense and longer mixing in the reactor prior to the start of the experiment. The stock clay suspension was also mixed for longer period than usual and was discarded when it dropped below the 25-L mark in the stock clay tank. The problem was consistent throughout the later stage of this research. But the curves in any one figure or between two figures, from these listed above, can be compared both qualitatively and quantitatively without any confusion. Any curve from these figures should not be compared quantitatively (flocculation index and turbidity values) with the curves in figures that are not mentioned in the above list. But qualitatively, (to observe the effect of a certain variable) any figure from this listed group can be compared with any figure that is not present in this list.

Moreover, the main concern was the mixing variables, and not the other physico-chemical issues (e.g. effect of temperature change, coagulation chemistry etc.). Different mixing variables were tested with different combinations of physico-chemical variables. Almost all the experiments were done with low coagulant dose, presumably under the adsorption/destabilization coagulation condition with the zeta potential of rapid mixed sample near -10 mv. The following subsections will describe the results of the experimental study.

6.1.2. Effect of impeller geometry

One of the prime objectives of this research was to identify the optimum impeller geometry for the coagulation-flocculation process, so the maximum number of experiments were performed to observe the effect of geometry under a large number of

physico-chemical conditions. For this reason, five different impellers were employed under varying conditions. One impeller was commercially available (A 310), one was used by other researchers (2-blade) as mentioned earlier, and the other three (wire mesh, modified stake and 2-blade stack) were designed and fabricated in the laboratory as a part of this study. The G versus rpm curves for all the impellers were developed by a photographic technique (mentioned earlier) in the laboratory.

The effect of geometry is shown in **Figures 6.1 through 6.19**. **Figures 6.1 through 6.11** represent the results of experiments performed with ferric nitrate coagulant and the rest were performed with alum coagulant. **Figures 6.4 through 6.8** illustrate the results of the cold temperature (5° C) experiments. The rest contain warm temperature (23° C) experiments.

Figure 6.1 illustrates the performance of three different impellers at warm temperature (23° C) and at pH = 7.8. From this figure, it is evident that geometry has significant impact on flocculation kinetics. This is demonstrated by both the sharp increase of flocculation index and marked decrease in turbidity reading at a particular point of measurement. Keeping all the other variables constant, only by changing the geometry of impeller, one can change the kinetics of flocculation to a significant extent. From this figure, it is obvious that the wire mesh (3x3 mesh) impeller was the best among the three impellers tested and the A 310 impeller performed worst. The difference in performance among the impellers was quite significant.

Figure 6.2 illustrates the performance difference among the three impellers at a different coagulant dose. Here the dose was 2.5 times the dose shown in the previous

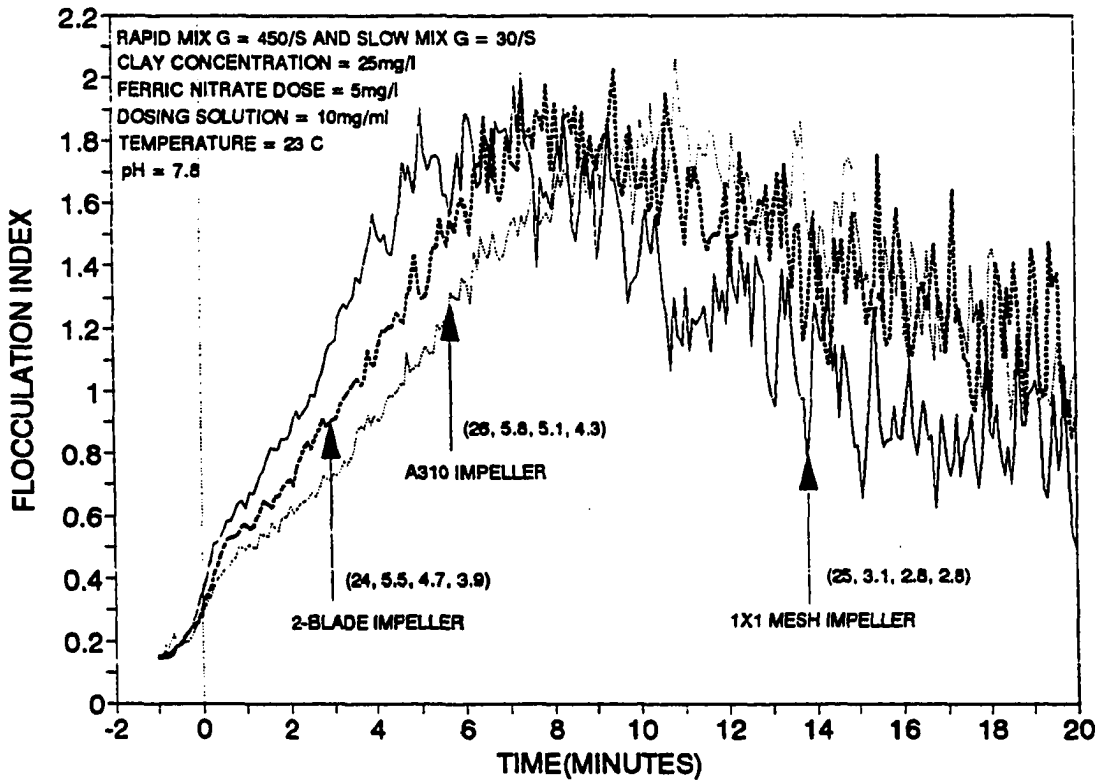

Figure 6.2. Effect of impeller geometry on flocculation kinetics at pH = 7.8 and temperature = 23° C with ferric nitrate as the coagulant.The G value of 450/s corresponds to 493, 248, and 112 rpm for A 310, 2-blade and the 1x1 mesh impellers respectively. The G value of 30/s corresponds to 63, 40, and 20 rpm for A 310, 2-blade, and 1x1 mesh impellers respectively. Numbers in parenthesis represent the homogenized turbidity and 10, 20, and 30 minute settled turbidity respectively following flocculation

figure and the mesh size was larger (1x1) than the previous mesh size (3x3). It can be seen that the kinetics were much faster and turbidity removal was better with the higher dose (compared with prior **Figure 6.1**). When the performance of the impellers is critically observed in the **Figures 6.1 and 6.2**, it becomes clear that the impeller geometry is very important in flocculation kinetics. If the performance of 3x3 mesh impeller in **Figure 6.1** is compared with the other two impellers (2-blade and A 310) in **Figure 6.2**, it can be seen that 3x3 mesh impeller in **Figure 6.1** removed more turbidity at all periods of sedimentation than the other two impellers, in spite of the lower dosage used in **Figure 6.1**.

Figure 6.3 shows the performance of the three impellers mentioned in **Figure 6.1** at different pH and ferric nitrate dose. All the other conditions of **Figure 6.1** were kept unchanged here. A dose of 1 mg/l ferric nitrate at pH = 6.0 gave a zeta potential reading near -5 mv which is optimum condition for A/D coagulation. But the inherent chemical characteristics of ferric nitrate produced considerably worse flocculation kinetics at this pH than at pH = 7.8.

From the results shown in **Figures 6.1, 6.2 and 6.3** it appears that the better impeller performs better in each of these three conditions. Although the spread between the curves generated by 3x3 mesh and 2-blade impellers in **Figure 6.3** is not substantial, the turbidity readings generated by those two impellers were substantially different. The 3x3 mesh impeller achieved much better results than the 2-blade impeller in terms of turbidity removal. By comparing the performance of these two impellers here, it can be stated that even though the flocs produced by the two impellers created similar blockage

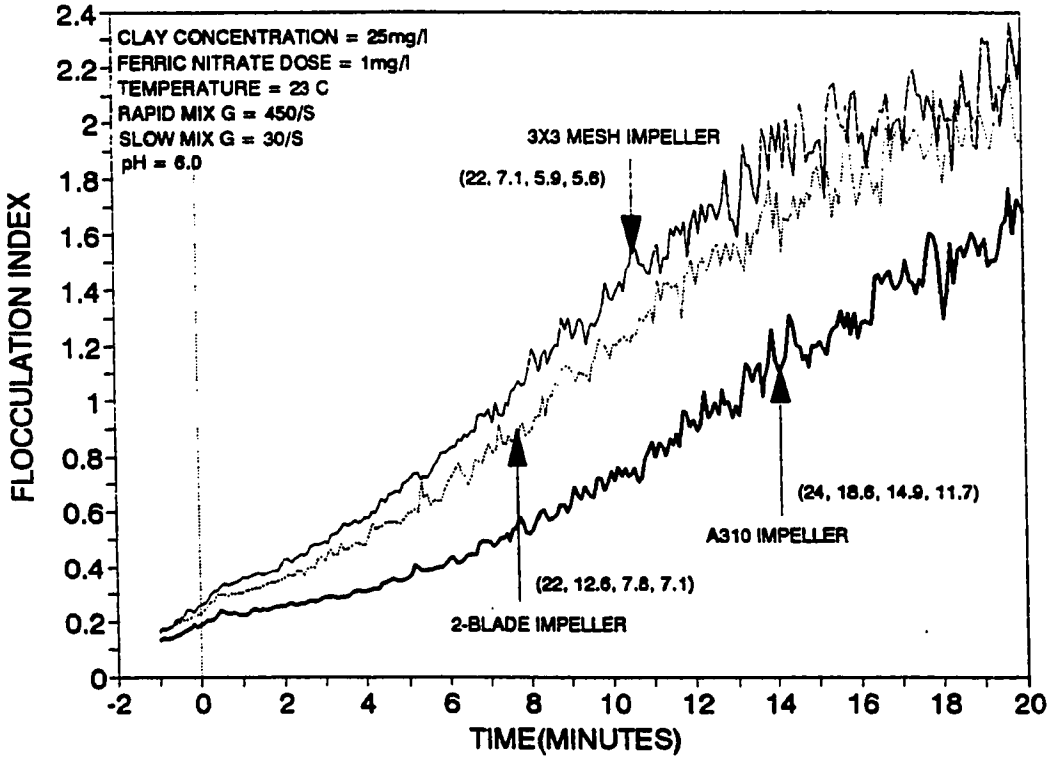

Figure 6.3. Effect of impeller geometry on flocculation kinetics at pH = 6.0 and temperature = 23° C with ferric nitrate as the coagulant.The G value of 450/s corresponds to 493, 248, and 112 rpm for A 310, 2-blade and the 3x3 mesh impellers respectively. The G value of 30/s corresponds to 63, 40, and 17 rpm for A 310, 2-blade, and 3x3 mesh impellers respectively. Numbers in parenthesis represent the homogenized turbidity and 10, 20, and 30 minute settled turbidity respectively following flocculation

to the light in the PDA instrument, the flocs produced by the 3x3 mesh impeller had a higher settling velocity than those produced by the 2-blade impeller. So the 3x3 mesh impeller produced larger and heavier flocs than the other two impellers.

Figure 6.4 illustrates the performance difference of the three impellers mentioned in **Figure 6.1** at cold temperature (5° C). Here, the dose was increased to 3 mg/l to achieve zeta potential reading near -10 mv and to achieve measurable kinetics with a slow mix G = 24/s. With ferric nitrate dose of 2 mg/l, the zeta potential was more negative (around -16 mv) and kinetics were much worse with a slow mix G of 24/s. The experimental conditions for **Figures 6.5 and 6.6** were identical to those for **Figure 6.4**, except for the slow mixing G. As opposed to slow mix G = 24/s in **Figure 6.4**, the G values are 48 and 72/s in **Figures 6.5 and 6.6**, respectively. From these three figures it is evident that the impeller geometry has a pronounced effect on flocculation kinetics at cold temperature also, and the performance difference is even more dramatic at cold temperature as shown by the wider spread between "flocculation index" versus time curves and higher difference of turbidity readings produced by the three impellers. The performance ranking also remains unchanged here. The 3x3 mesh impeller performed best and the A 310 impeller performed worst.

The experimental conditions for **Figure 6.7** were similar to those for **Figure 6.4**, except the ferric nitrate dose. In experiments to generate **Figure 6.7** the coagulant dose was two times (6 mg/l) of that (3 mg/l) used in experiments to generate **Figure 6.4**. This resulted in a zeta potential of -3 mv at the 6 mg/l dosage compared with -13 mv at 3 mg/l. With this higher dose of coagulant the performance difference between two

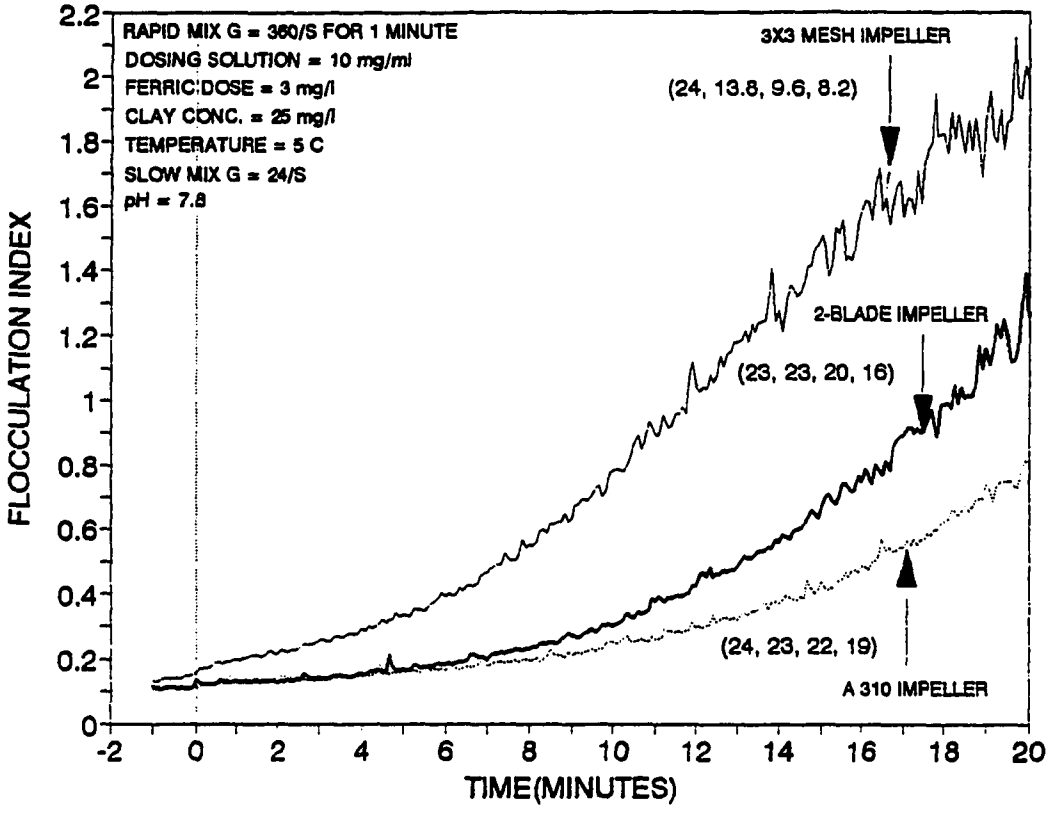

Figure 6.4. Effect of impeller geometry on flocculation kinetics at pH = 7.8 and temperature = 5° C with ferric nitrate as the coagulant. The G value of 360/s corresponds to 493, 248, and 112 rpm for A 310, 2-blade and the 3x3 mesh impellers respectively. The G value of 24/s corresponds to 63, 40, and 17 rpm for A 310, 2-blade, and 3x3 mesh impellers respectively. Numbers in parenthesis represent the homogenized turbidity and 10, 20, and 30 minute settled turbidity respectively following flocculation

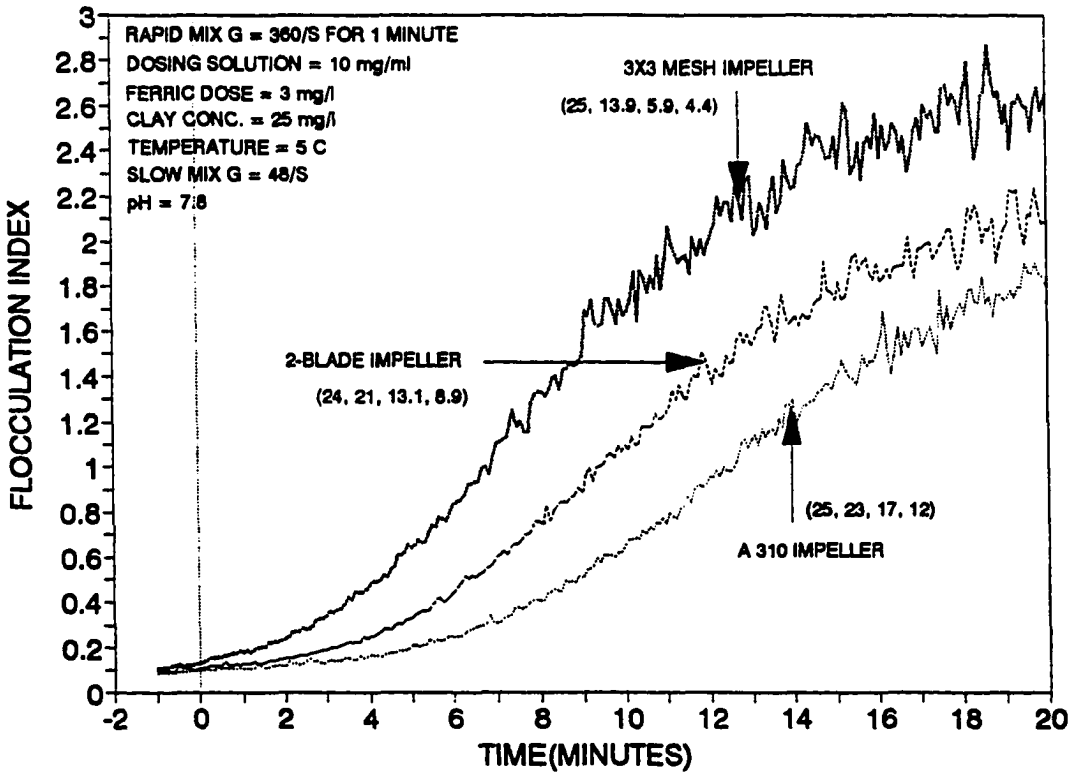

Figure 6.5. Effect of impeller geometry on flocculation kinetics at pH = 7.8 and temperature = 5° C with ferric nitrate as the coagulant. The G value of 360/s corresponds to 493, 248, and 112 rpm for A 310, 2-blade and the 3x3 mesh impellers respectively. The G value of 48/s corresponds to 93, 64, and 27 rpm for A 310, 2-blade, and 3x3 mesh impellers respectively. Numbers in parenthesis represent the homogenized turbidity and 10, 20, and 30 minute settled turbidity respectively following flocculation

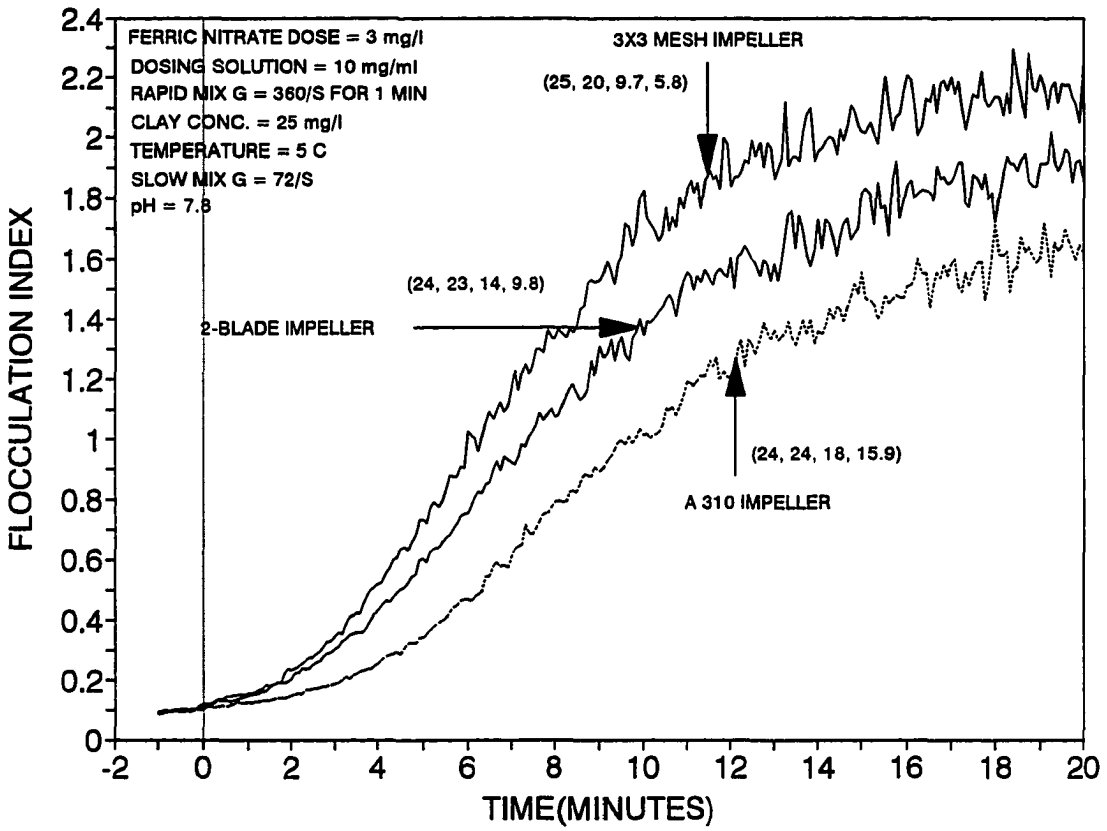

Figure 6.6. Effect of impeller geometry on flocculation kinetics at pH = 7.8 and temperature = 5° C with ferric nitrate as the coagulant. The G value of 360/s corresponds to 493, 248, and 112 rpm for A 310, 2-blade and the 3x3 mesh impellers respectively. The G value of 72/s corresponds to 124, 84, and 36 rpm for A 310, 2-blade, and 3x3 mesh impellers respectively. Numbers in parenthesis represent the homogenized turbidity and 10, 20, and 30 minute settled turbidity respectively following flocculation

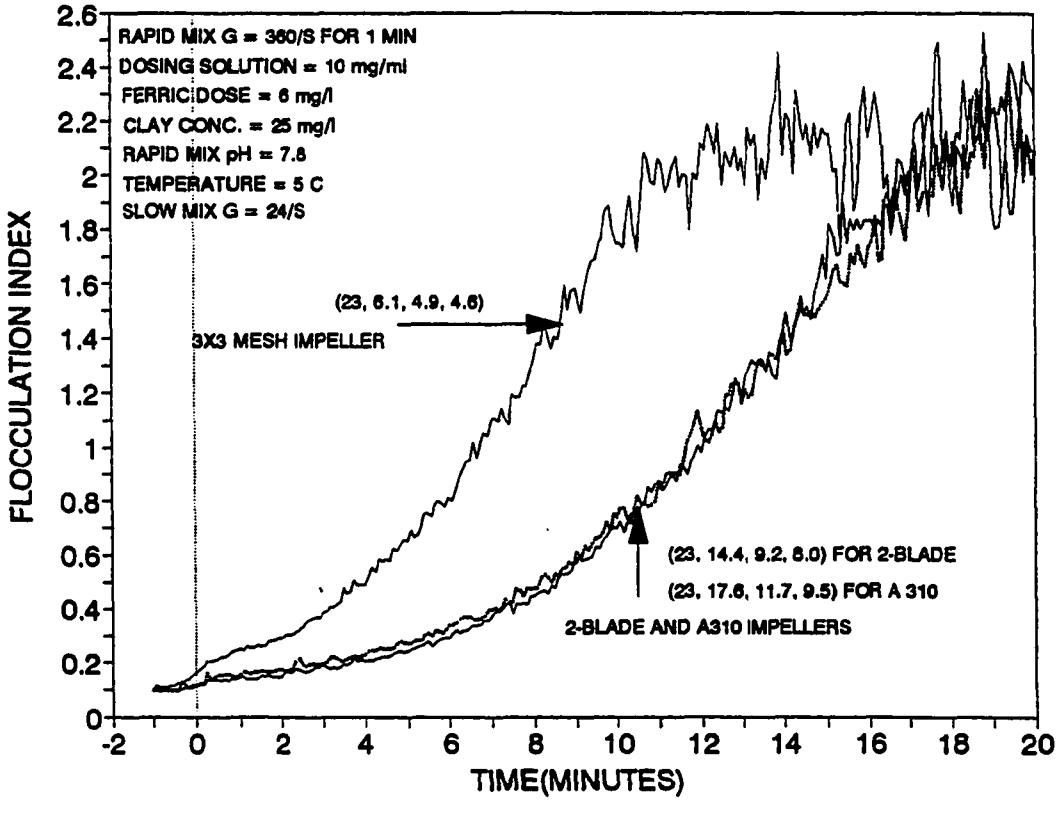

Figure 6.7. Effect of impeller geometry on flocculation kinetics at pH = 7.8 and temperature = 5° C with ferric nitrate as the coagulant. The G value of 360/s corresponds to 493, 248, and 112 rpm for A 310, 2-blade and the 3x3 mesh impellers respectively. The G value of 24/s corresponds to 63, 40, and 17 rpm for A 310, 2-blade, and 3x3 mesh impellers respectively. Numbers in parenthesis represent the homogenized turbidity and 10, 20, and 30 minute settled turbidity respectively following flocculation

turbine impellers (2-blade and A 310) decreased to a significant degree in terms of turbidity removal and the flocculation index readings almost overlapped. From this figure it is once again seen that even though the PDA readings produced by the two impellers were almost identical, their turbidity readings showed noticeable differences. The 2-blade impeller produced better settling flocs resulting in better turbidity removal than the A 310 impeller. The 3x3 mesh impeller performed much better than the other two impellers with this higher dosage at cold temperature.

When **Figures 6.4 and 6.7** are compared, it can be visualized again that the higher dose of ferric coagulants increased the flocculation kinetics and the floc settleability at this particular pH value. If these two figures are critically compared then the importance of impeller geometry can also be revealed. In terms of turbidity removal, the 3x3 mesh impeller in **Figure 6.4** with less coagulant dose performed better than or equal to the other two impellers in **Figure 6.7** with high coagulant dose.

Figure 6.8 illustrates the impact of impeller geometry on flocculation kinetics. Two impellers were compared: 3x3 mesh and A 310. This figure also indicates better performance of the 3x3 mesh impeller (curve 1) than the A 310 turbine impeller (curve 3). But due to inherent chemical characteristics of ferric coagulant, this better performance by the 3x3 mesh impeller was still not enough to produce similar results produced by the other two impellers at pH = 7.8 as shown in **Figure 6.5**. The kinetics of flocculation with ferric coagulant are much worse at pH = 6.0 than at pH = 7.8. When the dose was increased 10 times, the particles were restabilized and the kinetics became even worse (compare curves 1 and 2 in **Figure 6.8**). It would not be advisable

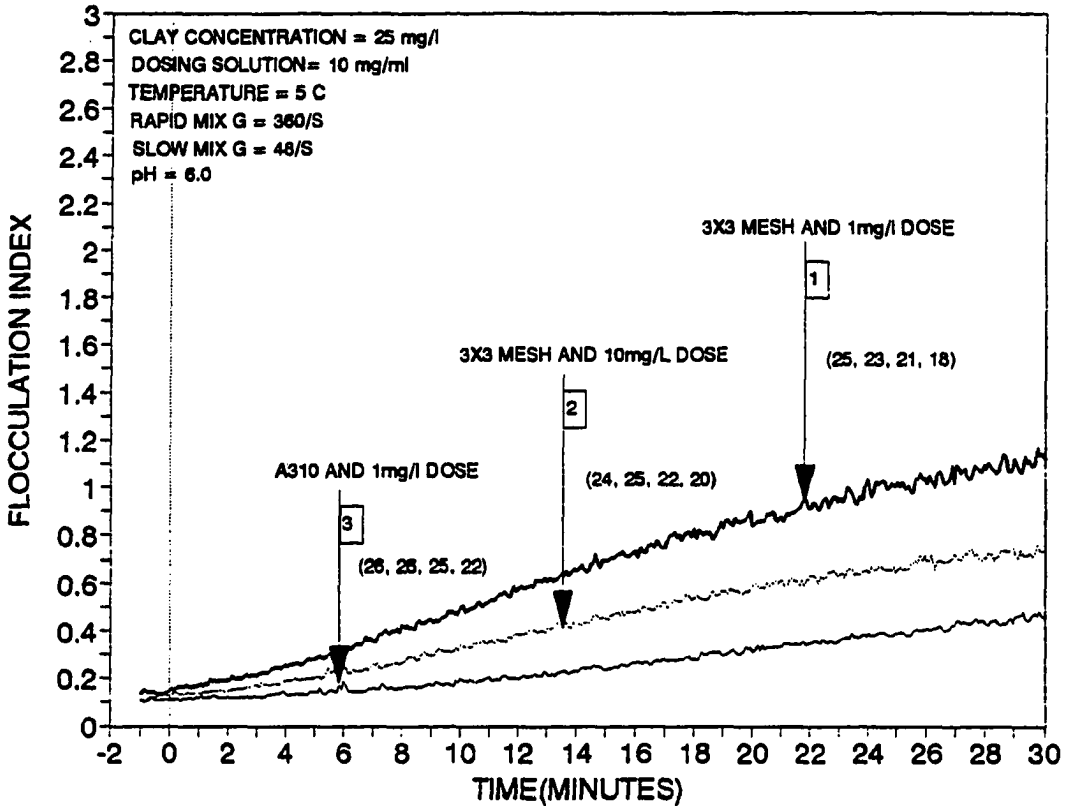

Figure 6.8. Effect of impeller geometry on flocculation kinetics at pH = 6.0 and temperature = 5° C with ferric nitrate as the coagulant. The G value of 360/s corresponds to 493 and 112 rpm for A 310 and the 3x3 mesh impellers respectively. The G value of 48/s corresponds to 93 and 27 rpm for A 310 and 3x3 mesh impellers respectively. Numbers in parenthesis represent the homogenized turbidity and 10, 20, and 30 minute settled turbidity respectively following flocculation

to flocculate the clay particles at low temperature and at low pH with ferric nitrate coagulant under the prevailing water chemistry of these experiments, because of the problem with restabilization.

So far, two turbine type impellers were compared with one paddle type impeller. **Figure 6.9** illustrates the performance of one turbine type impeller (2-blade) with three paddle type impellers. The 2-blade stack impeller was considered a paddle type impeller, because of the decentralized nature of its power input to the flocculation tank. **Figure 6.10** also illustrates the performance difference of these four impellers at a different pH (6.0) and coagulant dose. From these two figures, it is certain that all the paddle type impellers that deliver power into the reactor in a decentralized fashion, performed equally, and far better than the 2-blade turbine impeller under both sets of physico-chemical conditions. Some spread among the flocculation index versus time curves generated by different paddle impellers was observed at pH = 7.8, but they all produced almost identical turbidity readings.

When the 1x1 mesh impeller was compared with the 2-blade stack impeller at a higher slow mixing intensity (G = 60/s) as shown in **Figure 6.11**, it produced almost the same turbidity readings as those produced by the other impeller, even though their PDA readings were different. Even though the particles generated by the 1x1 mesh impeller gave slightly lower flocculation index values, their settling velocity was similar to those generated by the other impeller.

Figures 6.12 through 6.19 illustrate the effect of impeller geometry (two impellers: 3x3 mesh and 2-blade were used) on the kinetics of alum flocculation. All the

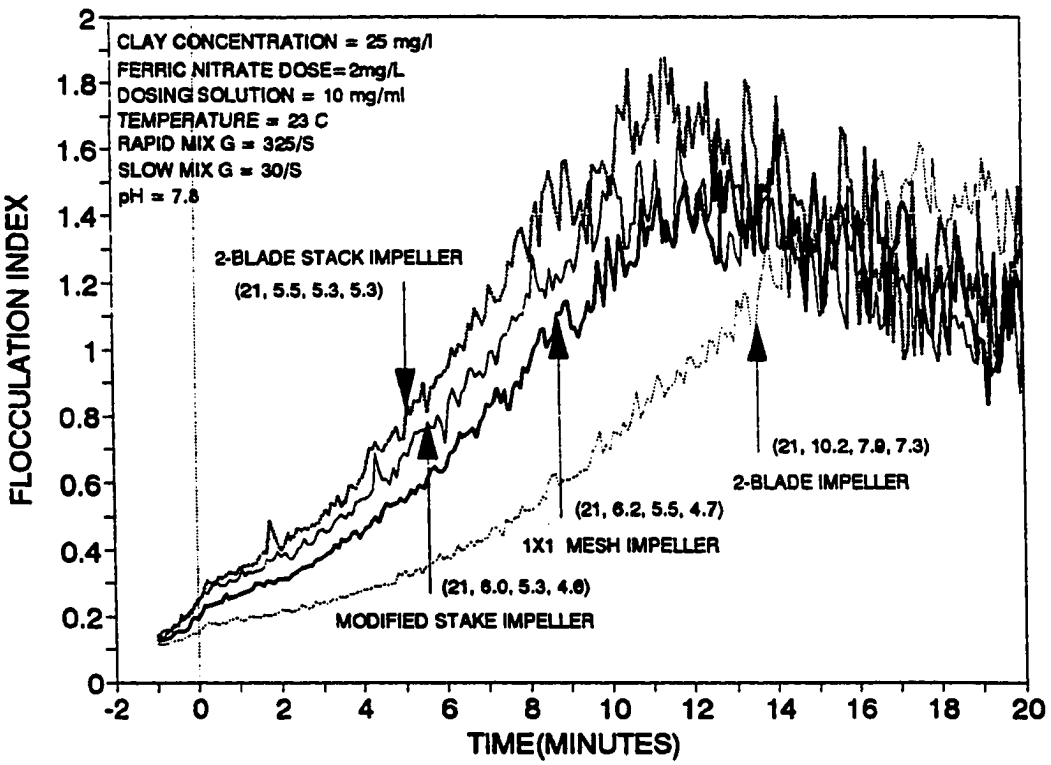

Figure 6.9. Effect of impeller geometry on flocculation kinetics at pH = 7.8 and temperature = 23° C with ferric nitrate as the coagulant. The rapid mix G value of 325/s corresponds to 200, 93, 105, and 180 rpm for 2-blade, 1x1 mesh, modified stake, and 2-blade stack impellers respectively. The slow mix G value of 30/s corresponds to 40, 20, 20, and 33 rpm for 2-blade, 1x1 mesh, modified stake, and 2-blade stack impellers respectively. Numbers in parenthesis represent the homogenized turbidity and 10, 20, and 30 minute settled turbidity respectively following flocculation

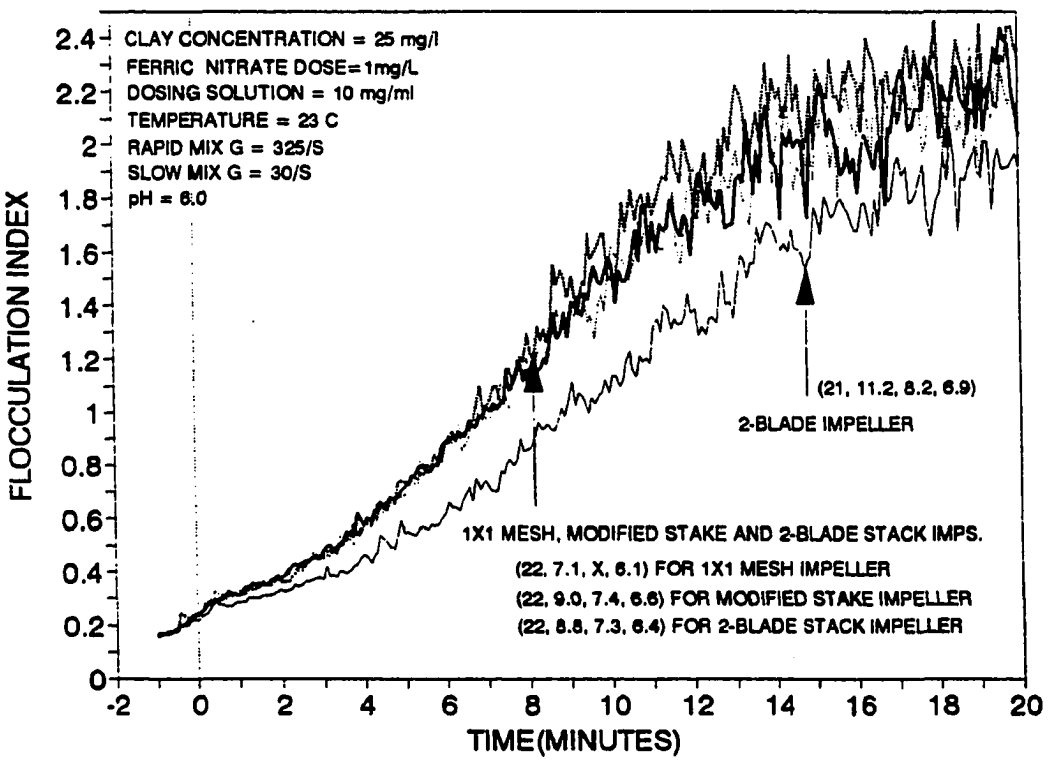

Figure 6.10. Effect of impeller geometry on flocculation kinetics at pH = 6.0 and temperature = 23° C with ferric nitrate as the coagulant. The rapid mix G value of 325/s corresponds to 200, 93, 105, and 180 rpm for 2-blade, 1x1 mesh, modified stake, and 2-blade stack impellers respectively. The slow mix G value of 30/s corresponds to 40, 20, 20, and 33 rpm for 2-blade, 1x1 mesh, modified stake, and 2-blade stack impellers respectively. Numbers in parenthesis represent the homogenized turbidity and 10, 20, and 30 minute settled turbidity respectively following flocculation

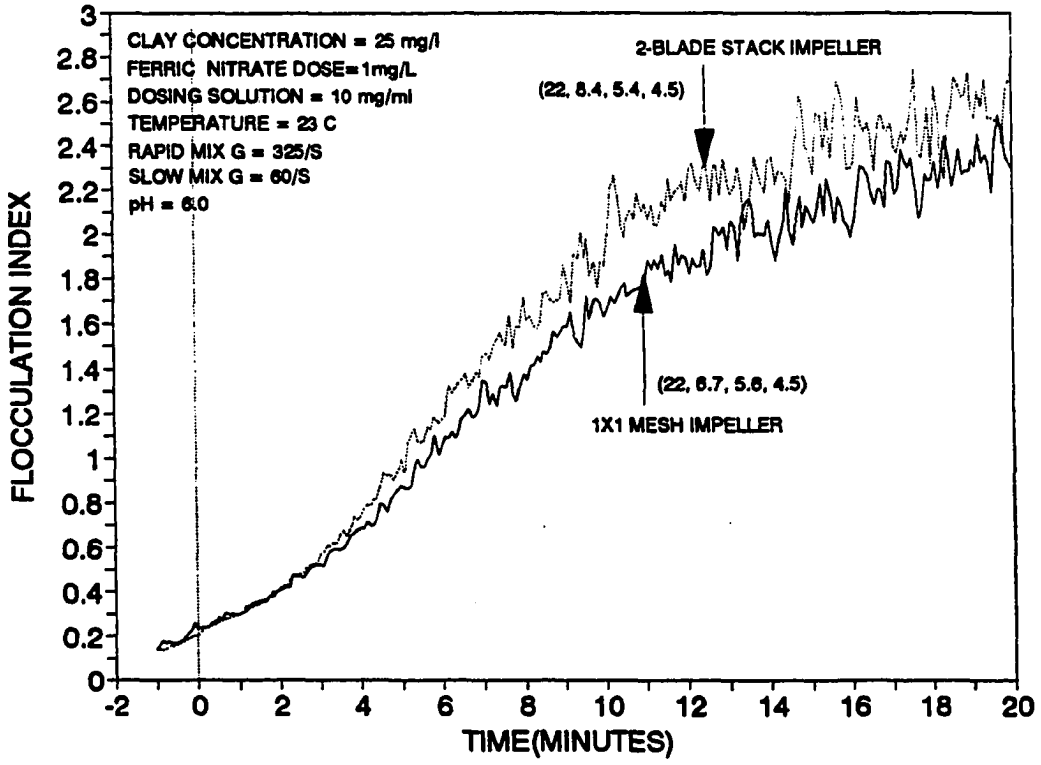

Figure 6.11. Effect of impeller geometry on flocculation kinetics at pH = 6.0 and temperature = 23° C with ferric nitrate as the coagulant. The rapid mix G value of 325/s corresponds to 93 and 180 rpm for 1x1 mesh and 2-blade stack impellers respectively. The slow mix G value of 30/s corresponds to 20 and 33 rpm for 1x1 mesh and 2-blade stack impellers respectively. Numbers in parenthesis represent the homogenized turbidity and 10, 20, and 30 minute settled turbidity respectively following flocculation

experiments to generate the above mentioned figures, were performed at warm temperature (23° C). Also a rapid mix G = 325/s was used in all those experiments. In general, it will be evident in most of these figures that alum was not as effective in turbidity reduction as ferric nitrate under comparable experimental conditions. **Figure 6.12** shows the performance difference between two impellers flocculating a 25 mg/l clay suspension with 1.5 mg/l alum dose at a pH = 7.8. These conditions produced a zeta potential around -10 mv with this clay suspension. So the mechanism of flocculation was adsorption/destabilization. This figure also indicates the importance of impeller geometry.

The experimental conditions for **Figure 6.13** were similar to those for **Figure 6.12** except for the clay concentration, coagulant dose and slow mixing pattern. An alum dose of 2.25 mg/l was used to achieve a zeta potential around -10 mv with 50 mg/l clay suspension in these experiments. Two slow mixing patterns were used in this figure (constant G of 30/s for curves 2 and 4, and tapered G for curves 1 and 3 of 30/s for 15 minutes, followed by 20/s up to the end of flocculation). Significant impeller geometry effect was noticed in both of these slow mixing conditions. The 3x3 mesh impeller performed far better than the 2-blade impeller.

Figure 6.14 shows the impact of impeller geometry on alum flocculation at pH = 6.0 with several alum dosages. For the 2-blade impeller when the alum dose was increased from 2.25 mg/l (curve 3) to 10 mg/l (curve 5), the particles became restabilized with positive zeta potential, producing much worse kinetics. With further increase of dose from 10 mg/l to 20 mg/l (curve 2) the flocculation index values were

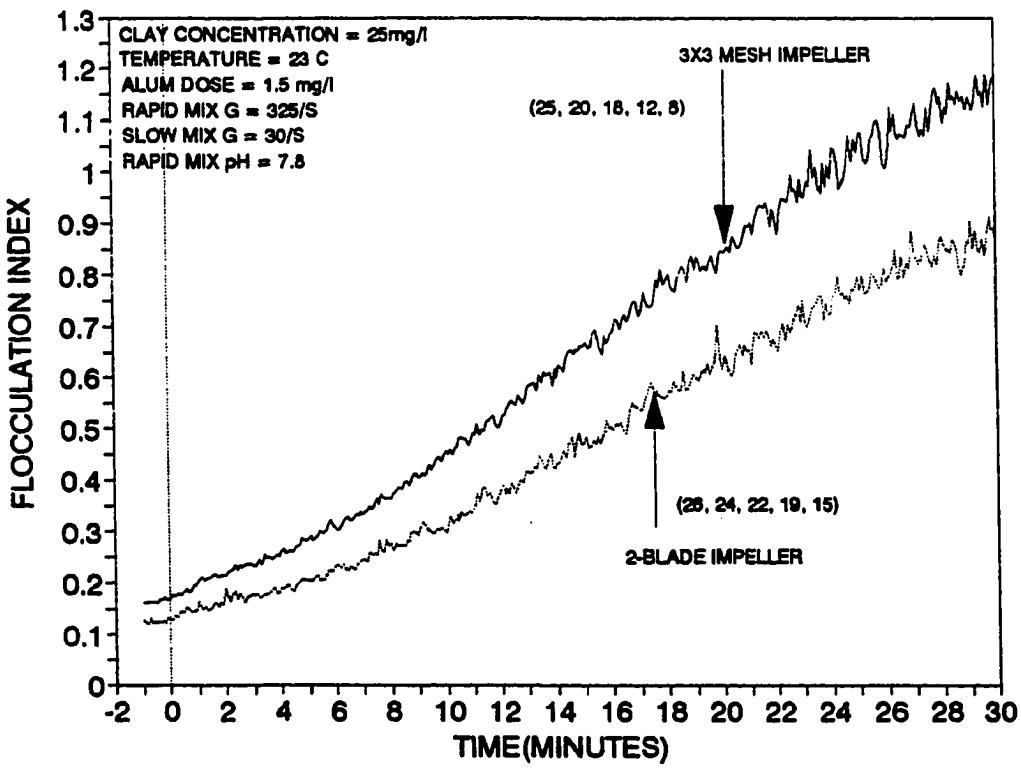

Figure 6.12. Effect of impeller geometry on flocculation kinetics at pH = 7.8 and temperature = 23° C with alum as the coagulant. Clay concentration is 25 mg/l. The rapid mix G value of 325/s corresponds 200 and 90 rpm for 2-blade and the 3x3 mesh impellers respectively. The G value of 30/s corresponds to 40 and 17 rpm for 2-blade and 3x3 mesh impellers respectively. Numbers in parenthesis represent the homogenized turbidity and 10, 20, 30, and 40 minute settled turbidity respectively following flocculation

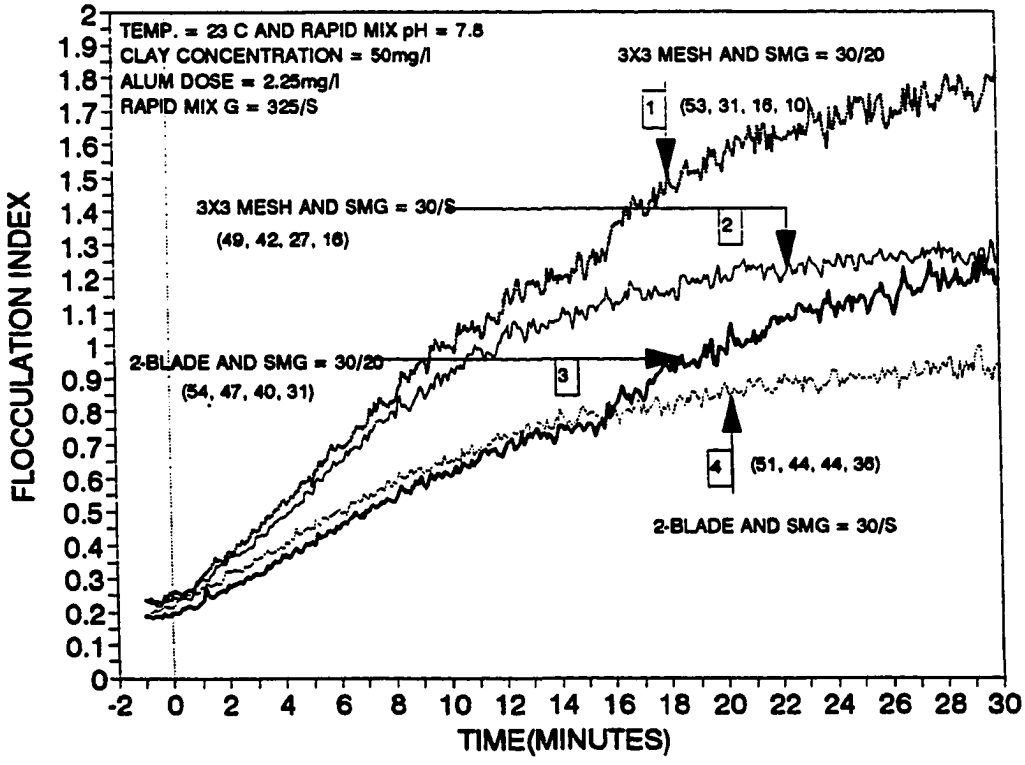

Figure 6.13. Effect of impeller geometry and slow mixing pattern on flocculation kinetics at pH = 7.8 and temperature = 23° C with alum as the coagulant. Clay concentration is 50 mg/l. The rapid mix G value of 325/s corresponds 200 and 90 rpm for 2-blade and the 3x3 mesh impellers respectively. The G value of 30/s corresponds to 40 and 17 rpm for 2-blade and 3x3 mesh impellers respectively. The slow mix G value of 20/s corresponds to 29 and 12 rpm for 2-blade and 3x3 mesh impellers respectively. Numbers in parenthesis represent the homogenized turbidity and 10, 20, and 30 minute settled turbidity respectively following flocculation

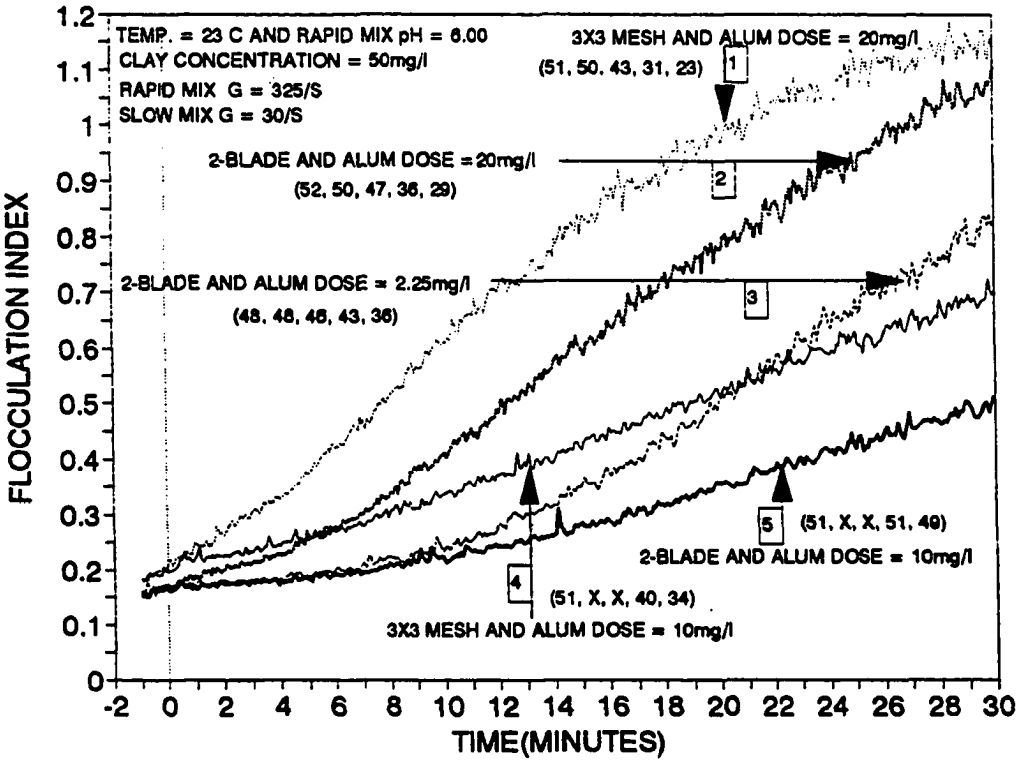

Figure 6.14. Effect of impeller geometry and coagulant dose on flocculation kinetics at pH = 6.0 and temperature = 23° C with alum as the coagulant. Clay concentration is 50 mg/l. The rapid mix G value of 325/s corresponds 200 and 90 rpm for 2-blade and the 3x3 mesh impellers respectively. The G value of 30/s corresponds to 40 and 17 rpm for 2-blade and 3x3 mesh impellers respectively. Numbers in parenthesis represent the homogenized turbidity and 10, 20, 30, and 40 minute settled turbidity respectively following flocculation. X means that the turbidity measurement was not taken at that particular time.

higher, probably due to the massive precipitation of $Al(OH)_{3(s)}$, but flocculation was not effective due to high positive zeta potential resulting in high remaining turbidity after 30 minutes of flocculation and 40 minutes of settling. In spite of generally poor performance overall, the 3x3 mesh performed far better than the 2-blade impeller under both sets of conditions (compare curve 1 versus 2, and curve 4 versus 5).

Figure 6.15 illustrates the performance difference of two impellers at pH = 6.0 with 2.25 mg/l alum dose. The slow mixing was tapered from G = 30/s to 20/s after 20 minutes. This figure also shows the tremendous impact of impeller geometry on alum flocculation as evidenced by much wider difference of PDA and turbidity readings (compare top curve for 3x3 mesh with middle curve for 2-blade) generated by the two impellers. From this figure and also from **Figure 6.13**, it can be visualized that the alum flocs are weak and breakage of flocs occur at the later period of flocculation, even with a slow mix G of 30/s at both pH levels. Tapering the slow mix G from 30/s to 20/s resulted in better kinetics at the later stage of flocculation and better turbidity removal.

Figure 6.16 illustrates the performance of the above mentioned impellers in a fully sweep floc region. An alum dose of 20 mg/l at pH = 7.8 (with no buffer) satisfies the condition of a fully sweep floc mode of flocculation. The kinetics were very fast with a very high positive zeta potential (about +30 mv). With only 20 minutes of slow mix and 20 minutes of settling both the impellers removed about 90% of the total turbidity. The flocculation index readings show that the impellers performed almost identically, but turbidity readings illustrate the importance of impeller geometry to some degree. This figure indicates that the impeller geometry is not that crucial in a sweep

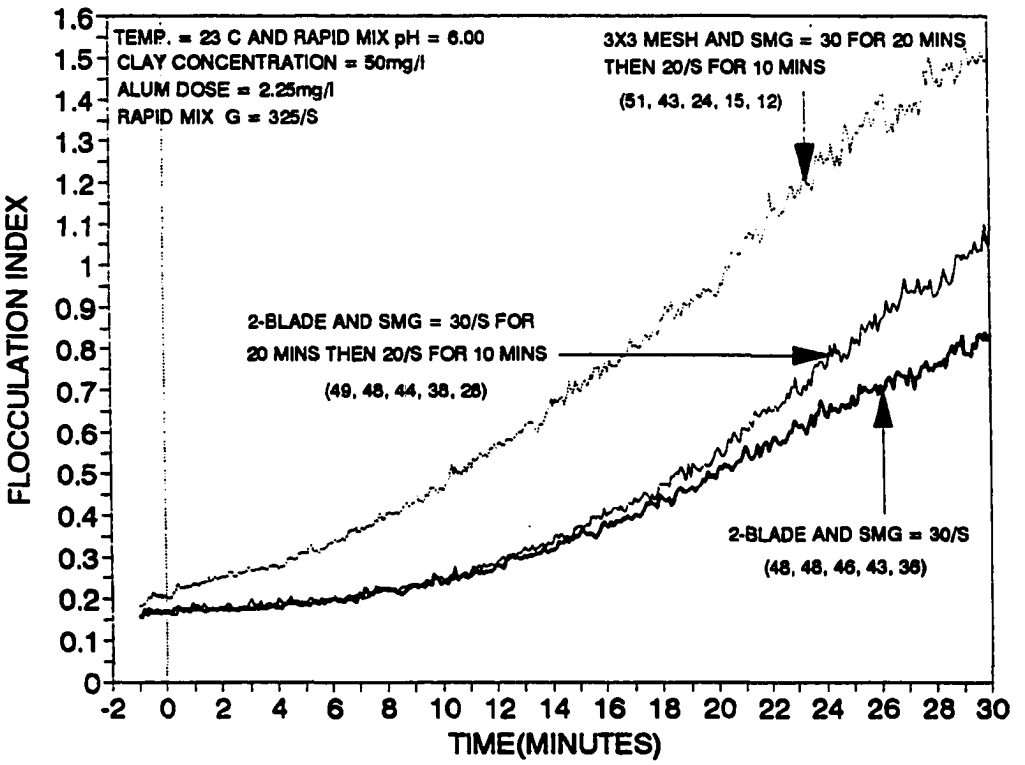

Figure 6.15. Effect of impeller geometry and slow mixing pattern on flocculation kinetics at pH = 6.0 and temperature = 23° C with alum as the coagulant. Clay concentration is 50 mg/l. The rapid mix G value of 325/s corresponds 200 and 90 rpm for 2-blade and the 3x3 mesh impellers respectively. The G value of 30/s corresponds to 40 and 17 rpm for 2-blade and 3x3 mesh impellers respectively. The slow mix G value of 20/s corresponds to 29 and 12 rpm for 2-blade and 3x3 mesh impellers respectively. Numbers in parenthesis represent the homogenized turbidity and 10, 20, 30 and 40 minute settled turbidity respectively following flocculation.

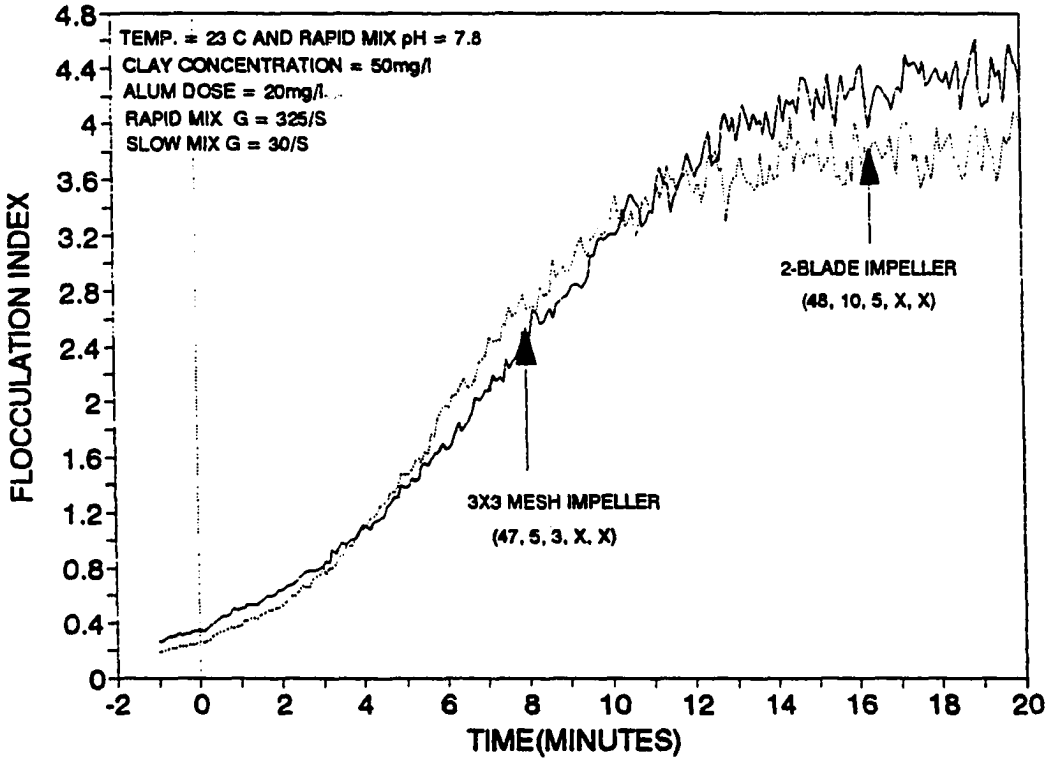

Figure 6.16. Effect of impeller geometry on flocculation kinetics at pH = 7.8 and temperature = 23° C with alum as the coagulant. Clay concentration is 50 mg/l. The rapid mix G value of 325/s corresponds 200 and 90 rpm for 2-blade and the 3x3 mesh impellers respectively. The slow mix G value of 30/s corresponds to 40 and 17 rpm for 2-blade and 3x3 mesh impellers respectively. Numbers in parenthesis represent the homogenized turbidity and 10, 20, 30, and 40 minute settled turbidity respectively following flocculation. X means that the turbidity measurement was not taken at that particular time

floc mode of flocculation, as compared to the A/D mode. But the 3x3 mesh impeller performed better in this mode, also.

Figures 6.17 through 6.19 illustrate the effect of impeller geometry on alum flocculation with three different clay concentrations in the presence of buffer. In these experiments only, several combinations of $NaHCO_3$ and Na_2CO_3 (very little amount of) were used as buffer to maintain a constant pH. The bicarbonate ion is a specifically adsorbed anion such as sulfate ion, and tends to influence the coagulation mechanism. Letterman and Vanderbrook (1983) cited the work of Hohl et al. (1978) which stated that the sulfate ion decreases the charge of aluminum hydroxide surface by increasing the number of neutral (AlOH and Al_2SO_4) and negative (AlO^- and $AlSO_4^-$) surface groups through ionization and complex formation reactions. Even though the effect is less severe, bicarbonate ion also reacts in similar fashion and competes with OH^- in the coordination around the aluminum.

Letterman and Vanderbrook (1983) also stated that low pH values tend to favor the flocculation with alum in presence of sulfate. Probably same is true for bicarbonate ion. But at high pH such as 7.8 used in this study, the flocculation kinetics became worse due to the formation of above mentioned neutral and negative surface groups and the reduction of positive charge of aluminum hydroxide surface. Letterman et al. (1979) illustrated that the turbidity removal with 10 mg/l alum was much worse when pH was increased from 7.0 to 8.0 in presence of bicarbonate ion. The current study also indicated that at pH = 7.8 the kinetics were worse in the presence of buffer when the dose was kept constant. Two times the coagulant used in **Figure 6.13** (without buffer)

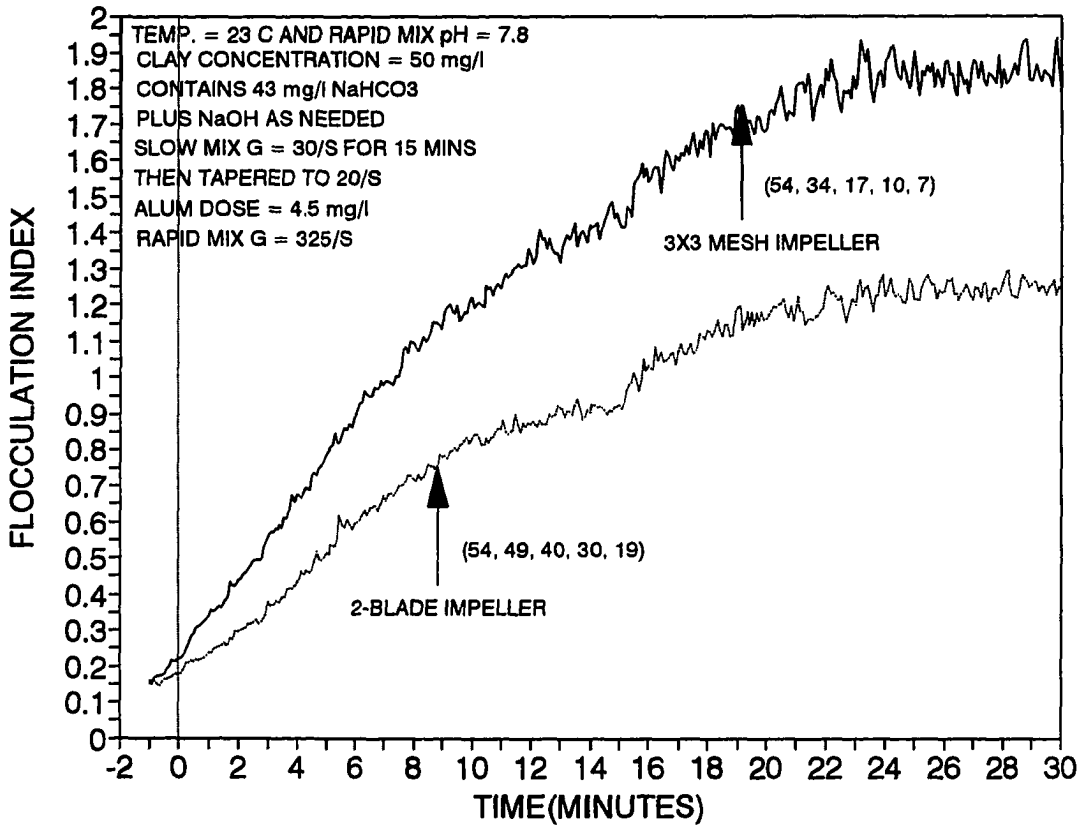

Figure 6.17. Effect of impeller geometry on flocculation kinetics at pH = 7.8 and temperature = 23° C with alum as the coagulant and buffer present. Clay concentration is 50 mg/l. The rapid mix G value of 325/s corresponds to 200 and 90 rpm for 2-blade and the 3x3 mesh impellers respectively. The G value of 30/s corresponds to 40 and 17 rpm for 2-blade and 3x3 mesh impellers respectively. The slow mix G value of 20/s corresponds to 29 and 12 rpm for 2-blade and 3x3 mesh impellers respectively. Numbers in parenthesis represent the homogenized turbidity and 10, 20, 30 and 40 minute settled turbidity respectively following flocculation

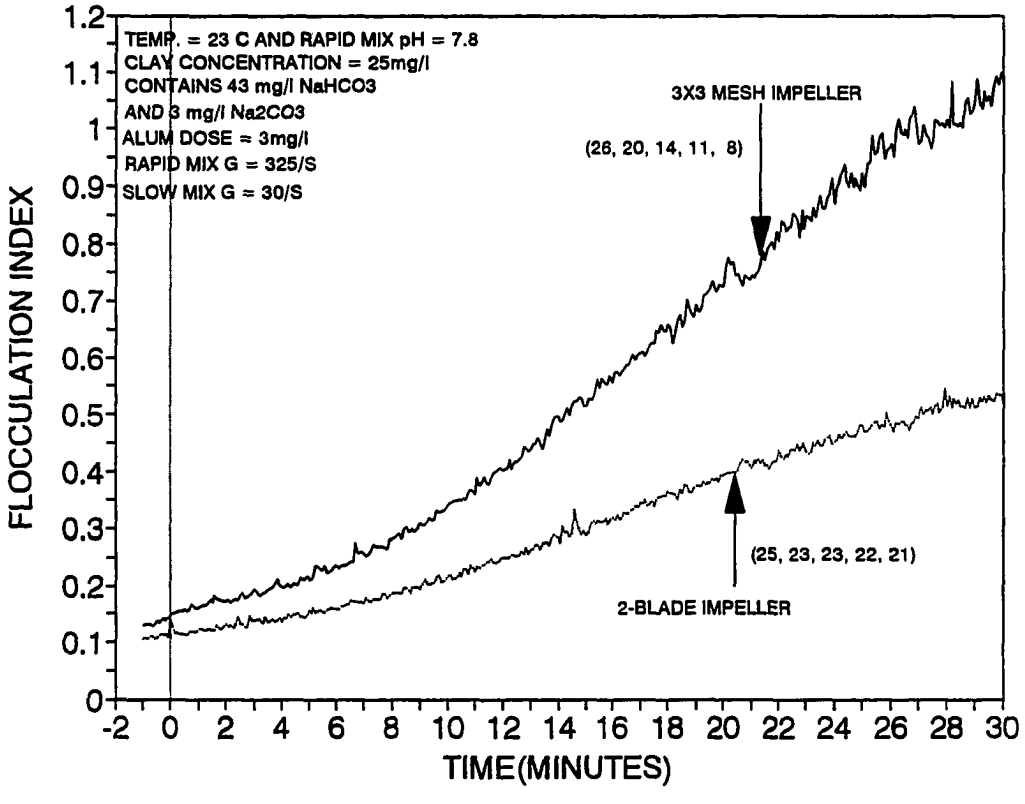

Figure 6.18. Effect of impeller geometry on flocculation kinetics at pH = 7.8 and temperature = 23° C with alum as the coagulant and buffer present. Clay concentration is 25 mg/l. The rapid mix G value of 325/s corresponds 200 and 90 rpm for 2-blade and the 3x3 mesh impellers respectively. The slow mix G value of 30/s corresponds to 40 and 17 rpm for 2-blade and 3x3 mesh impellers respectively. Numbers in parenthesis represent the homogenized turbidity and 10, 20, 30, and 40 minute settled turbidity respectively following flocculation

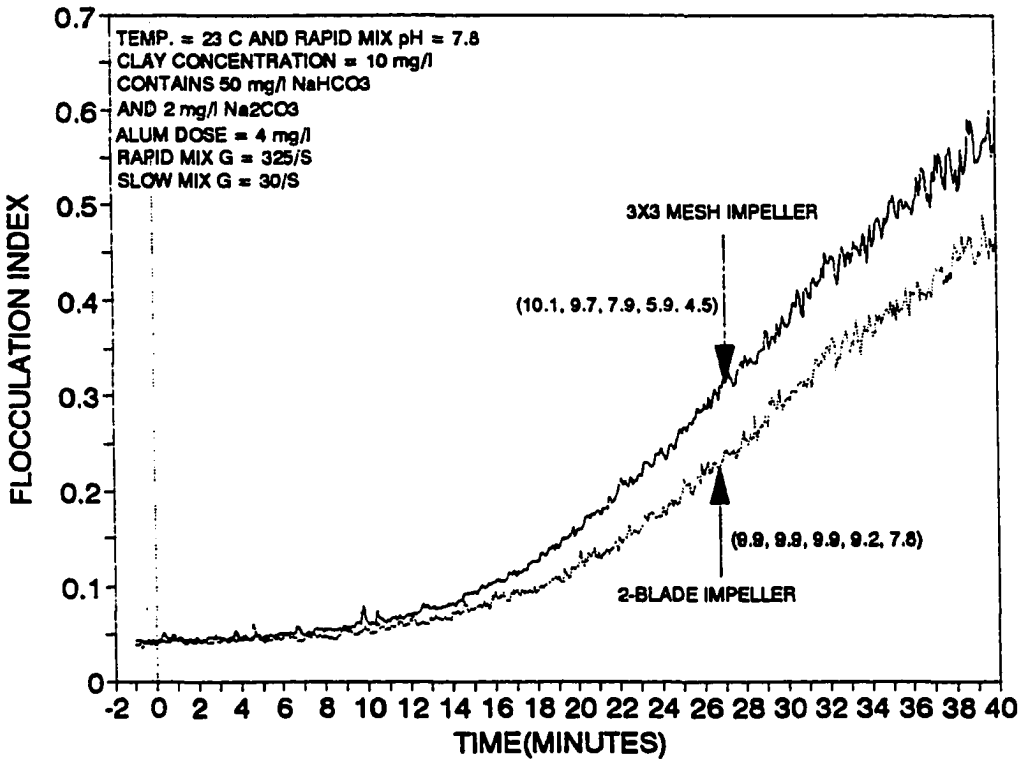

Figure 6.19. Effect of impeller geometry on flocculation kinetics at pH = 7.8 and temperature = 23° C with alum as the coagulant and buffer present. Clay concentration is 10 mg/l. The rapid mix G value of 325/s corresponds 200 and 90 rpm for 2-blade and the 3x3 mesh impellers respectively. The slow mix G value of 30/s corresponds to 40 and 17 rpm for 2-blade and 3x3 mesh impellers respectively. Numbers in parenthesis represent the homogenized turbidity and 10, 20, 30, and 40 minute settled turbidity respectively following flocculation

was required in **Figure 6.17** in presence of 43 mg/l $NaHCO_3$ to achieve similar zeta potential (around -13 mv) and flocculation kinetics with 50 mg/l clay suspension. In both the situations (with buffered and unbuffered suspension) the 3x3 mesh impeller was superior to the 2-blade impeller and the margin of difference was similar.

When the results are compared between **Figures 6.12** and **6.18**, a slightly different picture was seen. The dose was doubled in **Figure 6.18** in order to provide for the effects of the buffer, but the destabilizing characteristics were different this time for the two cases. The zeta potential for experiments in **Figure 6.18** was around -15 mv as compared to that found in **Figure 6.12**, around -10 mv. In both situations, the mesh impeller performed almost identically, but the performance of the 2-blade impeller was noticeably impaired in presence of buffer with minor modification of destabilization characteristics. This indicates that the 3x3 mesh impeller can maintain its performance over a broader range of destabilization characteristics of suspended particles than the 2-blade impeller.

Figure 6.19 contains the results of alum flocculation performed with 10 mg/l clay concentrations. Even with more favorable destabilization characteristics of particles (zeta potential around -7 mv in **Figure 6.19** as compared to -13 mv in **Figure 6.17**), the flocculation kinetics were much worse in **Figure 6.19**. The kinetics were severely limited by the number of particle contacts in **Figure 6.19**, due to much lower particle number concentration. In spite of the generally slow kinetics under these conditions, the 3x3 mesh impeller was significantly better than the 2-blade impeller.

6.1.3. Effect of rapid mixing intensity

Figures 6.20 through 6.23 illustrate the effect of rapid mixing intensity on flocculation kinetics under four different physico-chemical conditions. In **Figures 6.20 and 6.21**, all the physico-chemical conditions are the same, except the temperature and the dose. As mentioned earlier, the ferric nitrate dose was increased from 2 mg/l to 3 mg/l when temperature was changed from 23° to 5° C in order to achieve similar zeta potential reading after the rapid mixing stage. In both of these figures, the performance became worse when the rapid mix G was increased beyond a certain value. The rapid mix G values of 575/s and 460/s were found to be optimum at 23° and 5° C respectively with ferric nitrate coagulant at pH = 7.8 with a zeta potential reading around -10 mv. It should be kept in mind that the energy input was the same at both temperatures in order to achieve those rapid mix G values.

A rapid mix G of 450/s was found to be optimum for alum coagulation at pH = 7.8 and temperature = 23° C under A/D region as shown in **Figure 6.22**. The performance was worse when the intensity was increased to a G value of 575/s. The rapid mixing intensity of 450/s was also found to be optimum for flocculation with ferric nitrate at pH = 6.0 and temperature = 23° C under A/D region, as shown in **Figure 6.23**. The kinetics became significantly worse when the intensity was raised to a G value of 575/s. This was evidenced by both the PDA and the turbidity readings. It should be noted that all the rapid mixing intensity tests were performed with the 2-blade impeller.

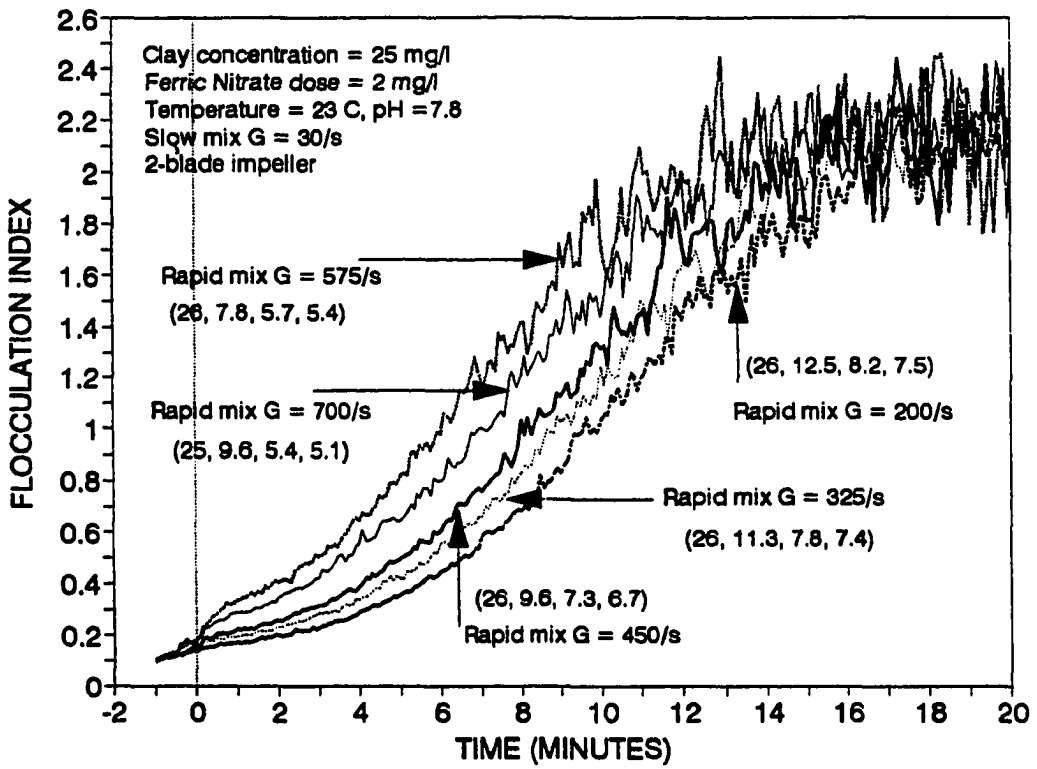

Figure 6.20. Effect of rapid mixing intensity on flocculation kinetics at pH = 7.8 and temperature = 23° C with ferric nitrate as the coagulant. The rapid mix G values of 200, 325, 450, 575, and 700/s correspond to 143, 200, 248, 293, and 335 rpm respectively. The slow mix G value of 30/s corresponds to 40 rpm. Numbers in parenthesis represent the homogenized turbidity and 10, 20, and 30 minute settled turbidity respectively following flocculation

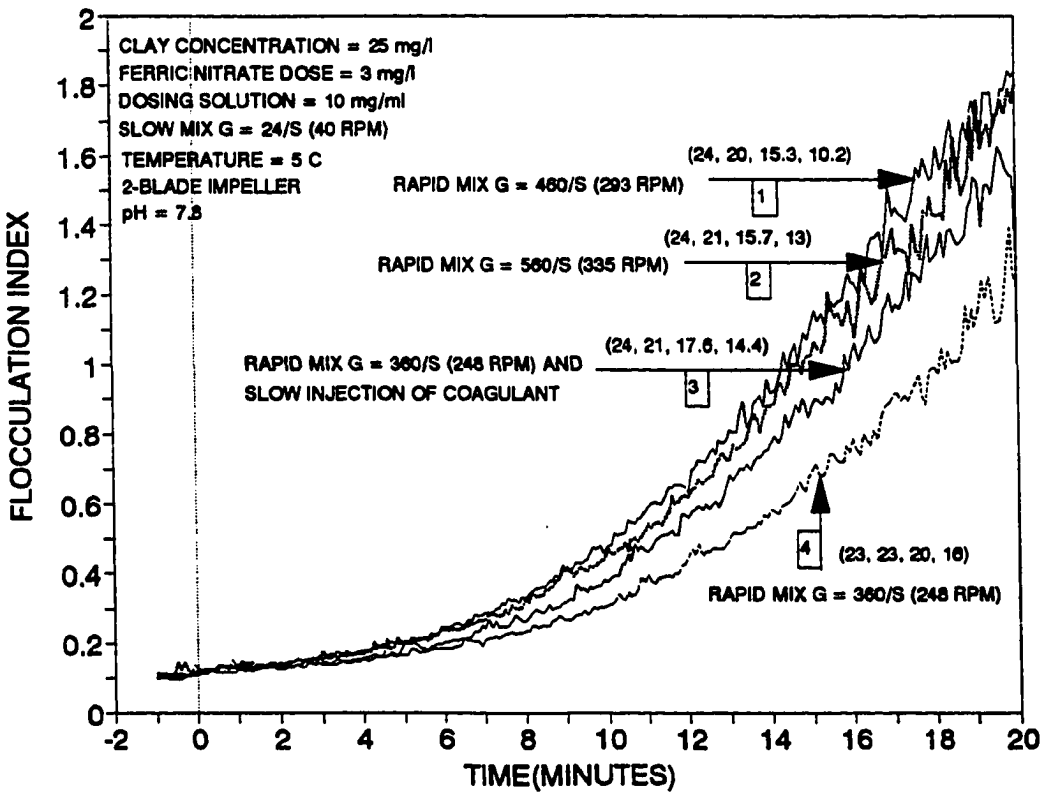

Figure 6.21. Effect of rapid mixing intensity and coagulation injection pattern on flocculation kinetics at pH = 7.8 and temperature = 5° C with ferric nitrate as the coagulant. Numbers in parenthesis represent the homogenized turbidity and 10, 20, and 30 minute settled turbidity respectively following flocculation

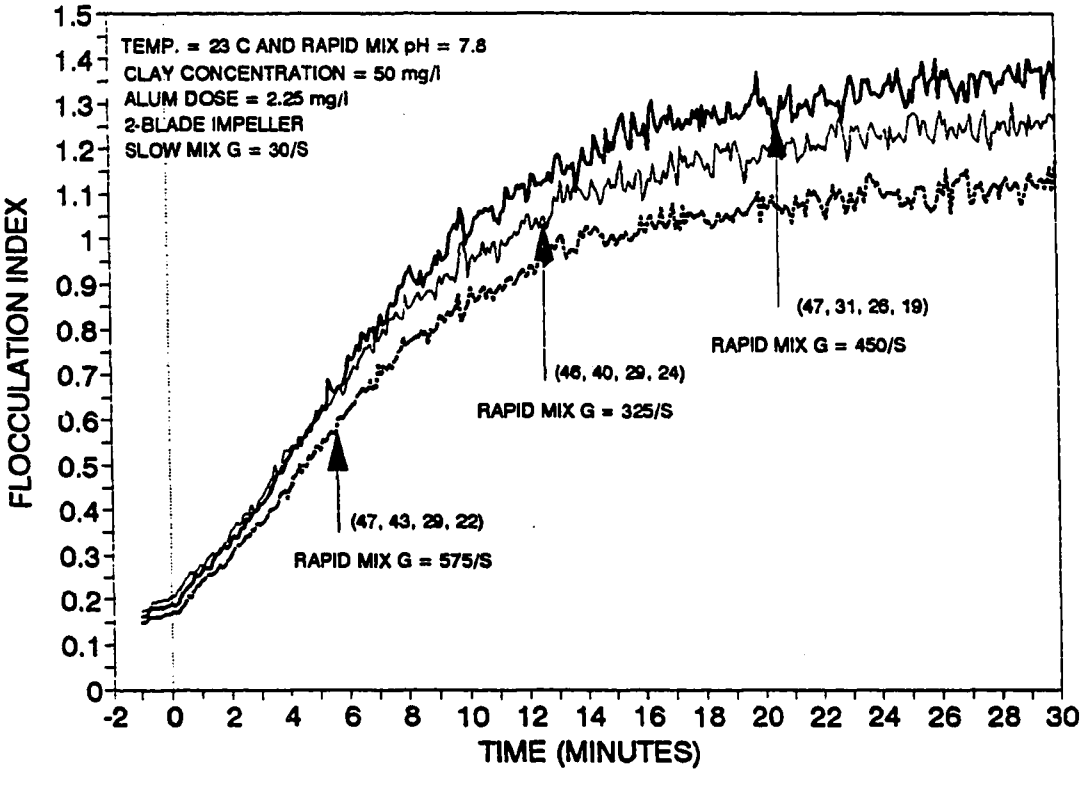

Figure 6.22. Effect of rapid mixing intensity on flocculation kinetics at pH = 7.8 and temperature = 23° C with alum as the coagulant. The rapid mix G values of 325, 450, and 575/s correspond to 200, 248, and 293 rpm respectively. The slow mix G value of 30/s corresponds to 40 rpm. Numbers in parenthesis represent the homogenized turbidity and 10, 20, and 30 minute settled turbidity respectively following flocculation

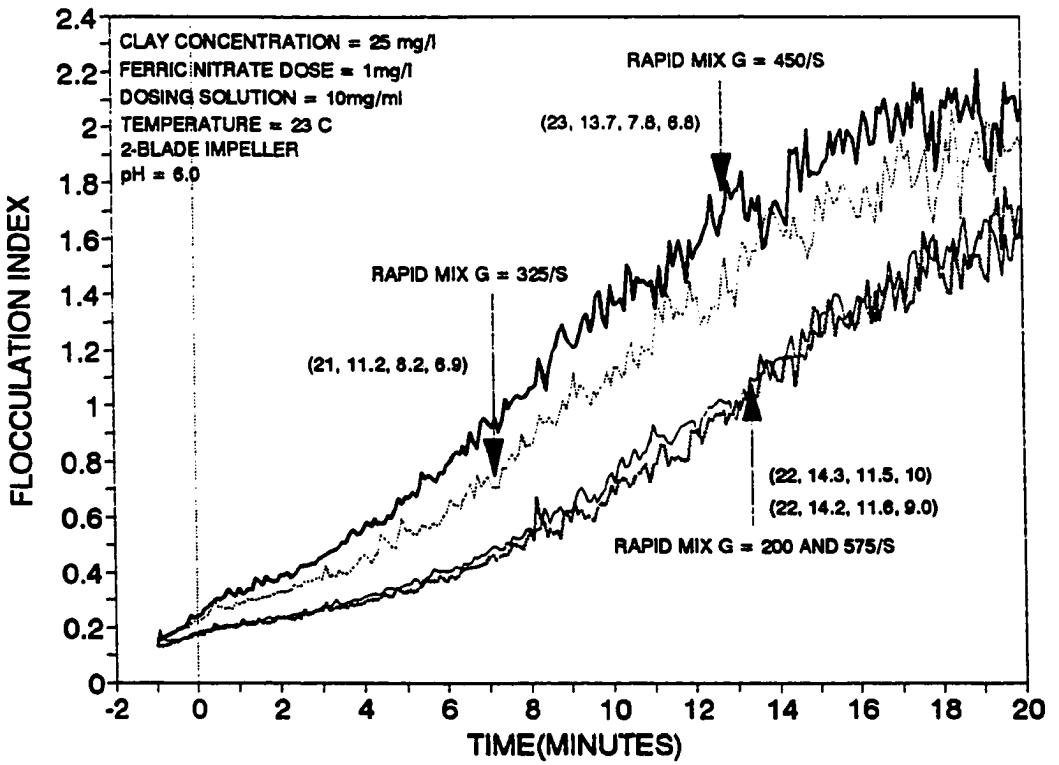

Figure 6.23. Effect of rapid mixing intensity on flocculation kinetics at pH = 6.0 and temperature = 23° C with ferric nitrate as the coagulant. The rapid mix G values of 200, 325, 450, and 575/s correspond to 143, 200, 248, and 293 rpm respectively. The slow mix G value was 30/s (40 rpm). Numbers in parenthesis represent the homogenized turbidity and 10, 20, and 30 minute settled turbidity respectively following flocculation

6.1.4. Effect of rapid mixing pattern

Figures 6.24 through 6.27 illustrate the results of rapid mixing pattern on flocculation kinetics of kaolin clay with ferric nitrate as the coagulant. Using a dimensionless Gt value of 27000, two rapid mixing patterns were tested under four different physico-chemical conditions. The two patterns include, high intensity (G = 450/s) mixing with short duration (1 minute), and low intensity (G = 225/s) mixing with longer duration (2 minutes). From these figures, it can be perceived that the low intensity-longer duration mixing outperformed the high intensity-short duration mixing, in almost all the situations. This was observed irrespective of impeller geometry, as well as the dose and temperature variations. **Figure 6.25** appears to be the only exception where the performance was almost the same. The performance differences in the other three figures were more pronounced at low dose and low temperature situations (Compare **Figure 6.27** with **Figures 6.24 and 6.26**).

6.1.5. Effect of coagulant injection pattern

Curves 3 and 4 of **Figure 6.21** and curves 2 and 3 of **Figure 6.28** portray the effect of coagulation injection pattern during rapid mix on flocculation kinetics of kaolin clay with ferric nitrate as the coagulant at pH = 7.8 at two temperatures. Two types of coagulation injection patterns were employed as mentioned earlier: slow injection over a period of 10 second duration, and pulse injection within a second. By comparing those curves of the mentioned figures it can easily be visualized that slow injection of coagulant yields better results than the pulse injection and the difference was more

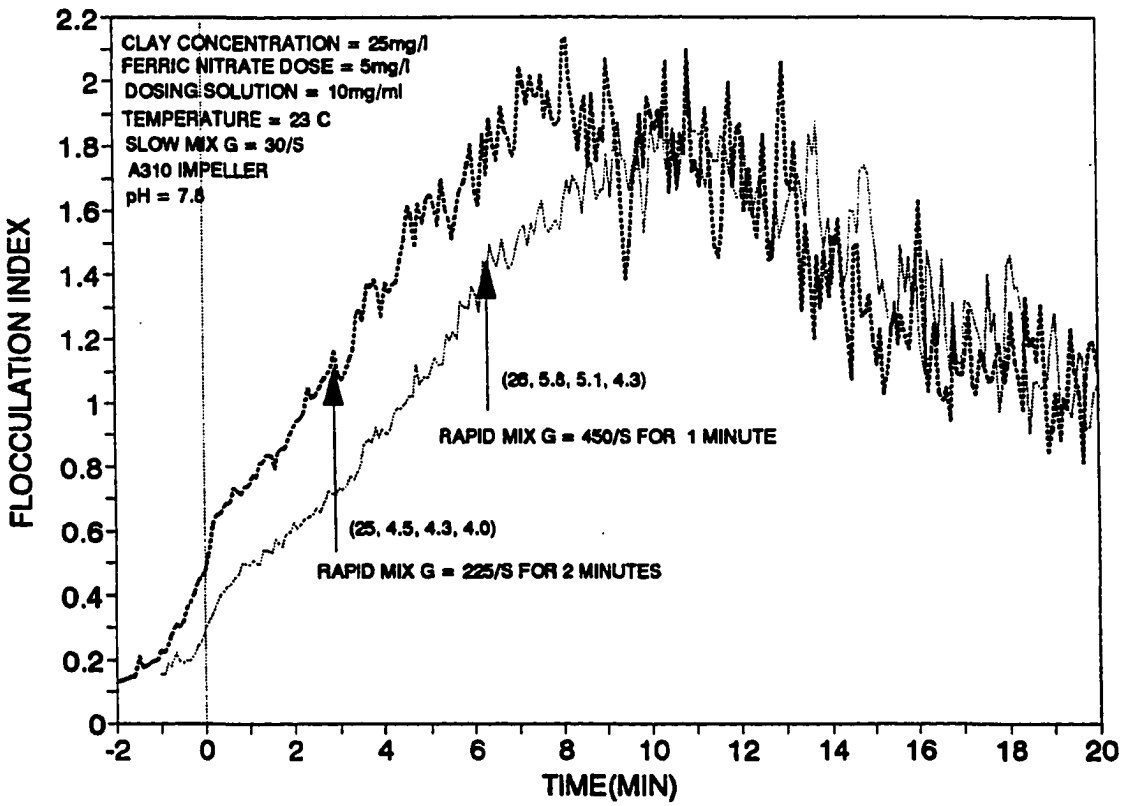

Figure 6.24. Effect of rapid mixing pattern on flocculation kinetics at pH = 7.8 and temperature = 23° C with ferric nitrate as the coagulant. The G values of 30, 225, and 450/s correspond to 63, 256, and 493 rpm respectively. Numbers in parenthesis represent the homogenized turbidity and 10, 20, and 30 minute settled turbidity respectively following flocculation

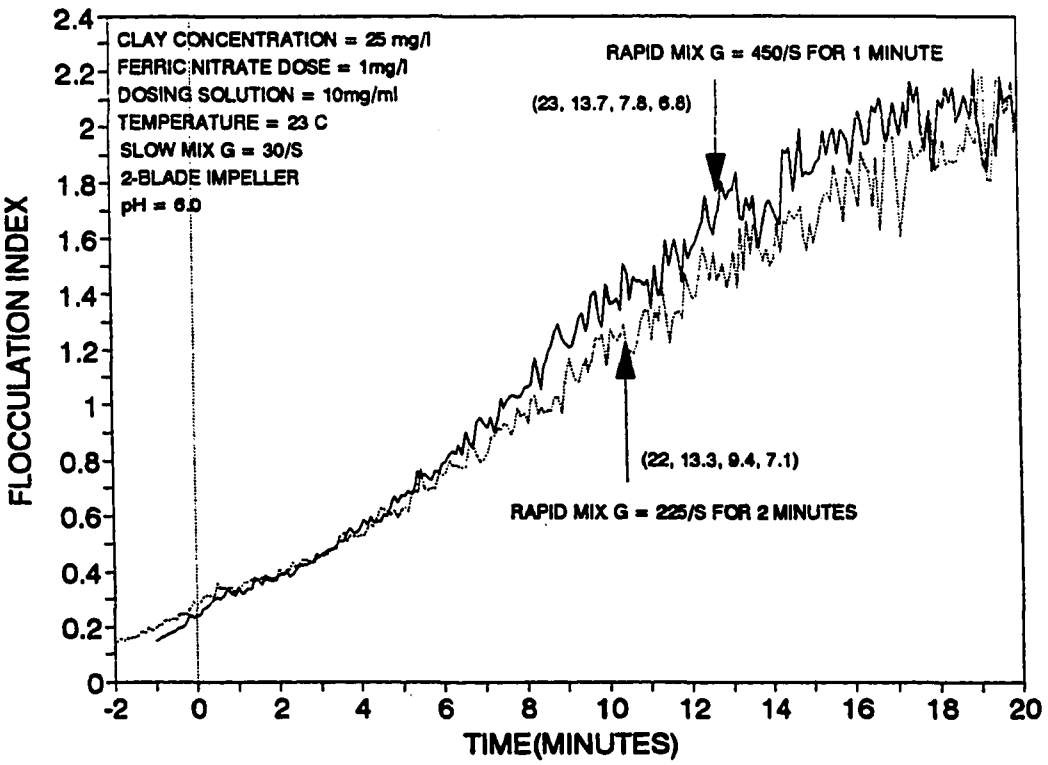

Figure 6.25. Effect of rapid mixing pattern on flocculation kinetics at pH = 6.0 and temperature = 23° C with ferric nitrate as the coagulant.The G values of 30, 225, and 450/s correspond to 40, 155, and 248 rpm respectively. Numbers in parenthesis represent the homogenized turbidity and 10, 20, and 30 minute settled turbidity respectively following flocculation

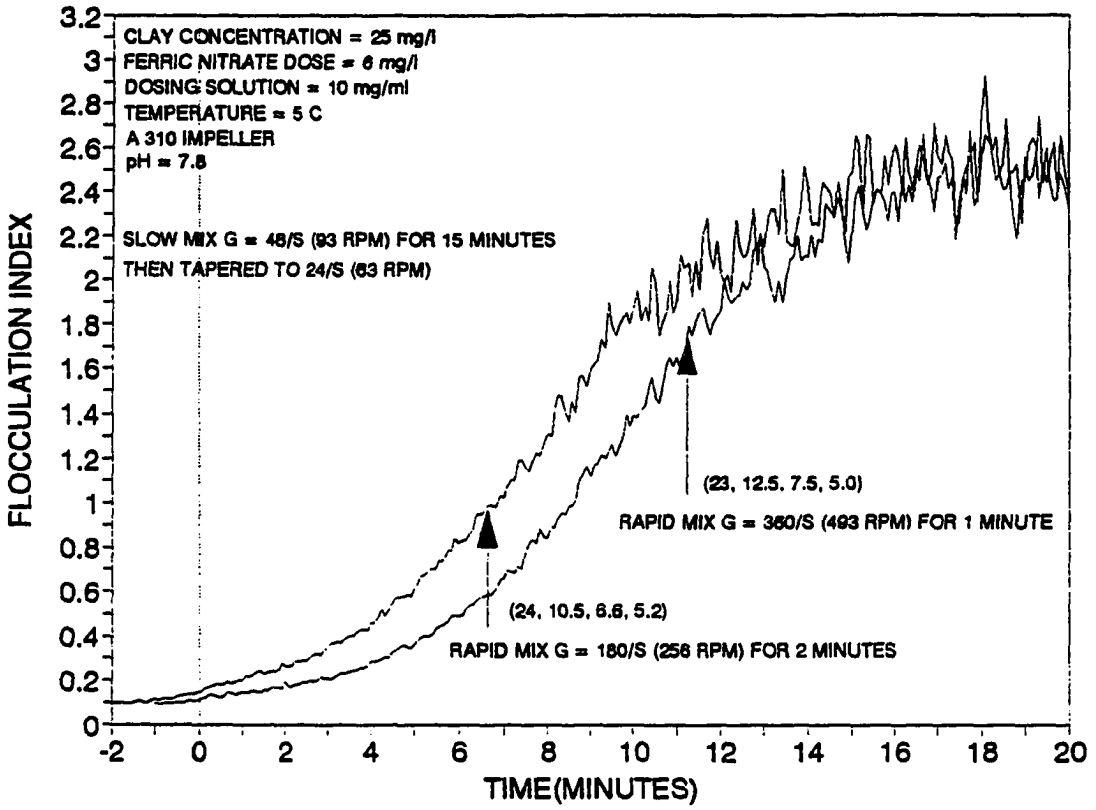

Figure 6.26. Effect of rapid mixing pattern on flocculation kinetics at pH = 7.8 and temperature = 5° C with ferric nitrate as the coagulant.
Numbers in parenthesis represent the homogenized turbidity and 10, 20, and 30 minute settled turbidity respectively following flocculation

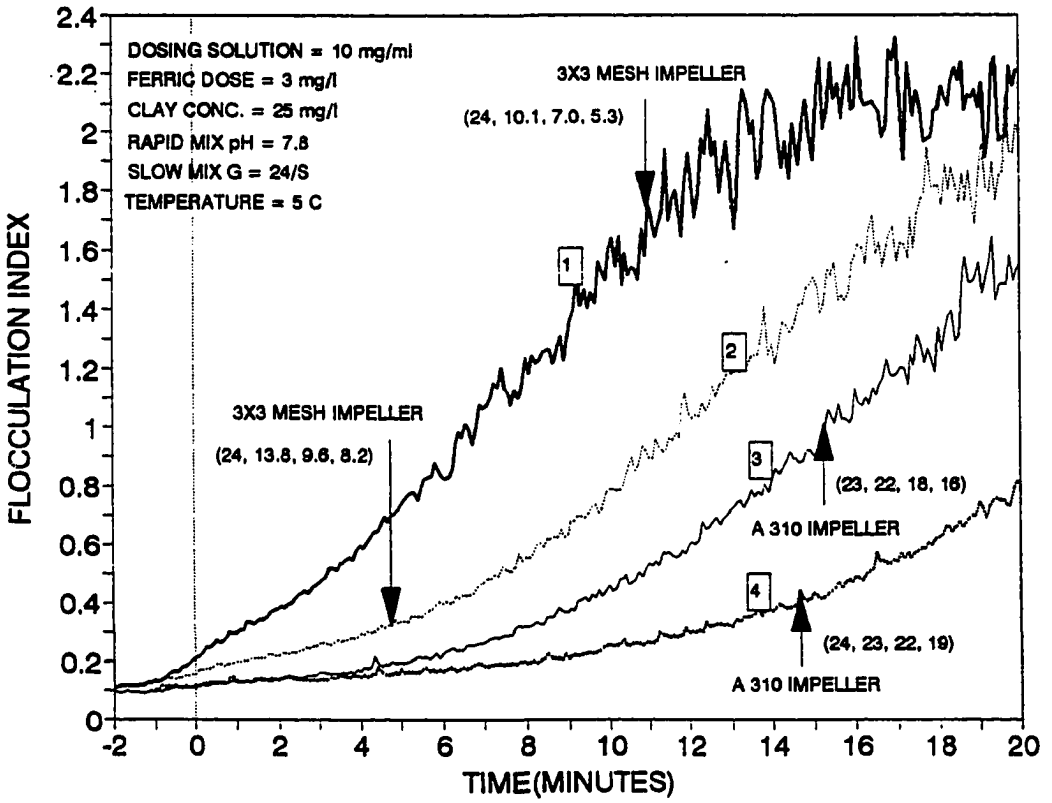

Figure 6.27. Effect of rapid mixing pattern on flocculation kinetics at pH = 7.8 and temperature = 5° C with ferric nitrate as the coagulant. Odd numbered curves represent a rapid mix G value of 180/s for 2 minutes (70 and 256 rpm for 3x3 mesh and A310 impellers respectively) and the even numbered curves represent a rapid mix G value of 360/s for 1 minute (112 and 493 rpm for 3x3 mesh and A 310 impellers respectively). Slow mix G value of 24/s corresponds to 17 and 63 rpm for 3x3 mesh and A310 impellers respectively. Numbers in parenthesis represent the homogenized turbidity and 10, 20, and 30 minute settled turbidity respectively following flocculation

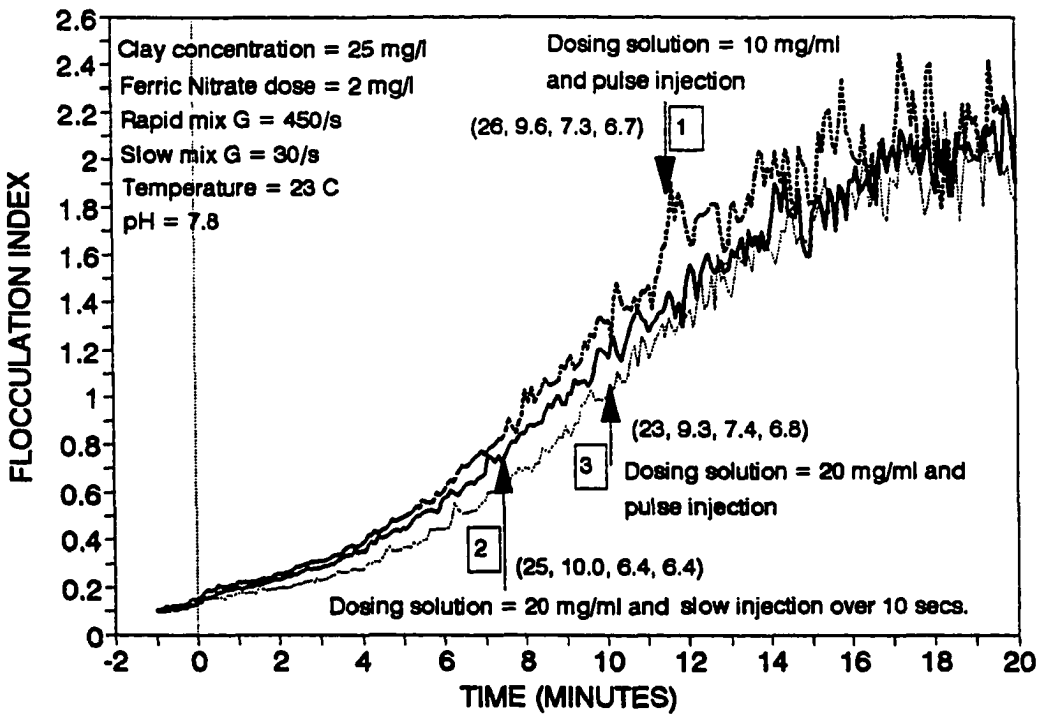

Figure 6.28. Effect of dosing solution concentration and coagulant injection pattern on flocculation kinetics at pH = 7.8 and temperature = 23° C with ferric nitrate as the coagulant. The 2-blade impeller was used. The G values of 450 and 30/s correspond to 248 and 40 rpm respectively. Numbers in parenthesis represent the homogenized turbidity and 10, 20, and 30 minute settled turbidity respectively following flocculation

pronounced at cold temperature than at warm temperature. This was confirmed by both PDA and turbidity readings. The experiments were done with 2-blade impellers.

6.1.6. Effect of dosing solution concentration

The curves 1 and 3 of **Figure 6.28,** and the **Figures 6.29 and 6.30** indicate that the concentration of dosing solution has a measurable impact on flocculation kinetics with ferric nitrate coagulant. When curves 1 and 3 of **Figure 6.28** are compared, better kinetics are seen with the dilute dosing solution as evidenced by the PDA reading. But the turbidity readings are almost the same in both cases. From **Figure 6.29** it is seen that measurable improvement of kinetics was achieved as evidenced by both PDA and turbidity readings, when the dosing solution was diluted from 20 mg/ml to 10 mg/ml, but further dilution to 5 mg/ml did not yield better results. Some difference in PDA reading was observed due to difference in initial PDA readings. Both the above situations were at warm temperature (23° C). **Figure 6.30** illustrates the effect of dilution at cold temperature. This figure shows that the earlier kinetics and the 30 minute settled turbidity reading were better when the dosing solution was diluted to 10 mg/ml from 20 mg/ml. The later period kinetics and the intermediate settled turbidity removals were better for 20 mg/ml dosing solution. But much better kinetics were observed when the dosing solution was further diluted to 5 mg/ml as seen by marked improvement of both the PDA and turbidity removal readings.

From these results one can easily understand that the concentration of coagulant dosing solution definitely has some impact on flocculation kinetics with ferric nitrate

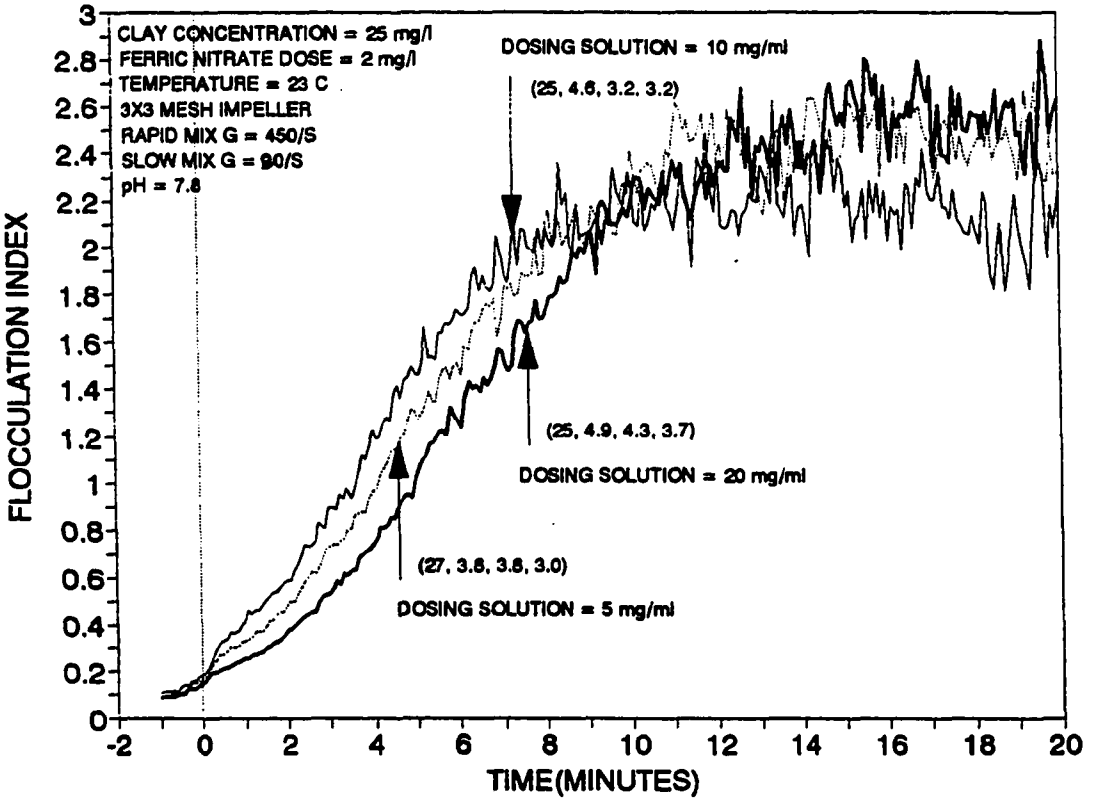

Figure 6.29. Effect of dosing solution concentration and on flocculation kinetics at pH = 7.8 and temperature = 23° C with ferric nitrate as the coagulant. The G values of 450 and 30/s correspond to 112 and 17 rpm respectively. Numbers in parenthesis represent the homogenized turbidity and 10, 20, and 30 minute settled turbidity respectively following flocculation

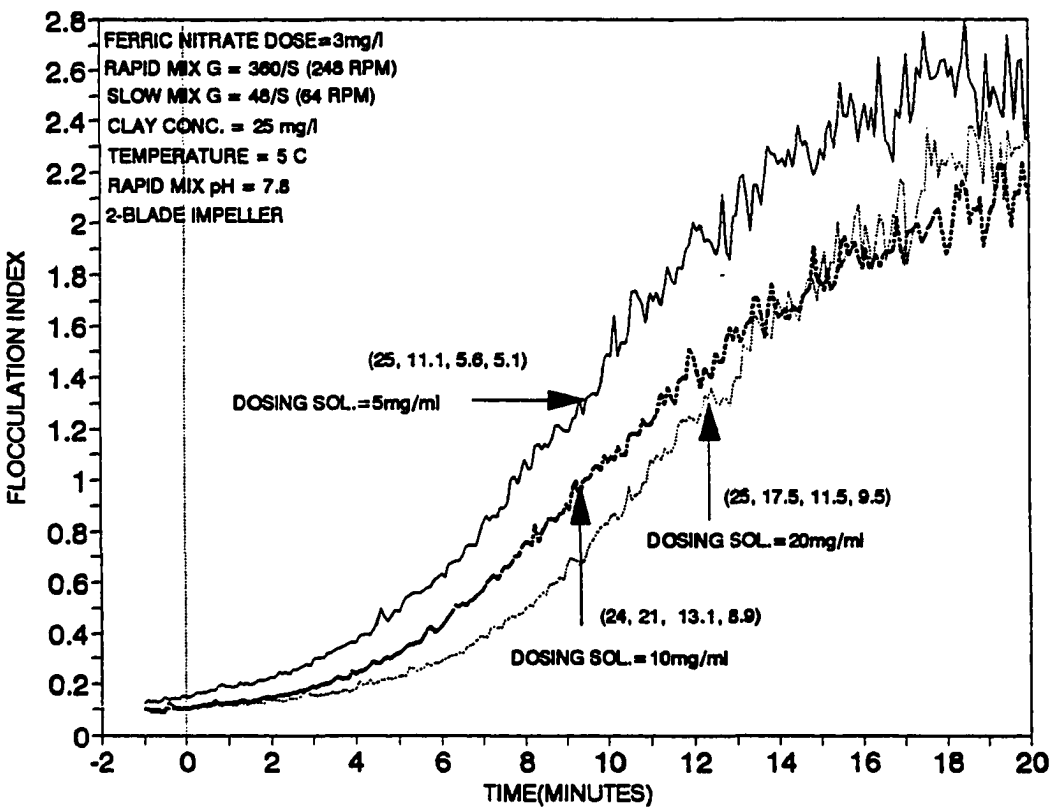

Figure 6.30. Effect of dosing solution concentration and on flocculation kinetics at pH = 7.8 and temperature = 5° C with ferric nitrate as the coagulant. Numbers in parenthesis represent the homogenized turbidity and 10, 20, and 30 minute settled turbidity respectively following flocculation

coagulant, and that the optimum dilution varies for different conditions.

6.1.7. Effect of number of coagulant injection ports

Figure 6.31 illustrates the performance difference between 1-point injection and 2-point injection of coagulant. The PDA readings generated by the two injection methods are almost identical but the turbidity readings indicate that 2-point injection performed better than 1-point injection. The 2-point injection removed more primary particles and created better settling, even though the flocculation index values were not much different from those produced by 1-point injection.

6.1.8. Effect of slow mixing intensity

From **Figures 6.32 through 6.36** it appears that slow mixing intensity is also an important mixing variable. **Figures 6.32 through 6.34** illustrate the results at cold water temperature with ferric nitrate coagulant. From these figures it is evident that if the constant-G mode is used for flocculation, then the optimum performance can be obtained near a certain G value. Below this value the kinetics are worse and above that value, the breakage of flocs occurs during the later period of flocculation. Compared to 24/s, a G value of 48/s produced a significantly better result with both PDA and turbidity readings. But further increase of G value to 72/s apparently resulted in floc breakup during the later period of flocculation evidenced by worse turbidity readings. This has been observed with all the three different impellers tested here. The slow mixing intensity is also important at warm temperature as shown in **Figures 6.35 and**

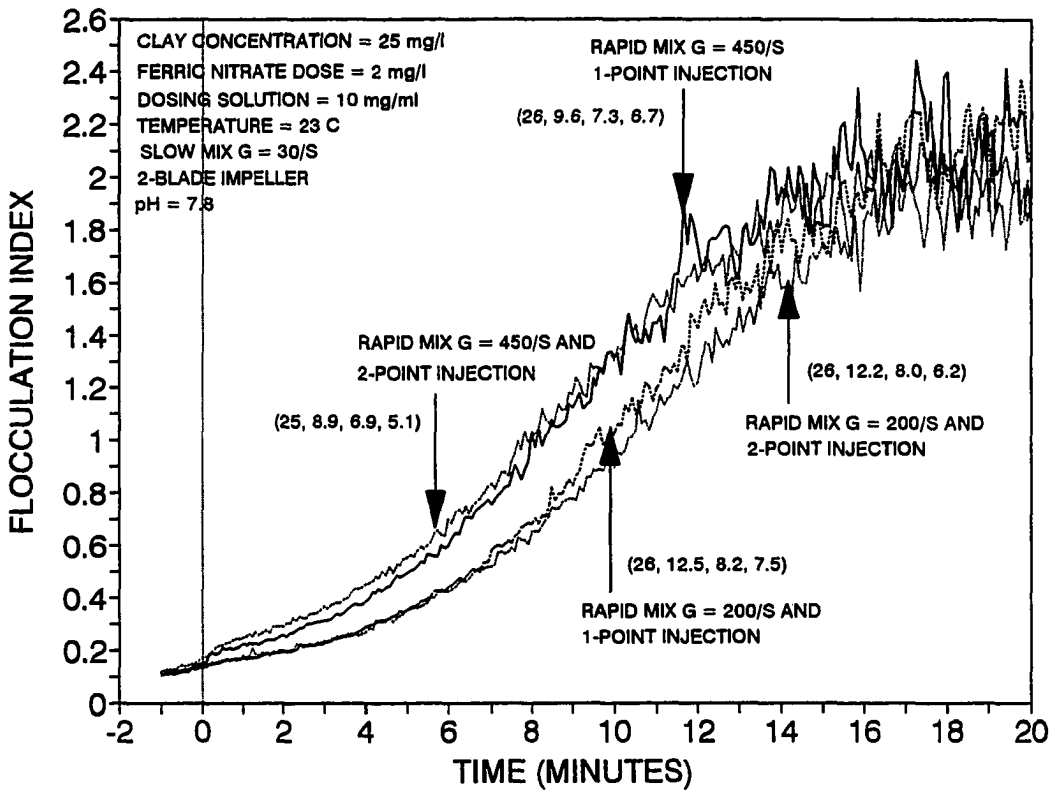

Figure 6.31. Effect of rapid mixing intensity and number of coagulation injection ports on flocculation kinetics at pH = 7.8 and temperature = 23° C with ferric nitrate as the coagulant. The G values of 450, 200, and 30/s correspond to 248, 143 and 40 rpm respectively. Numbers in parenthesis represent the homogenized turbidity and 10, 20, and 30 minute settled turbidity respectively following flocculation

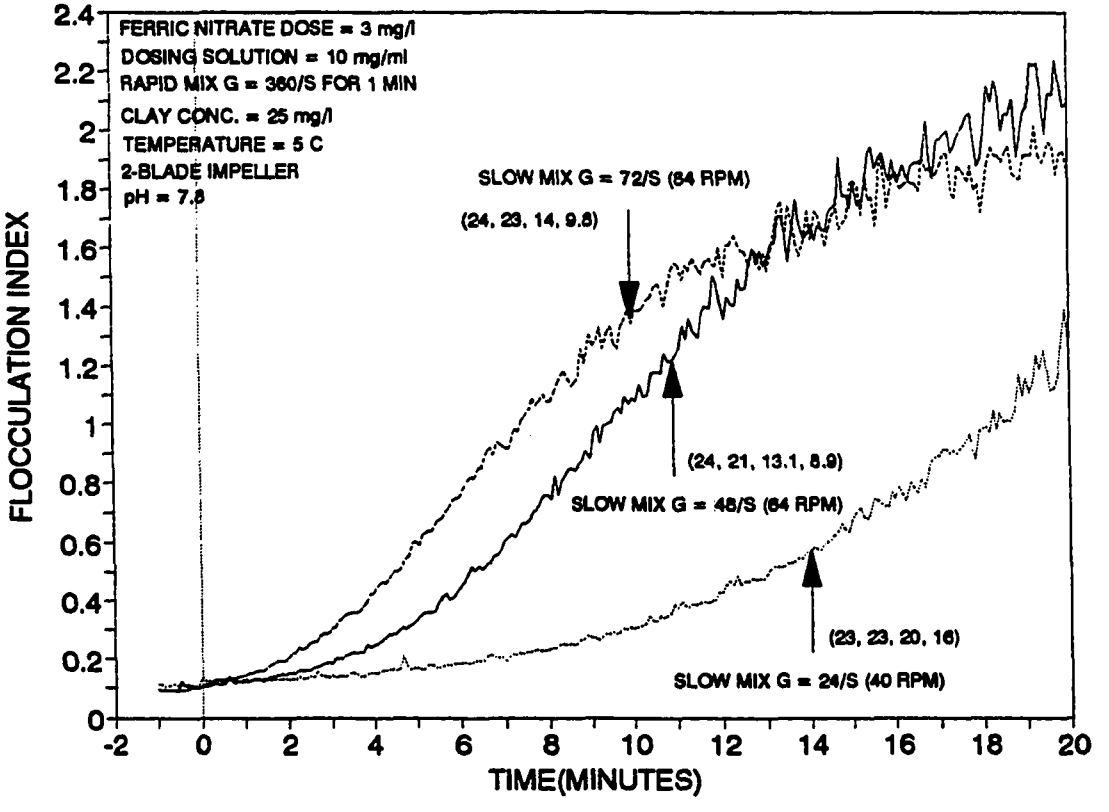

Figure 6.32. Effect of slow mixing intensity on flocculation kinetics at pH = 7.8 and temperature = 5° C with ferric nitrate as the coagulant. 2-blade impeller was used. The rapid mix G value of 360/s corresponds to 248 rpm. Numbers in parenthesis represent the homogenized turbidity and 10, 20, and 30 minute settled turbidity respectively following flocculation

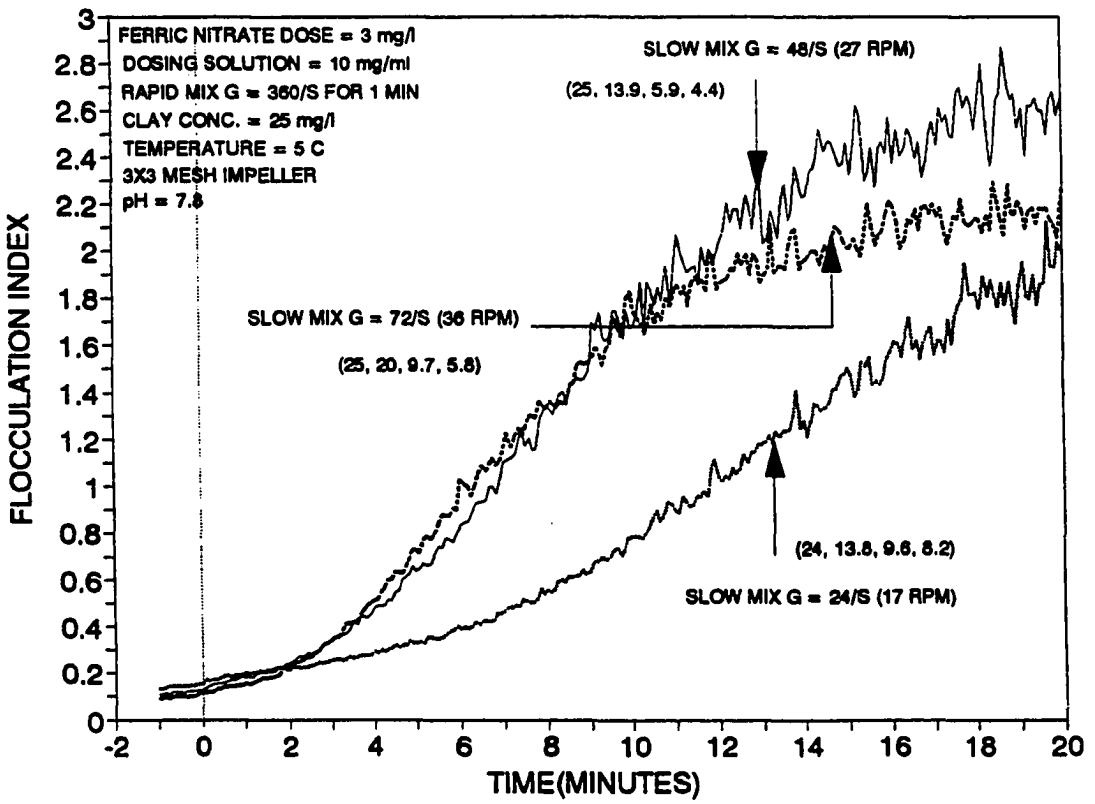

Figure 6.33. Effect of slow mixing intensity on flocculation kinetics at pH = 7.8 and temperature = 5° C with ferric nitrate as the coagulant. 3x3 mesh impeller was used.The rapid mix G value of 360/s corresponds to 112 rpm. Numbers in parenthesis represent the homogenized turbidity and 10, 20, and 30 minute settled turbidity respectively following flocculation

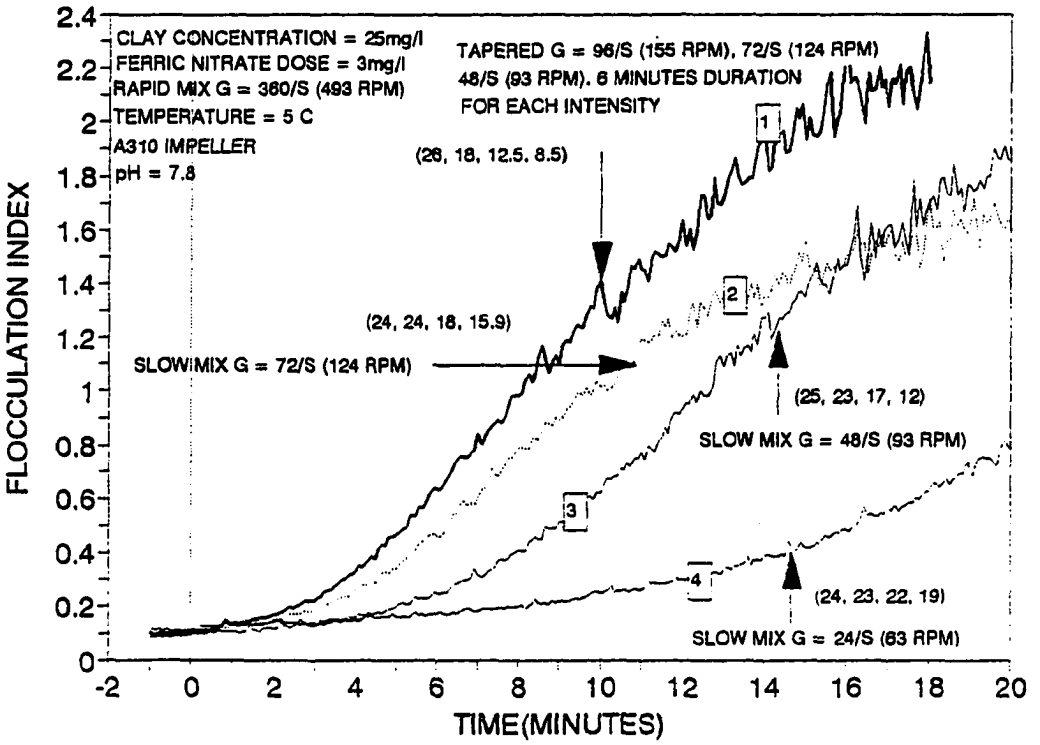

Figure 6.34. Effect of slow mixing intensity and pattern on flocculation kinetics at pH = 7.8 and temperature = 5° C with ferric nitrate as the coagulant. A 310 impeller was used.The rapid mix G value of 360/s corresponds to 493 rpm. Numbers in parenthesis represent the homogenized turbidity and 10, 20, and 30 minute settled turbidity respectively, following flocculation

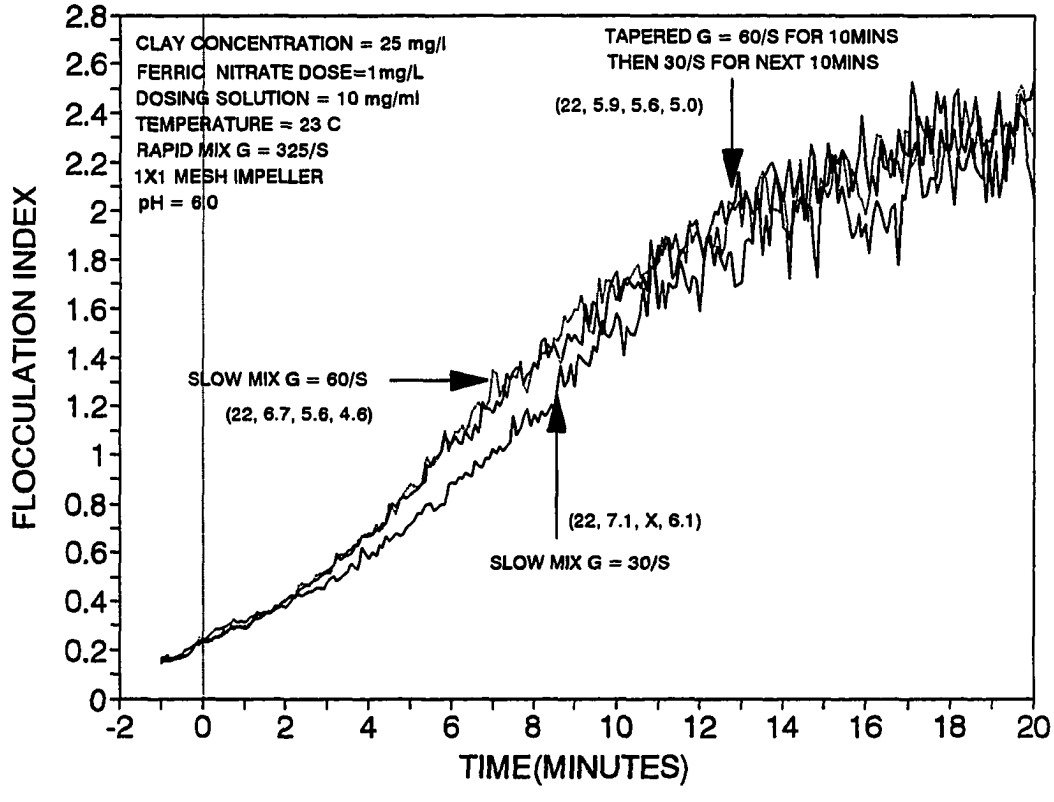

Figure 6.35. Effect of slow mixing intensity and pattern on flocculation kinetics at pH = 6.0 and temperature = 23° C with ferric nitrate as the coagulant. 1x1 mesh impeller was used. The G values of 325, 60, and 30/s correspond to 93, 31, and 20 rpm respectively. Numbers in parenthesis represent the homogenized turbidity and 10, 20, and 30 minute settled turbidity respectively, following flocculation. X means that the turbidity reading was not taken at that particular time

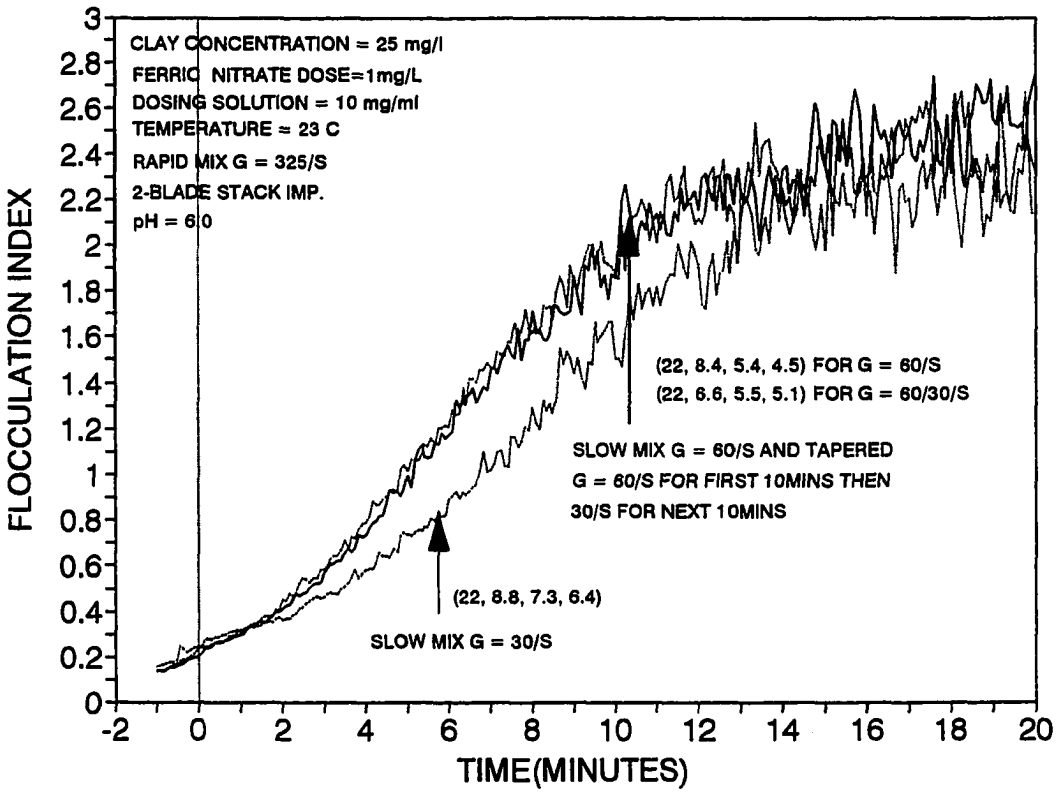

Figure 6.36. Effect of slow mixing intensity and pattern on flocculation kinetics at pH = 6.0 and temperature = 23° C with ferric nitrate as the coagulant. 2-blade stack impeller was used. The G values of 325, 60, and 30/s correspond to 180, 53, and 33 rpm respectively. Numbers in parenthesis represent the homogenized turbidity and 10, 20, and 30 minute settled turbidity respectively following flocculation

6.36, but the importance is not as crucial as that found at cold temperature.

6.1.9. Effect of slow mixing pattern

From **Figures 6.13, 6.15 and 6.34 through 6.36**, it appears that slow mixing pattern is also an important factor in flocculation efficiency. By tapering the intensity to a lower G value during the later period of flocculation, much better or comparable flocculation efficiency can be achieved with significant energy savings. This was seen irrespective of impeller geometry, coagulant type, water temperature, and pH values. Significant improvement of kinetics was seen with both the 3x3 mesh and 2-blade impellers in alum flocculation at pH = 7.8 and temperature 23° C when the slow mixing G was reduced from 30/s to 20/s after 15 minutes of flocculation as shown in **Figure 6.13**. Similar improvement was also noticed at pH = 6.0 when the slow mixing G was reduced to 20/s from 30/s after 20 minutes of flocculation as shown in **Figure 6.15**.

Curves 1 and 2 of **Figure 6.34** illustrate that flocculation can be improved significantly by tapering the slow mixing intensity at the different stages of mixing, even with a lower total dimensionless Gt value. Similarly, in **Figures 6.35 and 6.36**, a tapered flocculation with G = 60/s for 10 minutes followed by a G = 30/s for the next 10 minutes, performed as good as a constant G = 60/s for 20 minutes as shown for 1x1 mesh and 2-blade stack impellers, respectively.

6.1.10. Effect of opening size of wire mesh impeller

Two sets of experiments were conducted to determine the impact of opening size of the wire mesh impeller at constant power input as shown in **Figures 6.37 and 6.38**. Larger opening wire mesh achieved better results in both of these conditions (low dose at low pH in the A/D region and high dose at high pH in the sweep flocculation region) with constant power input as shown in those figures. Smaller mesh opening impeller dissipates more energy due to the drag between the fluid and the larger number of wires present in the flow area. Therefore, at constant power input, the impeller with smaller mesh opening had to be rotated at lower speed to achieve constant power input, which resulted in lower tip speed and lower local velocity and velocity fluctuations and therefore, lower probability of particle collisions. **Figure 6.39** illustrates the performance among four impellers at constant speed (20 rpm for all). Three mesh impellers with different opening sizes (one, nine and sixty four square openings per square inch) and one without mesh, only with the 7 mm wide outer frame (frame only). The flocculation index versus time curves for 3x3 mesh, 1x1 mesh, and the frame only impellers were almost identical at constant speed, but the turbidity readings produced by those three impellers were noticeably different. The 3x3 mesh and the frame only impeller performed best and worst respectively, in terms of turbidity removal. The 8x8 and 3x3 mesh impellers achieved almost identical turbidity readings even though they produced different flocculation index versus time curves.

From the above figures it is evident that the particle aggregation during flocculation is caused not only by the large scale flows generated by the effective radius

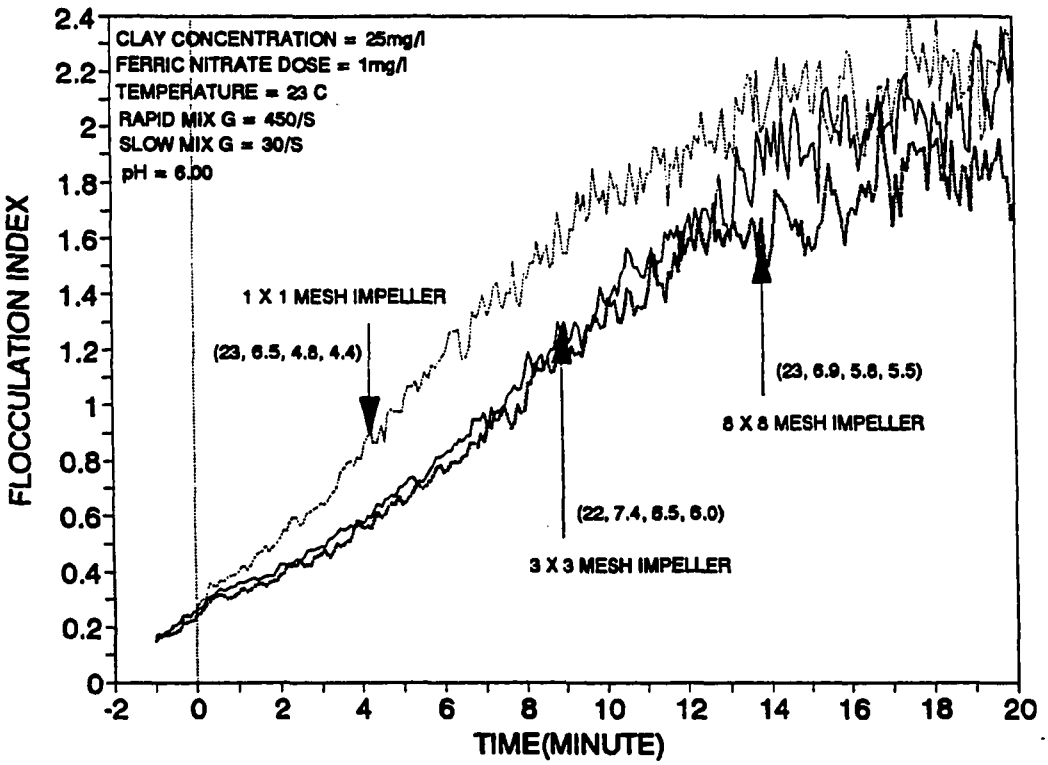

Figure 6.37. Effect of opening size of the mesh impeller on flocculation kinetics at pH = 6.0 and temperature = 23° C with ferric nitrate as the coagulant. The G value of 450/s corresponds to 112 rpm for all the three impellers and a value of 30/s corresponds to 15, 17, and 20 rpm for 8x8, 3x3, and 1x1 mesh impellers respectively. Numbers in parenthesis represent the homogenized turbidity and 10, 20, and 30 minute settled turbidity respectively following flocculation

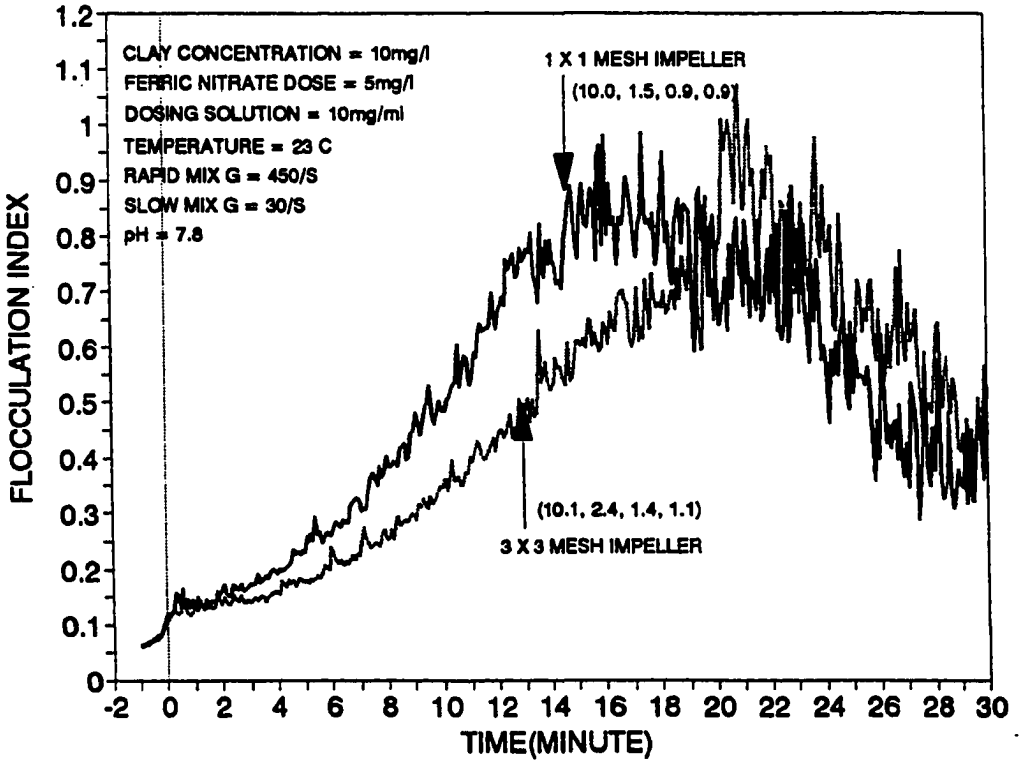

Figure 6.38. Effect of opening size of the mesh impeller on flocculation kinetics at pH = 7.8 and temperature = 23° C with ferric nitrate as the coagulant. The G value of 450/s corresponds to 112 rpm for both the impellers and a value of 30/s corresponds to 17 and 20 rpm for 3x3 and 1x1 mesh impellers respectively. Numbers in parenthesis represent the homogenized turbidity and 10, 20, and 30 minute settled turbidity respectively following flocculation

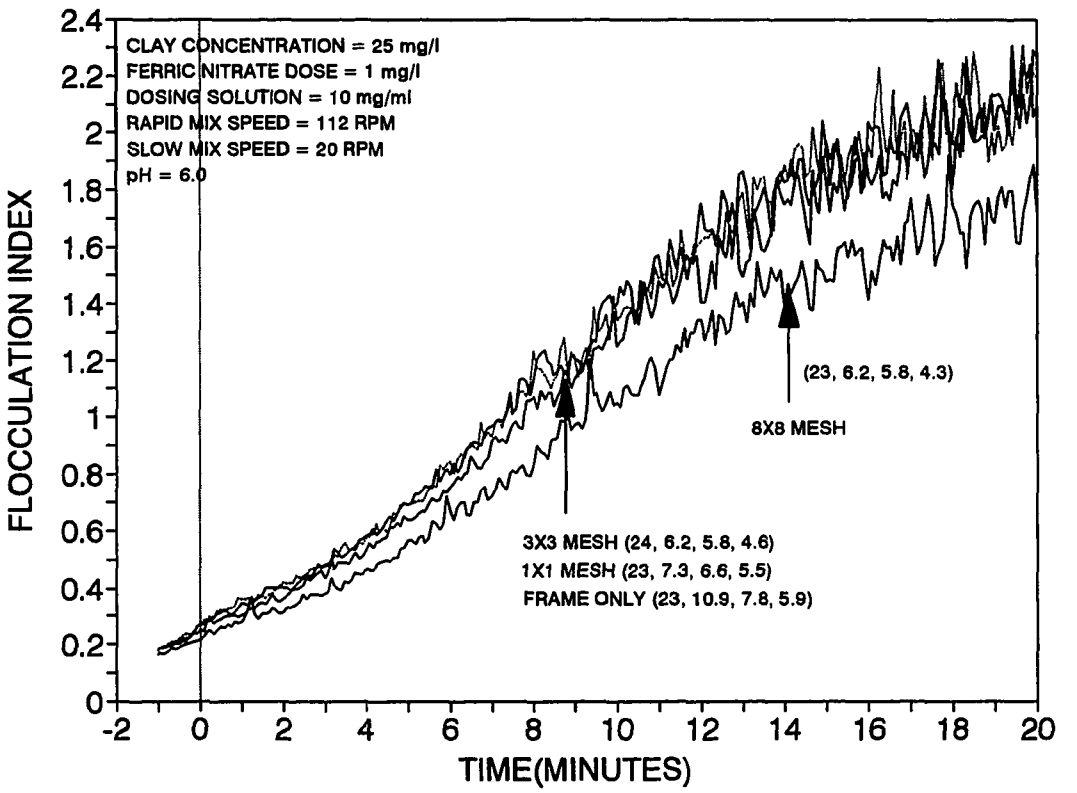

Figure 6.39. Effect of opening size of the mesh impeller on flocculation kinetics at pH = 6.0 and temperature = 23° C at constant speed with ferric nitrate as the coagulant. No G versus rpm curve was developed for the frame only impeller.The 112 rpm speed corresponds to G value of 450/s for three opening size mesh impellers. The 20 rpm speed corresponds to G values of 30/s, 40/s, and 49/s for 1x1, 3x3, and 8x8 mesh impellers. Numbers in parenthesis represent the homogenized turbidity and 10, 20, and 30 minute settled turbidity respectively following flocculation

(distance to the outer edge of the stirrer from the axis of its shaft) of the impeller or the tip speed, but also by the small scale motions generated by local velocity (proportional to impeller rotational speed and the distance of wire from the center of impeller shaft) and velocity fluctuations (created by wire mesh). The capture of primary particles as evidenced by the turbidity removal was improved by the wire mesh. More energy was required for the impellers with smaller mesh openings due to more drag between the larger number of wires and the fluid. Thus at constant speed, energy input increases as mesh size decreases which should benefit flocculation kinetics. However, no improvement of turbidity readings was observed when the number of mesh was increased from nine (3x3 mesh) to sixty four (8x8 mesh) per square inch. It is possible that the smallest opening wire mesh did not assist that much in particle growth. Rather, it restricted the growth of flocs after some time of flocculation by constricting their passage through the opening, or as the flocs grew rapidly, they also broke up more due to higher energy input and/or due to more frequent collisions with the larger number of wires present per unit flow area. As a result, the smallest mesh opening produced more uniform sized particles but fewer big floc particles (which was visually observed) resulting in lower flocculation index readings.

6.1.11. Effect of combination of impellers

These experiments were conducted to observe the contribution of two different impellers during two mixing stages of the coagulation-flocculation process. **Figure 6.40** contains the results of these experiments. Curves 1 and 4 correspond to the experiments

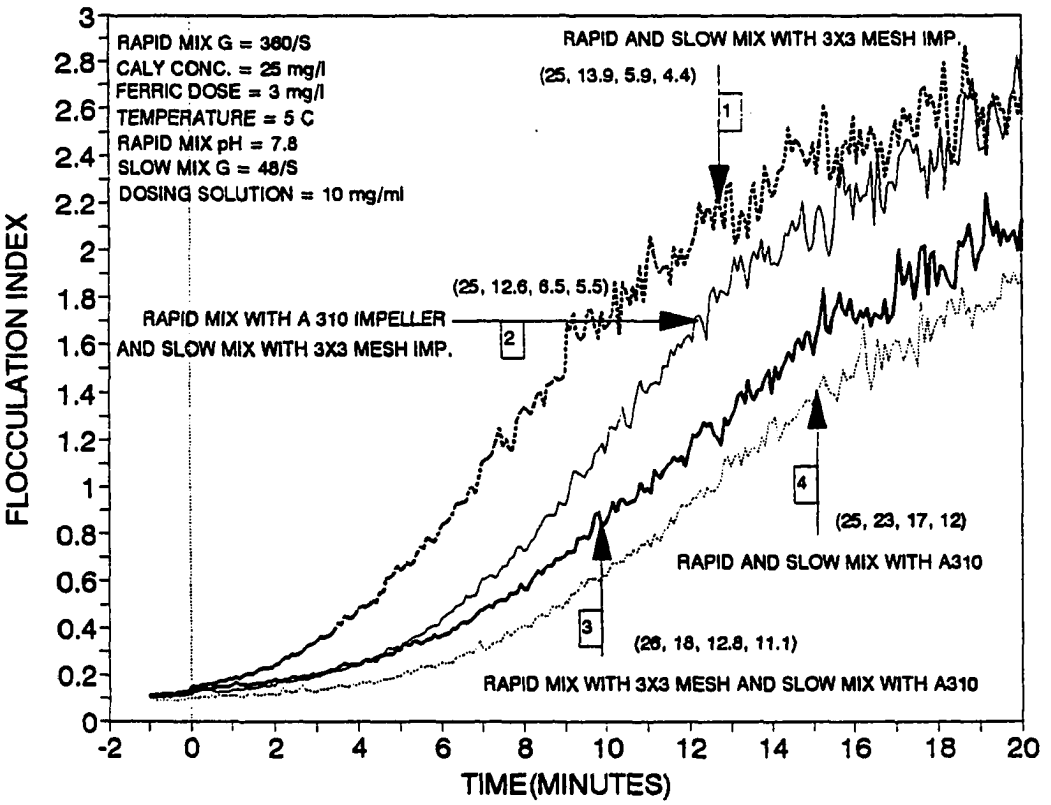

Figure 6.40. Effect of impeller type and mixing pattern on flocculation kinetics at pH = 7.8 and temperature = 5° C with ferric nitrate as the coagulant. The G value of 360/s corresponds to 493 and 112 rpm for A 310 and 3x3 mesh impellers respectively and the G value of 48/s corresponds to 93 and 27 rpm for A 310 and 3x3 mesh impellers respectively. Numbers in parenthesis represent the homogenized turbidity and 10, 20, and 30 minute settled turbidity respectively following flocculation

performed with the 3x3 mesh and the A 310 impellers respectively. A single impeller was used for both rapid and slow mixing stages as was done in all the other previous cases. Curve 2 corresponds to the experiment where the rapid mix was done with the A 310 impeller and the slow mix was done with the 3x3 mesh impeller. The sequence was reversed in the experiment corresponding to curve 3.

The worst result was obtained when both rapid and slow mixing operations were performed with the A 310 impeller (curve 4). Performance was slightly improved when the 3x3 mesh was used for rapid mixing only (curve 3). The performance was even more dramatic when the 3x3 mesh impeller was used for slow mixing only (curve 2). The best performance was obtained when both the mixing operations (rapid and slow) were performed with the 3x3 mesh impeller (curve 1). From these results it is clear that the better impeller (3x3 mesh) performs better in both the mixing stages, and that this impeller contributes more during slow mixing stage than during rapid mixing stage.

6.2. Discussion of Results

Figures 6.1 through 6.19 presented the comparisons among different impeller geometries studied during this research. The fundamental question of interest in these experiments deals with the homogeneity of turbulent flow field in a batch reactor. How important is it to introduce the energy over 90% of the suspension volume inside the reactor as opposed to only 5% of the suspension volume? All the turbulent flow field parameters commonly used in coagulation-flocculation process, such as, G, η_k, and ε,

assume a volume averaged ε. This assumption implies that the energy put into the suspension is evenly distributed over 100% of the suspension volume contained in the reactor. **Figures 4.11.and 4.12** give an indirect indication of the non-homogeneity of ε in the reactor flow field. These two figures show that the turbine impellers must turn quite rapidly to put the same energy into the suspension as the paddle impellers. So it follows that the energy dissipation near the blade of these impellers must be high.

Many research works (Cutter, 1966; Okamoto et al., 1981; and Placek et al., 1986) have shown that the local energy dissipation rate is highly position dependent, and an order of magnitude of available energy variation can be seen between the impeller region and the bulk of the tank inside a batch reactor equipped with Rushton turbine impeller. Several research works, (Clark, 1994; McConachie, 1991; Hanson and Cleasby, 1990; Ives, 1984; Bhole and Limaye, 1977; Patwardham and Mirajgaonkar, 1970; Argaman and Kaufman; 1970) observed an impact of impeller geometry on the coagulation-flocculation process. All of those studies indicated a measurable effect of geometry on flocculation kinetics.

From this study also, a significant effect of geometry has been observed on flocculation kinetics. Three impeller geometries (A310, 2-blade, and 3x3 mesh) were employed in most of the flocculation experiments with ferric nitrate coagulant under varying physico-chemical conditions. Four impeller geometries (2-blade, 1x1 mesh, modified stake, and 2-blade stack) were compared to observe the geometry effect under two sets of physico-chemical conditions. The performance difference between two paddle type impellers (1x1 mesh and 2-blade stack) was tested in another set of

conditions. All the alum flocculation experiments were performed with 2-blade and 3x3 mesh impellers under a variety of conditions.

Among the three impellers (A310, 2-blade, and 3x3 mesh) used in most of the treatment sets, the 3x3 mesh performed best and the A310 impeller performed worst under all physico-chemical conditions. From **Figure 6.40** it can be seen that the 3x3 mesh impeller performs better than the A310 impeller in both the rapid and slow mixing stages. This means that the better impeller will give better efficiency in both stages of the coagulation-flocculation process. The better geometry is the one which distributes energy inside the reactor in a more decentralized fashion. If the flow patterns generated by the two turbine impellers (A310 and 2-blade) are considered (**Figure 4.13**), then it is seen that the 2-blade impeller distributes energy through two circulating loops and this distribution of energy is more decentralized than that by the A310 impeller through a single circulating loop.

The mesh impeller generates more homogeneous turbulence than the turbine impellers and reduces the characteristic mixing time through direct contact with the maximum possible fluid volume. This direct contact of the mixing equipment with almost the entire volume of fluid reduces the necessity of bulk flow and increases velocity fluctuation of fluid particles with respect to time and space for a given energy input, and thereby increases the number of collisions among suspended particles per unit time per unit volume of suspension. Therefore, this impeller will perform better in all types of physico-chemical conditions as shown in **Figures 6.1 through 6.19** than the other two impellers (turbine type). Hanson and Cleasby (1990) and Argaman and

Kaufman (1970) found that the Stake and Stator impeller which distributes power throughout the tank was superior to the 2-blade turbine impeller. From the results of experiments by Ives (1984), it was seen that the mesh impeller performed best or near best among nine different impellers in terms of both turbidity removal and filtration number.

Patwardham and Mirajgaonkar (1970) concluded that the impeller that displaced the water most performed best in flocculation experiments. From their flocculation results shown in **Figure 3.52** it appears that impeller 5 with the largest paddle edge length (proportional to water displacement) achieved the highest percentage of turbidity removal. Clark et al. (1994) studied four impeller types in flocculation. Their results were not conclusive, but "there was some tendency toward a mild degradation in performance moving from the rake to the foil to the pitched blade to the Rushton impeller" (p. 125).

From **Figures 6.9 and 6.10** it appears that three impellers, 1x1 mesh, modified stake and 2-blade stack, performed almost identically and the 2-blade impeller performed much worse than the other three. The 1x1 mesh and the modified stake impellers put energy into the reactor in the most decentralized or distributive fashion (over 90% of the reactor volume). The 2-blade impellers delivers energy into the reactor in the most centralized fashion (within 5% of the reactor volume). The 2-blade stack impeller puts energy into the reactor in a fashion in between these two extremes. When the geometry was changed from 2-blade to 2-blade stack, a significant improvement in flocculation kinetics was observed with the same energy input. This is due to a three

fold upgrade towards the distributive energy input in the reactor. Six circulating loops generated by the 2-blade stack impeller as shown in **Figure 4.14**, circulates energy in a way to generate much more homogeneous turbulence flow field inside the reactor than that present with only two circulating loops generated by the 2-blade impeller.

When the 2-blade stack impeller was compared with two paddle impellers (1x1 mesh and modified stake) in terms of flocculation efficiency, it performed as good as those two impellers under the two sets of physico-chemical conditions used here. This indicates that the extent of homogeneity of turbulence produced by these three impellers inside the reactor under these conditions is comparable and/or not sufficiently different to cause any change in flocculation efficiency.

The following concepts are important, in order to have a better understanding of the difference in performance between the turbine and mesh impellers.

1. As mentioned previously in Chapter 3, the largest (i.e., the initial) eddy size is always associated with the impeller geometry (i.e. for 2-blade impeller the diameter of the initial vortex can be considered to be roughly the same size as the impeller blade width). This vortex is then stretched by interacting with other vortices around it by a mechanism called vortex stretching. The smallest diameter this vortex stretches to (through gradual energy cascade and size reduction) is approximately the size of the Kolmogorov microscale, where the energy is dissipated by viscosity. Below this microscale, flocculation is the result of localized shear fields induced by the vortex stretching process as shown in **Figure 3.39**. The smaller the microscale of turbulence,

the more intense the localized velocity gradients (or localized shear fields).

2. With the turbine impellers, energy is put into a central location with the largest eddies and then energy is transferred through vortex stretching to other eddies of different size in remote locations through a space filling process like heat or mass diffusion to achieve global mixing. This process of energy transfer or eddy cascade can be expedited only by increasing the energy input (the product of power input and mixing time) which accomplishes the mixing. However there is no one-to-one correspondence between power input and mixing time, since power input may go on to mix material that has already been mixed. From **Figures 3.48 and 3.49** it is clear that more energy is dissipated in the more energetic region. So it is quite possible that a significant energy could be lost near the impeller before it reaches the other locations of the tank causing poor global mixing.

3. **Figure 3.31** illustrates that with every step of energy cascade some energy is directly lost to the internal energy of the fluid. So the more the steps in the cascade the greater the amount of energy that will be lost to internal energy of the fluid, reducing the available kinetic energy for particle transport. Casson and Lawler (1990) illustrated that the wire mesh grid impeller produced small scale eddies directly inside the reactor. The wire mesh impellers used here produced similar production scale eddies throughout the reactor, which are supposed to be much smaller than the production scale eddies generated by the turbine impellers. It is possible that these production scale eddies

generated by the mesh impeller, require fewer number of steps in the cascade and thereby much shorter time to be stretched to an effective size for flocculation.

4. From the above discussion it is now clear that the mesh impeller produces much smaller initial eddies distributed all over the tank by significantly reducing the time of the vortex space filling process and the energy transfer process from largest eddies to smallest eddies, than the turbine impellers. Probably, if not definitely, it takes only one to two generations of eddies for the 3x3 mesh impeller to achieve a homogenous isotropic turbulent flow field as opposed to many generations of eddies required for the turbine impellers. Hanson (1989) stated, "If the flocs in the reactor are much smaller than the production scale eddies, then any variability introduced by geometry change is due to the non-homogeneous, anisotropic nature of the flow field. If the flocs are similar in size to the production scale eddies, the variability may be due to either the change in the eddy distribution at the production scale, or it may be due to non-homogeneous, anisotropic nature of the flow field" (p. 309).

Figures 6.20 through 6.23 illustrated the effect of rapid mixing intensity on flocculation kinetics under four different physico-chemical conditions. From the figures it was seen that there is an optimum rapid mixing intensity for each set of conditions. Beyond that optimum intensity, the kinetics become worse. This can be explained in a fashion similar to Gregory's (1989) "electrostatic patch" theory of polymeric flocculation which states, "*polyelectrolyte adsorbs on an oppositely charged particle in such a way that there are "patches" of excess charge because of local charge reversal and areas of*

unoccupied surface still bearing the original particle charge. Particle with polymer adsorbed in this "patchwise" manner can interact in such a way that positive and negative areas of different particles are adjacent, giving strong electrical attraction" (p. 203).

For optimum coagulation, a certain percentage of particle surface area must be covered with polyelectrolytes. Gregory further stated that the patch type adsorption occurs when the charge density of the polyelectrolyte is much greater than that of the particle surface. So it is possible that for each set of physico-chemical conditions, there has to be a certain rapid mixing intensity that will produce the required coverage ratio with particular types of polymeric species for optimum coagulation.

Another point of importance to be noted, is the role of rapid mixing. The duration of rapid mixing employed in this study was 60 seconds. Usual practice is to use 30 to 60 seconds. This duration of rapid mixing not only disperses the coagulant throughout the reactor before any significant chemical change has occurred, but also brings about the initial stages of particle collisions and subsequent aggregation. These aggregates act as the nuclei for further growth. This was evidenced by a gradual change of flocculation index during rapid mix. When the mixing intensity is beyond the optimum value, this aggregation or the growth of the particles is somewhat prevented due to excessive shear, slowing down the overall kinetics of flocculation. It should be kept in mind that various rapid mixing intensities did not produce any noticeable difference in zeta potential readings of samples taken immediately after rapid mix.

Srivastava (1988) also proved by particle counting technique that flocculation was occurring during the period of rapid mixing with either alum or cationic polymer. He found a significant reduction in the number of primary particles at the end of the rapid mixing period.

Figures 6.24 through 6.27 also indicate that particle aggregation occurs during rapid mix. These figures demonstrate that low energy mixing for longer duration is better than high energy mixing for short duration in most cases. It was observed that the zeta potential readings produced by the two rapid mixing intensities were comparable, but a larger increase of the flocculation index was observed at the end of rapid mixing for the low intensity-longer duration pattern, than for the high intensity-short duration pattern. This indicated that the hydrolysis products of metal coagulants produced during the two rapid mixing patterns were not much different. Any deficiency in the formation of optimum species with lower intensity was surpassed by the formation of more nuclei during the additional 1 minute of rapid mixing.

The occurrence of particle aggregation during rapid mix can be further confirmed from **Figure 6.40**. The zeta potentials after rapid mix were near -10 mv in all the four experiments. But if curves 3 and 4 are compared, it appears that the kinetics are better for rapid mixing with the 3x3 mesh impeller. The 3x3 mesh impeller produced a larger number of nuclei during rapid mix, that accelerated the aggregation process during slow mixing stage. Slow mixing was done with the A 310 impellers in both cases.

From **Figures 6.28 through 6.30** it appears that the concentration of dosing solution has some effect on flocculation kinetics. Diluting the dosing solution gives the

opportunity to add more volume of coagulant in the reactor for the same coagulant dose, thereby reducing the volume ratio of the coagulant stream and the clay suspension. Baldyga and Bourne (1984c) and Bourne et al. (1981a) have demonstrated that the product distribution parameter, X_s was lower and the mixing efficiency was higher when the volumetric ratio of two reacting streams was lowered during a series parallel reaction. It should be remembered that the X_s is an indirect measure of mixing efficiency, the value of which decreases with higher efficiency of mixing. During the rapid mixing stage in the coagulation-flocculation process, the provision of a lower volume ratio between two reacting streams improves mixing by increasing the relative interfacial surface area between two reacting streams. More and more clay primary particles come in contact with the larger initial volume of coagulant, and later with a larger number of coagulant clumps after it has been broken down by the shear fields. That is why some improvement was seen when the coagulant dosing solution was diluted. But there should be a limit to the extent of dilution, in order to avoid any chemical change of the coagulant, such as the onset of precipitation of metal hydroxides, before the diluted solution is used.

The 2-point injection performed slightly better than 1-point injection in turbidity removal, as shown in **Figure 6.31**. When a small liquid stream is added to a larger volume of liquid, the simplistic model shows that the small stream will be broken down into smaller clumps due to shear produced in the turbulent field, before the concentration gradients of the two liquids are eliminated by the diffusion process. One stream is broken down to two or more clumps and then into many smaller clumps.

When the same volume of coagulant is divided into two injection portions and injected through two ports of the reactor into the clay suspension, the dispersion process of the coagulant stream (inside the reactor) is somewhat accelerated, providing the opportunity for more primary particles to come in contact with the coagulant in a certain time period. As a result, the flocculation kinetics are accelerated. The 2-point injection also reduces the localized overdose and distributes the coagulant in a more uniform manner than the 1-point injection.

Slow injection of coagulant also improves the kinetics (shown in **Figures 6.21 and 6.28**) by bringing the fresh clay suspension in contact with each additional drop of coagulant solution, thereby distributing the coagulant more uniformly throughout the reactor content without any localized overdose. Slow injection accelerates the initial size reduction process of the coagulant stream through dispersion, creating much larger interfacial area between the coagulant and the clay suspension for increased mass transport. David and Clark (1991) indicated that the product distribution parameter X_s varies inversely with the square root of the power input per unit mass in case of drop wise addition (slow injection of coagulant in the current study) and that X_s varies inversely with the one third power of the power input per unit mass for pulse addition. That means, for a constant power input the X_s is lower and mixing efficiency is higher with dropwise addition (or slow injection of coagulant).

Slow mixing intensity and pattern are the two most important mixing variables, after impeller geometry. Desired flocculation results can not be obtained if the proper slow mixing intensity and pattern are not chosen. Even after destabilization to a

comparable zeta potential and the same slow mix energy input (energy corresponding to G = 30/s at 23° C and to G = 24 at 5° C) the flocculation kinetics were much worse at 5° C than at 23° C (**Figure 6.41**). The reason was that energy input at 5° C was not enough to generate the required number of particle contacts to produce kinetics similar to those observed at 23° C. At 5° C, fluid viscosity is significantly higher (almost 50%) than the viscosity at 23° C. The Kolmogorov length scale is also larger and more energy is lost through viscous dissipation to the internal energy of the fluid in every step of cascade, providing less energy available for particle transport.

Kinetics were significantly better when the energy input was increased from a G value of 24/s to 48/s at 5° C. But flocculation became worse when the G value was increased from 48/s to 72/s at 5° C due to increased floc breakup by viscous shear. The initial kinetics were better with G = 72/s at 5° C, but at the end, the resulting flocculation was worse due to breakage of flocs. This was observed with all the three impellers, as shown in **Figures 6.32 through 6.34**. This phenomenon of floc breakup was noticed by several other researchers (Camp, 1955; Argaman and Kaufman, 1970; Tambo and Hozumi, 1979; and Michaels and Bolger, 1962a and b). Tambo and Hozumi (1979) and Argaman and Kaufman obtained an inverse relationship between maximum floc diameter and G. Tapered flocculation is a wise choice for minimizing the problem of floc breakup. From **Figure 6.34** it is clear that better overall flocculation can be obtained even with smaller energy input, by varying the slow mixing intensity at different stages of flocculation. This is called tapered flocculation. At 23° C the flocculation was improved with the increase of intensity from 30/s to 60/s (**Figures 6.35**

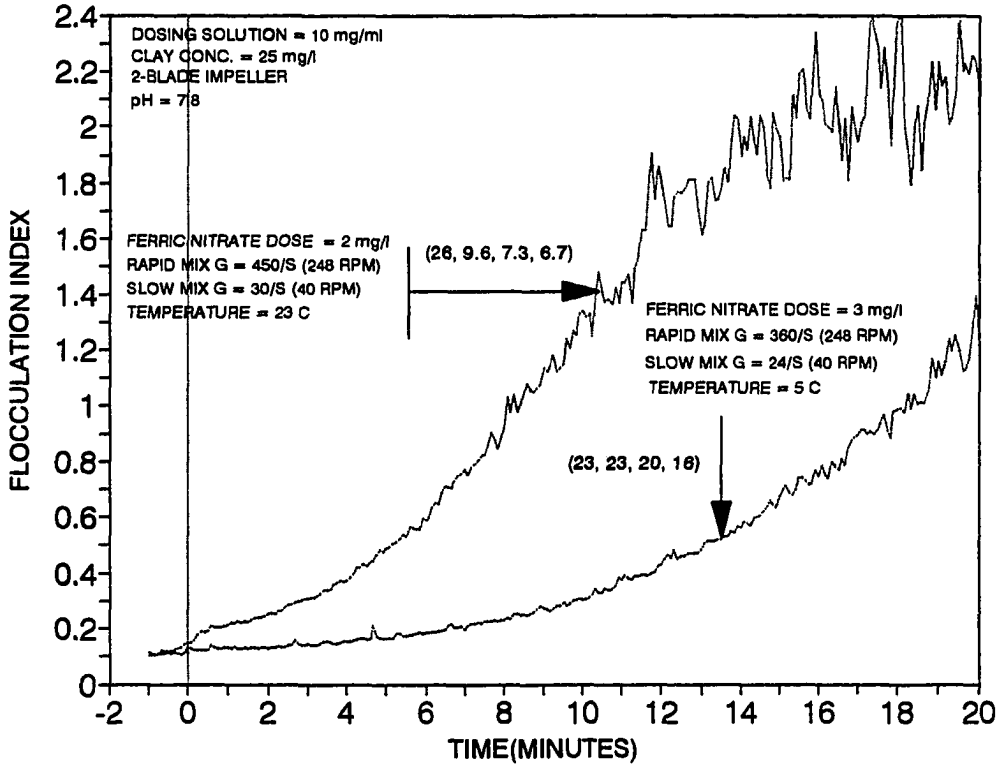

Figure 6.41. Effect of temperature on flocculation kinetics of kaolinite clay with ferric nitrate as the coagulant at pH = 7.8. Numbers in parenthesis represent the homogenized turbidity and 10, 20, and 30 minute settled turbidity respectively following flocculation

and 6.36), but the improvement was not as great as that seen at 5° C. Tapered intensity from 60/s to 30/s at the later stage of flocculation gave almost comparable but slightly worse results in 30 minute turbidity reading (**Figures 6.35 and 6.36**), than the constant G of 60/s indicating a net positive particle growth with G = 60/s. This means that the flocs grown with ferric nitrate coagulant at pH = 6.0 and temperature = 23° C with zeta potential around -10 mv are capable of withstanding a slow mixing intensity of G≈ 60/s.

From **Figure 6.15** it is clear that alum flocs are much weaker than the flocs produced by ferric nitrate (**Figures 6.35 and 6.36**). Under similar physico-chemical conditions, floc breakage was taking place at the later stage of alum flocculation even with slow mix G of 30/s. Tapering the slow mixing intensity from G = 30/s to 20/s improved the end results to a significant degree. This same phenomenon was observed in **Figure 6.13** at pH = 7.8 and 23° C during alum flocculation with two different impellers.

Even at cold temperature (5° C), the flocs produced with ferric nitrate were strong enough to withstand a slow mixing intensity of G ≈ 48/s (corresponding to G = 60/s at 23° C) at pH = 7.8 with zeta potential near -10 mv (**Figures 6.32 through 6.34**). But Hanson (1989) reported that the alum flocs are much weaker at cold temperature. From current study it was observed that the breakage of alum flocs took place during the later stage of flocculation with a G value of 30/s at 23° C (**Figure 6.15**). If the flocs are weaker at 5° C, then the alum flocs probably would break with a slow mixing G of 30/s or less at 5° C at the later stage of flocculation (no experiments were conducted with alum at 5° C). So an optimum combination of slow mixing intensity and

pattern should be chosen with several trial experiments for a particular set of experimental conditions depending on coagulant type, temperature, pH, mode of coagulation (A/D or sweep floc) and impeller type. **Figure 6.42** demonstrates that the flocculation kinetics of kaolin clay using alum are substantially worse than the kinetics using ferric nitrate as the coagulant. The poorer performance by alum is confirmed by both flocculation index and turbidity readings.

Figures 6.37 and 6.38 illustrate the effect of the opening size of the wire mesh impeller. It was hypothesized that the wire mesh impeller would produce small scale motions similar to grid generated motions used by Casson and Lawler (1990). These small scale motions generate a more homogenous turbulent flow field than the other impellers used in this study. It was expected that the smaller mesh size would produce the best flocculation kinetic results. However, the larger mesh sizes performed better at constant power input. This generated the concern that the contribution of the tip speed and large scale motions might dominate the flocculation performance. However, when the impellers with different size of opening were rotated at the same speed, turbidity removal improved moving from no mesh (frame only) to the 1x1 mesh to the 3x3 mesh to the 8x8 mesh impeller (**Figure 6.39**). This indicates that the wire mesh is playing a role in improving the removal of the primary particles. At the same speed, the wires located at a particular distance from the center of impeller shaft for all the impellers are producing same velocity (proportional to angular velocity of the impeller and the distance of the wire from the center of the shaft) and velocity fluctuations at that particular location. The impellers with smaller openings are generating more such

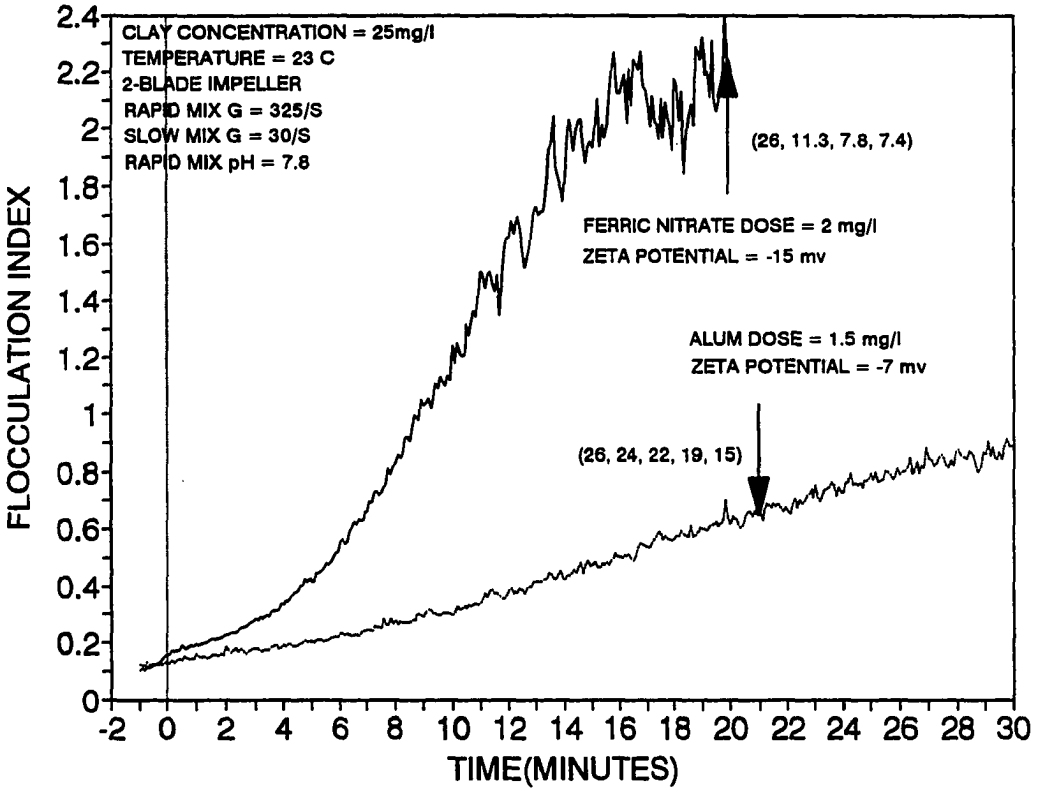

Figure 6.42. Effect of coagulant type on flocculation kinetics of kaolinite clay at temperature = 23° C and pH = 7.8. Slow mixing durations were 20 and 30 minutes for ferric nitrate and alum respectively. G values of 325/s and 30/s correspond to 200 rpm and 40 rpm respectively. Numbers in parenthesis represent the homogrnized and 10, 20, 30, and 40 minute settled turbidity. Forty minute settled turbidity was not measured for flocculation experiment with ferric nitrate

velocity and velocity fluctuations between two locations (both in vertical and radial directions) than an impeller with larger openings. As a result, the probability of particle collisions increases. These local velocity and velocity fluctuations are effective for initiating contact during rapid mix and at the early stage of flocculation when primary particles are forming doublets, triplets, quadrupulates, and so on. In contrast, when operated at constant power input to the system, the impellers with smaller opening sizes had to be rotated at lower speed, which reduced the velocity and velocity fluctuations at those locations resulting in lower probability of particle contact and worse flocculation kinetics. When the floc particles grow to a much larger size, then the large scale motions bring those large particles in contact with other particles of similar or different size. These larger floc particles contribute most to increasing flocculation index readings. A smaller number of very large particles may produce relatively better flocculation index readings than very large number of intermediate sized particles even though the overall flocculation performance (less number of primary particles present) is better for the second case. This point is evident from **Figure 6.39**. The 8x8 mesh impeller with lower flocculation index readings achieved better turbidity removal than 1x1 mesh and no mesh (frame only) impellers. Although the steeper rising limb of the flocculation index versus time curve indicated better flocculation results most of the time, it might not always reflect the actual flocculation efficiency evidenced by the turbidity removal. The overall flocculation efficiency is usually expressed as the total number of primary particles removed or turbidity removed rather than by the formation of a few number of very big particles.

The turbidity readings produced by the 3x3 mesh and the 8x8 mesh impellers were almost identical at constant speed (**Figure 6.39**). It is possible that the reduction of opening size beyond a certain size did not assist that much in flocculation performance. Rather, it restricted the growth of flocs after some time of flocculation by constricting their passage through the smaller openings, or that more breakup of flocs occurred due to higher energy input and/or due to more frequent collisions with the larger number of wires present per unit flow area. From all the phenomena described above, it appears that the large scale motions arising from bulk flow (pseudo-turbulence) and generated by tip speed or effective radius are generating contacts between large particles when they have grown to a certain size, on the other hand, the small scale motions generated by local velocity and velocity fluctuations (true turbulence) are effective for contacts among primary particles. Wire mesh impellers achieve both of these; and the choice of particular opening size of wire mesh impeller and its operation pattern for optimum flocculation should be determined by experiment.

6.3. What is Next?

Flocculation research has taken a ride on a slow boat during the past several years. Prior to that, a significant number of research works were conducted, unraveling the mystery of the chemical aspects of the coagulation-flocculation process. Very few researchers have conducted research for understanding the hydrodynamic aspects associated with the coagulation-flocculation process. Thanks to Argaman and Kaufman

(1968, 1970) who opened the door of this new area of research, followed by Hanson and Cleasby (1990) and Casson and Lawler (1990) who tried to describe the characteristics and limitations of the turbulent flow field usually found in the flocculation reactor.

This research was designed and conducted to advance further into this arena. From extensive literature review it was realized that a homogenous and isotropic turbulent flow field inside a reactor brings forth uniform particle destabilization and subsequent flocculation, and the degree of homogeneity and isotropicity depends on the intensity and/or uniformity of mixing. It was also found from literature and experimental observations that several mixing variables (rapid and slow mixing variables mentioned and discussed earlier) have a remarkable impact on flocculation kinetics. These mixing variables with several other physico-chemical variables lead to a large number of experiments that have to be performed in order to observe the impact of each mixing variable under each set of conditions, which is not possible within the scope of a dissertation. But this study opened the scope for a much broader field of flocculation research. Some of the areas that can be pursued are as follows:

1. All the experiments performed here involved metal coagulants and most of the mixing variables were tested with ferric nitrate coagulant only. Study with polymeric coagulant will be a promising area of research to observe the impact of various mixing variables. Usually the polymers are high molecular weight compounds and they are used in small dosages. Variables like impeller geometry, rapid mixing intensity, pattern,

coagulant injection pattern, concentration of dosing solution etc. should influence the destabilization mechanism of particles (A/D or interparticle bridging), especially at cold temperature. Srivastava (1988) demonstrated that rapid mixing intensity and pattern had a dramatic impact on polymeric flocculation at both warm and cold temperatures.

2. The effects of impeller geometry and other mixing variables have been tested only in one reactor size. It will be a promising area of research to observe and determine whether the scale has anything to do with the effect of various mixing variables on flocculation kinetics. Are the effects and their extent similar in all scales? If not, what will be the scale-up rules for various impeller geometries and other mixing variables? It will be helpful for the design engineers to design a flocculation unit based on batch reactor results, if these information are available. Clark et al. (1994) investigated the effect of scale on flocculation efficiency and found that flocculation efficiency tended to decrease as the reactor increases in size with constant power input and constant D/T ratio. But their research is not conclusive, so more research needs to performed in this area of scale effect.

3. Only two sets of experiments have been performed to observe the effect of various paddle type impellers (mesh, modified stake and 2-blade stack). From these results, no performance difference was observed among these three impellers. It would be interesting to investigate their performance in other physico-chemical conditions, especially at cold temperature with polymeric coagulant. Similar research can be done

with different mesh sizes. Among the three sizes tested in three physico-chemical conditions, the largest mesh size (1x1 mesh) performed best in two cases at constant power input and performed worst at constant speed. More research needs to be done to determine the optimum opening size and its optimum operation pattern (rapid and slow mixing intensity and pattern) under various physico-chemical conditions. It is quite possible that a particular mesh opening size would perform best in a particular set of rapid and slow mixing intensity and pattern. It will be also be a worthwhile research area to measure the turbulence intensity produced by mesh impellers with various opening size with different speeds and energy inputs.

4. An entire area of research can be opened with grid generated turbulence in baffled flocculation. A number of wire meshes with various opening sizes can be placed at different locations of a baffled flocculator to observe the effect of grid generated turbulence on baffled flocculation. This can be observed under various physico-chemical conditions.

5. Another area, probably the most promising area of research, can be opened with the title "Effect of various mixing variables on continuous flow flocculation" to determine the effect of the mixing variables tested in this study on continuous flow flocculation.

6.4. Conclusions

The following conclusions can be drawn from this research:

1. Different flocculation impellers deliver energy differently into the reactor. Paddle impellers such as the mesh and the modified stake impeller deliver energy into the reactor in a decentralized fashion (throughout the volume of the reactor), whereas the turbine impellers deliver power into the reactor in a centralized location. That is why the paddle type impellers consume more power at the same rpm than the turbine impellers (A 310 and 2-blade). The 2-blade stack impeller delivers power in a fashion somewhere in between these two extremes.

2. The PDA instrument gave flocculation kinetics measurements that were consistent with the settled water turbidity readings in most cases. In those cases, a steeper slope of the flocculation index curve generated by the PDA instrument corresponded to better settled water turbidity readings at all settling times after flocculation. But, because there were some exceptions to this general pattern, the flocculation performance should not be judged only from flocculation index readings. The flocculation index results should always be verified either by residual settled water turbidity readings or by evaluation of the number of primary particles at different time intervals during flocculation.

3. Impeller geometry was the most important mixing variable from an engineering

viewpoint. From this study it was observed that the paddle type mesh impeller performed far better than the turbine type impellers (A 310 and 2-blade) under all conditions tested. The mesh, the modified stake, and the 2-blade stack impellers performed almost identically under the conditions tested here. It was also observed at cold temperature that the turbine type impellers (2-blade and A 310) could not produce as good results (both turbidity and flocculation index) with higher G as the 3x3 mesh impeller with lower G.

4. When the 3x3 mesh and the A 310 impellers were compared, it was observed that the 3x3 mesh impeller performed better than the A 310 impeller in both stages of mixing (rapid and slow). But the performance difference was more pronounced during slow mixing stage. From this observation it can be concluded that the better impeller (3x3 mesh) performs better in both stages of mixing in a coagulation-flocculation process. This better performance by the mesh impeller is attributed to both better large scale motions (pseudo-turbulence) generated by larger effective radius and more intense, small scale, turbulence generated by the wires. The two smaller mesh openings studied gave better turbidity removal than the larger mesh, or frame only impellers.

5. Both rapid mixing intensity and pattern had a remarkable impact on flocculation kinetics. An optimum value of rapid mix G was obtained for each set of conditions. This optimum value was different under different conditions tested in this study. With a constant dimensionless Gt value, a low intensity, extended duration, rapid mix pattern

proved to be more beneficial than the high intensity, short duration, rapid mix pattern in almost all the conditions studied.

6. Other rapid mixing variables, such as coagulant injection pattern, concentration of dosing solution, number of ports of coagulant injection also showed some noticeable influence on flocculation kinetics. Slow injection, dilute dosing solution and multi port injection proved more beneficial than the pulse injection, concentrated dosing solution, and the single port injection respectively.

7. Slow mixing intensity and patterns also affected flocculation kinetics. There should be an optimum slow mix G for each set of experimental conditions when constant G-slow mixing is adopted. Reducing the slow mix G as flocculation progressed (i.e., tapered flocculation) resulted in higher flocculation index as flocculation progressed and better settled water turbidity due to less danger of floc breakup.

8. All the mixing variables tested in this study demonstrated a more pronounced effect on flocculation kinetics at cold temperature than at high temperature. Overall, cold temperature kinetics were much slower than the warm temperature kinetics. Ferric nitrate was more efficient in turbidity removal than alum under similar experimental conditions and the flocs produced during flocculation with ferric nitrate were stronger than the flocs produced during alum flocculation under comparable conditions (same temperature and similar zeta potential values)

BIBLIOGRAPHY

Adamson, A. W. 1979. A Text Book of Physical Chemistry. Second Edition. Academic Press, New York, N.Y.

Amirtharajah, A. 1987. Rapid Mixing and Coagulation Processes. In AWWA Seminar Proceedings: Influence of Coagulation on the Selection, Operation, and Performance of Water Treatment Facilities. AWWA, Denver, CO.

Amirtharajah, A., and K. M. Mills. 1982. Rapid Mix Design for Mechanisms of Alum Coagulation. Jour. AWWA, 74, 4, 210-216.

Amirtharajah, A. and C. R. O'Melia. 1990. Chapter 6: Coagulation Process: Destabilization, Mixing, and Flocculation. Water Quality and Treatment, 4th Edition, McGraw-Hill, New York, N.Y.

Amirtharajah, A., and N. Tambo. 1991. Chapter 1: Mixing in Water Treatment. In A. Amirtharajah, M. M. Clark, and R. R. Trussell Ed. Mixing in Coagulation and Flocculation. AWWA Research Foundation, Denver, CO.

Arboleda-Valencia. 1991. High Rate Flocculation. Progress Report. Personal Communication to Professor John L. Cleasby of Iowa State University.

Argaman, Y. and W. J. Kaufman. 1968. Turbulence in Orthokinetic Flocculation. SERL Report No. 68-5. Sanitary Engineering Research Laboratory, University of California, Berkeley, California.

Argaman, Y. and W. J. Kaufman. 1970. Turbulence and Flocculation. Jour. San. Eng. Div., ASCE, 96, SA2, 223-241.

Ayesa, E., M. T. Margeli, J. Florez, and J. L. Garcia-Heras. 1991. Estimation of Breakup and Aggregation Coefficients in Flocculation by a New Adjustment Algorithm. Chemical Eng. Sci., 46, 1, 39-48.

AWWA Coagulation Committee. 1989. Committee Report: Coagulation as an Intregated Water Treatment Process. Jour. AWWA, 81, 10, 72-78.

Batchelor, G. K. 1960. The Theory of Homogenous Turbulence. Cambridge University Press, Cambridge, England.

Baes, C. F. and R. E. Mesmer. 1976. The Hydrolysis of Cations. John Wiley and Sons, New York, N.Y.

Baldyga, J. and J. R. Bourne. 1984a. A Fluid Mechanical Approach to Turbulent Mixing and Chemical Reaction. Part I - Inadequacies of Available Methods. Chem. Engr. Commun., 28, 231-241.

Baldyga, J. and J. R. Bourne. 1984b. A Fluid Mechanical Approach to Turbulent Mixing and Chemical Reaction. Part II - Micromixing in the Light of Turbulence Theory. Chem. Engr. Commun., 28, 243-258.

Baldyga, J. and J. R. Bourne. 1984c. A Fluid Mechanical Approach to Turbulent Mixing and Chemical Reaction. Part III - Computational and Experimental Results for the New Micromixing Model. Chem. Engr. Commun., 28, 259-281.

Beek, J. J. and R. S. Miller. 1959. Mixing. Chem. Engr. Prog. Sym. Ser., 55, 25, 23.

Belevi, H., J. R. Bourne, and P. Rys. 1981. Mixing and Fast Chemical Reaction - II. Diffusion-Reaction Model for CSTR. Chem. Engr. Sci., 36, 10, 1649-1654.

Benefield, L. D., J. F. Judkins and B. L. Weand. 1982. Process Chemistry for Water and Wastewater Treatment. Prentice-Hall Inc., Englewood Cliffs, NJ.

Bhole, A. G. and P. Limaye. 1977. Effect of Shape of Paddle and Container on Flocculation Process. Journal of Institution of Engineers (India), 57, 52-57.

Bird, R. B., W. E. Stewart, and E. N. Lightfoot. 1960. Transport Phenomena. John Wiley and Sons, New York, N.Y.

Boadway, J. D. 1978. Dynamics of Growth and Breakage of Alum floc in the Presence of Fluid Shear. Jour. Env. Eng. Div., 104, EE5, 901-915.

Bourne, J. R. 1982. Characterization of Micromixing Using Fast Multiple Reactions. Chem. Engr. Commun., 16, 79-90.

Bourne, J. R. and P. Dell'ava. 1987. Micro- and Macro-mixing in Stirred Tank Reactors of Different Sizes. Chem. Engr. Res. Des., 65, 180-186.

Bourne, J. R., F. Kozicki, and P. Rys. 1981a. Mixing and Fast Chemical Reaction - I. Test Reactions to Determine Segregation. Chem. Engr. Sci., 36, 10, 1643-1648.

Bourne, J. R., F. Kozicki, U. Moergeli, and P. Rys. 1981b. Mixing and Fast Chemical Reaction - III. Model-Experiment Comparisons. Chem. Engr. Sci., 36, 10, 1655-1663.

Bradshaw, P., T. Cebeci, and J. H. Whitelaw. 1981. Engineering Calculation Methods For Turbulent Flow. Academic Press, London, U.K.

Bratby, J. 1980. Coagulation and Flocculation Tests. In Coagulation and Flocculation. Upland Press, Croydon, U.K. 263-289.

Bratby, J., H. W. Miller, and G. R. Marais. 1977. Design of Flocculation Systems from Batch Test Data. Water S. A., 3, 4, 173-182.

Brodkey, R. S. 1975. Chapter 2: Mixing in Turbulent Fields. In Robert S. Brodkey Ed. Turbulence in Mixing Operations: Theory and Application to Mixing and Reaction. Academic Press, Inc., New York, N.Y.

Brodkey, R. S. 1967. The Phenomena of Fluid Motions. Addison-Wesley Publishing Company, Reading, MA.

Burgess, J. 1988. Ions in Solution: Basic Principles of Chemical Interactions. Ellis-Horwood Limited, Chichester; John Wiley and Sons, New York, N.Y.

Camp, T. R. 1968. Floc Volume Concentration. Jour. AWWA, 60, 6, 656-673.

Camp, T. R. 1955. Flocculation and Flocculation Basins. Transactions, ASCE, 120, Paper 2722, 1-16.

Camp, T. R. and P. C. Stein. 1943. Velocity Gradients and Internal Work in Fluid Motion. Jour. Boston Society of Civil Engineers, 30, 4, 219-237.

Casson, L. W. and D. F. Lawler. 1990. Flocculation in Turbulent Flow: Measurement and Modeling of Particle Size Distributions. Jour. AWWA, 82, 8, 54-68.

Chakrabarti, M. 1991. Numerical Studies of Chemical Selectivity and Heat Transfer in Decaying Homogenous Turbulence. Ph. D. Thesis, Iowa State University Library, Ames, IA.

Ching, H., M. Elimelech, and J. G. Hering. 1994. Dynamics of Coagulation of Clay Particles with Aluminum Sulfate. JEED, ASCE, 120, 1, 169-189.

Clark, M. M. 1985. A Critique of Camp and Stein's RMS Velocity Gradient. JEED - ASCE, 111, 6, 741-754.

Clark, M. M., R. M. Srivastava, J. S. Lang, R. R. Trussell, L. J. McCollum, D. Bailey, J. D. Christie, and G. Stolaric. 1994. Selection and Design of Mixing Processes for Coagulation. AWWA Research Foundation, Denver, CO.

Cleasby, J. L., A. H. Dharmarajah, G. L. Sindt, and E. R. Baumann. 1989. Design and Operation Guidelines for Optimization of the High-Rate Filtration Process: Plant Survey Results. Subject Area: Water Treatment and Operations. AWWA Research Foundation, Denver, CO.

Corrsin, S. 1961. Turbulent Flow. American Scientist, 49, 300-325.

Currie, I. G. 1993. Fundamental Mechanics of Fluid. McGraw-Hill, Inc., New York, N.Y., 35-45.

Cutter, L. A. 1966. Flow and Turbulence in a Stirred Tank. AIChE Jour., 12, 1, 35-44.

Danckwerts, P. V. 1958. The Effect of Incomplete Mixing on Homogeneous Reactions. Chem. Engr. Sci., 8, 83.

Dann, R. 1988. Ferric Chloride Favored Over Alum for Cost Saving Coagulation. Waterworld News, March-April, 16-17.

David, R. and M. M. Clark. 1991. Chapter 5: Micromixing Models and Applications to Aluminum Neutralization Precipitation Reactions. In A. Amirtharajah, M. M. Clark, and R. R. Trussell Ed. Mixing in Coagulation and Flocculation. AWWA Research Foundation, Denver, CO.

Delichatsios, M. A. and R. F. Probstein. 1975. Coagulation in Turbulent Flow: Theory and Experiment. Jour. Colloid and Inter. Sci., 51, 3, 394-405.

Dentel, S. K. 1987. Optimizing Coagulant Additions From Laboratory and Field Test Methods. In AWWA Seminar Proceedings: Influence of Coagulation on the Selection, Operation, and Performance of Water Treatment Facilities. AWWA, Denver, CO.

Dentel, S. K. and J. M. Gossett. 1988. Mechanisms of Coagulation with Aluminum Salts. Jour. Am. Wat. Works Assoc., 80, 4, 187-198.

Drobny, N. L. 1963. Effect of Paddle Design on Flocculation. Jour. San. Engr. Div. ASCE, 89, SA2, 17-30.

Edzwald, J. K. 1981. "Coagulation". Back to the Basics. Proceedings of an American Water Works Association Seminar, St. Louis, MO, 23-44.

Eilbeck, W. J. and G. Mattock. 1987. Chemical Progress in Wastewater Treatment. Ellis-Horwood Limited, Chichester, U.K.

Ernst, M. H. 1986. Kinetics of Clustering in Irreversible Aggregation. In L. Pietronero and E. Tosatti Ed. Fractals in Physics. Elsevier Science Publishers, Netherlands, 289-302.

Fitchett, D. E. and J. M. Tarbell. 1990. Effect of Mixing on the Precipitation of Barium Sulfate in an MSMPR Reactor. AIChE Jour., 36, 4, 511-522.

Francois, R. J. and A. A. van Haute. 1983. Floc Strength Measurements Giving Experimental Support for a Four Level Hydroxide Floc Structure. In Pawlowski, Verdier, and Lacey Ed. Proceedings of an International Conference - Chemistry for Protection of the Environment. Elsevier, Toulouse, France.

Frost, W. 1977. Chapter 4: Spectral Theory of Turbulence. In Walter Frost and Trevor H. Moulden Ed. Handbook of Turbulence. Volume 1. Fundamentals and Applications. Plenum Press, New York, N.Y.

Frost, W. and J. Bitte. 1977. Chapter 3: Statistical Concepts of Turbulence. In Walter Frost and Trevor H. Moulden Ed. Handbook of Turbulence. Volume 1. Fundamentals and Applications. Plenum Press, New York, N.Y.

Glasgow, L. A. and J. Hsu. 1984. Floc characteristics in Water and Wastewater Treatment. In Particulate Science and Technology, 2. Hemisphere Publishing Company, 285-303.

Gleick, J. 1987. Chaos: Making a New Science. Viking Press, New York, N.Y.

Gregory, J. 1989. Fundamentals of Flocculation. Critical Reviews in Environmental Control, 19, 3, 185-230.

Gregory, J. 1985. Turbidity Fluctuations in Flowing Suspensions. Jour. Colloid and Inter. Sci., 105, 2, 357-371.

Gregory, J. 1987. Laminar Dispersion and the Monitoring of Flocculation Process. Jour. Colloid and Inter. Sci., 118, 2, 397-409.

Gregory, J. and D. W. Nelson. 1986. Monitoring of Aggregates in Flowing Suspensions. Colloids and Surfaces. Elsevier Science Publishers B. V., Amsterdam, The Netherlands, 175- 188.

Gregory, J. and D. W. Nelson. 1984. A New Optical Method for Flocculation Monitoring. In J. Gregory Ed. Solid-Liquid Separation. Ellis Horwood, Chichester, England, 172- 182.

Gregory, J. 1978. Effects of Polymers on Colloidal Stability. In K. J. Ives Ed. The Scientific Basis of Flocculation. Sijthoff and Noordhoff, The Netherlands.

Hall, E. S. 1965. The Zeta Potential of Aluminum Hydroxide in Relation to Water Treatment Coagulation. Jour. Appl. Chem., 15, 197-205.

Han, M. and D. F. Lawler. 1992. The (Relative) Insignificance of G in Flocculation. Jour. Am. Wat. Works Assoc., 84, 10, 79-91.

Hannah, S. A., J. M. Cohen, and G. G. Robeck. 1967a. Measurement of Floc Strength by Particle Counting. Jour. Am. Wat. Works Assoc., 59, 7, 843-858.

Hannah, S. A., J. M. Cohen, and G. G. Robeck. 1967b. Control Techniques for Coagulation-Filtration. Jour. Am. Wat. Works Assoc., 59, 9, 1149-1163.

Hanson, A. T. 1989. The Effect of Water Temperature and Reactor Geometry on Turbulent Flocculation. Ph.D. Thesis, Iowa State University Library, Ames, IA.

Hanson, A. T. and J. L. Cleasby. 1990. The Effect of Temperature on Turbulent Flocculation: Fluid Dynamics and Chemistry. Jour. Am. Wat. Works Assoc., 82, 11, 56-73.

Harnby, N., M. F. Edwards, and A. W. Nienow (Editors). 1985. Mixing in Process Industries. Butterworths, London.

Hayden, P. L. and A. J. Rubin. 1974. Systematic Investigation of the Hydrolysis and Precipitation of Aluminum(III). In A. J. Rubin Ed. Aqueous Environmental Chemistry of Metals. Ann Arbor Science Publishers, Inc., Ann Arbor, MI, 317-381.

Hill Jr., C. G. 1977. An Introduction to Chemical Engineering Kinetics & Reactor Design. John Wiley & Sons, New York, N.Y.

Hinze, J. O. 1975. Turbulence. McGraw-Hill Series in Mechanical Engineering. Second Edition. McGraw-Hill, Inc., New York, N.Y.

Hinze, J. O. 1955. Fundamentals of Hydrodynamic Mechanisms of Splitting in the Dispersion Process. AIChE. Jour., 1, 1, 289-295.

Hirtzel, C. S. and R. Rajagopalan. 1985. Advanced Topics in Colloidal Phenomena. Monograph. Department of Chemical and Environmental Engineering, Rensselaer Polytechnic Institute, Troy, New York.

Hohl, H., L. Sigg, and W. Stumm. 1978. Characterization of Surface Chemical Properties of Oxides in Natural Waters: The Role of Specific Adsorption in Determining the Surface Charge. Paper Presented at the Symposium on Particulates in Water. 175th ACS National Meeting, Anaheim, CA.

Hong-Xiao, T. and W. Stumm. 1987a. The Coagulating Behavior of Fe(III) Polymeric Species - I; Preformed Polymers by Base Addition. Water Research, 21, 1, 115-121.

Hong-Xiao, T. and W. Stumm. 1987b. The Coagulating Behavior of Fe(III) Polymeric Species - II; Preformed Polymers in Various Concentrations. Water Research, 21, 1, 123-128.

Hudson Jr., H. E. 1965. Physical Aspects of Flocculation. Jour. Am. Wat. Works Assoc., 57, 7, 885-892.

Hunter, R. J. 1987. Foundations of Colloid Science. Oxford University Press, Oxford, U.K.

Israelachvili, J. N. 1985. Intermolecular and Surface Forces: with Applications to Colloidal and Biological Systems. Academic Press, Orlando, Fl.

Ives, K. J. 1984. Experiments in Orthokinetic Flocculation. In J. Gregory Ed. Solid-Liquid Separation. Ellis Horwood Limited, Chichester, England, 196-220.

Ives, K. J. and A. G. Bhole. 1973. Theory of Flocculation for Continuous Flow System. Jour. Env. Eng. Div., ASCE, EE1, 17-34.

James, R. D. and T. W. Healy. 1972a. Adsorption of Hydrolyzable Metal Ions at the Oxide-Water Interface. I. Co(II) Adsorotion on SiO_2 and TiO_2 as Model Systems. Jour. Colloid and Inter. Sci., 40, 1, 42-52.

James, R. D. and T. W. Healy. 1972b. Adsorption of Hydrolyzable Metal Ions at the Oxide-Water Interface. II. Charge reversal of SiO_2 and TiO_2 Colloids by Adsorbed Co(II),La(III), and Th(IV) as Model Systems. Jour. Colloid and Inter. Sci., 40, 1, 53-63.

James, R. D. and T. W. Healy. 1972c. Adsorption of Hydrolyzable Metal Ions at the Oxide-Water Interface. III. A Thermodynamic Model of Adsorption. Jour. Colloid and Inter. Sci., 40, 1, 65-81.

Johnson, P. N. and A. Amirtharajah. 1983. Ferric Chloride and Alum as Single and Dual Coagulants. Jour. Am. Wat. Works Assoc., 75, 5, 232-239.

Kavanaugh, M. C. and J. O. Leckie. 1980. Preface to Particulates in Water. Characterization, Fate, Effects and Removal. In Michael C. Kavanaugh and James O. Leckie Ed. Advances in Chemistry Series 189. American Chemical Society, Washington, D.C., 9-11.

Kayode, T. O. and J. Gregory. 1988. A New Technique for Monitoring Alum Sludge Conditioning. Wat. Res., 22, 1, 85-90.

Koh, P. T. L. 1984. Compartmental Modeling of a Stirred Tank for Flocculation Requiring a Minimum Critical Shear Rate. Chem. Engr. Sci., 39, 12, 1759-1764.

Koh, P. T. L., J. R. G. Andrews, and P. H. T. Ulherr. 1987. Modeling of Shear Flocculation by Population Balance. Chem. Engr. Sci., 42, 2, 353-362.

Koh, P. T. L., J. R. G. Andrews, and P. H. T. Ulherr. 1984. Flocculation in Stirred Tanks. Chem. Engr. Sci., 39, 6, 975-985.

Kulov, N. N., E. K. Nikolaishvili, V. M. Barabash, L. N. Braginsky, V. A. Malyusov, and N. M. Zhavoronkov. 1983. Dissolution of Solid Particles Suspended in Agitated Vessels. Chem. Engr. Commun., 21, 259.

Lagvankar, A. L. and R. S. Gemmell. 1968. A Size-Density Relationship for Flocs. Jour. Am. Wat. Works Assoc., 60, 1040-1046.

Lawler, D. F., C. R. O'Melia, and J. E. Tobiason. 1980. Chapter 16: Integral Water Treatment Plant Design: From Particle Size to Plant Performance. In Kavanaugh and Leckie Ed. Particulate in Water. Advances in Chemistry Series 189. American Chemical Society Publishers, Washington, D.C.

Lesieur, M. 1987. Turbulence in Fluids. Martinus Nijhoff Publishers, Dordrecht, The Netherlands.

Letterman, R. D. and S. G. Vanderbrook. 1983. Effects of Solution Chemistry on Coagulation with Al(III); Significance of the Sulfate Ion and pH. Water Research, 17, 195-204.

Letterman, R. D., M. Tabatabaie, and R.. S. Ames Jr. 1979. The Effect of the Bicarbonate Ion Concentration on Flocculation with Aluminum Sulfate. Jour. Am. Wat. Works Assoc., 71, 8, 467-472.

Lichtenbelt, J. W. T., C. Pathmamanoharan, and P. H. Wiersema. 1974. Rapid Coagulation of Polystyrene Latex in a Stopped Flow Spectrophotometer. Jour. Colloid and Inter. Sci., 49, 3, 281-296.

Marcant, B. and R. David. 1991. Experimental Evidence for and Prediction of Micromixing Effects in Precipitation. AIChE Jour., 37, 11, 1698-1710.

Marchal, P., R. David, J. P. Klein, and J. Villermaux. 1988. Crystallization and Precipitation Engineering: An Efficient Method for Solving Population Balance in Crystallization with Agglomeration. Chem. Engr. Sci., 43, 59.

Margeli, M. T. and J. L. Garcia-Heras. 1987. Mathematical Model of the Flocculation Process Applied to the Elimination of Color of Bleaching Effluents of a Paper Mill. Internal Report 0189, Department of Environmental Studies of the CEIT, Apartado 1555, San Sebastian 20080, Spain.

Matijevic, E. and N. Kolak. 1967. Coagulation of Lyophobic Colloids by Metal Chelates. Jour. Colloid and Inter. Sci., 24, 441-450.

Matz, G. 1985. Ostwald Ripening - A Modern Concept. Ger. Chem. Engr., 8, 225.

McConnachie, G. L. 1991. Turbulence Intensity of Mixing in Relation to Flocculation. JEED, ASCE, 117, 6, 731-750.

McDonough, R. J. 1992. Mixing for the Process Industries. Van Nostrand Reinhold Publisher, New York, N.Y.

Michaels, A. S. and J. C. Bolger. 1962a. Settling Rates and Sediment Volumes of Flocculated Kaolin Suspensions. Industrial Eng. Chemistry Fund., 1, 1, 69-77.

Michaels, A. S. and J. C. Bolger. 1962b. Plastic Flow Behavior of Flocculated Kaolin Suspensions. Industrial Eng. Chemistry Fund., 1, 3, 153-162.

Miller, L. B. 1925. A Study of the Effects of Anions upon the Properties of Alum Floc. Public Health Reports, 40, 351-367.

Monin, A. S. and A. M. Yoglom. 1971. Statistical Fluid Mechanics: Mechanisms of Turbulence. Volume 1. MIT Press, Cambridge, MA.

Montgomery, J. M., Consulting Engineers Inc. 1985. Chapter 6: Precipitation, Coagulation, Flocculation. In Water Treatment Principles and Design. John Wiley & Sons Inc., New York, NY, 116-134.

Morris, J. K. and W. R. Knocke. 1984. Temperature Effects on the Use of Metal-ion Coagulants for Water Treatment. Jour. Am. Wat. Works Assoc., 76, 3, 74-79.

Nishikawa, M., Y. Okamoto, K. Hashimoto, and S. Nagata. 1975. Mixing: Principle and Applications. Jour. Chem. Engr. Japan, 9, 489.

Nyvlt, J. and M. Karel. 1985. Crystal Agglomeration. Cryst. Res. Technol., 20, 173.

O'Brien, E. E. 1975. Chapter 1: Theoretical Aspects of Turbulent Mixing of Reactants. In R. S. Brodkey Ed. Turbulence in Mixing Operations: Theory and Application to Mixing and Reaction. Academic Press, Inc., New York, N.Y.

Odegaard, H. 1985. Engineering Aspects of Flocculation. Schr-Reihc Ver. Wass.-Boden- u. Lufthyg., 62, 81-102.

Okamoto, Y., M. Nishikawa, and K. Hashimoto. 1981. Energy Dissipation Rate Distribution in Mixing Vessels and its Effects on Liquid-Liquid Dispersion and Solid-Liquid Mass Transfer. Inter. Chem. Engr., 21, 1, 88-94.

O'Melia, C. R. 1978. Coagulation in Wastewater Treatment. In K. J. Ives Ed. The Scientific Basis of Flocculation. NATO Advanced Study Institute Series, Series E, Applied Science - No 27. Sijthoff & Noorhoff, Netherlands.

O'Melia, C. R. 1972. Chapter 2: Coagulation and Flocculation. In W. J. Weber Ed. Physicochemical Process for Water Quality Control. Wiley-Interscience, New York, N.Y.

Panton, R. L. 1984. Incompressible Flows. John Wiley and Sons, New York, N.Y.

Parker, D. S., W. J. Kaufman, and Jenkins. 1970. Characteristics of Biological Flocs in Turbulent Regimes. Sanit. Engr. Lab. Rept. 70-5. Univ. of California, Barkeley, CA.

Patterson, G. K. 1985. Chapter 3: Modeling of Turbulent Reactors. In J. Ulbrecht and G. K. Patterson Ed. Mixing of Liquids by Mechanical Agitation. Gordon and Breach Science Publishers, New York, N.Y.

Patwardham, S. V. and A. G. Mirajgaonkar. 1970. Hydraulics of Flocculation and Paddle Characteristics. Journal of Institution of Engineers (India), 50, 60-64.

Placek, J. and L. L. Tavlarides. 1985. Turbulent flow in Stirred Tanks. Part I: Turbulent Flow in the Turbine Impeller Region. AIChE Jour., 31, 7, 1113-1120.

Placek, J., L. L. Tavlarides, and G. W. Smith. 1986. Turbulent flow in Stirred Tanks. Part II: Two Scale Model of Turbulence. AIChE Jour., 32, 11, 1771-1786.

Rao, M. A. and R. S. Brodkey. 1972. Continuous Flow Stirred Tank Turbulence Parameters in the Impeller Stream. Chem. Engr. Sci., 27, 137-156.

Rice, R. W. and R. E. Baud. 1990. The Role of Micromixing in the Scale-Up of Geometrically Similar Batch Reactors. AIChE Jour., 36, 2, 293-298.

Ritchie, A. R. 1956. Theoretical Aspects of Flocculation Coagulation. Proceedings of the Society for Water Treatment and Examination, 5, 81.

Saffman, P. G. and J. S. Turner. 1956. On the Collision of Drops in Turbulent Clouds. Jour. Fluid Mechanics, 1, 16-30.

Shapiro, A. H. 1961. Vorticity. Parts I and II. Educational Services Inc., circa, Cambridge, MA.

Sricharoenchaikit, P. and R. D. Letterman. 1987. Effect of Al(III) and Sulfate Ion on Flocculation Kinetics. Jour. Env. Eng. Div., 113, 5, 1120-1138.

Srivastava, R. M. 1988. Impact of Rapid Mixing and Temperature on Flocculation of Clay Suspensions in Water. M. S. Thesis, Iowa State University Library, Ames, Ia.

Stewart, R. W. 1969. Turbulence. (Motion Picture Film). Educational Services Inc., Cambridge, MA.

Stumm, W. and C. R. O'Melia. 1968. Stoichiometry of Coagulation. Jour. Am. Wat. Works Assoc., 60, 5, 514-539.

Stumm, W. and J. J. Morgan. 1981. Aquatic Chemistry. 2nd Edition. John Wiley and Sons, New York, N.Y.

Tambo, N. and H. Hozumi. 1979. Physical Characteristics of Flocs. II. Strength of Floc. Water Research, 13, 421-427.

Tambo, N. and Y. Watanabe. 1979a. Physical Characteristics of Floc. I. The Floc Density Function and Aluminum Floc. Water Research, 13, 409-419.

Tambo, N. and Y. Watanabe. 1979b. Physical Aspect of Flocculation Process. I. Fundamental Treatise. Water Research, 13, 429-439.

Tang, H. and W. Stumm. 1987. The Coagulation Behaviors of Fe(III) Polymeric Species, II. Preformed Polymers in Various Concentrations. Water Research, 21, 122-128.

Tatterson, G. B. 1991. Fluid Mixing and Gas Dispersion in Agitated Tanks. McGraw-Hill, Inc., New York, N.Y.

Tennekes, H. and J. L. Lumley. 1972. A First Course in Turbulence. MIT Press, Cambridge, MA.

Tomi, D. T. and D. F. Bagster. 1977. The Behavior of Aggregates in Stirred Vessels: Part I - Theoretical Considerations on the Effects of Agitation. Transactions Institution of Chemical Engineers, 56, 1, 1-8.

Toor, H. L. 1969. The Non-Premixed Reaction: A + B $\rightarrow$ Products. Ind. Engr. Chem. Fund., 8, 655.

Van't Reit, K., W. Brijn, and J. M. Smith. 1976. Real and Pseudo-turbulence in the Discharge Stream from a Rushton Turbine. Chem. Engr. Sci., 31, 407-412.

Voke, P. E. and M. W. Collins. 1983. Large Eddy Simulation: Retrospect and Prospect. Physico Chemical Hydrodynamics, 4, 2, 119-161.

Vrale and Jorden. 1971. Rapid Mixing in Water Treatment. Jour. AWWA, 63, 1, 52-59.

Yao, K. M., M. T. Habibian, and C. O'Melia. 1971. Water and Wastewater Filtration: Concepts and Applications. Environmental Science & Technology, 5, 1105-1112.

Zeta-Meter, Inc. 1986. Promotinal Literature. 1720 First Ave, New York, N.Y.

ACKNOWLEDGEMENTS

I wish to thank my major professor, Dr. John L. Cleasby for his support, guidance and advice during this research. I really appreciate the time he has invested in guiding me and the understanding he has shown at all times.

This project was supported financially by the National Science Foundation (NSF) under grant number BCS - 9117043, and the support has been greatly appreciated. The able assistance of Lim-Seok Kang and Bashaar Ammary during the course of this study is also appreciated.

I am indebted to my mother and three brothers for their patience and support throughout my academic life. I would like to thank all my maternal uncles for their support throughout my life. I would also like to thank my in-laws for their inspiration and support in every step of my graduate study. Above all, I am grateful to my wife, Rumana for her all out support both at home and at school. My dreams would never be realized without her support, patience and inspiration.

Finally, I would like to thank my high school teacher, Mr. Ashrafuzzaman, who implanted the following words in my mind:

"He who knows not and knows not that he knows not,
he is a fool, shun him.
He who knows but knows not that he knows,
he is asleep, wake him.
He who knows not and knows that he knows not,
he is teachable, teach him.
He who knows and knows that he knows,
he is wise, follow him."

APPENDIX

Summary of physico-chemical conditions used in this study

Figure No.	Temp. (° C)	Clay Conc. (mg/l)	Coagulant type	Dose (mg/l)	pH	ZP (mv)	IFI
6.1	23	25	FN	2	7.8	-10	0.15
6.2	23	25	FN	5	7.8	0	0.15
6.3	23	25	FN	1	6.0	-6	0.15
6.4	05	25	FN	3	7.8	-13	0.12
6.5	05	25	FN	3	7.8	-14	0.10
6.6	05	25	FN	3	7.8	-12	0.09
6.7	05	25	FN	6	7.8	-4	0.09
6.8	05	25	FN	1	6.0	-7	0.12
6.9	23	25	FN	2	7.8	-9	0.14
6.10	23	25	FN	1	6.0	-4	0.15
6.11	23	25	FN	1	6.0	-4	0.15
6.12	23	25	Alum	1.5	7.8	-7	0.13-0.16
6.13	23	50	Alum	2.25	7.8	-13	0.18-0.22
6.14	23	50	Alum	2.25 10 20	6.0	-13 +23 +30	0.17-0.21
6.15	23	50	Alum	2.25	6.0	-12	0.16-0.18

6.16	23	50	Alum	20	7.8	+25	0.20-0.23
6.17	23	50	Alum	4.5	7.8	-14	0.16
6.18	23	25	Alum	3	7.8	-13	0.10-0.13
6.19	23	10	Alum	4	7.8	-7	0.04
6.20	23	25	FN	2	7.8	-15	0.10
6.21	05	25	FN	3	7.8	-13	0.10
6.22	23	50	Alum	2.25	7.8	-12	0.16
6.23	23	25	FN	1	6.0	-6	0.15
6.24	23	25	FN	5	7.8	-3	0.15
6.25	23	25	FN	1	6.0	-5	0.15
6.26	05	25	FN	6	7.8	-3	0.10
6.27	05	25	FN	3	7.8	-13	0.10
6.28	23	25	FN	2	7.8	-13	0.10
6.29	23	25	FN	2	7.8	-12	0.10
6.30	05	25	FN	3	7.8	-13	0.10
6.31	23	25	FN	2	7.8	-15	0.10
6.32	05	25	FN	3	7.8	-13	0.10
6.33	05	25	FN	3	7.8	-13	0.10
6.34	05	25	FN	3	7.8	-13	0.10
6.35	23	25	FN	1	6.0	-4	0.15
6.36	23	25	FN	1	6.0	-4	0.15
6.37	23	25	FN	1	6.0	-6	0.16

6.38	23	10	FN	5	7.8	0	0.07
6.39	23	25	FN	1	6.0	-8	0.17
6.40	05	25	FN	3	7.8	-14	0.10
6.41	05	25	FN	3	7.8	-13	0.10
	23	25	FN	2	7.8	-15	0.10
6.42	23	25	FN	2	7.8	-15	0.10
	23	25	Alum	1.5	7.8	-7	0.10

Note: FN - Ferric Nitrate and IFI - Initial flocculation index
Error in ZP measurement is ∓2 mv